NTNU
Norwegian University of
Science and Technology

R744 HVAC unit for NSB Flirt trains

Eirik Trygstad

Master of Energy Use and Energy Planning
Submission date: June 2017
Supervisor: Armin Hafner, EPT
Co-supervisor: Trygve Eikevik, EPT

Norwegian University of Science and Technology
Department of Energy and Process Engineering

NTNU

Norwegian University
of Science and Technology

Department of Energy
and Process Engineering

EPT-M-2017-90

MASTER THESIS

for

Student: Eirik Trygstad
Spring 2017

R744 HVAC unit for NSB Flirt trains
CO_2 klimaanlegg til NSBs Flirt togene

Background and objective

Currently available HVAC units for trains are commonly using either HFC-134a (75%) or HFC-407C (25%) as working fluids, which have a significant global warming potential when released into the environment. These units typically rely on inefficient direct electrical heating to cover heating demands. However, some system suppliers can offer HFC-134a HVAC systems with heat pump capabilities able to supply heating to the coach at ambient temperatures above -5 °C.

Deutsche Bahn has analysed the energy consumption of their Railway Rolling Stock in detail over several years. Up to 30 % of their total energy consumption has to be spent to operate the HVAC units of the passenger trains in Germany. Only the propulsion system requires a larger share of the total energy. In Norway the energy consumption for heating up the train compartments is dominating, due to the high amount of operating hours at low ambient temperatures.

During the Master Thesis, the newly developed energy efficient and environmentally friendly HVAC unit applying R744 will be monitored during bench tests in Germany and when it is installed in a NSB train operated in the Oslo area. The test campaigns of the on-board HVAC systems (both conventional HFC-134a and R744) will be performed in close cooperation with the researcher team at NTNU/SINTEF.

The objective of the Master Thesis is to follow up the implementation process of the two test HVAC units (one with HFC-134a and one with two different R744 circuits [with and without ejector]). Document and evaluate the results of the measurement campaigns.

The following tasks are to be considered:

1. Literature review: HVAC systems for public transport systems, data acquisition systems (Manuals of the applied units), and define criteria's for the passenger survey during the test campaign with the NSB train.
2. Prepare HSE documents required for the field work, to be implemented in the Appendix
3. Describe the implemented HVAC sytems, the obtained measurement results during bench tests, the attached measurement units and the log files of the data acquisition systems.
4. Analise and process the measured data and develop ways of evaluation various operation modes
5. Summary report
6. Draft popular science article about the test campaign
7. Draft scientific paper related to the findings of the Master Thesis work
8. Proposals for further work

Within 14 days of receiving the written text on the master thesis, the candidate shall submit a research plan for his project to the department.

When the thesis is evaluated, emphasis is put on processing of the results, and that they are presented in tabular and/or graphic form in a clear manner, and that they are analyzed carefully.

The thesis should be formulated as a research report with summary both in English and Norwegian, conclusion, literature references, table of contents etc. During the preparation of the text, the candidate should make an effort to produce a well-structured and easily readable report. In order to ease the evaluation of the thesis, it is important that the cross-references are correct. In the making of the report, strong emphasis should be placed on both a thorough discussion of the results and an orderly presentation.

The candidate is requested to initiate and keep close contact with his/her academic supervisor(s) throughout the working period. The candidate must follow the rules and regulations of NTNU as well as passive directions given by the Department of Energy and Process Engineering.

Risk assessment of the candidate's work shall be carried out according to the department's procedures. The risk assessment must be documented and included as part of the final report. Events related to the candidate's work adversely affecting the health, safety or security, must be documented and included as part of the final report. If the documentation on risk assessment represents a large number of pages, the full version is to be submitted electronically to the supervisor and an excerpt is included in the report.

Pursuant to "Regulations concerning the supplementary provisions to the technology study program/Master of Science" at NTNU §20, the Department reserves the permission to utilize all the results and data for teaching and research purposes as well as in future publications.

The final report is to be submitted digitally in DAIM. An executive summary of the thesis including title, student's name, supervisor's name, year, department name, and NTNU's logo and name, shall be submitted to the department as a separate pdf file. Based on an agreement with the supervisor, the final report and other material and documents may be given to the supervisor in digital format.

☐ Work to be done in lab (Water power lab, Fluids engineering lab, Thermal engineering lab)
☒ Field work

Department of Energy and Process Engineering, 15. January 2017

Prof. Dr.-Ing. Armin Hafner
Academic Supervisor

Research Advisor: Prof. Trygve M. Eikevik

Abstract

The vast majority of current air conditioning systems, for railway HVAC applications, utilize high global warming potential (GWP) hydrofluorocarbon (HFC) refrigerants in a vapor compression cycle. In Europe, the dominating refrigerants are R134a and R407C, constituting 75 and 25% of the total stock, respectively.

Fluorinated greenhouse gases (GHG), such as HFCs, accounts for 2.5% of the overall GHG emissions, expressed in GWP (EU 2013), and are as a consequence being regulated at an increasing rate, through the revised F-Gas regulation of 2014, (EU) No 517/2014, that aims to reduce EU fluorinated GHG emissions by two thirds of the 2010 levels by 2030.

Because of the legislations and incentives put into place, both at the national and international level, the demand for environmentally benign HVAC&R technology, with viability in terms of achieved system efficiency and cost, is high, and can be expected to increase in a range of sectors the forthcoming years.

A review of current railway HVAC technology, gives strong indication that R744 (CO_2) vapor compression units are one of the most viable candidates for the future, able to meet virtually all requirements with regard to environmental impact, safety, reliability and energy efficiency.

A newly developed, energy efficient and environmentally friendly prototype R744 HVAC unit, will be tested onboard a commuter trainset, operated in the Oslo area, during a test campaign to be initiated late 2017. The goal of the test campaign is to evaluate the viability of the prototype in terms of being a replacement for the current standard R134a HVAC units, outfitted on the Norwegian railway operator NSB's railway fleet.

The prototype have the ability to operate in reversed mode, thus enabling delivery of heat to the passenger compartment through the ventilation air, down to an ambient temperature of -20℃. Moreover, the prototype utilize suction line heat exchangers, and offers ejector-supported fluid expansion during AC-mode operation, in order to minimize losses related to fluid expansion.

Results from laboratory bench tests of the prototype, presented in this thesis, indicate that performance requirements can be met, provided an attentive approach, with regard to system design and control strategy, is applied.

At the current stage of development, the prototype achieves a total cooling capacity of 18.6 kW, at the design summer conditions, specified in the European Standard for air conditioning of main line rolling-stock EN 13129.

Sammendrag

Den store majoriteten av dagens HVAC-enheter, om bord skinnegående materiell, benytter hydrofluorkarboner, med et høyt globalt oppvarmingspotensialet, som arbeidsmedium i dampkompresjonssystemer. I Europa, er de dominerende arbeidsmediene R134a og R407C, som utgjør henholdsvis 75 og 25% av den totale bestanden.

Fluoriserte drivhusgasser, som hydrofluorkarboner, utgjør 2,5% av de totale drivhusgassutslippene, uttrykt som CO_2 ekvivalenter (EU 2013). Følgelig blir de regulert i økende grad igjennom EU sitt reviderte F-gass direktiv, (EU) nr. 517/2014, som har som hensikt å redusere EU og samarbeidende nasjoners utslipp av fluoriserte drivhusgasser med to tre-deler innen 2030 sammenlignet med 2010.

Som følge av lover og insentiver, implementert både på et nasjonal og et internasjonalt nivå, er etterspørselen etter miljøvennlig luftkondisjonerings- og kjøle-teknologi, som tilfredsstiller bransjens krav med tanke på energieffektivitet og investeringskostnader, høy og forventet å øke de kommende årene.

En gjennomgang av dagen teknologi innenfor luftkondisjonering av skinnegående materiell, gir sterk indikasjon på at HVAC-enheter som benytter R744 (CO_2) som arbeidsmedium, er en av de mest lovende alternativene for morgendagens luftkondisjoneringssystemer i jernbanesektoren, ettersom de imøtekommer alle krav med hensyn til miljø, passasjer- og drift-sikkerhet og energieffektivitet.

En nyutviklet, energieffektiv og miljøvennlig prototype R744 HVAC-enhet, vil bli testet om bord et pendlertog driftet i Oslo-området, under en testkampanje som skal påbegynnes i utgangen av 2017. Målet med testkampanjen er å evaluere om prototypen kan være en passende kandidat til å erstatte dagens R134a HVAC-enheter, utstyrt på Norges Statsbaner (NSB) sin togflåte.

Prototypen kan driftes i reversert modus ned til en utetemperatur på -20°C, og kan dermed dekke deler av togvognens oppvarmingsbehov igjennom oppvarming av ventilasjonsluft. Gjennom utnyttelse av sugegassvarmevekslere og ejektor, minimerer prototypen irreversible ekspansjonstap. I tillegg legger prototypens todelte utformingen til rette for evaluering av to forskjellige systemer.

Resultater fra laboratorietester, presentert i denne oppgave, indikerer at nødvendige ytelseskrav kan oppnås, så fremt systemdesign og kontrollstrategi utføres på en gjennomført måte.

På det nåværende utviklingsstadium yter prototypen en kjølekapasitet på 18.6 kW ved dimensjonerende sommerforhold, i henhold til Norsk Standard for luftkondisjonering av rullende materiell på hovedlinje NS-EN 13129.

Preface

As this Master Thesis serves as the initial thesis of the pilot R744 HVAC unit project, I have invested a large amount of effort on obtaining sufficient information on the various implemented systems, in order to create detailed descriptions and illustrations, which will benefit future progress in the pilot project.

As have been disclosed in the introduction of the thesis, I uncovered several issues related to the data recorded by the reference unit DAQ system, which ultimately led to a change in thesis objective. Thus, the DAQ system and related record-file signal description became of little relevance for the results presented in the Master Thesis. However, as I consider the system description beneficial for the future progress in the pilot project, I have included it as an appendix to the thesis.

Parts of the literature presented in this thesis, have been extracted from an earlier project work I conducted during the autumn of 2016.

I wish to thanks to my Academic Supervisor Armin Hafner and Krzysztof Banasiak for constructive advice through the course of the thesis work. In addition, I would like to thank Christian Zieger and Michael Damm from *Faiveley Transport Leipzig GmbH & Co. KG* and Håkon Endresen from *NSB Matriell* for answering my many questions via email. Moreover, I would like to extend my thanks to the department of Energy and Process Engineering at NTNU for assistance and a seemingly endless supply of coffee.

Trondheim 11.06.2017

Eirik Trygstad

Table of contents

List of figures

List of tables

Nomenclature

AC: Air conditioning

AC*: Active current

BLEVE: Boiling liquid expanding vapor explosion

CAN: Controller area network

CAV: Constant air volume

CF: Continuous flow

CFC: Chlorofluorocarbon

COP: Coefficient of performance

COP_{HP}: COP for heat pump application

COP_{R}: COP for refrigeration application

CP: Heat capacity flow rate [kW/K]

DAQ: Data acquisitioning

DTU: Technical University of Denmark

DX: Direct expansion

EC: Electronically commuted

EEV: Electronic expansion valve

EN: European Standard

EPS: Energy performance simulation

ET: Eirik Trygstad

EV: Expansion valve

FTL: *Faiveley Transport Leipzig GmbH & Co. KG*

GC: Gas cooler

GHG: Greenhouse gas

GWP: Global warming potential

HC: Hydrocarbon

HCFC: Hydrochlorofluorocarbon

HFC: Hydrofluorocarbon

HFO: Hydrofluoro olefin

HP: Heat pump

HRD: Heat recovery device

HRS: Heat recovery system

HVAC: Heating, ventilation and air conditioning

HVAC&R: Heating, ventilation, air conditioning and refrigeration

HX: Heat exchanger

IAQ: Indoor air quality

IHX: Internal heat exchanger

ISO: the International organization for standardization

LMTD: Logarithmic mean temperature difference [K]

MAC: Mobile air conditioning

ODP: Ozone depletion potential

PPM_V: Parts per million by volume (0.01 vol%, percent volume fraction)

PRV: Passenger railway vehicle

PWM: Pulse width modulated

RH: Relative humidity [%]

R&D: Research and development

SCOP: Seasonal coefficient of performance, equal SPF [-]

SM: Stepper motor

SPF: Seasonal performance factor, equal SCOP [-]

TEV: Thermostatic expansion valve

TEWI: Total equivalent warming impact

TÜV: Technischer Überwachungsverein, Technical Inspection Association (English)

UIV: International Union of Railways

VAV: Variable air volume

VCC: Vapor compression cycle

VCU: Vapor compression unit

VFD: Variable frequency drive

VHC: Volumetric heating capacity [kJ/m^3]

VRC: Volumetric refrigeration capacity [kJ/m^3]

C_p: Specific heat capacity [kJ/(kg·K)]

E_{HP}: Electric energy supplied to the heat pump [kWh/year]

E_R: Electric energy supplied to the AC and refrigeration [kWh/year]

E_{PL}: Electric energy supplied to the top load [kWh/year]

E_{Sn}: Measured apparent power supplied to compressors [kW]

ΔE: Percentage energy savings [%]

I: Specific enthalpy of humid air [kJ/kg]

I_{sat}: Specific latent heat of vaporization [kJ/kg]

ΔI_{HX1} Specific enthalpy difference of humid air over HX1 [kJ/kg]

ΔI_{HVAC} Specific enthalpy difference of humid air over HVAC unit [kJ/kg]

$\dot{m}_{a1}$: Air mass flow rate through HX1, i.e. supply air, of the pilot R744 HVAC [kg/h]

$\dot{m}_{a2}$: Air mass flow rate through HX2 of the pilot R744 HVAC [kg/h]

$\dot{m}_{rb}$: Refrigerant mass flow rate basic circuit [kg/h]

$\dot{m}_{re}$: Refrigerant mass flow rate ejector circuit [kg/h]

$\dot{m}_{re,HX1}$: Low-side refrigerant mass flow rate ejector circuit [kg/h]

$\dot{m}_{re,HX2}$: High-side refrigerant mass flow rate ejector circuit [kg/h]

P_{is}: Isentropic power [kW]

P_{cs}: Crankshaft power [kW]

p_{ws}: Saturation pressure of water vapor

p_{tot}: Total pressure of humid air mixture

p_{gc}: Gas cooler pressure [bar]

p_c: Critical pressure [bar]

$\dot{P}_c$: Active/ true electrical input power supplied to the compressor [kW]

Q_{HP}: Heat delivered by the heat pump [kWh/year]

Q_R: Cooling delivered by the AC and refrigeration [kWh/year]

Q_{PL}: Energy delivered by the top load [kWh/year]

$\dot{Q}_{evap}$: Heat transferred from the heat-source to the refrigerant inside the evaporator [kW]

$\dot{Q}_{cond}$: Heat transferred from the refrigerant to the heat sink inside the condenser [kW]

$\dot{Q}_{Gain}$: Sensible internal system heat gains of the pilot R744 HVAC unit [kW]

$\dot{Q}_{gc}$: Heat transferred from the refrigerant to the heat sink inside the gas cooler [kW]

$\dot{Q}_{HVAC}$: The resulting cooling capacity of the pilot R744 HVAC unit [kW]

$\dot{Q}_{HX1}$: Cooling capacity of the pilot R744 HVAC interior heat exchanger [kW]

$\dot{Q}_{HX1,lat}$: Latent heat transfer from air HX1 of the pilot R744 HVAC [kW]

$\dot{Q}_{HX1,sens}$: Sensible heat transfer from air HX1 of the pilot R744 HVAC [kW]

$\dot{Q}_{HX2}$: Heat transfer from HX2 to ambient air [kW]

$\dot{Q}_{SLHX,HP}$: Heat transferred from the liquid line to the suction line at the SLHX [kW]

$\dot{Q}_{SLHX,LP}$: Heat received by the suction line from the liquid line at the SLHX [kW]

s: Specific entropy [kJ/kg·K]

Δs: Difference in specific entropy [kJ/kg·K]

t_c: Critical temperature [°C]

t_m: Average refrigerant temperature during heat rejection [°C]

t_{evap}: Refrigerant temperature at the evaporator [°C]

t_{db}: Dry bulb air temperature [°C]

t_{dg}: Refrigerant discharge gas temperature [°C]

t_{sg}: Refrigerant suction gas temperature [°C]

$t_{a,i}$: Temperature of the source medium at the evaporator inlet (*Figure 2.8)*

$t_{a,o}$: Temperature of the source medium at the evaporator outlet (*Figure 2.8)*

$t_{r,i}$: Temperature of the refrigerant at the evaporator inlet (*Figure 2.(8,10))*

$t_{r,o}$: Temperature of the refrigerant at the evaporator outlet (*Figure 2.(8,10))*

$t_{s,o}$: Temperature of the sink medium at the condenser outlet *(Figure 2.10)*

$t_{s,i}$: Temperature of the sink medium at the condenser inlet *(Figure 210)*

t_{sat}: Saturation temperature [°C]

Δt_A: Temperature difference between refrigerant outlet and source/sink inlet (*Figure 2.(8,10))*

Δt_A: Temperature difference between refrigerant inlet and source/sink outlet (*Figure 2.(8,10))*

Δt_L: Temperature drop corresponding to pressure drop through heat exchanger (*Figure 2.(8,10))*

Δt_{sh}: Evaporator superheat (*Figure 2.8)*

Δt_{oh}: Discharge gas overheat (*Figure 2.10)*

Δt_{ap}: Temperature approach [K]

v_g: Specific gas volume [m^3/kg]

V_S: Theoretical volumetric compressor capacity [m^3/h]

V_i: Actual volumetric compressor capacity [m^3/h]

$\dot{W}$: Power delivered to compressor [kW]

$\Delta \dot{w}_{is}$: Specific enthalpy difference related to isentropic compression [kJ/kg]

q_{cond}: Enthalpy difference of condenser [kJ/kg]

q_{evap}: Enthalpy difference of evaporator [kJ/kg]

x: Humidity ratio of air [$mass_{H20}/mass_{dry\ air}$]

$\dot{X}_{cond}$: Rate of vapor condensation on the HX1 surface [kg/h]

$\dot{m}_r$: Refrigerant mass flow rate [kg/s]

U-value: Rate of heat transfer through a surface [W/(m^2·K)]

π: Pressure ratio [-]

λ: Volumetric efficiency [-]

η_{alt}: Efficiency of alternative heating system [-]

η_{ej}: Ejector efficiency [-]

η_{is}: Isentropic efficiency [-]

Π_s: Suction pressure ratio [-]

Φ_m: Mass entrainment ratio [-]

1 Introduction

The purpose of this Master Thesis is evaluate the performance of a prototype R744 (CO_2) HVAC unit, further referred to as the pilot unit, to be commissioned onboard one of NSB's *Stadler* FLIRT commuter trainsets, operated in the Oslo area. The evaluation will be based on a series of laboratory bench tests, conducted at the *Faiveley Transport Leipzig GmbH & Co. KG (FTL)* R&D headquarters in Schkeudits.

Moreover, the thesis include a literature review of current and near future, energy efficient and environmental benign, HVAC technology for heating and cooling of passenger railway vehicles, in addition to a general literature review of vapor compression system technology.

A detailed description of two distinct HVAC units for heating, ventilation and air conditioning of the passenger compartment onboard the NSB *Stadler* FLIRT trainsets, will be presented.

The HVAC unit referred to as the pilot unit, is a prototype R744 HVAC unit designed and developed in a joint collaboration between *FTL* and *SINTEF*. Whereas the HVAC unit referred to as the reference unit, is a standard R134a HVAC unit, retrofitted with additional measuring equipment; i.e. a data acquisitioning (DAQ) system with additional temperature and pressure sensors, and current meters.

The pilot unit holds two individually operated refrigerant circuit, a basic circuit, and an ejector circuit. The ejector circuit can offer an ejector-supported expansion process during AC mode operation. The dual circuit layout of the pilot unit facilitates performance evaluation of two different R744 systems, in the presented bench test results.

A large amount of effort have also been spent on developing a complete description of the reference unit DAQ system and the record-file data; however, due to the events disclosed in section 1.1, the majority of this have been moved to Appendix A.

1.1 Initial purpose of the thesis work

Initially, the main purpose of this Master Thesis was to follow up the implementation of the two test HVAC units, i.e. the pilot and the reference unit, by documenting and evaluating recorded data from field measurements, during regular operation onboard the NSB *Stadler* FLIRT, BM 75-41 commuter trainset. However, due to several major setbacks, the pilot unit was still being tested at the *FTL* laboratory in Sckeuditz while the thesis was being finalized.

Moreover, the analysis of the recoded field measurement data from the reference unit, uncovered numerous issues with the DAQ system, as have been explained in section 4.1. Thus, the analysis potential of the field data became severely limited.

Consequently, although an extensive amount of effort had been spent on describing the DAQ system and decoding the record-file signals, it was decided to focus on the laboratory bench tests of the pilot unit in the Master Thesis. Thus, most of work related to the reference unit have been taken out of the thesis, and included in Appendix A.

Although not of significant relevance for the topics disclosed in this thesis, the DAQ system, description included in Appendix A, is considered beneficial for the future work on the pilot R744 HVAC unit project.

1.2 Background

The vast majority of air conditioning and refrigeration applications onboard railway vehicles are vapor compression cycle (VCC) units, applying hydrofluorocarbon (HFC) refrigerants with a high global warming potential (GWP). As the majority of the global community seems determined to comply with ever more restrictive policies on greenhouse gas (GHG) emissions, the interest for natural refrigerants, with their negligible GWP, have seen a substantial growth in the past couple of decades.

Natural refrigerants was widespread used in early refrigeration and air conditioning applications of the mid-1800s. However, at that time "natural refrigeration" termed the natural ice harvesting industry, which up until the advent of mechanical refrigeration systems was a vibrant economy, shipping ice worldwide [1].

Subsequently, the first seemingly ideal, new synthetic refrigerants, like R12 (CFC-12) and R22 (HCFC-22), made their arrival in the 1930s, and was quickly adopted as a preferred refrigerant by the refrigeration and air conditioning industry. The quick market uptake of synthetic refrigerants was largely attributed to safety and performance concerns related to the various natural refrigerant systems of the day. The main arguments at the time being reliability, complete safety and harmlessness to the environment [2]; however, the latter argument was later found to be grossly incorrect.

The CFC and HCFC fluids continued to be the predominant refrigerants, until the late 1980s, when their ozone-depleting properties (ODP) came to light. This called for a phase out through the Montreal Protocol (1987), which came into effect 1 January 1989 [3]. Consequently, a

family of non-ODP synthetic hydrofluorocarbon (HFC) refrigerants, such as R134a and R407C, was developed as replacements for the CFCs and HCFCs. Moreover, in the wake of the CFC/HCFC phase-out Professor Gustav Lorentzen proposed the revival of carbon dioxide as a viable long-term replacement, in the 1993 paper "*Revival of carbon dioxide as a refrigerant*" [2]. Nevertheless, the HFCs were quickly accepted as replacements for the CFC/HCFCs in most HVAC applications. The HFCs were designed to mimic the CFC/HCFC fluids, thus, in some cases, facilitating relatively simple system conversions.

Fluorinated GHGs, such as HFCs, accounts for 2.5% of the overall GHG emissions expressed in GWP (EU 2013) [4]. Consequently, HFCs are being regulated at an increasing rate, through the 2006 European Union F-Gas regulation, (EC) No 842/2006 [5]. This regulation addresses the containment, use, recovery and destruction of fluorinated GHG. As well as the training and certification of companies and personnel handling fluorinated gases. Moreover, the revised F-Gas regulation of 2014, (EU) No 517/2014 [6] aims to reduce EU fluorinated GHG emissions by two thirds of the 2010 levels by 2030, see *Figure 1.1*, consequently phasing out HFC refrigerants. The large increase in HFC placing on the market (POM) in 2014, seen in *Figure 1.1*, is a result of the market reaction to the revised regulations of 2014 [6].

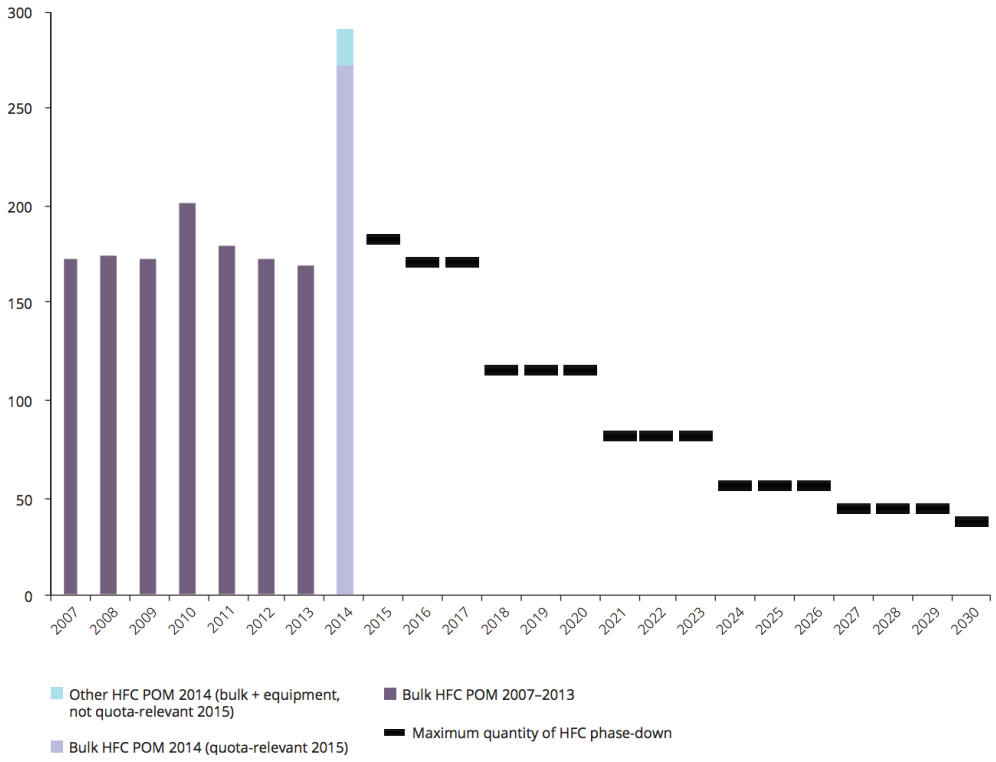

Figure 1.1: Outlook for the HFC phase-down, Placing on the market (POM) of HFCs (Mt CO_2-equivalent) (EU) [4].

Following the legislations and incentives put into place, both at the national and international level, the demand for environmentally benign HVAC&R technology with viability in terms of

achieved system efficiency and cost, is high and can be expected to increase the forthcoming years.

Research and development of new and improved HVAC technology, utilizing natural refrigerants, like that presented in this thesis, show viable results in terms of achieved efficiency, in some cases outperforming the traditional HFC systems at the relevant operating conditions; e.g. the use of transcritical R744 heat pumps for heating of domestic hot water [7], in automobile AC units [8], or supermarket refrigeration [9].

Analogous to the phase-out of CFC/HCFCs, new synthetic hydrofluorolefin (HFO) refrigerants are being developed as replacements for the HFCs. The HFOs have significantly lower GWP than the HFCs (GWP < 6). However, little is known about the long-term environmental effect of large-scale emission of these compounds into the atmosphere, as they eventually dissociate into other compounds. Back in 1993, late Professor Gustav Lorentzen wrote something that seems equally relevant today:

> The extensive use of ever-new compounds is one of the big problems of our time. In this situation it does not seem very sensible to replace the CFC/HCFCs with a new family of related halocarbons, equally foreign to nature, to be used in quantities of hundreds of thousands of tons every year [2].
>
> Gustav Lorentzen, 1993:1.

1.3 Norges statsbaner NSB

The Norwegian railway operator Norges Statsbaner (NSB), or Norwegian State Railways, is governed by the Norwegian Ministry of Transport and Communication, and is the owner of the pilot R744 HVAC project. As with many other government-owned companies, environmental policy is a central part of the NSB business strategy, striving to be one of the most environmentally friendly companies in Norway, as stated in their environment declaration [10]. Moreover, the declaration states that all purchases and actions made by the company, needs to be carefully considered from an environment point of view, and in accordance with the environmental management system ISO 14001.

Figure 1.2: NSB Stadler FLIRT (Stadler).

In 2008 NSB ordered 50 new five-part trainsets, of the model FLIRT, by the Swiss manufacturer *Stadler*, located in the small town of Bussnang north-east of Zürich. To this day (2017), NSB have ordered a total of 107 FLIRT trainsets, most of which have been commissioned into regular operation.

The FLIRT trainsets have been a huge success for NSB, since they were put into operation in 2012. According to a NSB press release, the introduction of the FLIRT trainset has led to an increase in travelers by 20% on certain routes, and is one of the main causes for the companies 30% energy reduction from 2004 to 2014 [11]. In 2015, half of all railway passengers in Norway traveled by a FLIRT, amounting to a total of 32 million individual trips [12]. Moreover, the FLIRT have proven to be very reliable in Norwegian climate, and the top speed of 200 km/h have significantly reduced travel time on certain routes.

The NSB Group have recently undergone extensive restructurations to comply with the implementation of the railway reform (Jernbanereformen) of 2017. A central objective of the reform is to facilitate increased competition in the passenger railway sector. As a consequence of the reform, the previous subsidiaries owning the rolling stock (Materiellselskapet AS), the ticket sales and distribution system (Entur AS), the maintenance activities (Mantena AS), and the property operations (ROM Eiendom AS) was demerged out of the NSB Group starting 1st of January 2017 [13].

2 Literature

2.1 Passenger rail HVAC

Not all energy consumed by a passenger railway vehicle (PRV) goes towards traction. PRVs are equipped with multiple auxiliary systems that ensure comfort to passengers and help provide a better transport service. These auxiliary systems include HVAC, lighting, power plugs, information screens and loud speakers, in addition to opening and closing of doors etc. Auxiliary loads are estimated to constitute about 10 to 15% and in some cases up to 50% of the total energy consumption of a PRV, according to numbers from International Union of Railways (UIC) [14].

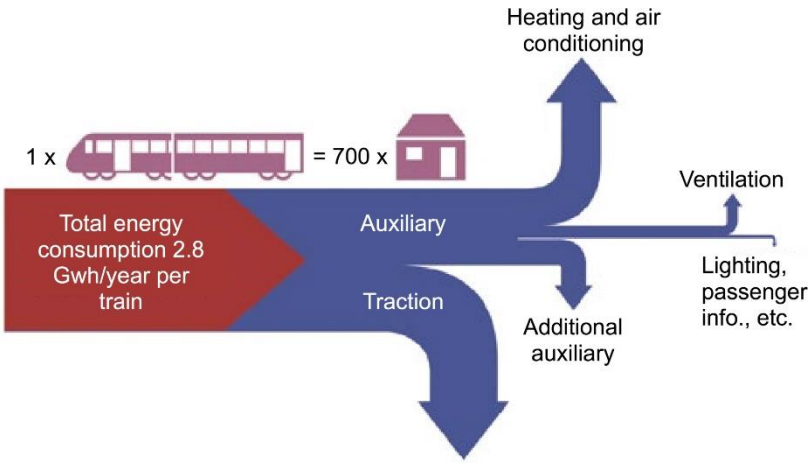

Figure 2.1: Load distribution in Swiss railways ICN trainsets (UIC [14]).

As one can observe in *Figure 2.1*, HVAC systems are by far the biggest energy consumer of the auxiliary systems, generally constituting 80% [15], depending on the climatic zone. Consequently, efficiency of the HVAC system, thermal isolation of the carriage envelope, and the transmission factor of window glazing can have a significant impact on the overall energy consumption a PRV.

In the search for improved efficiency and reduced energy demand, many energy measures and simulation tools have been adopted from the building sector, e.g. demand controlled ventilation, ventilation-air heat recovery, envelope insulation, low transmitting window glazing, adaptive system control strategies, etc.

A project originally initiated by the Physics Department of the University of Basil [16] monitored temperature, heating and cooling energy, GPS-positioning and ambient meteorological data for six passenger railway vehicles, from four different Swiss railway companies, over a three-year period. The main objective was to define and quantify measures

to reduce energy consumption of the HVAC system onboard the vehicles EWII of the Swiss Rhaetian Railway (RhB), without compromising comfort quality for the passengers. An energy performance simulation (EPS) software (IDA ICE) was used to establish the different load characteristics and seasonal heating demand.

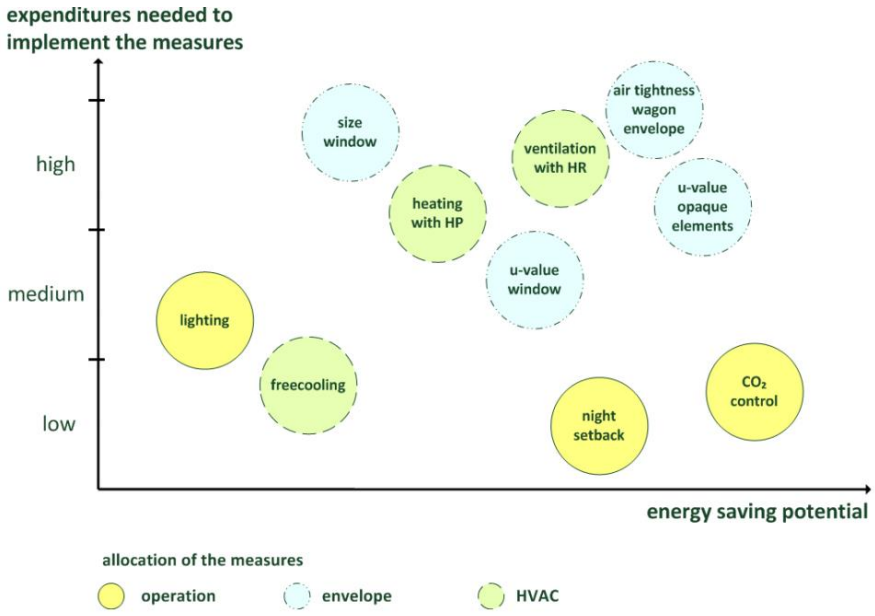

Figure 2.2: Qualitative cost-benefit assessment for the different energy measures[16].

The EPS data was then be used to identify the energy saving potential related to various energy measures. *Figure 2.2* shows the resulting cost-benefit of the evaluated measures. As can be observed in *Figure 2.2*, demand controlled ventilation regulated with regard to compartment CO_2 concentration was the measure related to the greatest energy saving potential (29% [16]). Moreover, the expenditures needed to implement this measure was regarded as low compared to most of the others; however, it is not completely clear what have been factored in for the different cost estimations.

2.1.1 Comfort parameters

The purpose of the HVAC system is to ensure sufficient thermal comfort and air quality for the passengers present in the passenger compartment. The thermal comfort is assessed based on, interior air temperature, air velocity, relative humidity (RH), surface temperatures (radiant temperature asymmetry), vertical and horizontal temperature gradients, and passengers clothing level and metabolism, as specified in the European Standard for air conditioning of main line rolling-stock EN 13129.

Additionally, the type of rail transportation service (e.g., urban rapid transit, commuter, long distance) and the corresponding comfort expectations, are important factors that should be

considered when selecting the control parameter and designing the equipment to attain them [17]. Thus, the following factors should also be considered:

- Changes in regional microclimates during travel.
- Air infiltration, draft, and temperature changes associated with door openings.
- Variations in solar loads due to dynamically changing solar orientation.
- Contribution of the HVAC system to overall vehicle noise.
- Length of journey.

2.1.2 Design conditions

Norway is located in climatic summer and winter zone III, according to EN 13129, thus yielding the external design, extreme, and limiting ambient operating conditions presented in *Table 1*. The HVAC system must ensure comfortable thermal environment at design conditions, have the ability to operate at full capacity during extreme conditions, while being able to operate at reduced capacity up to the limiting conditions.

Table 1: Design, extreme and limiting ambient conditions for passenger rail HVAC applications, as specified in EN-13129 7.1.1-Design conditions, 7.1.2-Extreme conditions and Limiting conditions.

Zone	Winter	Summer		
Ⅲ	Minimum exterior temperatures (T_a)	Maximum exterior-temperatures	Relative humidity(RH)	Equivalent solar load (E_n)
Design conditions	-40℃	28℃	45%	600 W/m^2
Extreme conditions	-45℃	33℃	30%	600 W/m^2
Limiting conditions		38℃	25%	600 W/m^2

When calculating the necessary HVAC unit heating capacity for design and extreme winter conditions, the thermal contribution from solar radiation and passengers should be zero, as this represents the maximum heating demand. Contrarily, when calculating the necessary HVAC unit cooling capacity for design and extreme summer conditions, the passenger sensible and latent load corresponding to full occupancy should be included, in addition to the humidity and solar gains listed in *Table 1* (EN 13129).

Design parameters for the interior of the passenger compartment, like temperature set points for heating and cooling, and fresh air demand, shall be established as specified in EN 13129. Additionally, The HVAC system should be able to respond quickly to sudden changes in thermal loads, as this is a common occurrence in PRVs.

2.1.3 Ventilation

In order to maintain sufficient indoor air quality (IAQ) in the passenger compartment, contaminated compartment air needs to be extracted and replaced with fresh outside air, as specified in EN 13129. In modern PRVs, ventilation is usually achieved through balanced mechanical ventilation systems, where an (almost) equal amount of air is supplied and extracted from the passenger compartment. The ventilation system comprise an air-handling unit (AHU), and a distribution ductwork.

2.1.3.1 Air handling unit

The function of the AHU is to supply and extract air from the distribution ductwork, as demonstrated in *Figure 2.3*. The amount of fresh air (a) needed to maintain sufficient IAQ is mainly a function of the continuously changing passenger occupancy, and a method for controlling the amount of supplied fresh air (b) based on demand (demand control) is crucial in order to ensure minimal energy consumption [16], as mentioned earlier (*Figure 2.2)*.

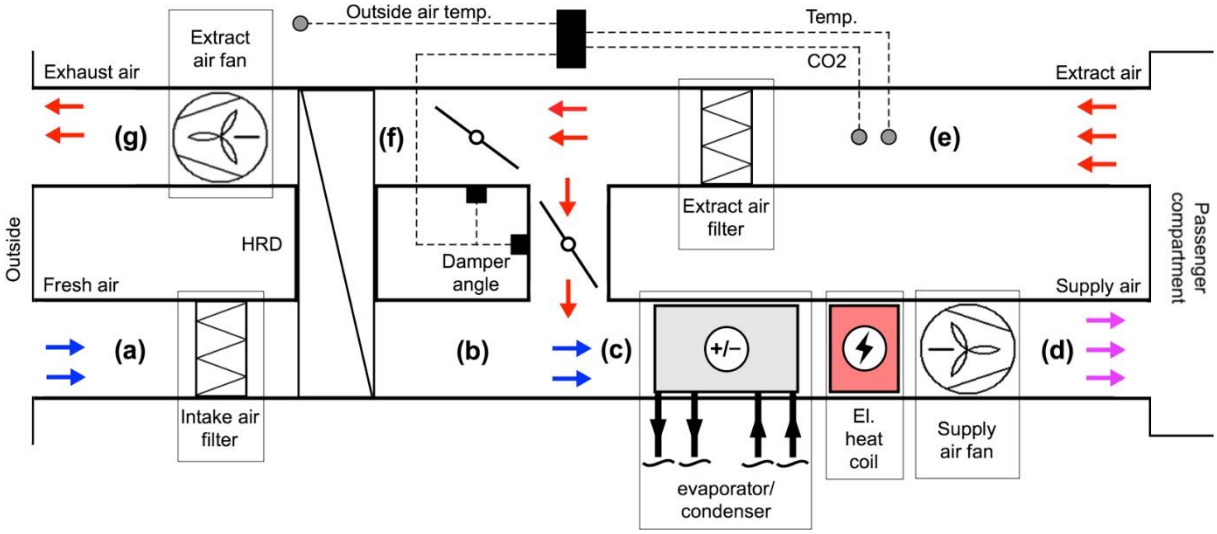

Figure 2.3: Principle sketch HVAC constant volume air handling unit

The ventilation fresh air (a) demand is usually determined based on continuously measured CO_2 concentration in the extract air (f). As most railway HVAC AHUs use constant-speed fan motors [17], a variable fresh air (a) volume rate is usually achieved by utilizing an integrated by-pass, as shown in *Figure 2.3*. By implementing the damper configuration depicted in *Figure 2.3*, the ratio of fresh and recirculated air can be controlled by automated damper, while keeping a constant supply air (d) volume rate. Moreover, by-pass with automated dampers also enables the operator to effectively shut off outside air from the vehicle if smoke or other hazardous exterior conditions are encountered [17].

The AHU depicted in *Figure 2.3* utilize a heat recovery device (HRD) transferring heat from the extracted air in point (f) to (b). The HRD type of choice is usually recuperative (no air cross contamination) plate heat exchangers. Proper frost protection and water drainage needs to be integrated into the HRD design, as conditions where moisture in the extract air (f) can condense on the cold heat exchanger surface during winter operation. Frost protection can be facilitated by an integrated a by-pass, enabling redirection of the airstreams when frost formation on the heat exchanger surface is a possibility.

2.1.3.2 Air distribution

The high occupant density and restricted space of a typical PRV can make effective HVAC air distribution very challenging. Moreover, the entire compartment cooling demand is usually provided by the supply air, which introduce further challenges with regard to passenger cold draught sensation.

The majority of PRV HVAC systems distributes the supply air from ceiling mounted grills or a perforated ceiling, as depicted in *Figure 2.4 a)*. The large flow area of the ceiling grills results in relatively low supply air velocities, and promote effective distribution of the supply air. Buoyancy forces cause the low temperature supply air to descend down to the breathing zone, where it receives heat and contaminants from, e.g. passengers, equipment, etc., and floats back up to ceiling level where it gets extracted by local extracts. This distribution principle is commonly known as displacement ventilation.

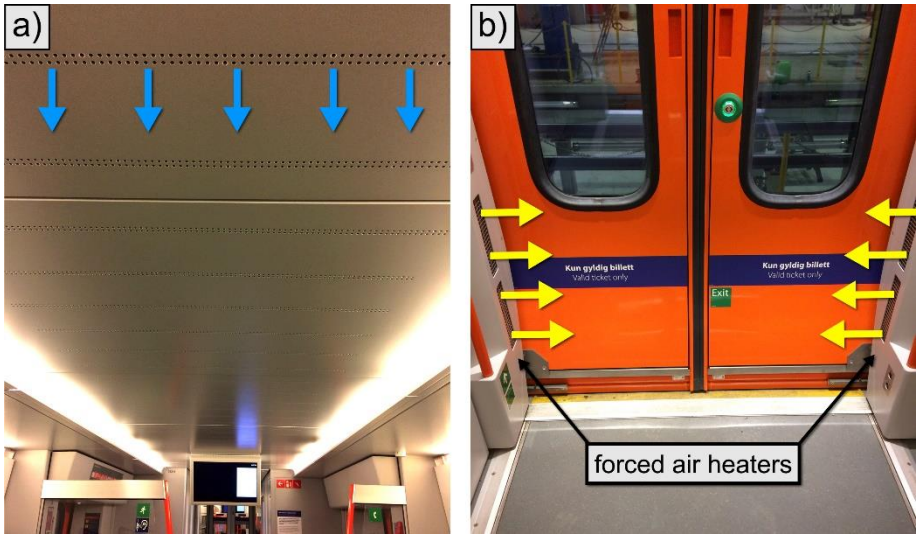

Figure 2.4: Air distribution of passenger railway coach a) Perforated ceiling for supply of ventilation air and b) forced air heaters, onboard a NSB Stadler FLIRT trainset.

In order to mitigate the entrainment of unprocessed outside air due to door openings, and envelope infiltration, the compartment is usually pressurized with 12 – 37 Pa positive pressure

[17]. For rail vehicles operating in cold climates supplementary equipment such as forced air heaters, as depicted in *Figure 2.4 b)*, can be implemented to help reduce rapid temperature changes caused by door openings.

2.1.4 Cooling

As previously mentioned, cooling for the passenger compartment is generally provided through the ventilation system supply air. During AC-mode operation the heat exchanger located in the AHU (*Figure 2.3)* functions as an evaporator, and the mixture of recirculated and fresh air (c) is cooled down to the desired supply air (d) temperature.

The supply air fans and fan motors are usually located in the supply airstream, thus constituting a sensible heat gain equal the total power of the fan motor [17]. Moreover, during AC-mode operation, moisture from the air (c) will often condense on the evaporator surface; consequently, proper drainage must be assured, and the latent heat corresponding to the amount of condensed moisture needs to be included in the load calculations.

The cooling demand per carriage is usually in the range of 20 to 40 kW, depending on climatic zone and maximum passenger capacity.

2.1.5 Heating

The passenger carriage usually include several heating devices, some located inside the passenger compartment, and some located in the AHU supply airstream. The control units for equipment making up the heating system, should be connected through a bus-system to facilitate efficient system control.

In general, the heating equipment located inside the passenger compartment consists of electrical heat convectors mounted along the sidewalls of the carriage, and in some cases electric floor heating. Additionally, forced air convectors can be installed to cover transient heating demands related to door openings, as previously mentioned (*Figure 2.4 b)).*

Electric heating coils integrated in the air-handling unit (AHU), usually covers heating of the supply air. As energy for heating of the ventilation fresh air generally constitutes one of the largest energy demands for a railway passenger vehicle operated in cold climate [16], the use of HRDs have become more common. Moreover, some system suppliers can offer reversible air to air HVAC units, able to deliver heat to the AHU down to an ambient temperature of -10°C [18]. The pilot R744 HVAC unit described in this paper (section 3.2.2), is designed to deliver heat to the AHU down to an ambient temperature of -20°C.

2.1.6 Maintainability

In general, railway HVAC equipment requires more frequent periodic maintenance than stationary equipment, due to the high reliability requirements and the harsh operating environment encountered during rail travel. Moreover, a passenger carriage without the ability to open windows can become unusable if the air conditioning equipment fails [17]. Consequently, the HVAC system should permit quick problem diagnosis and repair, facilitated by easy accessibility and digital, microprocessor-based controls.

2.1.7 Substituting HFCs in railway HVAC

As previously mentioned, the vast majority of air conditioning systems, for railway HVAC applications, utilize HFC refrigerants in a vapor compression cycle. In Europe the dominating refrigerants are R134a and R407C, making up 75% and 25%, respectively [18]. This amounts to a total HFC stock of 1180 metric tons (1605 kt CO_2 eq.) in railway vehicles, according to the 2006 EU-27 reported numbers [19]. Based on a survey establishing actual refrigerant refills at the biggest national railway operators in the EU, Schwarz et al. [19] estimated the yearly HFC emission rates from the railway sector to be 5% of the total HFC stock. Thus amounting to a total HFC emission of 63.6 metric ton (86.5 kt CO_2 eq.) from the EU railway sector.

As mentioned in section 1.2, the inevitable phase-out of HFCs, calls for new and environmentally benign air conditioning technology. The main requirements for these new replacement systems, from the system suppliers and railway operators point of view, will be safety, reliability, maintainability, size, weight, and cost. Additionally, the ultimate replacement technology should be easily adaptable for different climatic zones, as worldwide implementation would ensure mass production, reduced cost, and further incentivize R&D of energy efficient systems.

The safety requirements for railway vehicles prohibits the use of toxic or flammable refrigerants. System reliability is obviously of great importance, as a system failure can put the whole trainset out of commission for an extended period, consequently resulting in a substantial loss for the railway operator.

HVAC system efficiency have traditionally been given a relatively low priority, as HFC vapor compression systems generally achieve a decent COP without much effort; however, some of the proposed replacement technologies are burdened with low efficiencies. Moreover, UIC have committed to reduce average energy consumption by 50% by 2030 and 75% by 2050, relative to a 1990 baseline [20], thus making HVAC energy efficiency essential for future systems.

Currently, R744 (CO_2) seems to be one of the only viable replacements for railway vapor compression systems, owing to its complete safety, as opposed to the new HFOs with flammable characteristics and highly toxic combustion products [21]. Moreover, R744 offers low filling costs, superior thermodynamic properties, and generally achieve similar or better COP than the HFC system when operated in climatic zone III (EN 13129), as this paper will be covering in detail.

An alternative to vapor compression AC, is the air cycle [22]. Air cycle machines was widespread used in early refrigeration applications [23], and is currently gaining attention in the railway HVAC sector, due to the fact that it is completely safe and environmentally benign in terms of a refrigerant leakage, as the compression medium is air (R729). Moreover, air cycle systems offers high reliability, and relatively low cost. However, the achieved COP_R of air cycle systems are far lower than traditional vapor compression systems, as the COP_R of an air cycle always will be less than one.

Thermoelectric AC have also been suggested for use in railway HVAC [24], it was tested for a half year period, onboard a passenger railway coach operated in France, during a 1982 study conducted by Stockholm et al. [25]. The authors reported reliable operation for the test campaign, and pointed to the thermoelectric systems advantages with regard to quick response time, high reliability, and compactness. Ivanov et al. [26] concluded that thermoelectric AC was commercially viable for cooling of the locomotive drivers cabin, after successful trails conducted in Russia. However, thermoelectric AC have not yet been commercialized for railway HVAC applications, probably due to the high cost and low efficiency compared to traditional vapor compression systems [27].

2.1.8 Current test campaigns

At InnoTrans 2016 in Berlin, the manufacturer *Vossloh Kiep Austria* presented the HKL 751-CO_2, *Figure 2.5*. A reversible transcritical R744 HVAC unit, for heating and cooling of PRVs. The compact roof mounted unit, weighs 560 kg, holds a total refrigerant charge of 6.6 kg, and have a heating and cooling capacity of 20 kW and 24 kW respectively. Moreover, the unit have a frequency-controlled compressor and electronic expansion valves, for efficient capacity and high-pressure control, operating up to a maximum high-side pressure of 120 bar.

Figure 2.5: HKL/HVAC 751-CO_2 by Vossloh Kiepe Austria. Right: roof mounted reversible R744 HVAC-unit, left: DB ECO train (DB).

The system was to be commissioned in a new prototype Deutsche Bahn AG trainset September 2016 [28]; however, specifics are not available in the open literature.

An air cycle AC system is currently being tested in German high-speed intercity ICE-3 trains, provided by Deutsche Bahn. The aim of the project is to document the performance of the system, on a PRV in normal operation, over its entire life cycle, according to the manufacturer *Liebherr-Transportation Systems* [29]; however, specifics are not available in the open literature.

Figure 2.6: Air cycle AC onboard DB intercity ICE-3 trains. Right: DB ICE-3 [Deutche Bahn], left: air cycle AC unit from Liebherr for the ICE 3.1 Re-Design program (Liebherr).

2.2 Reversible heat pumps and comprising components

In its simplest form, a reversible heat pump usually comprises a compressor, two heat exchangers, two expansion devices, and a reversing valve, as depicted in *Figure 2.7*. The role of the two heat exchangers is switched depending on operating mode, heating (HP) or cooling (AC). This is achieved by reconfiguring the refrigerant flow through the system, facilitated by a reversing valve. *Figure 2.7* depicts a principle sketch of a simple reversible heat pump, where the red and blue arrows describes refrigerant flow in HP- and AC-mode respectively.

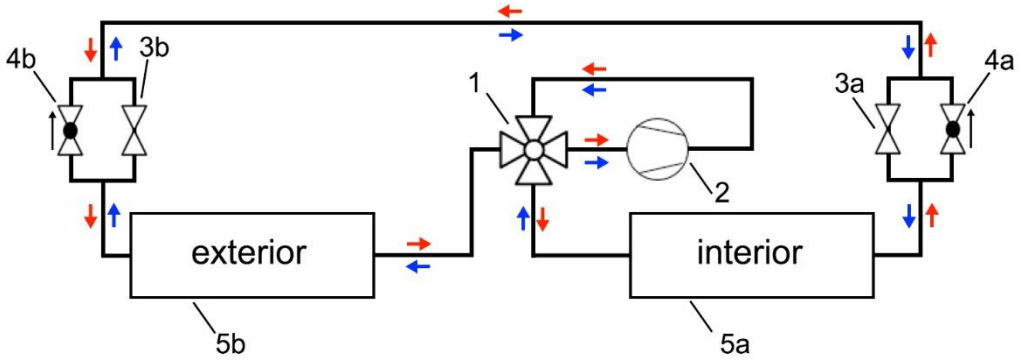

Figure 2.7: Simplified principle sketch of a reversible heat pump unit, with reversing valve (1) and compressor (2) two expansion valves (3a,b), two back pressure valves (4a,b), and two heat exchangers (5a,b).

2.2.1 Performance and energy saving

There are many ways to define the performance of the individual components of a heat pump, as will be described in the sub-sections below, but the momentary performance of the heat pump is usually stated as the coefficient of performance (COP). For HP-mode operation the COP_{HP} is defined as the ratio of heat delivered at the condenser ($\dot{Q}_{cond}$) and the work supplied to the compressor ($\dot{W}$), and for AC-mode operation the COP_R is defined as the ratio between absorbed heat at the evaporator ($\dot{Q}_{evap}$) and supplied work to the compressor. Eq.(3) presupposes that heat loss from the compressor is zero.

$$COP_{HP} = \frac{\dot{Q}_{cond}}{\dot{W}} \qquad \text{Eq.(1)}$$

$$COP_R = \frac{\dot{Q}_{evap}}{\dot{W}} \qquad \text{Eq.(2)}$$

$$COP_{HP} = COP_R + 1 \qquad \text{Eq.(3)}$$

As the COP is a measure of the momentary cycle performance, it says little about how the heat pump performs over time. Consequently, the COP is of little interest when assessing the "actual" performance and energy savings of the system over time.

The seasonal performance factor (SPF), sometimes referred to as the seasonal coefficient of performance (SCOP), is the ratio between supplied heat and received energy over a year or season (heating/cooling). The SPF also include the energy needed for additional drivers in the heat pump system, e.g. pumps, fans etc., and can be calculated according to Eq.(4) and Eq.(5).

$$SPF_{HP,Net} = \frac{Q_{HP}}{E_{HP}} \qquad \text{Eq.(4)}$$

$$SPF_{HP,Gross} = \frac{Q_{HP}+Q_{PL}}{E_{HP}+E_{PL}} \qquad \text{Eq.(5)}$$

Where $SPF_{HP,Net}$ represents the performance of the heat pump, and $SPF_{HP,Gross}$ represent the performance of the total heating system, including the peak load.

The SPF and COP are ratios, and do not reveal the "actual" energy savings as this is relative [7]. When evaluating the energy savings of a heat pump up against an alternative heating system, the percentage energy savings (ΔE) should be assessed.

$$\Delta E = \left(\frac{1}{\eta_{alt}} - \frac{1}{SPF}\right) \cdot 100\% \qquad \text{Eq.(6)}$$

Where η_{alt} is the average efficiency of the alternative heating system.

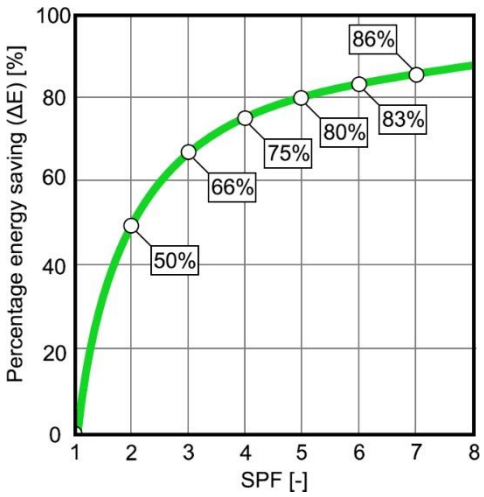

Figure 2.8: Graph showing percentage energy savings presupposing an efficiency of the alternative heating system (η_{alt}) of 1 (based on [7]).

The non-linear relation between the ΔE and SPF, depicted in *Figure 2.8*, means that the energy savings obtained by an increase in SPF, for "low-SPF" systems, is far greater than a similar increase in SPF, for a "high-SPF" system. E.g. when increasing the SPF from 2 to 3 or from 6 to 7, the corresponding increase in ΔE is 16 and 3 %-points, respectively. Consequently, this is something that needs to be considered when evaluating the cost of implementing efficiency

measures to an existing system, or comparing investment cost vs. performance between two systems.

2.2.2 Compressors

The compressor sucks saturated vapor from the evaporator, thus keeping a sufficiently low evaporator pressure and temperature, enabling heat flow from the heat source to the refrigerant inside the evaporator. The refrigerant line, between the evaporator and the compressor, is at compressor suction pressure, and commonly referred to as the suction line. Further, the refrigerant vapor downstream of the compressor is discharged at an elevated temperature and pressure. The refrigerant line downstream of the compressor, i.e. between the compressor and condenser/ gas-cooler, is at compressor discharge pressure, and commonly referred to as the discharge line. *Figure 2.9* depicts a transcritical R744 VCC in a log ph-diagram, where point 1 to 2 represents the compression process.

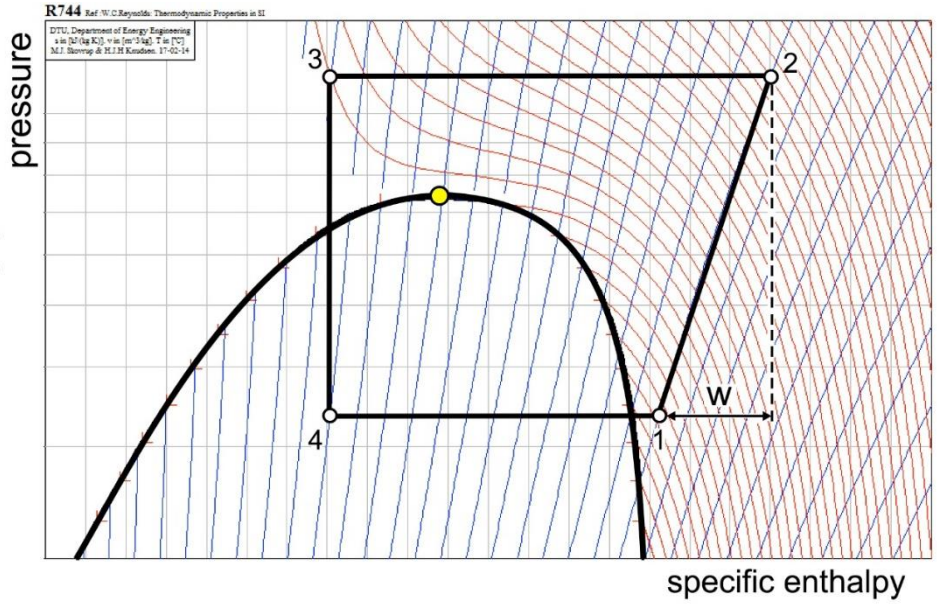

Figure 2.9: Log(p)-h diagram of transcritical R744 VCC, where the blue and red lines represents isenthalps and isotherms respectively (based on [30]).

The compressor is crucial with regard to system COP, achieved capacity, service life, and initial investment cost [31]. There is a wide range of compressors with different application area on the market. The following criteria should be considered when selecting a compressor: capacity and capacity regulation, volumetric flow rate (V_s), compression ratio (π), thermophysical properties of the refrigerant, in addition to temperature and pressure levels encountered during operation and standstill [32]. Practical factors like amount of system start-stops, maintenance intervals, vibration and noise, should also be considered.

There are mainly two types of compression devices, positive displacement and dynamic. For positive displacement compressors, a discrete volume of refrigerant vapor is compressed by physically reducing the volume, thus increasing the pressure [33]. The workings of dynamic compression devices, such as ejectors, utilize a momentum exchange driven entrainment effect, explained in section 2.2.5.2. The most common displacement compressors for VCCs are scroll, reciprocation and rolling piston, and screw. Only scroll and reciprocating piston compressors will be described in this thesis.

2.2.2.1 Compressor classification

As previously mentioned there are two types of compressors, positive displacement and dynamic. Additionally, compressors are classified with regard to how they are constructed (hermetic, semi-hermetic, open).

For hermetic compressors (*Figure 2.10 a)),* the motor and compressor parts of the unit are fixed in a factory welded shell, housing the refrigerant and the lubrication oil [32]. The simple construction usually results in low-cost, compact, and lightweight compressors, but preclude the possibility of servicing the internal components. Consequently, the whole unit has to be replaced at certain intervals or a during failure. Thus, the use of hermetic compressors are limited to small capacity systems (tens of kW [33]).

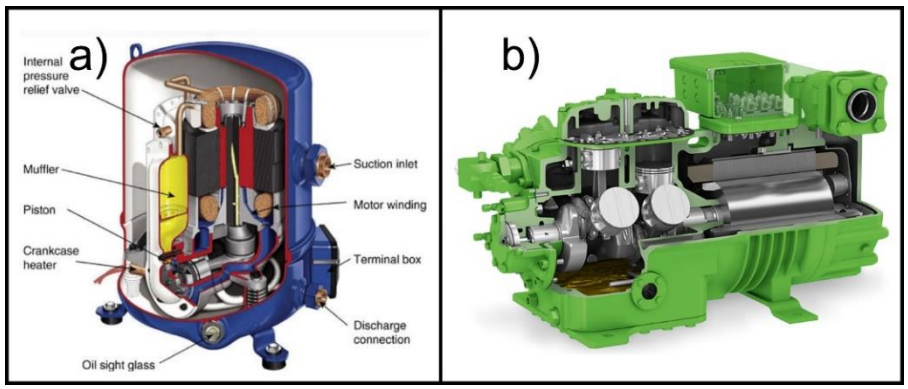

Figure 2.10: Cutaway view of compressors, a) hermetic reciprocating piston (Danfoss [33]), and b) semi-hermetic reciprocating piston (Bitzer).

For semi-hermetic compressors (*Figure 2.10 b),* the motor and the compressor parts are in direct contact, but the casing can be dissembled, thus making it serviceable. The cost of these compressors are generally substantially higher than hermetic, and are usually applied in small to medium capacity systems, with a maximum motor capacity of 300 kW [32].

Open compressors consists of two individual units, a compressor and a motor. Power is transferred from the motor to the compressor through a drivetrain (shaft or belt). The externally

coupled crankshaft extends through the compressor housing, and proper seals are required to avoid leakage of oil and refrigerant [34]. Open compressors are high-cost, very serviceable, and applied in large capacity systems.

2.2.2.2 Reciprocating/ piston compressors

Reciprocating compressors, further denoted as piston compressors, is adaptable for a large capacity range, spanning from small single cylinder units with capacity of a few hundred watts, to large 16 cylinder 1000 kW machines [34].

The piston compressor looks similar to a normal combustion engine, where one or more pistons are connected to each other by a rotating crankshaft, but instead of using chemical energy to produce mechanical energy, mechanical energy is spent to produce pressure energy.

The two-stroke principle of a piston compressor is depicted in *Figure 2.11*. On the suction-stroke refrigerant vapor flows into the cylinder chamber (b), from the suction line (a) through the open suction valve. Subsequently, the refrigerant is compressed on the compression-stroke, until the pressure inside the cylinder (b), exceeds discharge line pressure in point (c) plus the tension of the discharge valve spring, consequently assuring that the maximum cylinder pressure automatically adjusts to the condensation/gas-cooler pressure. This feature is a major advantage for piston compressors, and minimize losses related to shifting pressure ratio (π) in the system during operation [34].

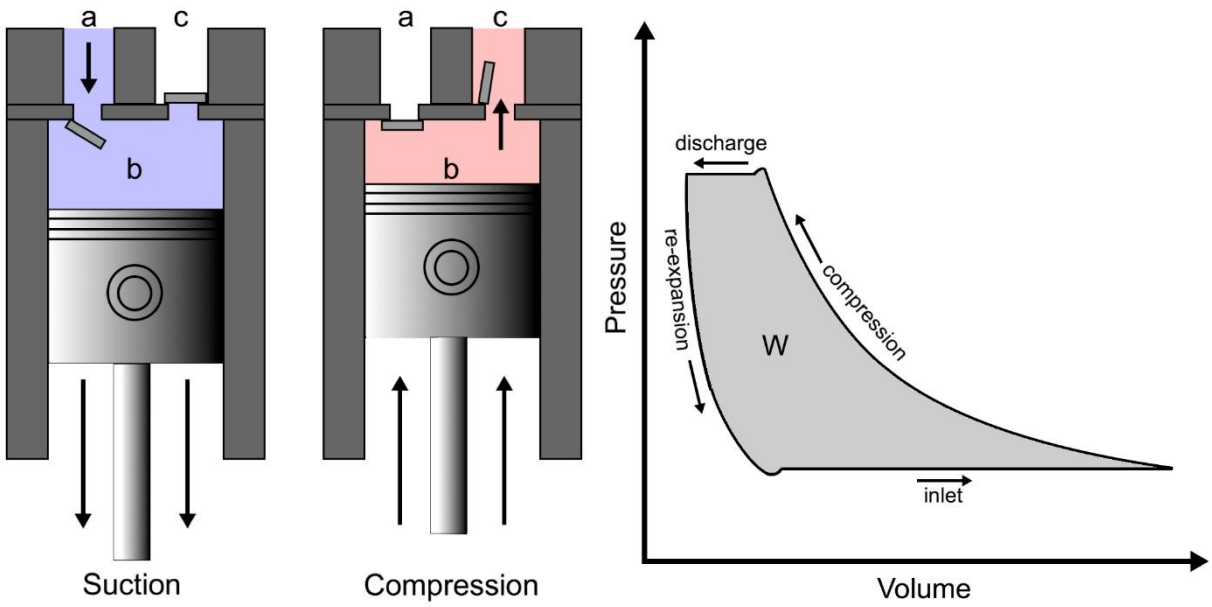

Figure 2.11: Two-stroke principle and pV-diagram of piston compressor Left: Suction- and compression stroke. Right: pV-diagram of the compression process, where W is the compression work (based on [33]).

2.2.2.3 Scroll compressors

The scroll compressor utilize two orbiting horizontal scrolls to compress the refrigerant vapor from the suction line. The upper scroll assembly is in a fixed stationary position, and the discharge port is located on the top. The bottom scroll is orbiting the crankshaft and the top scroll in an eccentric motion, enabled by the design of the motor shaft assembly. This motion traps vapor between the phase shifted scroll walls, pushing it in crescent shaped gas pockets towards the center of the upper scroll, where it flows through the discharge port, as depicted in see *Figure 2.12*.

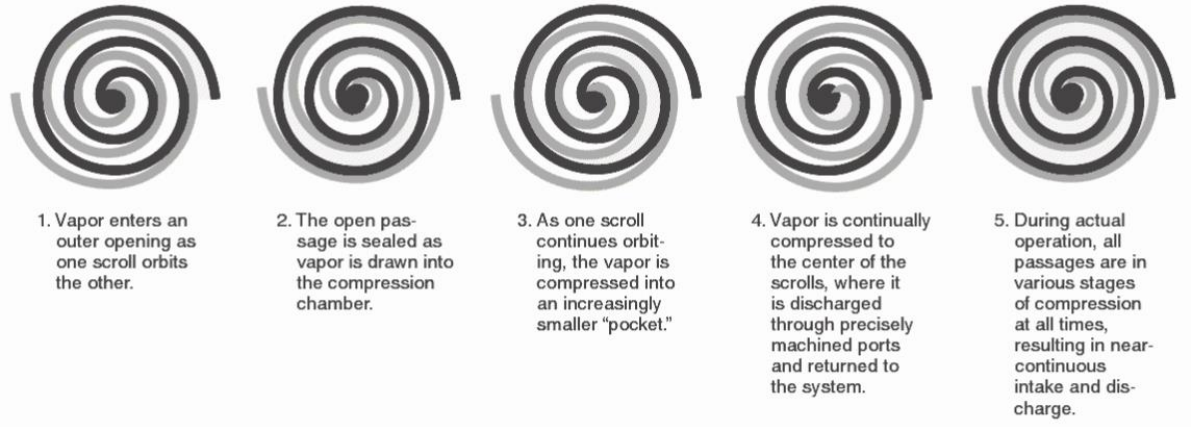

Figure 2.12: Compression process in scroll compressors. The movement of the scrolls, and how refrigerant vapor enters, compresses and discharges through the scroll compression process [35].

The volumetric ratio (λ) and thus the pressure ratio (π) of the scroll compressor is fixed, thus resulting in energy losses related to over and under compression. The scroll compressor is usually hermetically constructed, and include fewer parts than the piston compressor. They also generally achieve higher efficiency, better part-load performance and operation characteristics than the piston compressor. [32, 34]

2.2.2.4 Capacity control

Reversible heat pump systems are designed to cover a maximum heating or cooling load. However, most of the operating hours occurs outside design conditions, thus requiring less duty from the system. Moreover, the design load for heating and cooling can deviate; hence, the system will always operate at reduced capacity in one mode of operation (HP/AC). Consequently, reliable and efficient capacity control is crucial, and can be achieved in a number of ways, some of which disclosed below.

The simplest form of capacity control is On/off control, where the system capacity output is either 100% or 0%. This control method is mostly suitable for small systems with intermittent loads. However, relatively large heat pump systems can consist of a number of on/off controlled

units, thus improving the system capacity range. Moreover, on/off control can be applied in combination with water storage tanks to improve control and reduce number of system start/stops.

Capacity reduction by cylinder unloading is exclusive for piston compressors. The rotational speed of the crankshaft is constant, and compressor capacity is reduced in steps by keeping the suction valve open (or alternatively closed) on the discharge stroke, for a number of cylinders. This unloading method is called valve-lifting, and reduction increments vary with number of available cylinders. The method is normally used in medium to large sized systems. Cylinder unloading can also be utilized during system start-up, as this reduces the start torque and corresponding start current to the motor. Moreover, unloaded start will support proper oil pressure build-up before full load [33]. With this control method mechanical energy losses due to friction in the unloaded cylinders will occur.

Variable frequency drive (VFD) is a very efficient means of capacity control, suitable for applications in virtually all capacity ranges. An inverter regulates the voltage and frequency of power supplied to an electric AC* induction motor, thus reducing rotational speed and refrigerant mass flow rate ($\dot{m}_R$). Due to compressor lubrication, the capacity can normally not be reduced lower than 20-50%. Traditionally VFD has been a relatively high-cost control method, but technological advancements have reduced cost and size, and additionally improved the reliability of VFD. [33, 34]

2.2.2.5 Losses

Positive displacement compressors, like piston and scroll, have a fixed maximum theoretical volumetric capacity (V_S) defined by the compressor geometry and rotational speed. However, because of volumetric losses the actual volumetric capacity (V_i) is lower than V_s.

Volumetric losses accounts for all losses affecting the flow rate of the compressor [33]. They occur due to a number of factors, such as re-expansion of residual gas in the compressor chamber (mainly piston compressors because of non-displaced volume), and reduced specific suction-gas volume due to heat transfer from the high-pressure side and the cylinder walls. In addition, gas leakage occurs between the piston and cylinder walls, or between scroll walls. [34]

$$\lambda = \frac{V_i}{V_s} \qquad \text{Eq.(7)}$$

Volumetric efficiency (λ) is the ratio between V_i and V_s, see Eq.(7). As depicted in *Figure 2.13*, the scroll compressor outperforms piston compressors on volumetric efficiency especially during high pressure ratios (π).

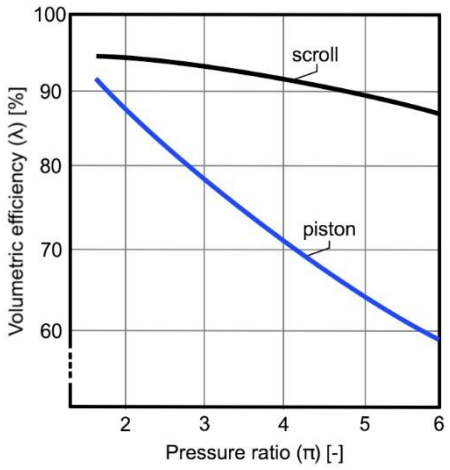

Figure 2.13: Volumetric efficiency for scroll and piston compressorsat changing pressure ratio (based on [34]).

Other losses related to the compressors include mechanical losses. The mechanical losses are caused by friction between compressor parts, friction between gas molecules and compressor parts, and inter molecular friction in the gas. The relationship between isentropic compression power (P_{is}), and the active electrical input power to the compressor motor motor (P_s) (for hermetic and semi-hermetic) is called the compressor isentropic efficiency (η_{is}).

$$\eta_{is} = \frac{P_{is}}{P_{cs}} \qquad \text{Eq.(8)}$$

For hermetic and semi-hermetic compressors, the motor efficiency is included in η_{is}. The isentropic efficiency is generally higher for large compressors [34]. The η_{is} is usually higher for scroll compressors than for piston compressors, as seen in *Figure 2.14*.

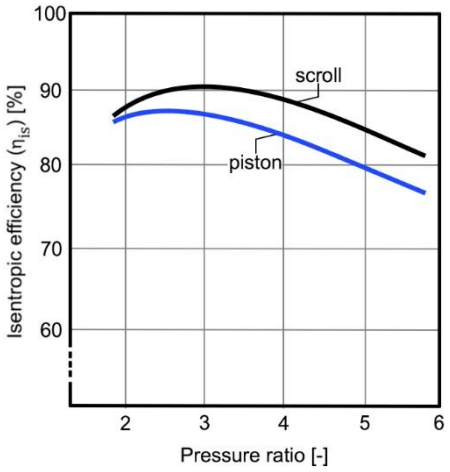

Figure 2.14: Isentropic efficiency for scroll and piston compressorsat changing pressure ratio (based on [34])

2.2.2.6 Lubrication

As a compressor consists of many moving parts, it requires proper lubrication. Moreover, the lubrication oil also helps to seal internal leakages within the compressor [36]. The lubrication oil needs to be chemically stable at all conditions occurring during operation, and have to be compatible with the refrigerant.

During operation, oil is carried along by the refrigerant as it flows through the system. Although lubrication oil serves a crucial purpose within the heat pump system, it also hampers performance by decreasing effective flow area and heat exchanger efficiency [36]. For safe and reliable operation, proper oil filtration and return to the compressor have to be ensured.

During system stand-still, the lubrication oil will contain a certain amount of dissolved refrigerant. The amount will depend on stand-still pressure and temperature, as well as lubrication oil and the refrigerant properties. At system start-up, liquid refrigerant diluted in the crankcase oil reservoir will start to evaporate as the suction pressure is reduced. The gas will boil off and cause oil-foaming in the crankcase. Heating devices are commonly fitted to the crankcase to reduce this phenomenon.[33]

2.2.2.7 Transcritical CO_2 compressors

There have been significant advancements in CO_2 compressor technology since the reintroduction in the early nineties. Due to the high maximum high-side pressures (100-160 bar), and the large pressure difference between high-side and low-side, challenges with regard to internal leakages have had to be overcome. Consequently, only piston compressor design was applied in early applications. Now, more or less all types of compressors have been developed and commercialized, from low to high capacity applications, as reported by Nekså et al. [37].

The thermophysical properties of CO_2 also enable the possibility for very efficient compression, as CO_2 have significantly higher VRC than traditional refrigerants, thus reducing the required volumetric compressor capacity by 80-90% when compared to R134a [37]. However, the relationship between a compressor's mass and its displacement is not an obvious one, and will depend on different deign tradeoffs like bore diameter, stroke, number and materials etc., as reported by Pettersen et al. [38]. Moreover, the pressure ratio (π), re-expansion losses, and negative effect of valve pressure drops tend to be lower for the CO_2 compression process, due to the high pressure level and shape in the pV-diagram, thus resulting in higher efficiency [38].

2.2.3 Heat exchangers

A heat pump unit generally consist of several components for heat exchange, depending on unit type and use. As explained earlier, the most basic HP units comprise two heat exchangers, an evaporator for heat absorption from the heat source, and a condenser for heat rejection to the heat sink. In addition, a variety of different heat exchangers can be implemented to optimize the system and ensure efficient operation. Because of the wide variety of different heat exchangers, this thesis is limited to evaporators, condensers, gas-coolers, and internal heat exchangers for suction gas heating.

The most common heat exchanger designs applied in air-to-air heat pumps are fin-and-tube and microchannel, depicted on left and right in *Figure 2.15*, respectively. The heat exchanger surface have to be maximized on the air-side, as air has a relatively low thermal conductivity, specific heat capacity, and density [34]; which combined with limited air velocities results in low values for heat transfer coefficients. Typically, the heat transfer coefficient on the air-side is only 5-20% of that on the refrigerant-side [39]. The air is usually fed to the heat exchanger by air blowing fans. As depicted in *Figure 2.15*, the air flows cross-directional relative to the tubes/channels holding the refrigerant. The fins should be vertical, to facilitate drainage of condensed moisture, and the tubes are constructed (and dimensioned) to promote turbulence on the refrigerant side, thus improving heat transfer [33].

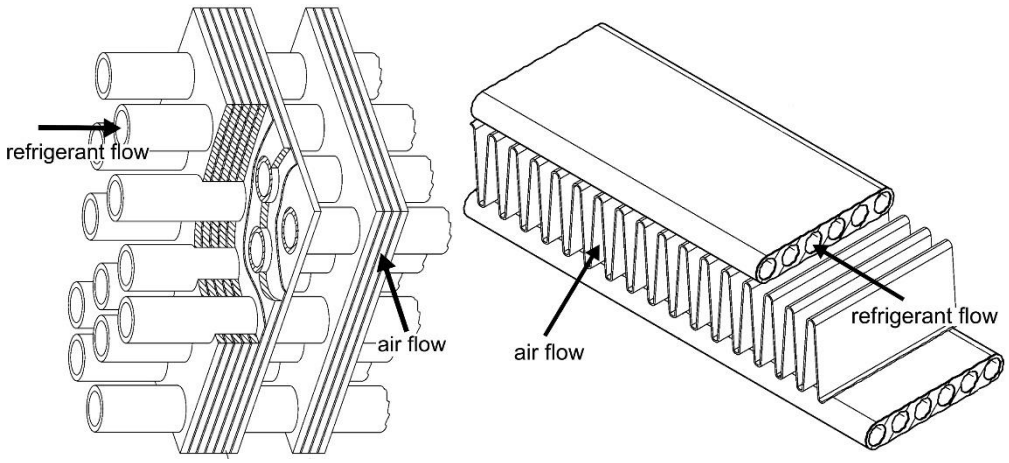

Figure 2.15: Air-to-air heat pumps heat exchanger design and flow Left: fin-and-tube heat exchanger [40]. Right: microchannel heat exchanger [41].

Microchannel heat exchanger design offers several advantages with regard to thermal performance, corrosion protection (single metal), reduced refrigerant charge, durability, and weight, when compared to the fin-and-tube design. However, the manufacturing process of microchannel heat exchangers requires defined casting blocks, resulting highly standardized sizes for high-volume production [33].

2.2.3.1 Evaporators

The evaporator is located on the low-pressure side of the heat pump system, and transfers low-grade heat from the heat source to the refrigerant by evaporation of refrigerant, thus keeping a constant refrigerant temperature, as depicted on the left in *Figure 2.16*. However, in reality the pressure drop through the evaporator will result in a temperature drop (Δt_L), corresponding to the $\Delta t/\Delta p$ characteristic of the refrigerant, as depicted on the right in *Figure 2.16*. Moreover, the right side of *Figure 2.6* include superheating of refrigerant vapor (Δt_{sh}) near the refrigerant outlet, as for direct expansion (DX) evaporators.

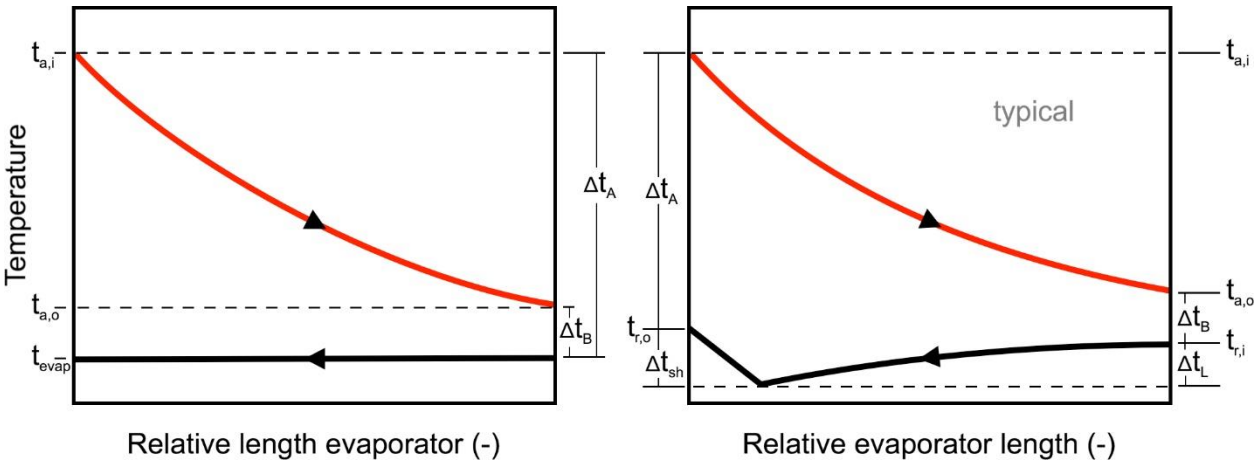

Figure 2.16: Temperature profile of counterflow evaporator.Left: ideal case excluding pressure drop and superheat (Δt_{sh}). Right: actual case including pressure drop and superheat (Δt_{sh}). The temperature profile through the relative length of an evaporator for heat source (red) and refrigerant (black) (based on [42]).

Given the equations for evaporator heat exchange, listed below, it's apparent that the cooling capacity of the evaporator ($\dot{Q}_{evap}$) is highly dependent on the evaporator temperature, as an increased cooling demand will require a higher logarithmic mean temperature difference (LMTD), and consequently a reduced evaporator temperature (t_{evap}). Similarly, an evaporator with good heat transferring characteristics (high U-value) will require a lower LMTD, or heat transfer surface, for a given capacity demand.

$$\dot{Q}_{evap} = (U \cdot A \cdot LMTD)_{evap} \qquad \text{Eq.(9)}$$

$$\dot{Q}_{evap} = \dot{m}_s \cdot C_{p,s} \cdot (t_{a,i} - t_{a,o}) \qquad \text{Eq.(10)}$$

$$\dot{Q}_{evap} = \dot{m}_r \cdot (h_{r,o} - h_{r,i}) \qquad \text{Eq.(11)}$$

$$LMTD = \frac{\Delta t_A - \Delta t_B}{\ln[\frac{\Delta t_A}{\Delta t_B}]} \qquad \text{Eq.(12)}$$

Where:

- $\dot{Q}_{evap}$: heat transferred from the heat source to the refrigerant inside the evaporator [kW]

- U: U-value of the heat transferring evaporator surfaces [W/m^2K]
- A: heat transfer surface of the heat exchanger [m^2]
- LMTD: logarithmic mean temperature difference [K]
- $t_{a,i}$, $t_{a,o}$, Δt_A and Δt_B (*Figure 2.16)*
- $\dot{m}_r$: mass flow rate of refrigerant [kg/s]
- $\dot{m}_s$: mass flow of the source medium [kg/s]
- $C_{p,s}$: specific heat capacity of the source medium [kJ/kg·K]
- $h_{r,o}$: specific enthalpy of the refrigerant at the evaporator outlet [kJ/kg]
- $h_{r,i}$: specific enthalpy of the refrigerant at the evaporator outlet [kJ/kg]

The evaporator design is determined by a range of factors, e.g. type of heat source, refrigerant, operating conditions, capacity demand, and requirements concerning size, weight and cost of the complete unit. There are three main groups of evaporators, direct expansion (DX), flooded, and recirculated. The evaporator types described further in this paper is the DX and recirculated evaporators, with air as heat-source.

DX evaporator, also known as dry-type, utilizes parts of the heat transferring surface for superheating of refrigerant vapor (Δt_{sh}). This ensures that all of the refrigerant is boiled off into a vapor before it enters the compressor, as incompressible liquid droplets impose wear on the compressor, and hampers volumetric efficiency (λ). Normally 10-20% of the evaporator area is utilized for superheating, and as the heat transfer coefficient declines with increasing vapor quality (kg vapor/kg liquid), the average U-value of the DX evaporator will typically be lower than that of the recirculated [34].

DX evaporators are commonly applied in small to medium size air-source HVAC units, and are associated with compact design, low cost and refrigerant load, as well as simple oil return [34]. To reduce mal-distribution of refrigerant, it is common practice to mount a refrigerant distributer at the inlet of DX evaporators. The distributer consists of a number of individual feeds to various sections of the coil [33].

In recirculated evaporators, the refrigerant leaving the evaporator is a two-phase mixture of vapor and gas. The mixture flows into a liquid separator, where the compressor sucks of the vapor, and the liquid is recirculated back to the evaporator, as depicted in *Figure 2.17*. A float valve can be used to control the amount of refrigerant supplied to the evaporator.

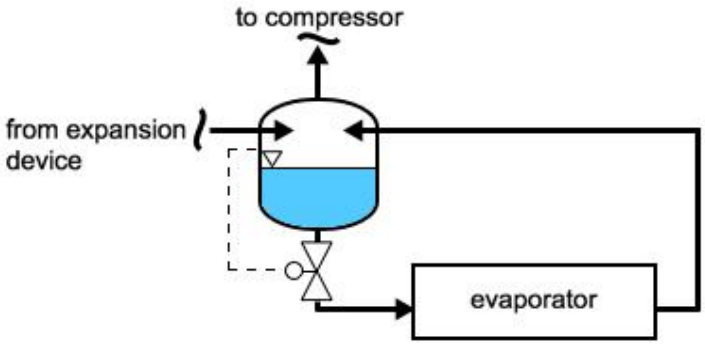

Figure 2.17: Component arrangement of recirculated evaporator (based on [34]).

Since a larger portion of the evaporator is filled with liquid refrigerant, the average U-value of a recirculating evaporator will be higher than that of a DX, thus reducing the necessary heat transfer surface (A_{evap}), or required LMTD, for a given capacity demand. However, the increased refrigerant load and additional components usually results in a higher initial system cost. Moreover, flooded evaporator also impose more challenges with regard to oil return to the compressor.

2.2.3.2 Condensers

The condenser is located on the high-pressure side of the heat pump system, and its function is to transfers heat from the refrigerant to the heat sink. The primary portion of this heat is latent heat, due to condensation of refrigerant vapor, thus keeping a constant refrigerant temperature, as depicted on the left in *Figure 2.18*. However, as the discharge gas temperature is higher than the saturation temperature, some sensible heat rejection will occur at the inlet section of the condenser, as depicted on the right in *Figure 2.18*. Moreover, the right side of *Figure 2.18* also include pressure drop through the condenser, resulting in Δt_L. The condensation temperature is highly dependent on the evaporator temperature.

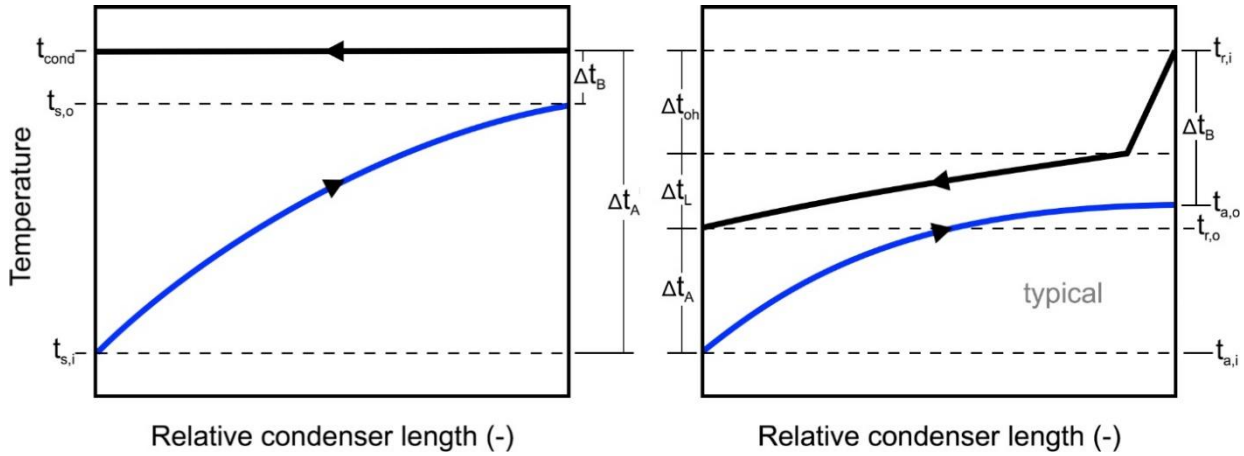

Figure 2.18: Temperature profile of counterflow condenser.Left: ideal case excluding pressure drop and overheat (Δt_{oh}). Right: actual case including pressure drop and overheat (Δt_{oh}). The temperature profile through the relative length of a condenser for heat sink (blue) and refrigerant (black) (based on [42])

The rate of heat transfer at the condenser can be described by the following equations:

$$\dot{Q}_{cond} = (U \cdot A \cdot LMTD)_{cond} \quad \text{Eq.(13)}$$

$$\dot{Q}_{cond} = \dot{m}_s \cdot C_{p,s} \cdot (t_{s,o} - t_{s,i}) \quad \text{Eq.(14)}$$

$$\dot{Q}_{cond} = \dot{m}_r \cdot (h_{r,A} - h_{r,B}) \quad \text{Eq.(15)}$$

$$LMTD = \frac{\Delta t_A - \Delta t_B}{\ln[\frac{\Delta t_A}{\Delta t_B}]} \quad \text{Eq.(16)}$$

Where:

- $\dot{Q}_{cond}$: is the heat output of the condenser [kW]
- U: U-value of the heat transferring surfaces of the condenser [W/m^{2}K]
- A: heat transfer surface of the condenser [m^2]
- LMTD: logarithmic mean temperature difference [K]
- $t_{s,i}$, $t_{s,o}$, Δt_A and Δt_B (*Figure 2.18)*
- $\dot{m}_s$: mass flow of the sink medium [kg/s]
- $C_{p,s}$: specific heat capacity of the sink medium [kJ/kg·K]
- $h_{r,B}$: specific enthalpy of the refrigerant at the condenser outlet [kJ/kg]
- $h_{r,A}$: specific enthalpy of the refrigerant at the condenser outlet [kJ/kg]

2.2.3.3 Gas coolers

When heat is rejected in supercritical area, as for transcritical R744 heat pumps, the process occurs in a gas-cooler (GC). The transfer of heat in a GC is very different from the condensation process in a subcritical HP, as can be seen by comparing *Figure 2.18* and *2.19*. In supercritical area, heat is transported from the refrigerant to the heat sink medium as sensible heat, thus resulting in a gliding refrigerant temperature, at a constant GC pressure (p_{gc}) [37], as depicted in *Figure 2.19* point (2) to (3).

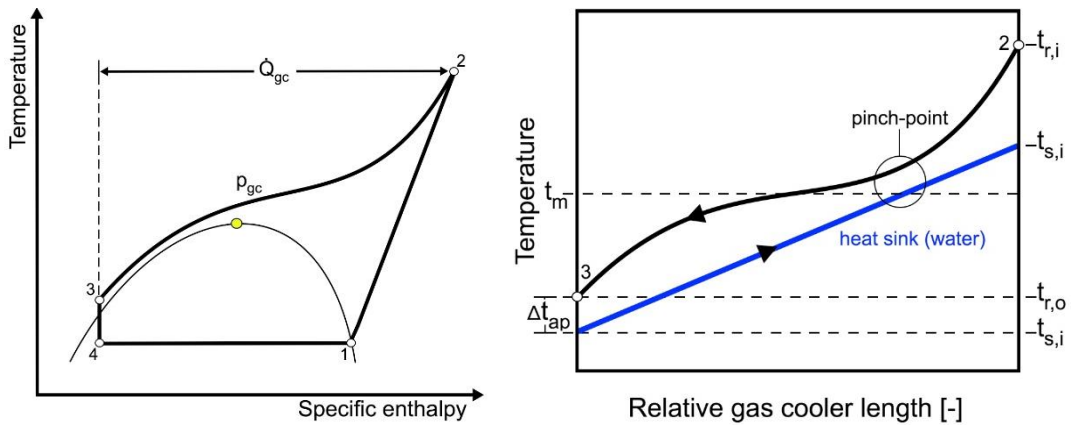

Figure 2.19: VCC and temperature profile of a gas cooler.Left: th-diagram of transcritical VCC. Right side: Temperature profile of gas-cooler (GC). Where: $t_{s,i}$ and $t_{s,o}$ is inlet and outlet temperature of the heat sink medium, and $t_{r,i}$ and $t_{r,o}$ is inlet and outlet temperature of the refrigerant and Δt_{ap} is the temperature approach at the GC-outlet (based on [7])

The temperature profile inside the GC is determined by the GC pressure (p_{gc}), inlet and outlet temperature of the heat sink medium ($t_{s,i}$, $t_{s,o}$) and the refrigerant ($t_{r,i}$, $t_{r,o}$), in addition to the heat capacity flow rates (CP) Eq.(17). The gliding temperature, of both refrigerant and heat sink medium, allows for a closer match between the two temperature profiles, thus improving heat exchanger effectiveness [43].

$$CP = C_p \cdot \dot{m} \qquad \text{Eq.(17)}$$

The point within the GC with the lowest temperature difference between the refrigerant and the heat sink medium is called the pinch-point. It is preferable to have the pinch-point at the GC outlet, as a pinch-point occurring within the relative length of the GC hampers heat transfer [7].

The shape of the isobar (point 2 to 3 in *Figure 2.19*) is determined by the specific heat capacity (C_p), which gets increasingly high near the critical point (t_c = 31.1°C, p_c = 73,8 bar, C_p > 10000 for CO_2 [30]), thus leading to a small change in temperature for a given heat output. For high pressure isobars ($p_{gc} \geq$ 150bar), the temperature glide is further away from the critical point, thus yielding a relatively constant C_p, and consequently a more linear characteristic on the isobar, as opposed to the "S-shape" for "low-pressure" isobars ($p_{gc} \leq$ 80 bar). A more in depth explanation have been presented by Stene [7], and Pettersen et al. [38].

The COP and capacity of the transicritical cycle, is usually limited to how low refrigerant temperature it is possible to achieve at the GC outlet ($t_{r,o}$) [44]. A small change in $t_{r,o}$, can produce a large change in enthalpy at the GC outlet, because of the high C_p near the critical point [38], as previously mentioned. Consequently, counterflow GC design is essential.

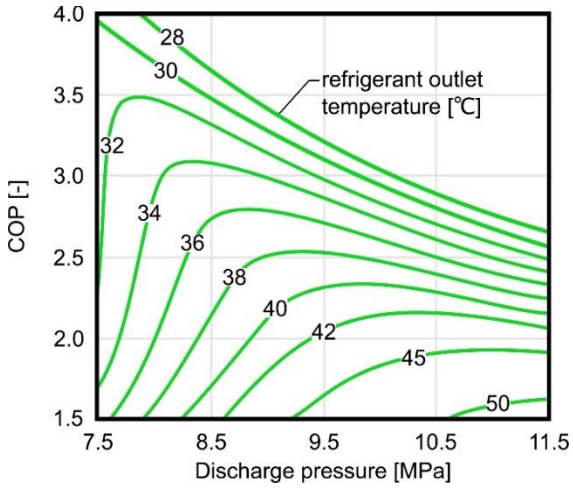

Figure 2.20: Effect of refrigerant exit temperature on COP for realistic high-side pressures.The evaporation temperature used in example is set to 3.9°C and effectiveness of the SLHX is set to 0.8. Pressure drop is neglected, and the compressor efficiency is fitted from a previous experiment by Boewe et al. [45] (based on [46]).

Figure 2.20 shows the predicted relationship between COP and discharge pressure for different R744 outlet temperatures, as reported by Bullard et al. [46]. As *Figure 2.20* shows, the discharge pressure needs to be increased in order to maximize cycle COP at elevated refrigerant outlet temperatures. Moreover, the COP curve tends to be flatter at higher refrigerant outlet temperatures.

Consequently, COP for the transcritical R744 cycle is largely dependent on the temperature of the heat sink, average temperature of the refrigerant during heat rejection (t_m), and the temperature difference between the refrigerant and the heat source medium at the GC outlet, called temperature approach (Δt_{ap}), see right side *Figure 2.19.*

Supercritical heat rejection introduce the need to control high-side pressure in order to achieve optimal efficiency. Ultimately, the optimal GC pressure (p_{gc}) for a transcritical R744 VCC is that which yields the highest COP. *Figure 2.21* shows variations in COP, heating capacity and compressor crankshaft power at different compressor discharge pressures, as originally presented by Nekså [44]. At low discharge pressures (≤ 90 bar) *Figure 2.21* show that a relatively small increase in compressor power yields a relatively large increase in GC heating capacity, provided that the refrigerant outlet temperature is constant.

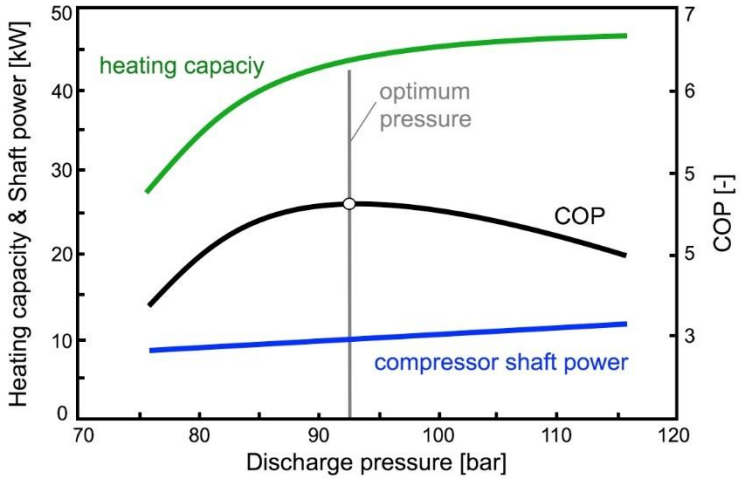

Figure 2.21: Optimum discharge pressure. Variation of heating capacity, heating-COP and compressor shaft power with the discharge pressure for CO_2 heat pump (based on [44]).

The design of compact GCs have to take the temperature glide into consideration to avoid heat conduction between "hot" and "cold" parts of the heat exchanger, as this hampers thermal efficiency considerably, especially when operating at large temperature glides [37, 44]. Consequently, long and slim GC design, or GCs in series could be preferable.

2.2.3.4 Suction line heat exchangers

A suction line heat exchanger (SLHX) is an internal heat exchanger (IHX) that transfers heat from the high-pressure liquid line to the suction line, i.e. between evaporator and compressor, as depicted in *Figure 2.22*. The SLHX is one of the most common ways to modify the original VCC so as to reduce losses related to fluid expansion [47].

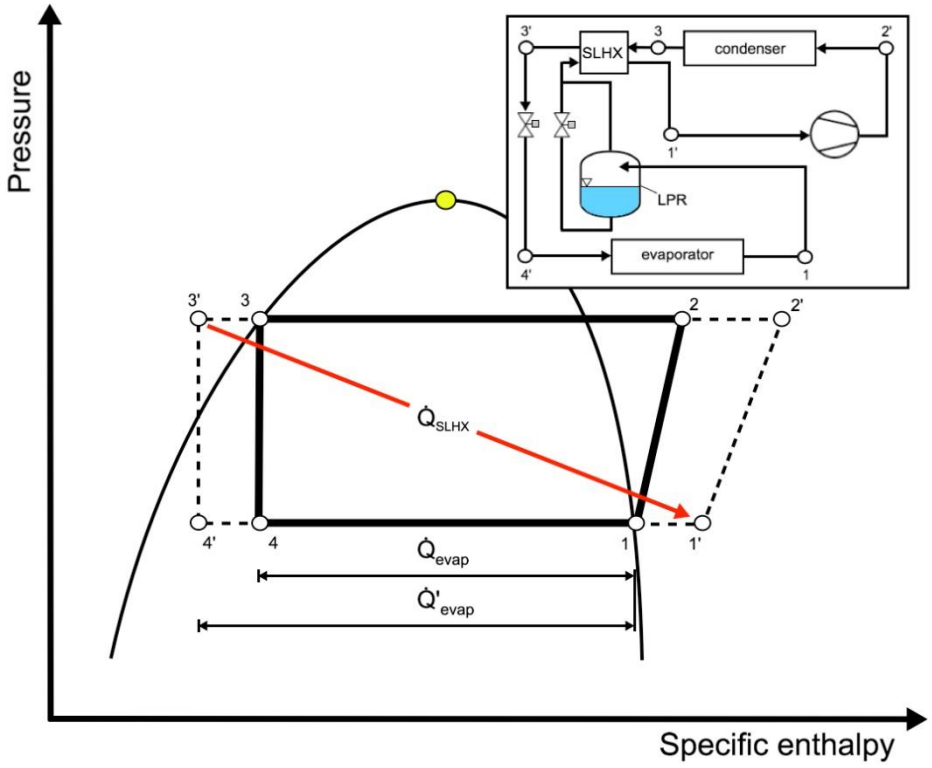

Figure 2.22: Log(p)-h VCC and component arrangement of HP-system utilizing SLHX.. Where LPR is a low pressure receiver, $\dot{Q}'_{evap}$ and $\dot{Q}_{evap}$ is heat absorption by the evaporator with and without SLHX respectively, and $\dot{Q}_{SLHX}$ is the heat transferred from the liquid line to the suction line by the SLHX (based on [47] & [48]).

The sub-cooling of the refrigerant in the liquid line, (3) to (3') in *Figure 2.22*, leads to a lower enthalpy level of the refrigerant at the evaporator inlet (less flash-gas), thus resulting in higher heat absorption at evaporator ($\dot{Q}'_{evap}$ vs. $\dot{Q}_{evap}$).

The heat transported to the suction line ensures superheated vapor at the compressor inlet, which is necessary for reliable operation, as mentioned in section 2.2.2. However, increased suction gas temperature (t_{sg}) also results in higher discharge gas temperature (t_{dg}), and volumetric losses. Consequently, this results in increased high-side superheating losses and lower volumetric compressor efficiency (λ) [34]. Moreover, high discharge gas temperatures can lead to increased degradation of refrigerant and lubrication oil.

Because of the above-mentioned factors, the positive/negative impact of implementing a SLHX is highly dependent on the initial VCC throttling losses [34]. Systems applying R744 and R134a

usually benefits from implementation of a SLHX, especially at high ambient temperatures. Robinson and Groll [49] reported a 7% increase in COP_{HP} when a SLHX was added to their simulation model of a basic transcritical R744 HP system. Moreover, experimental results from Torrella et al. [50] showed an increased COP_R and cooling capacity of 12% when utilizing a SLHX in their R744 refrigeration system.

2.2.3.5 Transcritical CO_2 heat exchangers

The high operating pressures and excellent thermophysical properties of CO_2 permits very small cross sectional flow area on the refrigerant-side of the heat exchanger. This enables increased air-side surface area per unit core volume, thus making compact heat exchanger design very feasible [38].

Heat exchangers for use in transcritical R-744 heat pumps have to be of a high build quality to withstand burst pressure requirements, thus resulting in limited assortment and high cost.

2.2.4 Additional circuit components

2.2.4.1 Accumulators

A HP unit can comprise several tanks for retention of the refrigerant charge during part load operation, some of which also holds other functions, e.g. liquid vapor separation and oil return. Accumulators located at the suction line, as depicted in *Figure 2.17* and *Figure 2.22*, are generally denoted as, low-pressure receivers (LPR), suction line accumulators, or suction line separators.

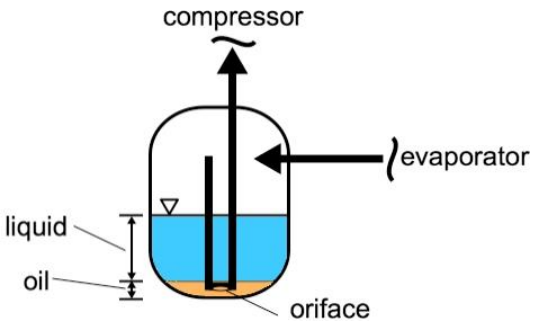

Figure 2.23: Low-pressure receiver with orifice for oil return (based on [35]).

In systems with high-side charge control, the high-side pressure is controlled by varying the high-side refrigerant charge. Consequently, a refrigerant buffer, like a LPR, must be implemented so that the high-side charge can be varied without flooding or drying up the evaporator [38].

Another function of the LPR is to safeguard against entrainment of liquid refrigerant to the compressor, this is achieved by the piping configuration of the LPR, see *Figure 2.23*. In systems

with recirculated evaporators, the LPR assures recirculation of saturated liquid refrigerant back to the evaporator, as shown earlier in *Figure 2.17*. In some cases, the LPR can include an integrated heating coil, e.g. receiving heat from the liquid line, consequently integrating the SLHX into the LPR [51].

As the LPR separates liquid from vapor, oil will also be separated in the LPR. Therefore, to avoid accumulation of oil in the LPR, an oil return function, ensuring proper oil return back to the compressor, should be part of the design, or a separate system. In *Figure 2.23* oil return is achieved by the orifice in the suction line, while *Figure 2.22* show a different solution with a separate line going from the bottom of the LPR, through a metering valve and back to the suction line.

2.2.4.2 Filter driers

The purpose of filter driers, *Figure 2.24*, is to filter out particles and foreign matter such as metal chips and moisture from the refrigerant line, as these pose a risk for the components comprising the HP unit [32]. In general, filter driers are constructed for one directional flow, but bidirectional filter driers are also on the market. The bidirectional filter driers are basically two one directional filter driers, with opposite arrangement, mounted in the same component, appropriate flow is directed by integrated check valve [51]. The intended flow direction is marked by an arrow, as depicted in *Figure 2.24*.

Figure 2.24: Filter driers for reversible R-744 heat pump

2.2.4.3 Reversing valve

The function of the reversing valve, or changeover valve, is to alter the refrigerant piping configuration, and thus refrigerant flow, according to the desired operating mode, HP or AC [51], as shown in *Figure 2.25*. Consequently, changing the function of the interior and exterior heat exchangers, as depicted earlier in *Figure 2.7*. Alternatively, flow reversing can be facilitated by two or more three-way valves.

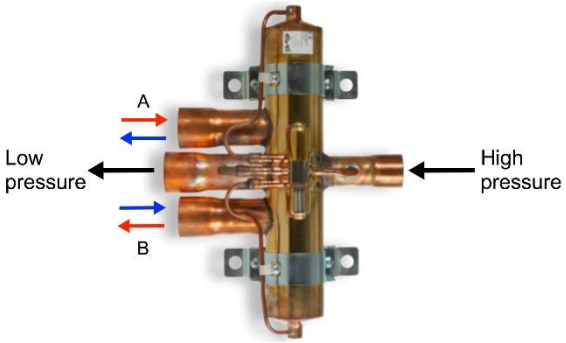

Figure 2.25: 4-way reversing valve. Where low pressure and high pressure represent flow to and from the suction line and discharge line, respectively. The flow through A and B is altered to reverse flow through the heat exchangers, consequently changing operating mode [Eliwell].

2.2.4.4 Check valves

The refrigerant flow through a check valve is only possible in one direction, marked by an arrow on the component. The purpose of the check valve, is to assure bypass of components constructed for one directional flow, when the system switches between operating modes [51]. Consequently, a reversible heat pump system can comprise several check valves.

2.2.5 Expansion devices

2.2.5.1 Expansion valves

In a traditional (subcritical) heat pump the function of the expansion valve (EV), or throttling valve, is to regulate refrigerant mass flow ($\dot{m}_r$) to the evaporator. For DX systems, the refrigerant flow should correspond to the amount evaporated in the evaporator, and additionally provide a certain amount of superheat at the evaporator outlet.

The evaporator type, usually determines the control principle of the EV. Systems comprising DX evaporators, usually apply EVs regulated with regard to the suction line temperature, these EVs are known as thermostatic expansion valve (TEV) [52]. The TEV, depicted in *Figure 2.26 a)*, holds a mechanism that detects the amount of refrigerant superheat at the evaporator outlet, the valve opening is adjusted to maintain a constant superheat, typically 5K [33]. Alternatively, DX systems can adopt electronic expansion valves (EEV), as depicted in *Figure 2.26 b)*.

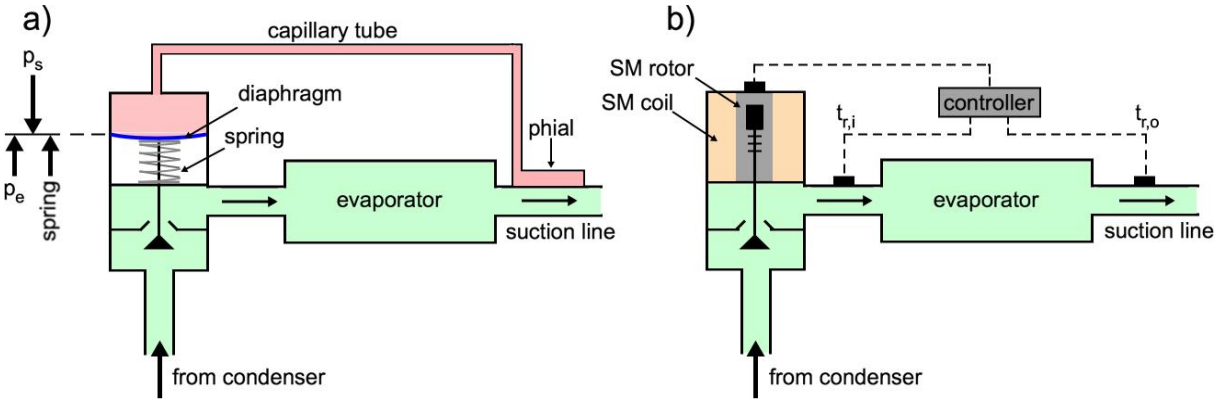

Figure 2.26: Principle sketch of expansion valves for DX systems.a) Thermostatic expansion valve, valve opening adjusts according to the balance between evaporator pressure p_e, spring tension and pressure in the separate container p_s. The separate container is filled with a suitable fluid for the relevant system (based on [33]). b) Continuous flow electronic expansion valve, a stepper motor (SM) change the valve opening with regard to measured temperature at the evaporator inlet and outlet.

Flooded/recirculated evaporators can be regulated with regard to the liquid level in the liquid receiver, measured by either a mechanical float or an electronic sensor.

There are mainly two types of EEV, continuous flow (CF) and pulse width modulating (PWM), both of which relies on a pre-configured signal output from a controller. When the CF-EEV (*Figure 2.26 b)*) receives a low voltage signal from the controller, a stepper motor (SM) rotates accordingly, the rotational movement is converted into axial movement by a drive mechanism, and the valve opening is adjusted to provide desired refrigerant flow. In the case of PWM-EEV, the valve is either in fully open or fully closed position. The intervals in which the valve is open and closed are regulated in order to achieve a desired average refrigerant mass flow rate [33]. Some valves also incorporate the functionality of both PWM and CF valves.

The EEV offers precise control over a wide capacity range, in addition to rapid response to changes in load [33]. Moreover, electrical connection between components enables adaptable and intelligent system control. Other throttling devices include, constant-pressure expansion valves and capillary tubes [32].

The process through an EV can be regarded as isenthalpic, if heat transfer to the surroundings is treated as negligible. Hence, the entropy generation related to the expansion process is determined by operating conditions and the refrigerant properties. For VCCs inhibited by high expansion losses it can be expedient to replace the EV with a recovery device, like an ejector or an expander, more on ejectors in section 2.2.5.2.

In the transcritical R744 cycle, the high-side pressure is primarily dictated by the balance between compressor capacity and flow resistance of the throttling device [53]. As described in section 2.2.3.3, the COP and capacity of the transcritical cycle is directly linked to the high-

side pressure. Consequently, EVs used in transcritical heat pumps should provide precise and responsive control, in order to optimize high-side pressure at various operating conditions.

2.2.5.2 Ejectors

As a measure to reduce losses related to isenthalpic fluid expansion (throttling loss), an expansion work recovery device, like an ejector, can be implemented. There are a number different ways to utilize ejectors for work recovery in VCCs, as explained by Elbel and Lawrence [54] and Sarkar [55]. The ejector cycle described in this thesis is commonly referred to as the standard two-phase ejector cycle, depicted in *Figure 2.27*.

The ejectors durable and simple design, low cost, reasonable efficiency, ability to handle a wide range of multi-phase flow, and the fact that it consists of no moving parts, makes it a very viable expansion work recovery device for refrigeration applications.

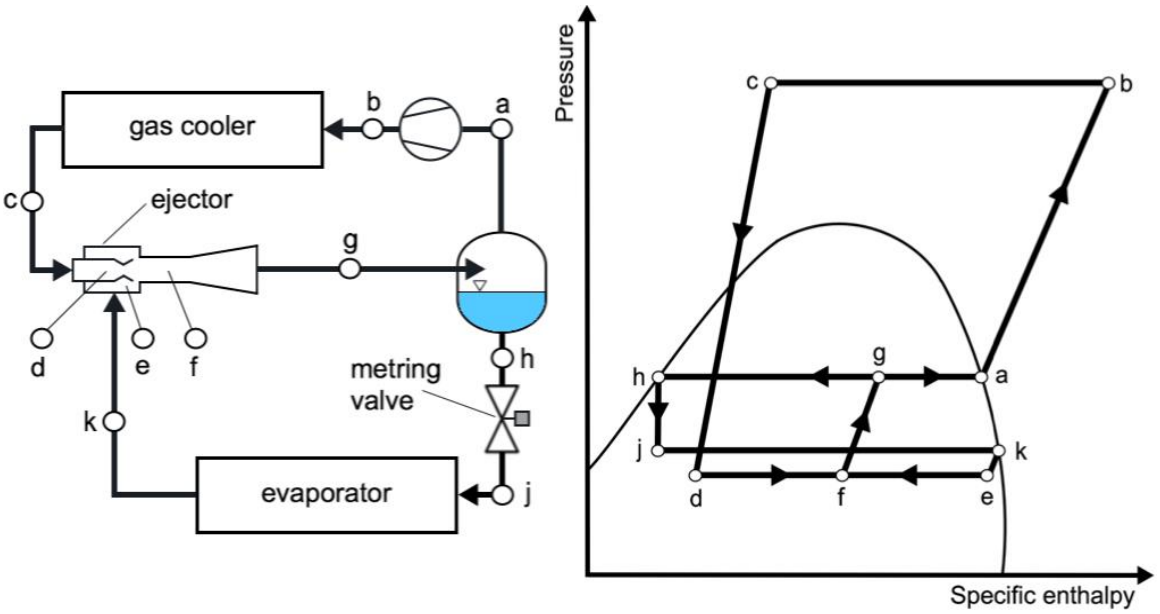

Figure 2.27: Transcritical R-744 standard two-phase ejector cycle. Left side: component diagram. Right side: ph-diagram with state points (based on [56] & [57]).

In the standard two-phase ejector cycle (*Figure 2.27)*, work is recovered from the refrigerant during the expansion process, by using the high-pressure refrigerant (c) as a motive fluid (d) in a two-phase ejector. The velocity of the motive fluid invokes a momentum exchange driven entrainment effect, thus ensuring refrigerant flow from the evaporator (k) to the mixer section of the ejector (f). Subsequently, parts of the kinetic energy of the mixture (f) is converted into pressure energy in the diffuser, and the two-phase fluid exits the ejector at an intermediate pressure (g), thus resulting in reduced compressor load.

As can be observed from *Figure 2.27*, the standard two-phase ejector cycle enables refrigerant with a lower vapor fraction at the evaporator inlet (j), thus improving heat transfer efficiency and capacity of the evaporator. Moreover, implementation of an additional evaporator at point (g), would enable heat absorption at an intermediate temperature [37].

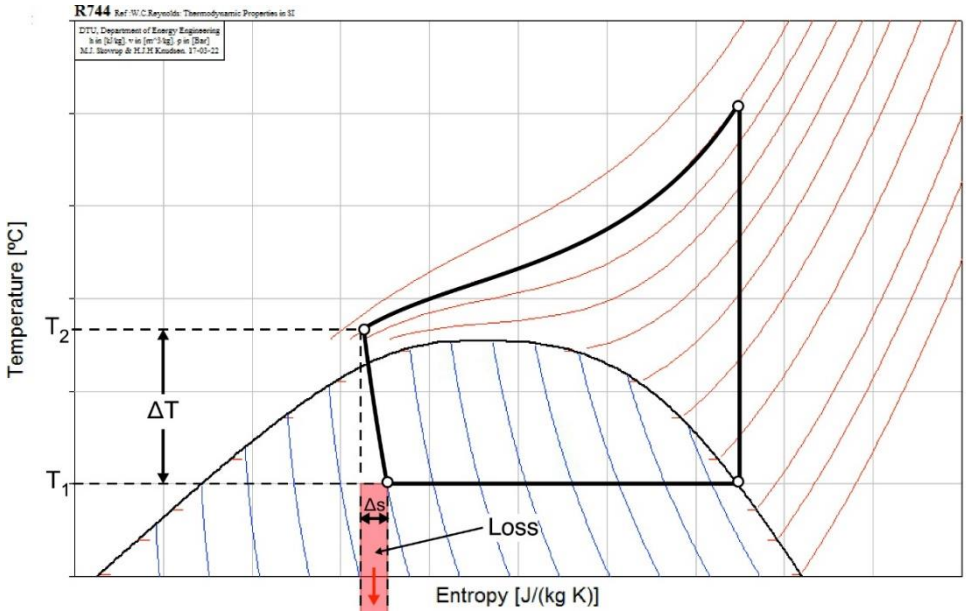

Figure 2.28:Throttling loss for the transcritical R-744 ideal Lorentzen cycle depicted in a t-s diagram. With isobaric heat exchange, isentropic compression and isenthalpic fluid expansion.Where T_1 and T_2 is CO_2 absolute temperature after and before expansion valve respectively, Δs is change in specific entropy [kJ/kg·K], blue and red lines represent isenthalps and isobars respectively (based on [30]).

Naturally, the possible cycle COP improvements obtained by ejector-supported expansion depends on the magnitude of the isenthalpic throttling loss, depicted for the transcritical R744 ideal Lorentzen cycle in *Figure 2.28*. The irreversibility of the expansion process is determined by the thermal properties of the refrigerant, and the temperature difference (ΔT) before (T_2) and after (T_1) fluid expansion, see Eq.(18) [58].

$$Loss = T_1 \cdot \Delta s \sim \frac{C_p \Delta T^2}{T_1 + T_2} \qquad \text{Eq(18)}$$

Additionally, refrigerants with higher mass flow rate for a given capacity may also benefit from ejector-supported expansion, as the total irreversibility of the expansion process is proportional to the mass flow rate [54].

The concept of utilizing multi-phase ejectors for performance enhancement in refrigeration systems was patented by Kemper et al. [59] in 1966. However, the modern day introduction of the two-phase ejector for use in refrigeration applications, is in many ways a result of extensive research on how to improve the transcritical R744 VCC for use in automotive air conditioning, as explained by Hrnjak [8].

The transcritical R744 VCC has a significant throttling loss compared to low-pressure refrigerants, e.g. R134a and R410A [30], especially at high ambient temperatures. Consequently, the possible COP improvements obtained by utilizing ejector-supported expansion in the transcritical R744 cycle is far greater than that for the traditional low-pressure fluids [54].

Although ejector-supported expansion seems most viable for R744 systems, the focus of recent experimental research has shifted from transcritical R744 to low-pressure refrigerants, with numerous studies being published starting 2014, as reported by Elbel and Lawrence [54]. Further, Elbel and Lawrence [54] reports that the focus of recent research on R744 ejector technology have shifted from experimental studies to multi-dimensional CFD-modeling, with several detailed studies starting 2012.

There are numerous ways to define the ejector efficiency (η_{ej}), many of which require detailed knowledge about the static pressure conditions at the motive nozzle exit (d), which is difficult to determine. Elbel and Hrnjak [60] introduced a method for determining ejector efficiency (η_{ej}) as a function of mass entrainment ratio (Φ_m) Eq.(19), and suction pressure ratio (Π_s) Eq.(20), thus threating the ejector as a "black box".

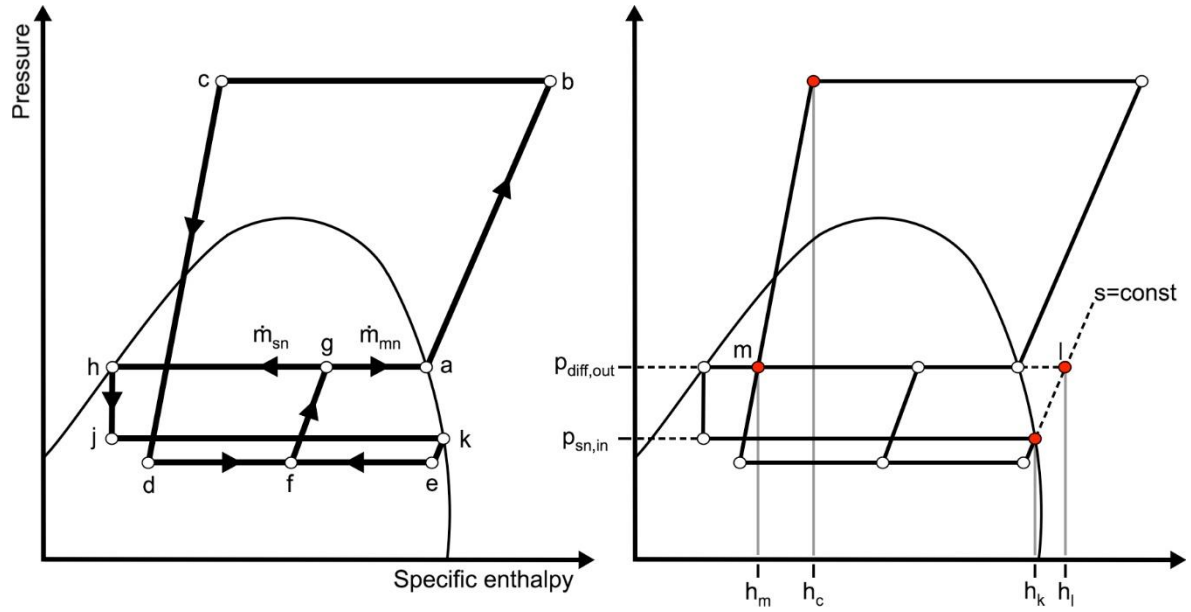

Figure 2.29:Transcritical R-744 standard two-phase ejector cycle efficiency metrics. Where $p_{diff,out}$ is pressure at the diffusor outlet $p_{sn,im}$ is pressure at suction nozzle inlet, $\dot{m}_{sn}$ is the mass flow through the suction nozzle equal to evaporator mass flow, $\dot{m}_{mn}$ is mass flow through the motive nozzle equal to gas-cooler mass flow (based on [60]).

$$\Pi_s = \frac{p_{diff,out}}{p_{sn,in}} \qquad \text{Eq.(19)}$$

$$\Phi_m = \frac{\dot{m}_{sn}}{\dot{m}_{mn}} \qquad \text{Eq.(20)}$$

$$\eta_{ej} = \frac{\dot{W}_{rec}}{\dot{W}_{rec,max}} = \Phi_m \cdot \frac{h_l - h_k}{h_c - h_m} \qquad \text{Eq.(21)}$$

Although the definition of Elbel and Hrnjak [60] seems to be the most commonly reported ejector efficiency [54], there are several other definitions, as previously mentioned. A summary of two-phase ejector efficiency definitions have been comprised by Lawrence and Elbel [61].

The first performance analysis of the standard ejector cycle was conducted by Kronhauser [56] in 1990. He investigated the ability of the standard ejector cycle to improve COP for several refrigerants (not R744), using a homogenous equilibrium model for the cycle, and assuming constant pressure in the mixing section of the ejector. The largest and lowest improvements in cycle COP were found for R502 (30%) and R717 (12%), respectively.

More recent experimental and CFD-modeling research on the transcritical R744 two-phase ejector cycle, like Elbel [62], Liu et al. [63] and Banasiak [57], have found that ejector geometry can have a significant effect on ejector performance, thus sometimes resulting in poor efficiency during "off-design" operation. Consequently, an ejector with fully adjustable geometry, able to adapt to different operating conditions would be optimal, however the construction of such ejector appears challenging. Alternatively, Hafner et al. [64] have investigated the possibility of using a parallel multi-ejector arrangement for larger scale supermarket refrigeration.

A review of recent developments in advanced ejector technology have been comprised by Elbel and Lawrence [54]. They found that experimental studies investigating performance of the transcritical R744 standard ejector cycle have shown COP improvements mostly in the range of 15-30%. Moreover, Elbel and Lawrence [54] suggests that the greatest opportunity for further work in the field of ejector technology is addressing practical issues related to compressor oil return, design of compact and efficient LPRs, and more efficient system control for small to medium capacity applications.

2.2.6 Air as heat source

Ambient air is the most commonly used heat source/sink for HP, AC and refrigeration applications around the world, mainly due to the fact that its readily available virtually anywhere. Moreover, ambient air requires no additional costly collector system for heat absorption/rejection, other than fans. However, ambient air is far from the ideal heat source as will be discussed below.

The ideal heat source should have a relatively high and stable temperature throughout the heating season, as this ensures a low temperature difference between the evaporator and the

condenser, consequently increasing the possible COP_{HP} of the system. Ambient air however, does not hold these traits as the temperature fluctuates from hour to hour and over the year. Moreover, the temperature of ambient air is usually in counter-phase with the heating and cooling demand, as the highest cooling and heating loads occurs at the highest and lowest ambient air temperatures, respectively.

Additionally, energy has to be spent for de-frosting of the evaporator air-side surface at certain ambient conditions. As the amount of humidity present in the ambient air normally is quite low during temperatures below -2°C, evaporator frosting is most problematic during approximately 7°C to -2°C. Moreover, the steep characteristic of the saturation curve at low temperatures result in a lower change in absolute humidity for a corresponding change in temperature ($\Delta x/\Delta t$), as shown in *Figure 2.30.*

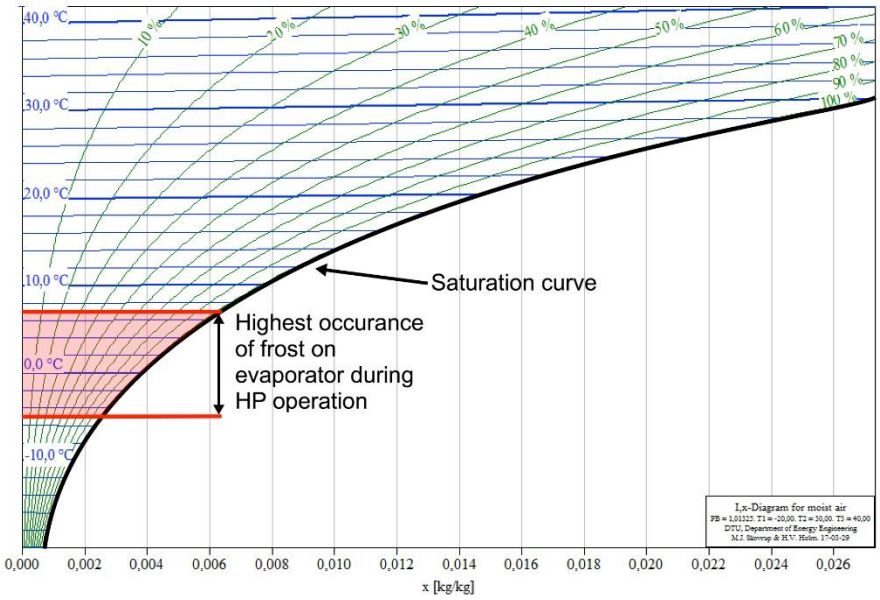

Figure 2.30: Occurrence of frost on evaporator depicted in a i-x diagram. Where the green and blue lines represent relative humidity (RH) constants and isotherms, respectively (based on [30]).

Accumulation of frost on the air side of the evaporator will reduce the U-value, and thus reduce the evaporation temperature, heat transfer rate, and COP, as explained by Martinez and Aceves [65]. Large amounts of accumulated frost can also impose structural wear, and subsequently damage, to the evaporator. De-frosting is usually achieved by cycle reversing or electric resistance heaters. Sufficient drainage of condensed water needs to be ensured, in order to avoid damage to equipment and microbiological growth.

As the thermophysical properties of air is rather poor with regard to heat transfer, the surface area and volume flow on the air-side of the evaporator needs to be relatively high. This is

achieved by the evaporator design and can be further improved with air fans, as explained in section 2.2.3.

To sum up the above-mentioned factors, ambient air is a cheap and readily available heat source, with some challenges with regard to system performance and reliability at unfavorable ambient conditions, in addition to heat transfer efficiency on the evaporator air-side.

2.2.7 Safety

There are many safety concerns that needs to be addressed in order to safeguard personnel, property and environment, from a heat pump system. These safety concerns are mainly related to the physical and chemical properties of the applied refrigerants, as well as the temperatures and pressures occurring in the system during operation. The design, construction, installation, operation and maintenance of the system must comply with the requirements specified in the European Standard EN 378.

2.2.7.1 Refrigerant safety classification and maximum charge

Refrigerants are safety classified in accordance to ISO 817. The safety classification consists of two alphanumeric characters, e.g. A2 or B1, in addition to a third character L designating low burning velocity, if relevant. The capital letter describes the toxicity of the refrigerant, whereas the Arabic number denotes the flammability. Refrigerant blends, consisting of two or more compounds, are assigned dual safety group classification separated by a dash (/). The toxicity classification, A and B, are based on the allowable exposure limit:

- Class A (lower chronic toxicity) have an occupational exposure limit ≥ 400 PPM_V
- Class B (greater chronic toxicity) have an occupational exposure limit ≤ 400 PPM_V

The flammability classification consists of four classes (1, 2L, 2 or 3), where 1 and 3 indicates no and higher flammability, respectively.

A non-toxic, non-flammable refrigerant can still pose a threat to the people occupying an adjacent zone, as most refrigerants are heavier than air (not R717), thus causing displacement of air in the dwelling zone.

Consequently, the maximum allowable refrigerant charge depends on the safety classification of the refrigerant (ISO 817), in addition to the room occupancy type, volume and ventilation rate (EN 378).

2.2.7.2 Pressure switches

To ensure that pressure is maintained within the design limits of the heat pump system, safety pressure switching should be implemented, as specified in EN 12263. The pressure switches are pressure actuated devices, designated with regard to placement in the refrigerant circuit. High-pressure switches and low-pressure switches, are located on the high- and low-pressure side of the refrigerant circuit, respectively. When the pre-set cut-off pressure is reached, the pressure switch signals the compressor control unit to stop operation. The heat pump system can also comprise several thermostatic switches, actuated by a pre-set cut-off temperature. In addition to high- and low-pressure switches, large capacity systems also comprise pressure switches actuated by a minimum oil pressure differential.

2.2.7.3 Safety and shut-off valves

Safety valves are passive safety devices that prohibits system rupture or explosion at abnormal conditions (e.g. fire, system failure, etc.), by evacuating the refrigerant charge, thus relieving the pressure. The refrigerant must be evacuated so that it pose minimal threat to persons and property.

A shut-off valve is a device that shuts off the refrigerant flow when signaled. The placement of several shut-off valves should ensure minimal refrigerant leakage during a pipe rupture or component failure.

2.2.7.4 Leakage detection

If the practical concentration limit of a refrigerant, as specified in EN 378-1, can be exceeded during a refrigerant leak, proper leakage detection must be implemented as specified in EN 378-3. Detector placement must be chosen in relation to refrigerant density, and needs to take the local air-flow patterns into consideration. At a pre-set refrigerant concentration value, the detector signals the system control unit to activate shut-off valves, the alarm system, and the emergency ventilation or controls. Systems utilizing refrigerants with safety classification A1 can use oxygen deprivation sensors instead of refrigerant concentration sensors.

2.2.7.5 Safety of transcritical R744 heat pumps

Refrigerant carbon dioxide (R744) has the safety classification A1, thus being non-toxic and non-flammable, as specified in ISO 817. However, there are some safety concerns related to the high pressures occurring during operation that needs to be considered. Additionally, the air displacing characteristics of R744 also have to be taken into consideration, as previously mentioned.

In the case of a rupture, the explosion (stored) energy may define the magnitude of the potential damage. The explosion energy of the system can be estimated based on the total refrigerant-side volumes, pressures, and refrigerant properties. Pettersen et al. [66] calculated and compared the explosion energies between a transcritical R744 and baseline R22 AC unit, both with a cooling capacity of 7 kW.

Pettersen et al. [66] used a closed-system model, assuming isenthalpic gas expansion during the explosion, as the rapid process would leave little to no time for heat transfer between the expanding gas and the ambient air. Moreover, the model assumed equalized pressure and temperature throughout the system. The released energy was then calculated as the difference in internal energy between the initial state of the refrigerant inside the system, and the final state after expansion at atmospheric pressure.

The results of Pettersen et al. [66], depicted in *Figure 2.31*, revealed that the explosion energies of the two systems were not as different as the large difference in pressure would suggest, due to the smaller volume and refrigerant charge of the R744 system.

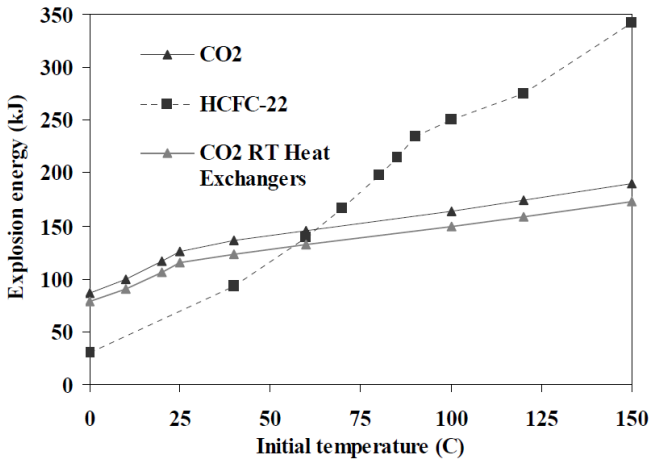

Figure 2.31:Calculated total explosion energy for HCFC-22 (R22) system and CO_2 (R744) system at varying initial temperature. Data for CO_2 system with round tube (RT) heat exchangers is also shown [66].

As can be observed in *Figure 2.31* the ratio of energies (R744/R22) is about 2 at room temperatures, and 0.7 at 100°C. The explosion energy of the R22 system is much more temperature sensitive than the R744 system, and the energy release from the R22 system is likely to be much higher than the R744 system for extreme situations such as fires.

Pettersen et al. [66] also conducted a number of experimental tests, investigating the possible occurrence of a boiling liquid expanding vapor explosion (BLEVE) in R744 systems. A BLEVE may occur during a rapid depressurization of a vessel containing a pressurized liquid or supercritical fluid. The rapid depressurization may leave a explosively vaporizing superheated

liquid, that could lead to a transient overpressure peak inside the vessel [66]; possibly resulting in a more severe blast effect, due to the shorter duration of the energy release [38]. A paper by Kim-E and Reid [67] pointed to the possibility of BLEVE of R744 systems. However, results from extensive experimental studies conducted by, Pettersen and Hakenjos [68], and Pettersen [69], have not given any reason to expect BLEVE of R744 systems.

The high system pressures may also lead to the occurrence of high intensity acoustic shock waves during a rupture.

2.3 Refrigerants

A refrigerant, or working fluid, transports thermal energy from a heat source to a heat sink, by going through phase changes in a vapor compression cycle (VCC). There is a wide range of different refrigerants both natural and synthetic, with different practical, thermodynamic and environmental properties.

A refrigerant may consist of a single compound (pure), or it can be a blend (mixture) of several. Moreover, a refrigerant blend can either be azeotrope, or zeotrope. An azeotrope refrigerant is a blend of two or more compounds, that at a given mixing ratio behaves like a pure compound. For this ratio the blend has the same evaporation and condensation temperature at a given pressure. While for zoetrope refrigerant, the different compounds condense and evaporate over a temperature range for a given pressure [34]. Systems using refrigerant blends should always be filled with liquid phase refrigerant to ensure correct ratio of the different compounds [33].

The identifying numbers assigned to the refrigerants in accordance to ISO 817, e.g. R22, R134a, etc., are such that the chemical composition of the compound can be explicitly determined based on the number (for most refrigerants).

The refrigerant selected for a system, should have thermophysical properties optimized for the systems intended use. The goal should be to achieve a good cycle efficiency (high COP) and safe operation at all operating conditions. The ideal properties for a refrigerant are listed as follows [33]:

- High specific heat of vaporization
- High suction gas density
- Good heat transferring and fluid dynamic characteristics
- Above atmospheric but not excessive pressures at evaporating and condensing conditions.

- Low pressure ratio (π) between evaporator and condenser
- Triple point and critical temperature well outside working range
- Chemically stable, compatible with system components and piping, and miscible with the lubrication oil
- Non-corrosive, non-toxic, non-flammable
- Environmentally benign
- Low cost

Naturally, no single one refrigerant hold all of these traits, and the choice of refrigerant for a particular application will always be a compromise [33].

The pressure level in the evaporator should be higher than atmospheric pressure to avoid leakage of air and thus moisture into the system. The pressure ratio (π) between the condenser and the evaporator is also an important factor, as this is closely linked to the compressors isentropic and volumetric efficiency (η_{is}, λ) [34], as previously mentioned in section 3.2.2.

The vapor density (ρ_v) of the refrigerant should be high, in order to achieve a high volumetric refrigeration and heating capacity (VHC (Eq.(23)) and VRC (Eq.(24))) which reduce the necessary compressor volume (V_S) as seen from Eq.(22). As the ρ_v is closely linked to the pressure, systems with high operating pressure, like R744, generally achieve a higher VRC.

$$V_s = \frac{\dot{m}_R}{\rho_{sg}} \qquad \text{Eq.(22)}$$

$$VHC = q_{cond} \cdot \rho_v \qquad \text{Eq.(23)}$$

$$VRC = q_{evap} \cdot \rho_v \qquad \text{Eq.(24)}$$

Where:

- $\dot{m}$: mass flow of circulated refrigerant [kg/s]
- ρ_{sg}: vapor density at compressor inlet [kg/m^3]
- q_{cond}: enthalpy difference of condenser [kJ/kg]
- q_{evap}: enthalpy difference of evaporator [kJ/kg]

2.3.1 Total equivalent warming impact (TEWI)

When comparing different systems lifetime impact on the global environment, the systems total equivalent warming impact (TEWI) should be evaluated. The TEWI describes the systems direct and indirect impact on global warming over its entire operational life, and is to a large extent affected by the choice of refrigerant. The TEWI includes losses related to refrigerant

leakage and recovery, in addition to the emissions related to the energy required to operate the system [33]. The TEWI factor should be calculated in accordance to EN 378-1 Eq.(25):

$$TEWI = (GWP \cdot L \cdot n) + \left(GWP \cdot m[1 - \alpha_{recovery}]\right) + (n \cdot E_{annual} \cdot \beta) \qquad \text{Eq.(25)}$$

Where:

- GWP: Global warming potential
- L: Leakage rate per year [kg/year]
- n: Number of operating years (system lifetime) [year]
- m: Refrigerant charge [kg]
- $\alpha_{recycling}$: Recycling factor
- E_{annual}: Energy consumption per year [kWh/year]
- β: CO_2 emission factor, kg CO_2 emitted per kWh of electricity [kWh/kg_{CO2}]

The emissions related to transport, construction and de-construction of the system are not included in the TEWI, and is only valid for comparing alternative systems or refrigerant options for one application in one location, as stated in EN 378-1.

2.3.2 R744 carbon dioxide

Refrigerant carbon dioxide has the refrigerant number R744. As specified in ISO 817, the compounds assigned numbers in the 700 and 7000 series specifies that they belong to the inorganic group. The number 44 is the molar mass of the molecule CO_2. R744 is a non-toxic and non-flammable refrigerant, thus belonging to the safety classification group A1 in the ISO 817, as described previously in section 3.2.7.

2.3.2.1 The rise, fall, and revival of R744

Carbon dioxide was one of the very first refrigerants applied in early vapor compression systems. Alexander Twining first proposed its use as a refrigerant in an 1850 British patent [70]. However, carbon dioxide first made its breakthrough as a refrigerant through the work of the self-thought scientist Thaddeus Lowe. In 1860, Lowe developed a compressor for filling military observation balloons with hydrogen. He later adapted his compressor for CO_2 in 1866, for use in the manufacture of artificial ice [23].

Further development in carbon dioxide VCC technology first came 20 years later, through the work of Franz Windhausen who patented an improved CO_2 compressor in 1886. Later, Windhausen's design was further improved by Evarard Hesketh of J&E Hall, and CO_2 was finally established as a viable refrigerant option from 1887 and onwards [23].

Owing to its non-flammable and non-toxic properties, R744 was the preferred refrigerant for the marine market in the 1880s. Up until then open-circuit air cycle had dominated this market, but the efficiency and reliability achieved by the R744 vapor compression systems proved superior. R744 continued to be the preferred refrigerant in applications where safety was a concern, until the 1930s. The decline and fall of CO_2 as a refrigerant is in large part contributed to the advent of the synthetic chlorofluorocarbon (CFC) refrigerants, in addition to the improved safety record of ammonia (R717) vapor compression systems.

The phase out of the synthetic CFC and HCFC refrigerants, due to their ozone depleting properties, dictated by the Montreal protocol (1987), sparked new life into the R&D of viable R744 VCC technology, headed by professor Gustav Lorentzen, starting early 1990s [2, 71]. The cycle proposed upon reintroduction, was a transcritical VCC, with supercritical heat rejection [2]. Thus enabling efficient and practically viable operation for several different heat pump and refrigeration applications.

Upon reintroduction, the main focus of R&D on R744 systems was in applications for mobile AC units (MACs), as these accounted for almost 60% of the global emissions from the refrigeration sector [48], in addition to heat pumps for heating of domestic hot water [37]. Still to this day (2017), R&D of new and efficient CO_2 heat pump systems are being conducted at an increasing rate, for a wide range of domestic, commercial and industrial applications.

2.3.2.2 Properties of R744

Although CO_2 is a GHG (GWP=1), abundant amounts of CO_2 are recovered from industry waste gas, thus the effective GWP of commercial CO_2, for instance used as refrigerant is zero [48]. Moreover, R744 have zero ozone depleting properties (ODP=0), thus currently (2017) being the only non-toxic, non-flammable, non-global-warming, non-ozone-depleting refrigerant available for vapor compression systems.

Because of its abundance, CO_2 is low-cost and easily obtained compared to the synthetic mediums [2]. Moreover, the use of natural refrigerants, is unquestionably more preferable from an environmental point of view, as they already have a natural role in the ecosystem, and their environmental effects are well established [48], as opposed to the HFCs and the newly developed HFOs.

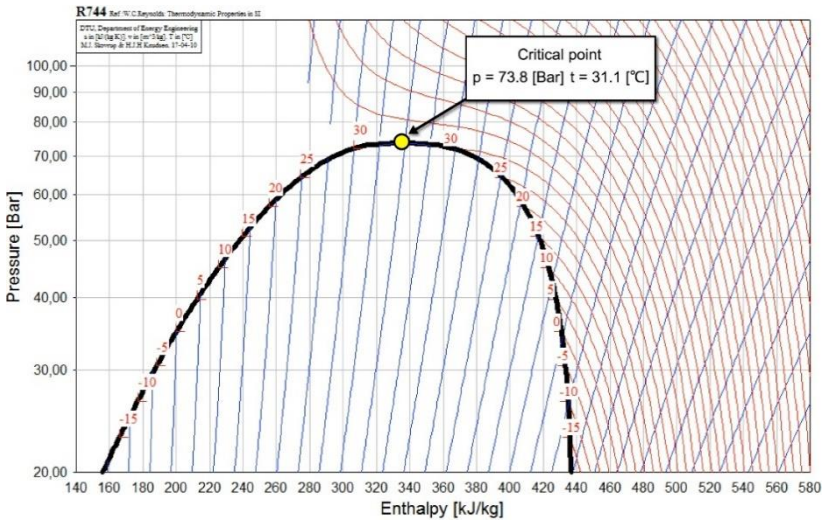

Figure 2.32: Log(p)-h diagram R744, where blue and red curves represent isentropes and isotherms, respectively (DTU [30]).

The properties of R744 are quite different from all of the conventional refrigerants. As can be observed in *Figure 2.32*, R744 has a low critical temperature (t_c) and moderate critical pressure (p_c), 31.1℃ and 73.8 bar, respectively [34]. Heat rejection by the means of condensation is limited to the critical temperature, thus most modern single-stage R744 vapor compression systems operate transcritically, as described in section 2.2.3.3.

Because of high operating pressures, typically 30-40 bar on low-side and 100-130 bar on high-side, R744 vapor compression systems achieve much higher VRC (Eq.(24)) than traditional system, generally 3-10 times higher than CFC, HCFC, HFC and HC systems [38], as depicted in *Figure 2.33 a)*. Consequently, this results in a much smaller required swept compressor volume, typically 80-90% smaller compared to R134a. Moreover, R744 has a low surface tension, which reduce the required superheat for nucleation and growth of vapor bobbles, which may positively affect heat transfer [38].

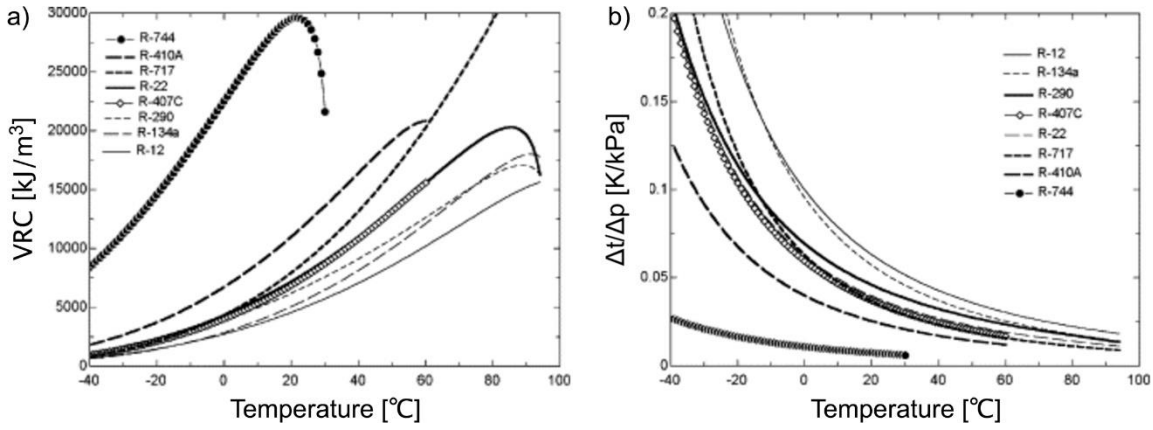

Figure 2.33: A comparison of VRC a) and slope of Δt/Δp curve b) for different refrigerants [38].

The high vapor pressure of R744 gives a very small temperature change for a given pressure change, generally 4-10 times lower than conventional refrigerants, as can be observed in *Figure 2.33 b)*. This can have a huge impact on the design of heat exchangers, as a larger pressure drop can be accepted, thus enabling compact and efficient heat exchangers design, as mentioned in section 2.2.3.5.

Additionally, R744 have high thermal conductivity, which is essential for heat transfer coefficients both in single-phase and two-phase flow [38]. Moreover, R744 has a relatively low liquid and vapor viscosity compared to the conventional refrigerants, which is an important parameter with regard to fluid flow behaviors, convection characteristics and two-phase heat transfer and pressure drop [38].

As a supercritical fluid gets close to the critical point its physical properties exhibits extremely rapid variations when temperature is changed in an isobaric process, especially near the pseudocritical point (the temperature which the specific heat becomes a maximum for a given pressure) [72], as may be observed from *Figure 2.34*.

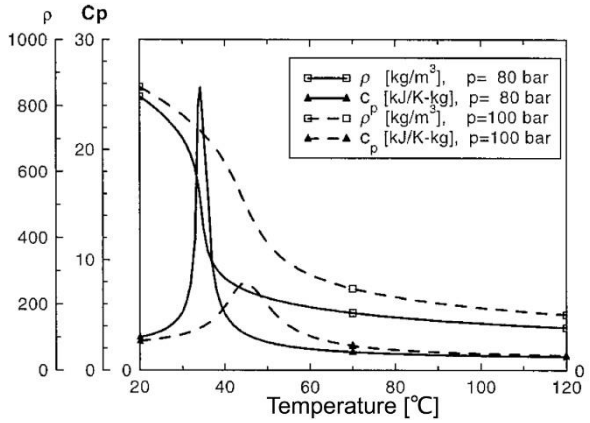

Figure 2.34: Variations of the specific heat (C_p) and density (ρ) of R744 at pressures of 80 and 100 bar [72].

Consequently, it is necessary to consider the changing properties when using the LMTD method for a supercritical fluid, as it presumes constant specific heat (C_p) throughout the evaluated section. Thus it should be carefully investigated whether this is a good approximation [38].

2.3.3 R134a tetrafluoroethane

Tetrafluoroethane, or R134a, is a non-toxic, non-flammable, HFC refrigerant without ozone-depleting properties. As it holds many of the same thermodynamic properties as CFC-12 and HCFC-22, it was early adopted as a suitable replacement, and is one of the most common refrigerants applied MACs. The newly developed HFOs have very similar properties as R134a and are being considered as long term alternatives where their flammability can be accepted.

Because of its high molecular weight (102), R-134a is well suited for high capacity systems, up to 100 MW. R-134a have a relatively high t_c of 101.1°C and a moderate p_c of 40.7 bar [30], as can be observed in *Figure 2.35*. Thus enabling heat rejection at up to 90°C (with special equipment), which is a lot compared to other HFCs like, R-407C and R-410A, able to deliver heat up to 70 and 60°C respectively. In addition, R134a vapor compression systems generally achieve higher COP than R407C and R410A systems [73].

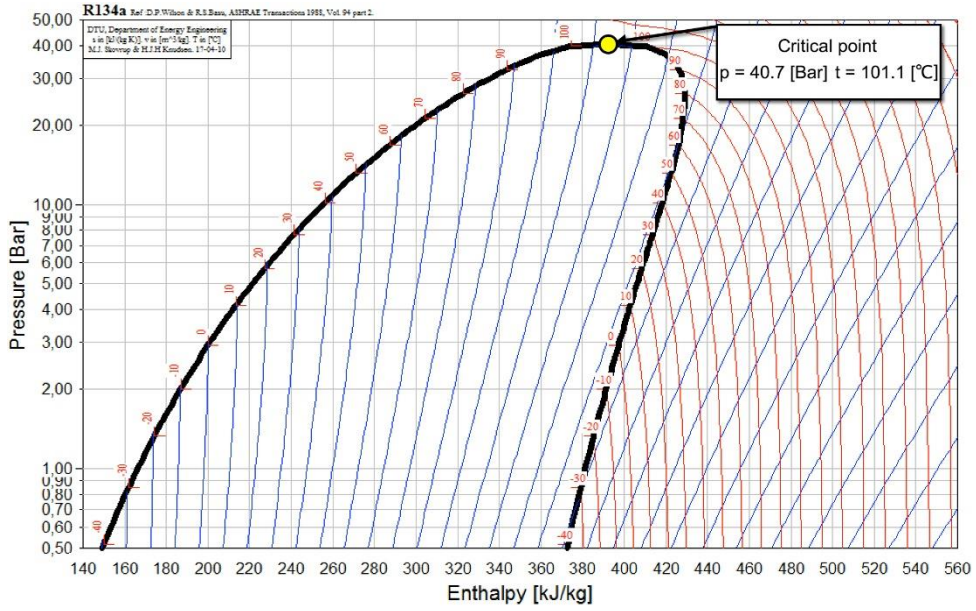

Figure 2.35: Log(p)-h diagram R134a , where blue and red curves represent isentropes and isotherms, respectively (DTU [30]).

The relatively low operating pressures, and high molar mass of R134a, results in a low VRC, thereby increasing the needed Vs, consequently leading to big and expensive compressors. In addition, R134a have minimal solubility with mineral oil, fully synthetic oil must therefore be applied as lubricant, which can lead to acid formation in the presence of moisture in combination with high temperatures [34].

Like other HFCs, R134a have a high GWP (1430), and strict requirements for leakage protection and sensors have been applied through the F-gas directive, as explained earlier in section 1.1. There are also GHG emissions related to the production process of R134a. According to McCulloch and Lindley [74], 6.6 tons of CO_2 is emitted during process of producing one ton of R134a. However, this is quite insignificant when compared to the environmental impact of a direct emission of R134a into the atmosphere.

R134a is a relatively high-cost refrigerant due to the complicated production process, explained in *Figure 2.36.*

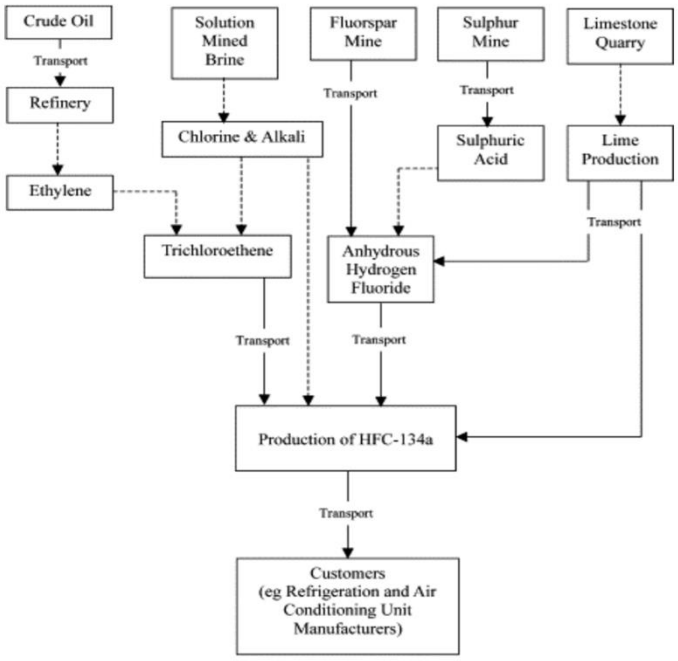

Figure 2.36: Block diagram representing the production process of R134a, showing major stages in the conversion of crude oil and other minerals into R134a [74].

3 HVAC onboard the NSB Stadler FLIRT

The HVAC system onboard the *NSB Stadler FLIRT* trainset consists of several roof mounted unitized HVAC and heat recovery system (HRS) modules, manufactured by *Faiveley Transport Leipzig GmbH & Co. KG (FTL).* The placement of these modules are shown in *Figure 3.1*.

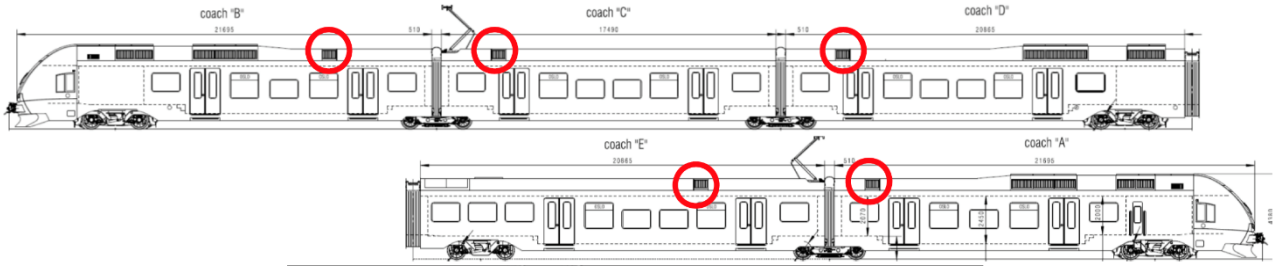

Figure 3.1: Location of HVAC & HRS modules onboard the NSB Stadler FLIRT (Stadler).

The particular trainset evaluated during the test campaign, a commuter type *BM 75-41*, holds a total of seven HVAC units; five serving the passenger compartment, and one serving the driver's cab on each side of the trainset. Only the HVACs serving the passenger compartment will be described further in this thesis.

Each roof mounted HVAC module is connected to a HRS module, as depicted in *Figure 3.2*. The HVAC module comprise three sub-assemblies, housing most of the air-handling unit (AHU), vapor compression unit (VCU), and electrical equipment components.

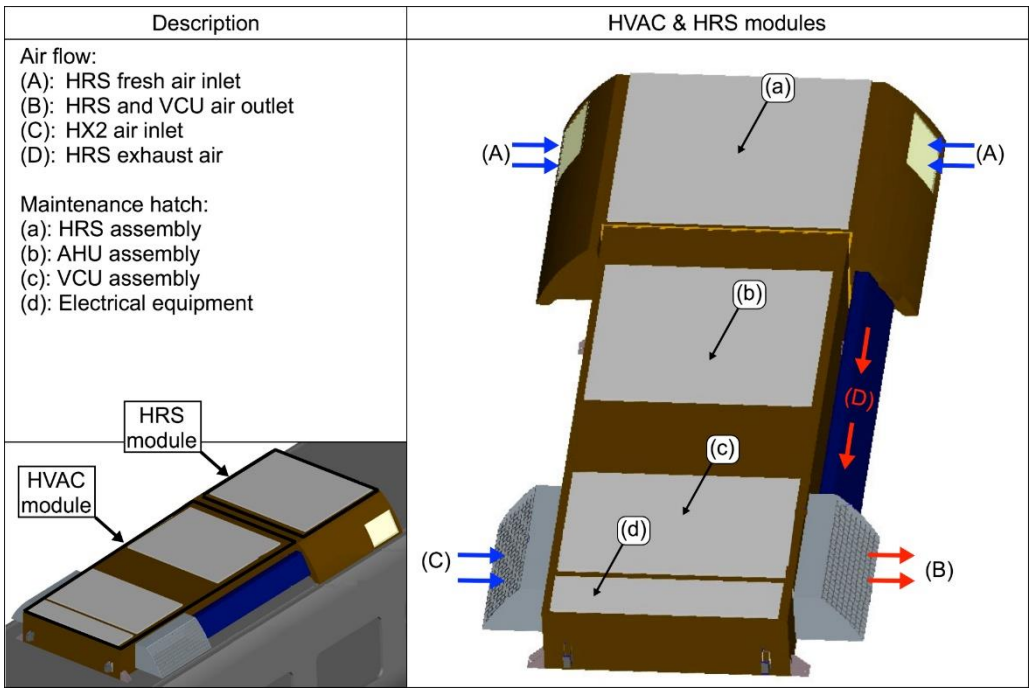

Figure 3.2: Visual representation of the HVAC module onboard NSB Stadler FLIRT, showing the maintenance hatches for the different assemblies and air flow.

The modules have four maintenance hatches, providing easy access for service personnel. Moreover, the unitized layout facilitates quick installation and removal.

Filters and grills helps safeguard against severe ambient conditions encountered during operation. The placement of the air inlets and outlets are such that heated air is discharged away from the vehicle and away from the fresh air inlet, thus precluding recirculation of discharge air, and minimize temporary extreme inlet air temperatures that may occur at passenger loading platforms or in tunnels. Consequently, the exhaust air from the ventilation system (D) and VCU is discharged at the same location, (B) in *Figure 3.2*. The component placement and spacing in the assembly facilitate maintenance and system repairs.

The HVAC module, depicted in *Figure 3.3*, house the HVAC unit components and is divided into two main parts, an interior part (AHU assembly) comprising the fresh air inlet, supply air fans and dampers, and the interior heat exchanger (HX1); and an exterior part (VCU assembly) comprising most of the vapor compression system components and acting as a machinery room.

As the majority of the refrigerant charge is confined to the VCU assembly, exposure to the passenger compartment during a refrigerant leak is minimal. The contactors, circuit breakers and climate controllers are located in a separate assembly (k). Both the standard and the pilot HVAC units are assembled in identical module casings.

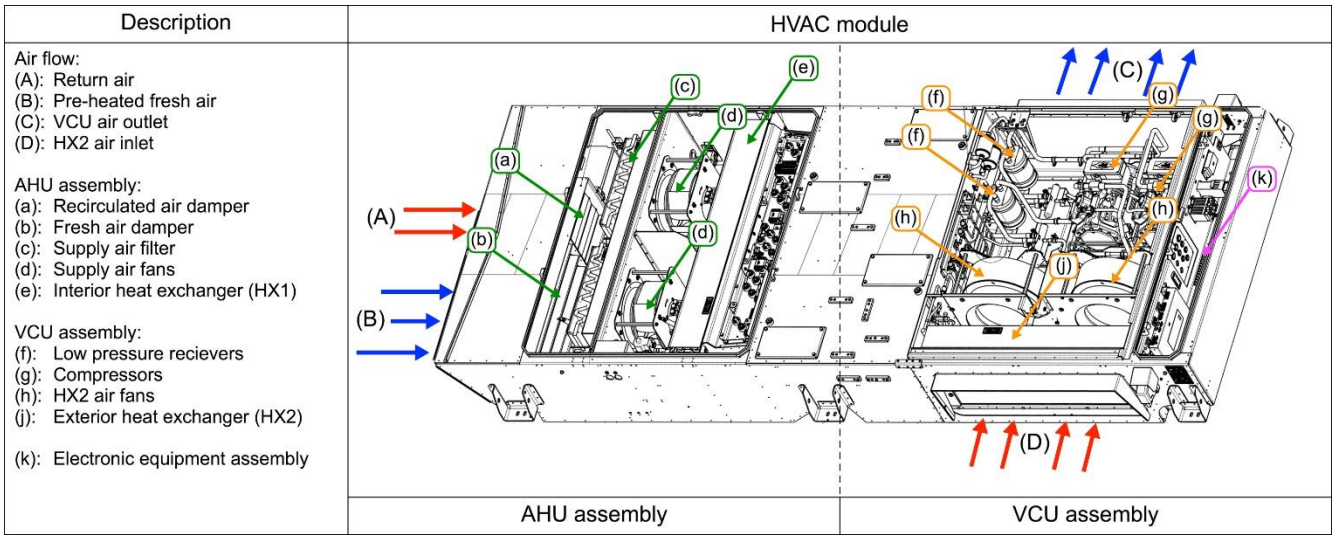

Figure 3.3:Sketch of the R134a HVAC module onboard NSB Stadler FLIRT, depicting the layout of components included in the AHU and VCU assemblies, and describing the different air flows.

The HVAC module is mounted to the carriage with six vibration reducing mounts, to mitigate transportation of vibration and noise to the passenger compartment through the carriage structure.

Photographs of both the pilot R744 and the reference R134a HVACs have been included in Appendix A.

Apart from the HVAC unit, the heating system onboard the NSB *Stadler* FLIRT trainsets consists of wall mounted electric heaters and floor heating systems, as described in section 2.1.5.

3.1 Ventilation system

The AHU onboard the NSB *Stadler* FLIRT trainset, supplies a mixture of fresh and recirculated air into the passenger compartment, established based on passenger load and ambient temperature, as specified in *Table 2*. Passenger load is determined based on sensor measurements of the carriage weight, this method offers very quick system response time; however, at a relatively low precision.

Table 2: Ratio of fresh and recirculated air supplied to the passenger carriage, onboard the NSB Stadler FLIRT, during different modes of operation corresponding to ambient temperatures (FTL).

air volumes	ambient temperature	passenger load	fresh air [m³/h]	supply air [m³/h]
heating	-40 °C < t_a < - 5 °C	3/3 2/3 1/3	690 460 230	2000
heating	-5 °C < t_a < + 13 °C	3/3 2/3 1/3	1035 690 345	2000
transition	+13 °C < t_a < +26 °C	3/3 2/3 1/3	1380 910 455	4000
cooling	+26 °C < t_a < 35 °C	3/3 2/3 1/3	1035 690 345	4000
Emergency ventilation			1800	1800

As can be observed in *Table 2*, system operation is grouped into four different modes of normal operation determined by ambient temperature, in addition to an emergency mode. Each mode has a different fresh air volume corresponding to the passenger load (<33%, <66%, or >66%). Moreover, the total supply-air volume rate during heating mode operation is reduced to 2000 m^3/h as opposed to 4000 m^3/h during transition and cooling mode operation.

The ratio of fresh and recirculated air is controlled by changing the damper angles of automated dampers, as depicted in *Figure 3.3 (a) & (b)* and *Figure 3.4 (d)*, and previously explained in section 2.1.3.1.

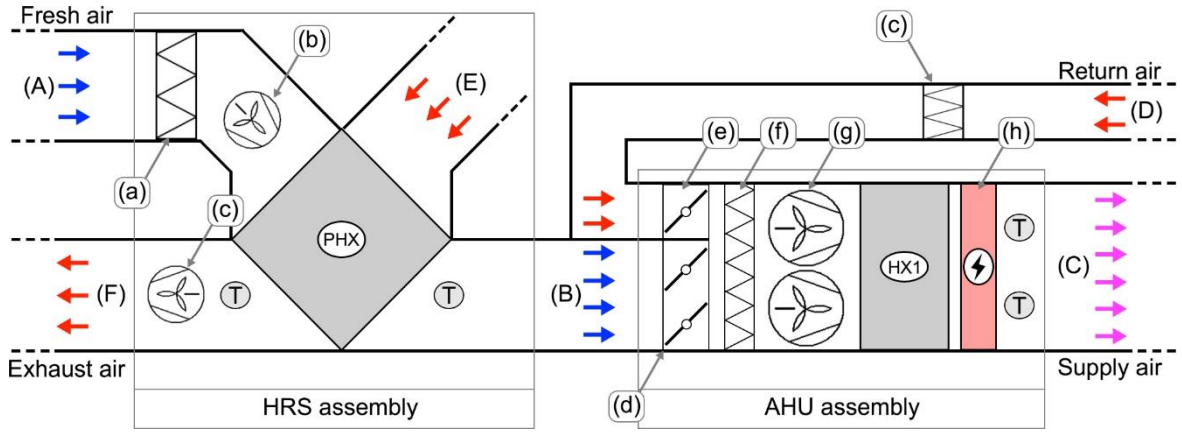

Figure 3.4: Passenger carriage air handling unit onboard NSB Stadler FLIRT,Where the air flows: (A) is the fresh intake air, (B) is the pre-heated fresh air, (C) is the supply air, (D) is the return/recirculated air, (E) the extract air, and (F) is the exhaust air. Components: (a) fresh air filter (two on real system), (b) support supply air fan, (c) return air filter, (d) fresh air dampers, (e) return air dampers, (f) mixed air filters, (g) main supply air fans, (h) electric heating coil (two on real system), (T) temperature sensors, (HX1) VCU interior heat exchanger (two independently operated circuits), (PHX) air-to-air plate heat exchanger.

Figure 3.4 represents the AHU onboard the NSB *Stadler* FLIRT trainset. As depicted in *Figure 3.(3 & 4)*, the AHU assembly house the VCU interior heat exchanger (HX1), which can supply or extract heat from the mixture of ventilation fresh and recirculated air, depending on operating mode (HP or AC). In addition, the AHU assembly house two electric heating coils, located downstream of HX1, with a heating capacity of 11 kW each.

As depicted in *Figure 3.4*, the supply air is driven by two main fans (g) located inside the AHU assembly, in addition to one support fresh-air fan (b) located in the HRS module; while the extract air is driven by one fan (c) located in the HRS module, motor specifications are listed in *Table 3*.

The main supply-air fans provide a constant air volume rate, corresponding to the active operating mode listed in *Table 2* (heating, transition, cooling). The support fresh-air and the exhaust air fans, located inside the HRS module, operate at variable speed. The exhaust air fan motor is controlled to maintain an overpressure of 10-29 Pa inside the passenger compartment.

Consequently, the amount of air extracted by the exhaust air fan is lower than the amount of fresh air supplied by the support fresh-air fan. All of the fan motors are located directly in the airstream, thus constituting a sensible heat gain to the supply air, equal to the total power of the fan motors.

Table 3: Technical specifications AHU & HRS fan motors onboard NSB Stadler FLIRT. Where EC stands for electronically commutated, which is a brushless, direct current, external rotor type of motor, with built in electronically PWM control. AC (active current) (FTL).*

AHU & HRS fan motor specification					
Fan motor	Power supply	Number	Location	Type	Total power at max load
Main supply	230V-3-50Hz AC*	2	AHU	EC	approx. 0.8 kVA (each)
Support fresh	110V DC	1	HRS	EC	365 W
Exhaust air	110V DC	1	HRS	EC	365 W

All of the AHU fan motors are electronically commuted (EC) motors, which use permanent magnet rotors and a series DC powered coils to create several PWM stator fields. These types of motors typically run cooler and achieve higher efficiency, both at maximum and part load operation, than similar capacity asynchronous motors. Moreover, EC motors offers low generation of noise and have a long service life.

The HRS transfer heat from the exhaust air to the fresh air, thus pre-heating the ventilation fresh air with the exhaust air, as depicted in *Figure 3.5*; consequently, leading to a substantial reduction in ventilation fresh air heating demand. The HRS utilize a cross-flow air-to-air plate heat exchanger. The recuperative heat exchanger design preclude cross-contamination of moisture, odors and particles between the two air streams.

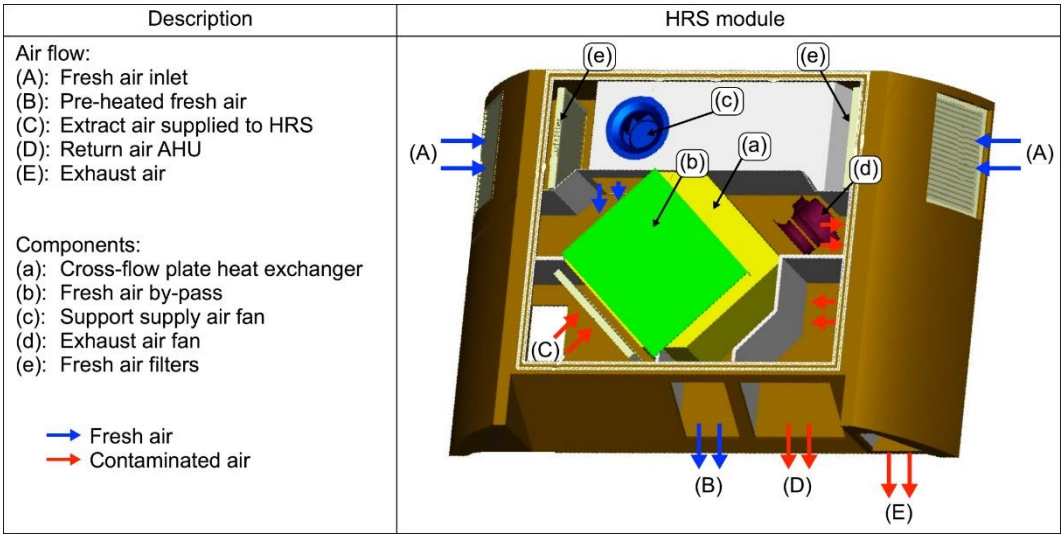

Figure 3.5: Visual representation of the HRS assembly onboard NSB Stadler FLIRT, describing the different airflows and comprising components.

Proper water drainage to the carriage roof is facilitated via a pipe socket, as large amounts of moisture from the exhaust air (C) will condense on the cold heat exchanger surface during low ambient temperature operation. The water is drained away from the carriage roof to avoid accumulation of ice. Moreover, the HRS has a built in fresh air bypass to avoid build-up of frost

on the heat exchanger surface. The bypass opening is regulated based on ambient temperature and effectively redirects a portion of the fresh air, thus allowing for a higher heat exchanger surface temperature; however, at the expense of heat recovery efficiency. Moreover, the bypass is active during cooling (AC) operation, specified in *Table 2.*

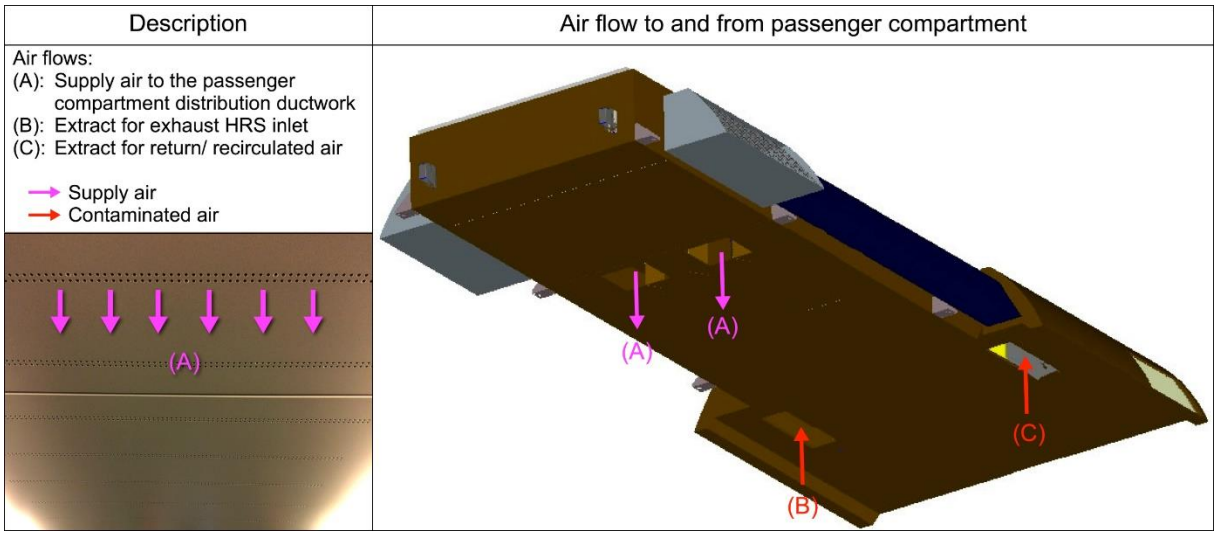

Figure 3.6: Visual representation of the airflow to and from the passenger compartment, onboard the NSB Stadler FLIRT.

The supply air is distributed to the passenger compartment at very a low impulse through grills extending over the whole ceiling surface, as depicted in *Figure 3.7*. Air is extracted from the passenger compartment at two separate ceiling height extracts. One extract is connected to the HRS (B), and the other is connected to the AHU recirculation duct AHU (C), as depicted in *Figure 3.6* and *3.7.*

Figure 3.7: Distribution of ventilation air onboard the NSB Stadler FLIRT. Where the blue arrows represent flow of fresh air, the red arrows represent flow of extract air, (A) is the supply air outlet of the HVAC unit connected to the supply air distribution ductwork, (B) is the extract air inlet of the HRS, and (C) is the return air inlet for the AHU.

3.2 Vapor compression unit

3.2.1 Standard R134a unit

The standard R134a HVAC units, developed by *FTL*, are specially designed for the Nordic conditions encountered by the NSB *Stadler* FLIRT trainsets. The reversible functionality, reportedly, enables the unit to operate as a heat pump down to an ambient temperature of -10°C.

The R134a unit holds two independently operated reversible circuits, A and B, as depicted in *Figure 3.8*. The dual circuit layout provides an additional capacity control range, in addition to improved system redundancy, as the need for simultaneous operation of both circuits seldom occurs. Moreover, during HP operation, one circuit can be intermittently operated in AC mode to provide de-frosting of the exterior heat exchanger (HX2).

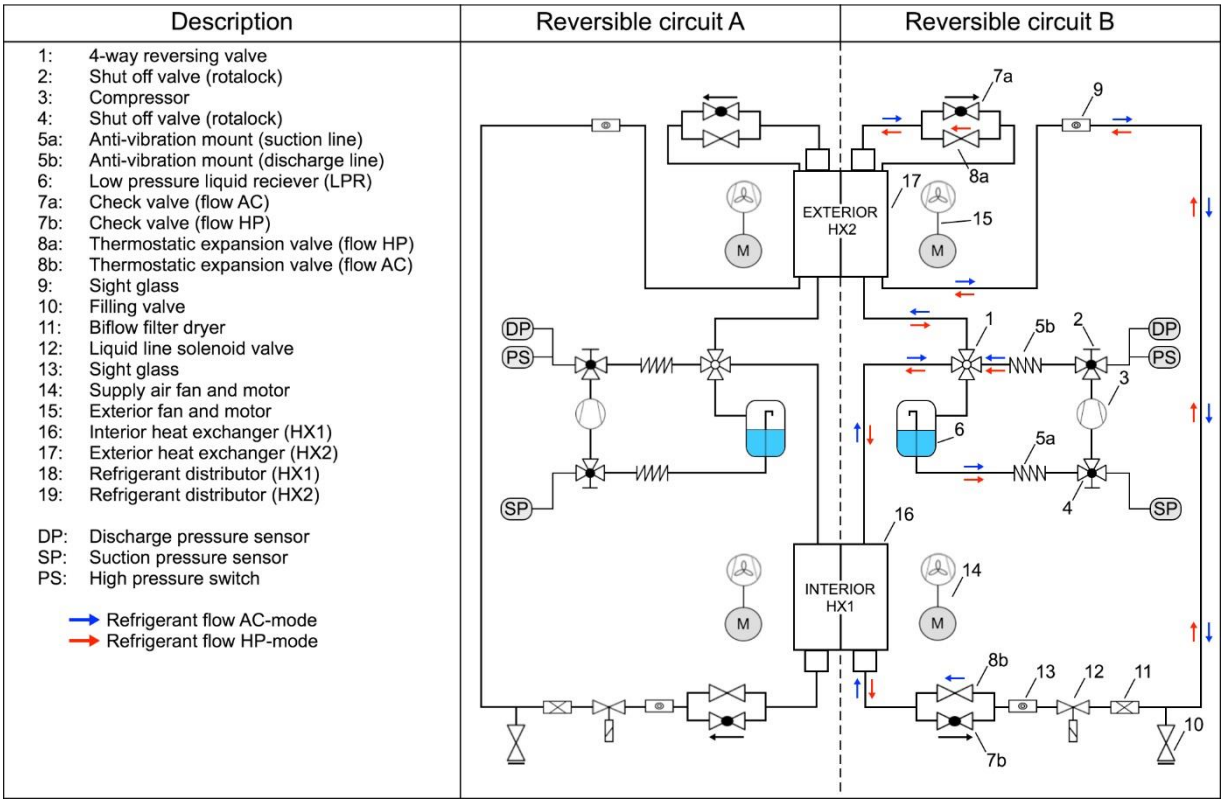

Figure 3.8: Float chart of the VCU in the reference R134a HVAC unit, describing refrigerant flow direction for different modes of operation, components.

Heating and cooling capacity for each individual circuit can be decreased 50% through the means of closed suction cylinder unloading; consequently, capacity of the unit can be reduced in four steps (100, 75, 50 and 25%).

The standard R134a HVAC unit have been designed to cover a compartment cooling demand of 23 kW at the design summer conditions specified in section 3.1.2 (EN 13129), according to specification sign on the physical HVAC unit.

Table 4: Heating and cooling capacity of the standard R134a HVAC, where specifications listed for cooling mode operation corresponds to the compartment demand during design conditions for climatic zone III specified in EN 13129 (FTL).

Statet heating & cooling cpacity of the standard R134a HVAC				
Operating mode	Circuits in operation	Capacity HX1 [kW]	Ambient condtions	
			Temperature [℃]	Relative humidity(RH) [%]
Cooling (AC)	2	23	28℃	45
Heating (HP)	2	15.4	-10℃	90
Heating (HP)	1	11.4	6℃	80

The HVAC unit includes two electric heating coils, able to cover the entire ventilation heating demand of 22 kW at design winter conditions; hence, there is no minimum capacity requirements for HP operation. However, *FTL* reports that the unit can supply 15.4 kW heat to the ventilation air at the limiting ambient temperature of -10℃, see *Table 4*.

As explained previously in section 2.2.6, the risk of frost formation on the exterior heat exchanger during HP operation is greatest during ambient temperatures of approximately 7 to -2℃. This have been taken into consideration when developing the control strategy for the HVAC unit; hence, only one circuit operates in HP operation during these ambient conditions, e.g. 6℃ and 80 % RH in *Table 4*. Thus, the idle circuit can be intermittently operated in AC mode to provide de-frosting of HX2.

3.2.1.1 Compressors

The R134a HVAC unit holds two four-cylinder semi-hermetic reciprocating compressors with integrated crankcase heater, developed by the German manufacturer *Bitzer*, depicted in *Figure 3.9.* The compressors are mounted to the unit with vibration reducing mounts to help mitigate transportation of noise and vibrations. Moreover, the suction and discharge line include a section of vibration reducing pipeline, depicted in *Figure 3.9* (5a and 5b).

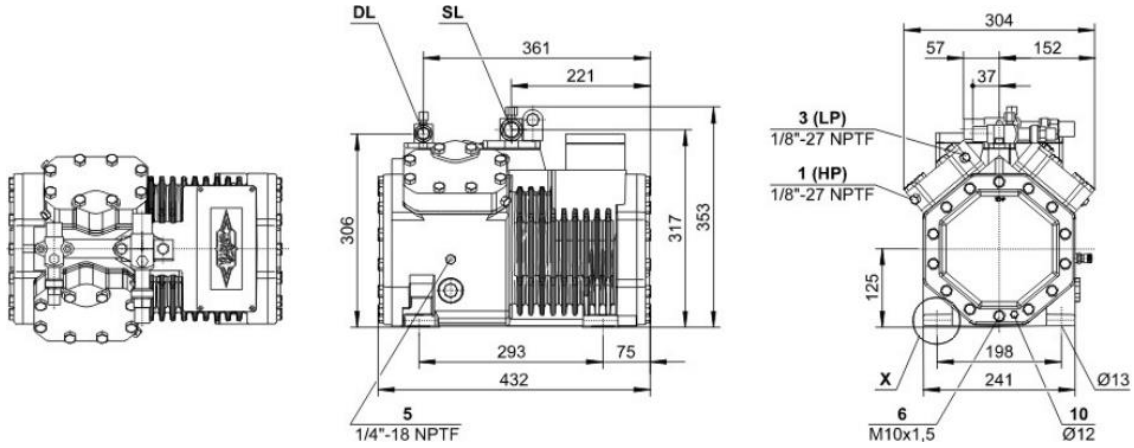

Figure 3.9: Dimensions and connections Bitzer 4EC-6.2 compressor, installed in the R134a HVAC. Where LP and HP refers to nipple mounts for suction and discharge pressure sensors and pressure switches, and DL and SL abbreviates discharge line and suction line, respectively (Bitzer).

The compressor is driven by an integrated asynchronous motor, which have a rotational speed of 1450 RPM for the constant supply frequency of 50 Hz. The compressor capacity can be reduced 50% through the means of closed suction cylinder unloading, provided by a solenoid valve mounted on the cylinder head. The closed suction effectively cuts of compression work from one cylinder block, i.e. two cylinders, when the solenoid is energized. *Table 5* lists an excerpt of the technical specifications for the *Bitzer* 4EC-6.2, listed data is for each compressor.

Table 5: Technical specifications Bitzer 4EC-6.2, data specified in the table is for each compressor while the HVAC unit comprise two (Bitzer,& FTL).

Bitzer 4EC-6.2							
Motor	Power supply	Type	Max operating current	Max starting current	Design load ta = 28°C RH = 45%		Extreme load ta = 35°C RH = 45%
	400V-3-50Hz AC*	Asyncronous	10.8 [A]	62.2 [A]	approx. 4.4 [kVA]		approx. 4.8 [kVA]
Compressor		Number of cylinders	Bore x stroke	Displacement (1450 RPM)	Max pressure		Oil charge
					DP	SP	
		4	46 [mm] x 39.5 [mm]	22.72 [m3/h]	28 [Bar]	19 [Bar]	2.00 [dm3]

The compressor motor have integrated overload protection, which effectively cuts off the power supply when an over temperature is measured on the motor windings. Moreover, a high-pressure switch connected to the discharge line, depicted in *Figure 3.8* (PS), ensures system shut down for pressures exceeding the design limitations.

3.2.1.2 Heat exchangers

The standard unit comprise two heat exchangers, one interior heat exchanger (HX1) located in the AHU assembly, and an exterior heat exchanger (HX2) located in the VCU assembly, as previously depicted in *Figure 3.3.* Both of these are constructed in aluminum fins and copper tube.

The function of HX1 is to exchange heat with the supply air, hence acting as an evaporator during AC mode and a condenser during HP mode. Consequently, air temperature and humidity at the air-inlet is determined by the state of the fresh- and return-air mixture, which in turn is dictated by the state of the ambient and compartment air, and the return/fresh air ratio, listed in *Table 2.*

As may be observed in *Figure 3.10* the two circuits of HX1 have a 50-50 vertical interlaced division with 10 columns and 8 rows each. Refrigerant flow direction through HX1 change depending on operating mode (AC or HP), whereas the direction of airflow remains unchanged;

consequently, one mode of operation will result in co-current flow while the other in cross-current flow. Cross-current flow through HX1 occurs in AC mode.

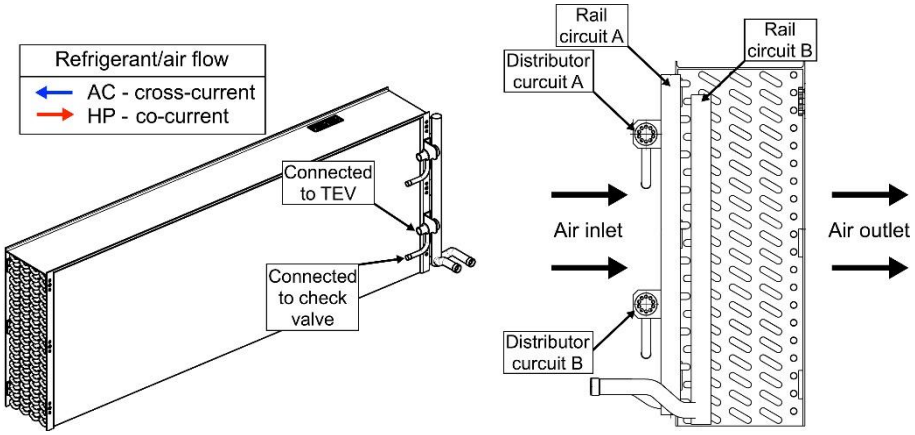

Figure 3.10: Interior heat exchanger (HX1) R134a HVAC, showing the division of the two circuits, in addition to vertical and horizontal distribution. Where distributor refers to refrigerant distributer and rail refers to refrigerant receiver rail.

The refrigerant tubes of HX1 are connected to refrigerant distributers on one side, and a refrigerant receiver rail on the other, depicted in *Figure 3.10*. The refrigerant distributor is coupled to the evaporator inlet, i.e. the refrigerant inlet of HX1 when system operates in AC mode. Some specifications for HX1 have been listed in *Table 6*.

Table 6: Technical specifications interior heat exchanger (HX1) R134a HVAC (FTL).

HX1 - R134a HVAC							
Fin	Material	Spacing		Thickness	Length	Heigth	Depth
	Au	2.0 mm		0.2 mm	1400 mm	500 mm	173 mm
Tube	Material	Spacing		Diameter		Number of passes	
		Horizontal	Vertical	Outer	Inner	Horizontal	Vertical
	Cu	25 mm	21.6 mm	9.53 mm	9.25 mm	8	10 (per circuit)
Fans	See AHU main supply fans *Table 3*						

The exterior heat exchanger (HX2) is located inside the VCU assembly and functions as a condenser during AC mode and an evaporator during HP mode. Circuit division and refrigerant flow through HX2 is quite different from HX1, as can be observed in *Figure 3.11*. Whereas HX1 have a vertical interlaced division, HX2 is horizontally split in two parts, an upper part and a lower part, as depicted in *Figure 3.11*. Moreover, a section of HX2 is used for sub-cooling of liquid refrigerant.

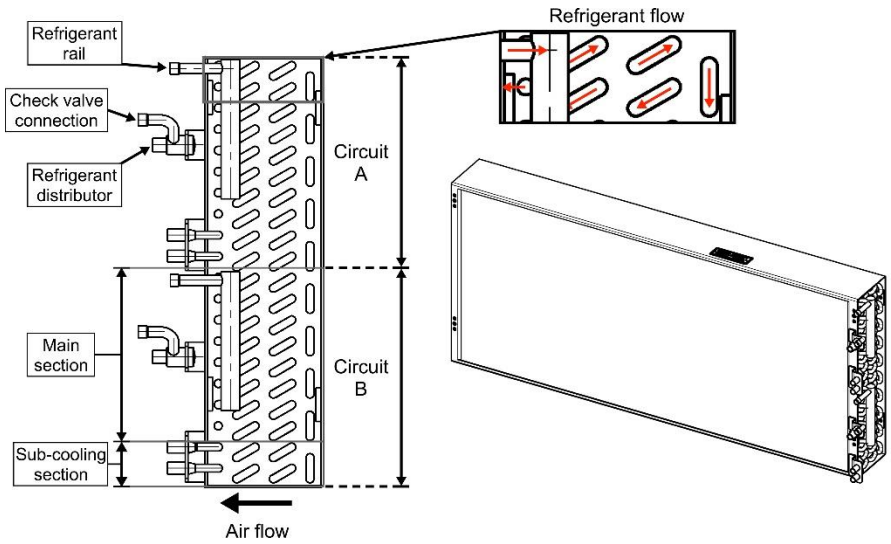

Figure 3.11: Exterior heat exchanger (HX2) R134a HVAC, showing the division of the two circuits, in addition to refrigerant and airflow through the heat exchange.

Refrigerant distributors are connected to the evaporator inlet, i.e. the refrigerant inlet when unit operates in HP mode.

The airflow through HX2 is supported by two fans located inside the VCU, as depicted in *Figure 3.3* (h). The two fans are driven by asynchronous motors and provide a total air volume rate of 8000 m^3/h for the constant supply frequency of 50 Hz. During low capacity demands one fan motor can be switched off, consequently reducing air volume rate by ≈ 50%. Some technical specifications for HX2 have been listed in *Table 6*.

Table 7: Technical specifications exterior heat exchanger (HX2) R134a HVAC (Faiveley).

HX2 - R134a HVAC							
Fin	Material	Spacing		Thickness	Length	Heigth	Depth
	Au	3.2 mm		0.3 mm	1100 mm	500 mm	130 mm
Tube	Material	Spacing		Diameter		Number of passes	
		Horizontal	Vertical	Outer	Inner	Horizontal	Vertical
	Cu	25 mm	21.6 mm	9.52 mm	9.25 mm	6	10 (per circuit)
Fans (each)	Power supply		Number	Air volume rate		Supplied power (each)	
	400V-3-50Hz		2	4000 m3/h		≈ 1.0 kVA	

3.2.1.3 Expansion device

The R134a HVAC unit holds four thermostatic expansion valves (TEV), two for each circuit. The active expansion valve, depending on operating mode, is mechanically adjusted based on evaporator outlet temperature, as described earlier in section 2.2.5. By-pass of the inactive expansion valve is achieved through check valves, as depicted in in *Figure 3.8* (7a) & (7b).

3.2.2 Pilot R744 unit

The pilot R744 HVAC unit have been designed to fit similar HVAC module casing as the standard R134a unit, and does, as the standard unit, hold two reversible refrigerant circuits; however, whereas the two circuits in the standard unit is identical, the layout of the two R744 circuits have some differences, as may be observed in *Figure 3.12*.

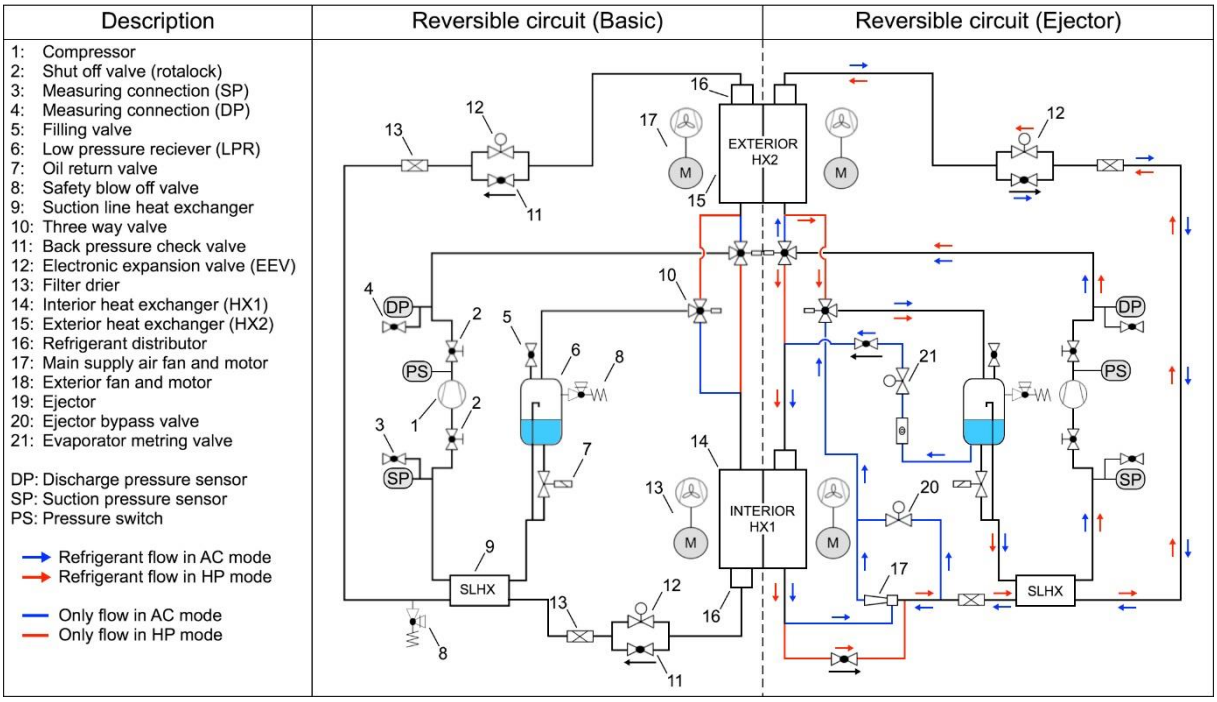

Figure 3.12: Float chart of the VCU in the pilot R744 HVAC unit, describing refrigerant flow direction for different modes of operation, and components.

The pilot R744 HVAC unit holds one basic circuit and an ejector circuit, as depicted in *Figure 3.12*. The difference between the two is that the ejector circuit utilize ejector-supported expansion when operated in AC mode. Reconfiguration of refrigerant flow upon mode switch, is facilitated by two three-way valves. Similarly to the standard unit, the two circuits can be independently operated.

Like the standard unit, the pilot unit is dimensioned to cover a compartment cooling demand of 23 kW at design summer conditions; however, some inconsistencies with regard to these requirements have been disclosed in section 4.2.4.4.

For heat pump operation, *FTL* expect similar capacities as for the standard unit; however, whereas operation of the standard unit is limited to an ambient temperature of -10°C, the pilot unit can offer operation down to -20°C. The larger range of operation can in itself offer substantial energy savings. Moreover, as previously explained the amount of fresh air bypassed

the HRS increase during low ambient temperatures; hence, increasing the potential energy savings of the pilot unit even further.

The refrigerant charge of the ejector circuit is higher than the basic circuit, due to additional piping and to enabling a flooded evaporator; consequently, the R744 charge is 5.44 kg and 6.59 kg for the basic and ejector circuit, respectively. To facilitate safe containment of the charge and mitigate excessive standstill pressure, the volume of the accumulator (LPR) in the ejector circuit is larger than the one installed in the basic, having a volume of 7.5 and 5 liters, respectively.

The AC and HP performance of the pilot unit was tested during laboratory bench tests at the *FTL's* R&D laboratory in Schkeuditz. The method behind the conducted tests and the results presented in this thesis have been described and presented in section 4.2 and chapter 5, respectively.

3.2.2.1 Compressors

The pilot unit holds two two-cylinder semi-hermetic reciprocating compressors with integrated crankcase heater, developed by the German manufacturer *Bitzer*, depicted in *Figure 3.13.* Even though the R744 compressors only have 15% of the R134a compressors displacement, the R744 compressor outweighs the R134a compressor by 10%, having a drained weight of 94 kg. The substantial weight of the R744 compressor is largely attributed to the high operating pressures.

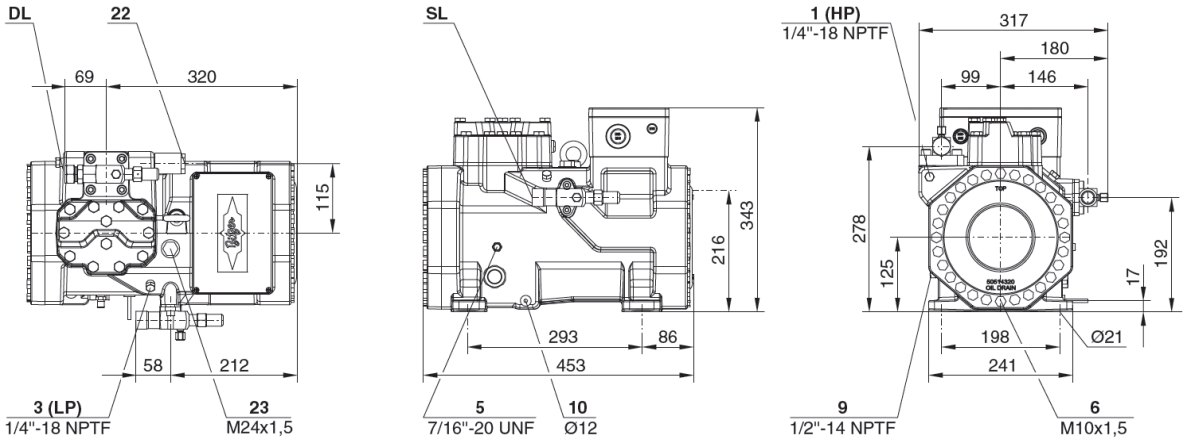

Figure 3.13: Dimensions and connections Bitzer 2MTE-5K compressor, installed in the pilot R744 HVAC. Where LP and HP refers to nipple mounts for suction and discharge pressure sensors and pressure switches, and DL and SL abbreviates discharge line and suction line, respectively (Bitzer).

The compressor motor operate at similar speed as the R134a compressor (1450 RPM at 50Hz), and include similar overload and overpressure protection, however, with set to a higher pressure limit (approx. 102 bar).

Both of the compressors utilize *Bitzer's* newly developed *CRII* capacity modulation system which, simply put, is PWM cylinder unloading.

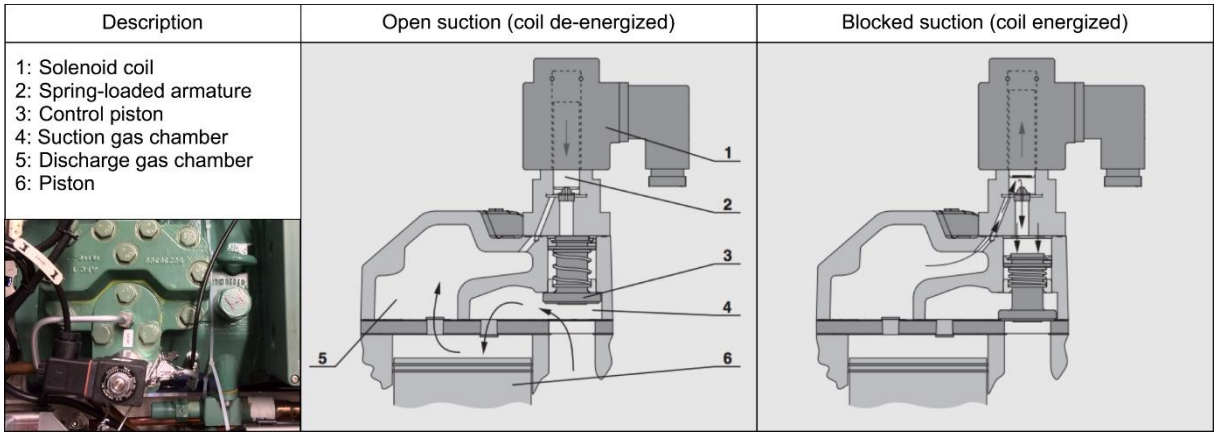

Figure 3.14: Bitzer CRII capacity modulation system, depiction of cylinder head with mounted PWM solenoid valve for capacity modulation (Bitzer).

The *CRII* system is based on the principle of blocked suction port, depicted in *Figure 3.14*. At part load, the solenoid coil is intermittently energized by a PWM signal, which opens up a port leading from the discharge gas chamber to the rear of the control piston; hence, pushing down the control piston, thus blocking the suction port. Consequently, the resulting reduction in capacity depends on the cycle intervals of the PWM signal, which is governed by the HVAC control unit.

The *CRII* system have been commercially available for a wide range of *Bitzer* compressors since 2014; however, not for two-cylinder compressors like the *2MTE-5K*, probably because the suction for the whole cylinder block, i.e. both cylinders, have to be intermittently cut off; consequently, leading to relatively large fluctuations in system conditions. This affects the range of controllability, as the lower the capacity output, the larger the fluctuation in system conditions will be. Nevertheless, *Bitzer* claims that capacity of the two-cylinder compressor can be reduced down to 20% without any problem, by using a 2-second open and 8-second close cycle; however, closing cycles of less than 2-seconds are not recommended.

Table 8 lists an excerpt of the technical specifications for the *Bitzer 2MTE-5K*, listed data is for each compressor.

Table 8: Technical specifications Bitzer 2MTE-5K, data specified in the table is for each compressor while the HVAC unit comprise two (Bitzer & FTL).

Bitzer 2MTE-5K							
Motor	Power supply	Type	Max operating current	Max starting current	Design load ta = 28°C RH = 45%		Extreme load ta = 35°C RH = 45%
	400V-3-50Hz AC*	Asyncronous	11.5 [A]	62.0 [A]	approx. 4.3 [kVA]		approx. 5.7 [kVA]
Compressor		Number of cylinders	Bore x stroke	Displacement (1450 RPM)	Max pressure		Oil charge
					DP	SP	
		2	30 [mm] x 27 [mm]	3.3 [m3/h]	100 [Bar]	160 [Bar]	1.20 [dm3]

3.2.2.2 Heat exchangers

The pilot unit, does like the standard unit, house an interior heat exchanger (HX1) located in the AHU assembly, and an exterior heat exchanger (HX2) located in the VCU assembly. Additionally, each of the circuits in the pilot unit include an internal heat exchanger for transportation of heat from the liquid line to the suction line, i.e. a suction line heat exchanger (SLHX).

It proved challenging to find a manufacturer willing and able to deliver the heat exchangers for the pilot unit. This can largely attributed to the low production volume, and the high burst pressure requirements for railway HVAC equipment, i.e. three times maximum operating pressure (approx. 300 bar).

Moreover, as the system is reversible, both HX1 and HX2 have to withstand high-side pressure. This led to a change of supplier in the summer of 2016, as the heat exchangers ruptured during the burst tests. Eventually, new heat exchangers were delivered by the Israeli manufacturer *Lordan.*

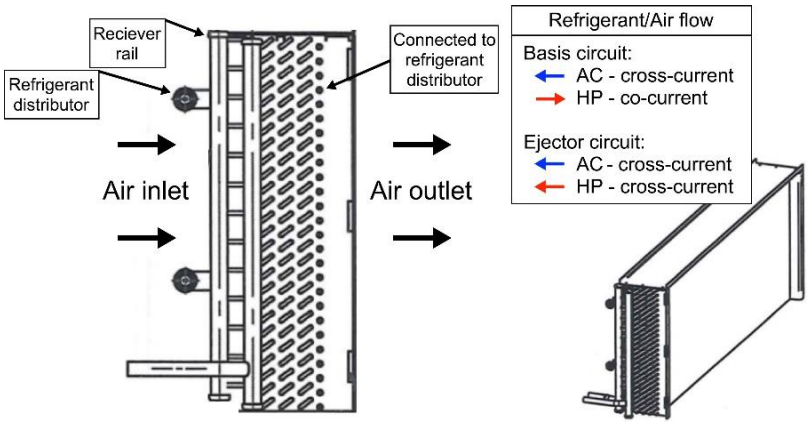

Figure 3.15: Interior heat exchanger (HX1) of the pilot R744 HVAC, showing the division of the two circuits, in addition to vertical and horizontal distribution, and flow. Where distributor refers to refrigerant distributer and receiver rail refers to refrigerant receiver rail (Lordan).

The interior heat exchanger (HX1) of the pilot unit, depicted in *Figure 3.15*, is a fin-and-tube heat exchanger with vertical fins and a 50-50 vertical interlaced tube division of the two circuits. HX1 functions as an evaporator during AC mode and a gas-cooler during HP mode.

Because of the piping configuration of the ejector circuit, shown in *Figure 3.12*, the flow through HX1 is similar for both modes of operation, whereas the flow direction is switched in the basic circuit. Thus, the two refrigerant circuits will be in flowing in opposite direction when both circuits are operated in HP mode; consequently, this can constitute a substantial loss in performance as HX1 functions as a gas-cooler when the pilot unit operates in HP mode, thus performance is highly linked to refrigerant outlet temperature, as explained in section 2.2.3.3. Moreover, the operation of the ejector circuit in HP mode should be prioritized over the basic circuit, as the refrigerant is in cross-current flow with the supply air.

The ejector circuit side of HX1 will be completely flooded during AC operation, facilitated by the standard two-phase ejector cycle layout, previously explained in section 2.2.5.2. Consequently, HX1 heat transfer efficiency of the ejector circuit is expected to be far greater than that of the basic cycle in AC mode operation. Additional specifications for HX1 on the pilot unit have been listed in *Table 9.*

Table 9: Technical specifications interior heat exchanger (HX1) of the pilot unit (Lordan)

HX1 - pilot R744 HVAC							
Fin	Material	Spacing		Thickness	Length	Heigth	Depth
	Au	-		0.15 mm	1350 mm	500 mm	173 mm
Tube	Material	Spacing		Diameter		Number of passes	
		Horizontal	Vertical	Outer	Inner	Horizontal	Vertical
	Cu	-	-	5.0 mm	4.59 mm	8	10 (per circuit)
Fans	See AHU main supply fans *Table 3*						

The exterior heat exchanger (HX2) of the pilot unit, depicted in *Figure 3.16*, functions as an evaporator during HP mode and a gas-cooler during AC mode. As can be observed in the *Figure 3.16*, the division of the two circuits is similar to HX1; however, HX2 is smaller and only have a six horizontal tube passes, whereas HX1 has eight.

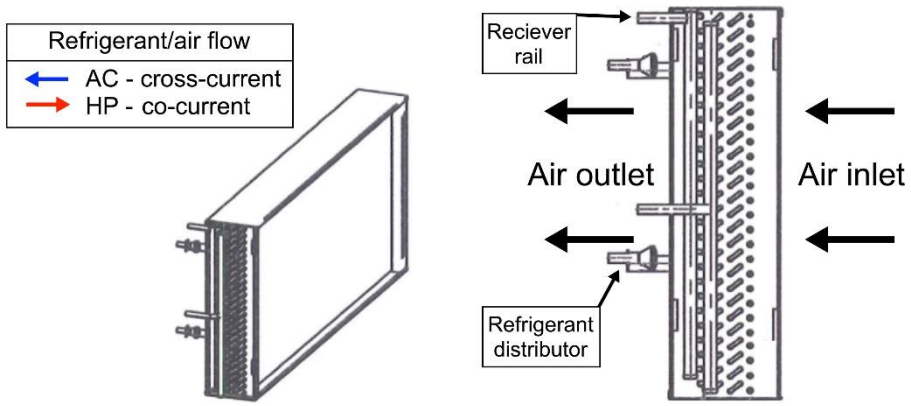

Figure 3.16: Exterior heat exchanger (HX2) of the pilot R744 HVAC, showing the division of the two circuits, in addition to vertical and horizontal distribution, and flow. Where distributor refers to refrigerant distributer and receiver rail refers to refrigerant receiver rail (Lordan).

The refrigerant flow direction through HX2 is altered for both circuits upon mode switch, resulting in cross-current flow between refrigerant and air in AC mode, when HX2 functions as a gas-cooler, as depicted in *Figure 3.16*. Additional specifications have been listed in *Table 10*.

Table 10: Technical specifications exterior heat exchanger (HX2) of the pilot unit [Lordan]

HX2 - pilot R744 HVAC							
Fin	Material	Spacing		Thickness	Length	Heigth	Depth
	Au	-		0.2 mm	1100 mm	495 mm	76.2 mm
Tube	Material	Spacing		Diameter		Number of passes	
		Horizontal	Vertical	Outer	Inner	Horizontal	Vertical
	Cu	-	-	5.0 mm	4.4 mm	6	10 (per circuit)
Fans (each)	Power supply		Number	Air volume rate (each)		Supplied power (each)	
	400V-3-50Hz		2	4000 m3/h		≈ 1.0 kVA	

Both refrigerant circuits of the pilot unit also include a small tube-in-tube SLHX, which transports heat from the liquid line to the suction line. Flow through the SLHX is parallel for HP mode and counter-flow in AC, as may be observed in *Figure 3.12*.

3.2.2.3 Expansion devices

The pilot unit include several expansion devices, serving a number of different purposes. The ejector circuit holds three identical EEVs by the Italian manufacturer *Carel*, in addition to a two-phase ejector specially made by the Danish manufacturer *Danfoss*; while the basic circuit holds two of the *Carel* EEVs.

As explained in section 2.2.5.1, the expansion device in a transcritical vapor compression system serves the crucial purpose of regulating the high-side pressure, in addition to ensure superheated vapor at the evaporator outlet (DX).

During HP mode operation, one of the three EEVs in the ejector circuit provides "regular" fluid expansion from high-side to low-side pressure (see *Figure 3.12* (12)), similar to the standard unit this valve is bypassed through a check valve in AC operation.

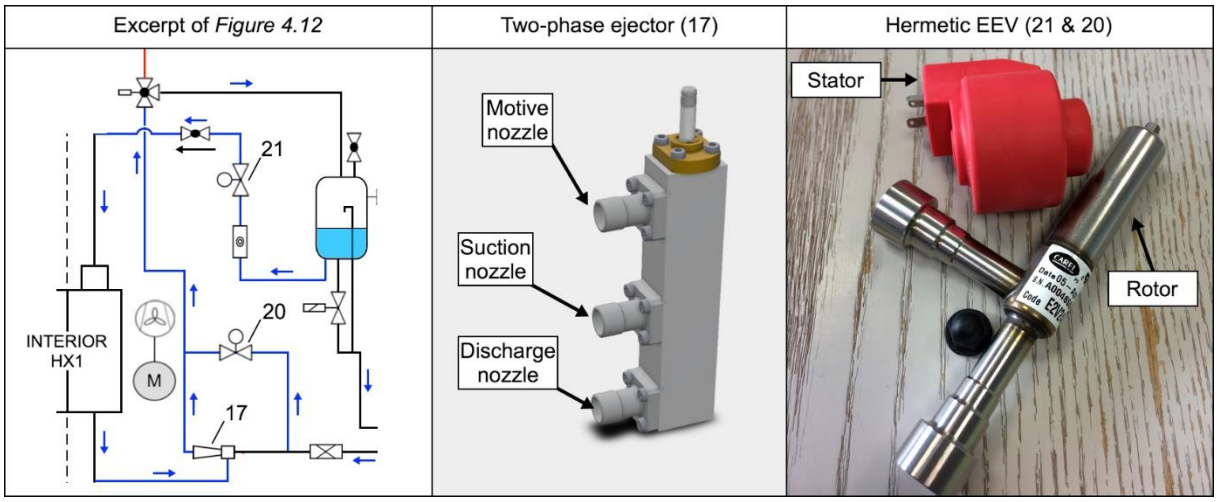

Figure 3.17: AC ejector circuit layout, two-phase ejector, and EEV. Where the middle figure depicts the Danfoss ejector, specially made for the R744 HVAC pilot project, and the left figure depicts the Carel E2V EEV with hermetically welded rotor (Dansfoss & Carel).

During AC mode operation the expansion process in the ejector circuit is supported by a two-phase ejector. As can be observed in *Figure 3.17*, the suction port of the ejector is coupled to the outlet of HX1 and is at evaporator pressure, maintained by a metering valve (21).

In order to facilitate high-side pressure control, a bypass leading from the line upstream of the motive inlet to the line downstream of the discharge outlet (of the ejector) can be regulated with an EEV (*Figure 3.17* (20)). Consequently, high-side pressure can be reduced or increased, by increasing or reducing the valve opening of EEV 20, respectively, for a constant compressor output.

In the basic circuit, fluid expansion in both HP and AC mode operation is occurring through EEVs regulated with regard to suction gas temperature. Similar to the standard R134a unit, the expansion valves are bypassed through check valves when not active, as depicted in *Figure 3.12*.

4 Methodology

4.1 Analyzing field data measurements from reference unit

As explained in the introduction of this thesis, one of the initial tasks to be conducted during the thesis work was to analyze and process the recorded field data measurements from the reference unit, and from the pilot unit when commissioned into operation.

However, due to several setbacks, the pilot unit was not commissioned onboard the trainset during the thesis work. Moreover, due to numerous issues with the reference unit DAQ system, disclosed below, analysis potential of the field data measurements became severely limited.

Consequently, although an extensive amount of effort was spent on describing the DAQ system and decoding the record file signals, it was decided to prioritize the laboratory bench tests of the pilot unit, described and presented in section 4.1 and chapter 5, respectively, in the Master Thesis. Thus, most of work related to section 4.1, have been included in Appendix A.

Although not of significant relevance for the topics disclosed in this thesis, the DAQ system, description included in Appendix A, greatly benefits future work on the pilot R744 HVAC unit project.

It must be noted that Appendix A should be reviewed in order to get a full understanding of the topics disclosed in the subsections below, i.e. 4.1.1 to 4.1.4.

4.1.1 Commissioning of the reference unit

Commissioning of the reference R134a HVAC unit, with the retrofitted DAQ system, took place at NSB main workshop in Sundland, Drammen. The installation of the reference unit was, conducted by a team from *Stadler*, and took approximately three days to complete. The student was present during two of these days, and took part in the initial system startup conducted by a service technician.

During the initial system startup, the reference unit was operated in service mode in order to verify its various functionality. After some initial problems with the DAQ system was sorted, the reference unit seemed to be functioning as intended.

In order to establish that the data-logger (CCM8) operated as expected, data from the service operation was uploaded from the SD card to a laptop, and briefly inspected. When the record file was imported into *Excel*, data from unknown sources, and stated as unknown values was presented in 82 columns. As no signal description had been provided by *FTL*, it was decided

that further analysis of the record data would be postponed pending a signal description from *FTL*.

As the *FTL* service software indicated reliable data from the retrofitted sensors on the reference unit, the BM 75-41 trainset was commissioned into regular operation the following day, assuming satisfactory functionality of the reference DAQ system.

4.1.2 Problems with CM4 current measuring relay

Three days after the BM 75-41 was commissioned into regular operation, the trainset had to be taken back to the workshop in Sundland, due to a malfunction with the reference unit. The malfunction was due to a communication error between the HVAC controller (FPC24/2) of the reference unit, and the train system CAN-bus. After four days at the workshop, the trainset was commissioned into regular operation again. However, after this event, data measured via the CM4 current measuring relay, was no longer listed with valid values in the record file. The reason for the defect CM4 was not disclosed by *FTL*.

Consequently, this put limitations as to what could be deduced from the recorded data, as the CM4 measured HVAC equipment energy consumption, as described in Appendix A.

4.1.3 De-coding the record file signals

FTL provided a signal description for the reference unit record-file. However, most of the information in this was vague and unclear. Consequently, a complete signal description was compiled by the student, based on email correspondences with the software developer at *FTL*, and by tracking each of the 82 signals in the in the DAQ system wiring diagrams.

The complete signal description of the reference unit DAQ system have been included in Appendix A.

4.1.4 Issues with the recorded data

As previously explained, issues occurred with the CM4 device, consequently eliminating the possibility to analyze energy consumption of the HVAC equipment. However, this was far from the only uncovered issue with the DAQ system of the reference unit, as will be explained in this subsection.

Provided the signal description included in Appendix A, the task of analyzing the recorded field data was initiated. A method for determining VCU operation was established, Appendix A7, and the temperature measurements from the refrigerant circuit, Appendix A1, was assessed. However, the values from these sensors did not seem to correspond well with realistic values

from operation of an R134a VCC unit. Moreover, when assessing the data from the pressure sensors, Appendix A2, the readout from the retrofitted sensors also showed unrealistic values.

Concern was also attributed the fact that the VCC unit seemed to be operated quit infrequently during the first few months of operation, i.e. January and February. When a method for determining operating mode was established, Appendix A7, it became evident that the VCC unit had not been operated in heat pump mode, even though a ventilation air heating demand was clearly present numerous times during the evaluated period, as the electric heating coils where frequently operated.

All of the issues uncovered during analysis, were presented for *FTL* during the second visit to Schkeuditz. It was concluded that there were severe issues with the data from all of the retrofitted sensors, i.e. Appendix A1, parts of Appendix A2, and Appendix A3. Moreover, it was confirmed by *FTL* that the standard units did not operate in heat pump mode, because of an insufficient capacity control range, and limited amount of ventilation air heating demand after the HRS.

A software miss-match between that installed on the CCM8 data-logger and on the reference unit HVAC controller (FPC24/2), was deemed the most probable cause for the issues with record file data. A *FTL* engineer would have to be on sight at the NSB workshop in Sundland in order to remediate the problem. However, a plan for this was not agreed upon.

The process of decoding the DAQ system signals was very time consuming, thus the full extent of the DAQ system issues was not established until quite late in the thesis work. Moreover, due to the extent of the uncovered issues, the vast majority of the recorded data proved useless.

Consequently, no further analysis of the measurement data from the reference unit was conducted.

4.2 Laboratory tests of the pilot R744 HVAC unit

Several laboratory cooling load bench tests of the pilot R744 HVAC unit, were conducted at the *Faiveley Transport (FTL)* R&D laboratory, in Schkeuditz Germany. These tests were conducted in accordance with *FTL's* safety procedures by a *FTL* test engineer. The students' role was to observe and later partake in the discussion of the gathered results with representatives from the developer, i.e. *FTL*, the project scientific adviser from *SINTEF*, and a representative from the project owners NSB.

The described tests and the corresponding results presented in this thesis, was performed and analyzed over the course of several months, whereas the student was present at the *FTL* test facilities during one week of testing. However, the student followed the development via e-mail correspondences and received summarizations of the progress. Hence, only averaged data from steady state operation, for a limited number of conditions was made available for the student.

Furthermore, due to several encountered difficulties and challenges, elaborated in subsection 4.2.4, laboratory bench testing of the pilot unit was still being conducted while this thesis was finalized. Moreover, no results from heat pump mode operation was made available to the student. Consequently, the test scenarios corresponding to the presented results, are from a limited number of maximum capacity cooling load tests.

Alterations were made to the ejector circuit after the initial laboratory tests highlighted issues resulting in excessive refrigerant superheating at the HX1 outlet, as will be explained in 4.2.4.1. A before and after comparison of the ejector circuit at design load conditions was conducted and have been described and presented in section 4.2.4.1 and 5.1, respectively. It should be noted that the all other test scenarios featured in this thesis corresponds with the ejector circuit layout depicted in Appendix C3

Challenges with regard to accurate high-pressure control of the ejector circuit, and crankcase oil foaming were also experienced, as have been elaborated in section 4.2.4.

The *FTL* reported measurement data from the laboratory tests was used to produce results describing the pilot unit performance at various ambient temperatures during individual operation of each circuit and for simultaneous operation of both circuits. However, the limited number of available test scenarios made comparable analysis challenging.

Due to insufficient cooling capacity at design conditions, performance enhancing measures were suggested, individually implemented, and tested, in order to identify the system components related to the highest drop inn performance, as will be elaborated in section 4.2.4.4.

4.2.1 Laboratory setup

In this subsection, the chamber and pilot unit setup during the laboratory bench tests, will been described. Unless specified otherwise, the design of the pilot unit during the laboratory tests corresponds with the description in section 3.2.2, and the illustration in Appendix C.

The chamber setup used during the cooling load tests have been illustrated in *Figure 4.1*. As may be observed, air was supplied to HX1, i.e. evaporator, through a closed ducting system, connected to an external HVAC. The external HVAC unit also included a humidifier; hence, it was possible to control both temperature and humidity of the supplied air (A) in order to simulate the return and fresh air mixture corresponding to "real" operation (*Table 2*).

Appendix C includes photographs of the test chamber and the pilot unit, in addition to float charts depicting the sensor layout for the two circuits (basic and ejector) used in the lab tests. The float charts in Appendix C2 and C3 illustrates the various measuring points throughout the basic and ejector circuit, respectively; whereas Appendix C4 illustrates the measuring points located in the air streams. Measuring points related to air, have been assigned names A1 to A6, whereas measuring points related to refrigerant, have been assigned names R7 to R33. The sensor addresses applied by *FTL* have also been included in Appendix C2 to C4, to facilitate comparison of results.

Both temperature and humidity was measured upstream and downstream of HX1, thus making it possible to establish total sensible and latent heat extraction. The state of the air was also measured further downstream of HX1, to include the sensible heat gain from all HVAC equipment, thus enabling the possibility of establishing the effective cooling capacity of the whole HVAC unit.

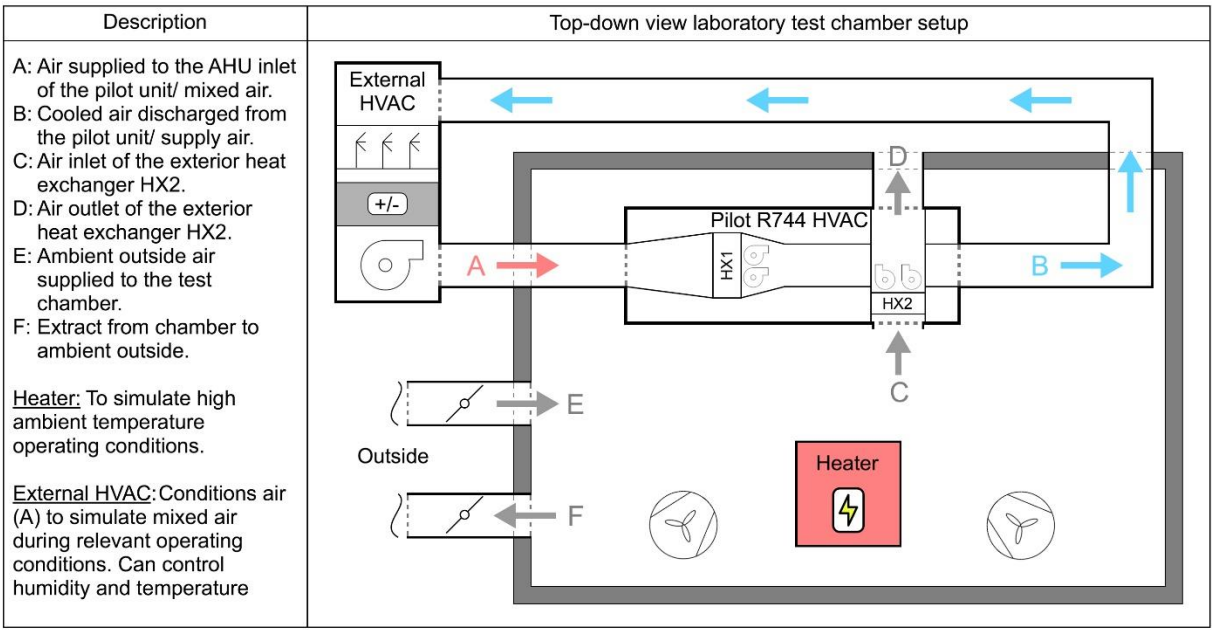

Figure 4.1: Top-down view of the FTL test chamber in Schkeuditz Germany used to conduct cooling load tests of the pilot R744 HVAC unit.

The inlet and outlet temperature of HX1 and HX2 was measured by several thermocouples spread over the inlet and outlet heat exchanger surface, as can be seen in the photograph of the AHU assembly in Appendix C1; whereas the temperature upstream and downstream of the HVAC unit was measured by single thermocouples.

As can be seen in *Figure 4.1* the air inlet (C) of HX2, i.e. gas-cooler, was exposed to the air inside the chamber. The temperature in the test chamber could be increased by an electric heater, while two air fans provided a sufficient temperature uniformity. Moreover, air could be supplied and extracted from the chamber through ducts leading outside, (F) and (E), respectively. Furthermore, the air downstream of HX2 was discharged out of the test chamber.

No personnel was allowed inside the test chamber during tests, due to *FTL's* safety protocol, with particular concerns attributed the high system operating pressures. Consequently, the control and monitoring of the test rig was conducted from an adjacent observation room.

The high-pressure switch of the pilot unit was set to 102 bar, which in practice meant a high-pressure limit of 100 bar. However, during some tests the high-pressure switch was disconnected in order to investigate 110 bar high-pressure operation, as described in section 4.2.4.4.

4.2.2 General methodology

In this section, the general methodology used to process the laboratory test data into the results presented in chapter 5, have been described.

Although, the *FTL* test summaries included relatively complete calculation results, the methodology and assumptions behind them had not been disclosed. Consequently, only measurement data, with a few disclosed exceptions, was taken from the *FTL* summaries in order to produce the results presented in this thesis.

Moreover, the process of creating the calculation model used to generate the results of this thesis, highlighted some inconsistencies related to some of the *FTL* calculations, as described and shown in section 4.2.5 and 5.5, respectively.

4.2.2.1 HVAC unit electrical power consumers

The total current and voltage supplied to the two compressor motors was measured during the tests, thus yielding the corresponding apparent (E_{sn}) and active ($\dot{P}_c$) power, whereas this was not the case for auxiliary HVAC equipment like the supply air (HX1) and HX2 fan motors.

Consequently, energy consumption of all auxiliary HVAC equipment was excluded from the calculations and the presented results. Moreover, during simultaneous operation of both circuits, the power supplied to each individual compressor could not be determined based on the measurement data. However, a polynomial provided by *Bitzer*, was used to estimate individual effective compressor power during simultaneous operation.

4.2.2.2 Air state calculations

As previously mentioned the test rig included several sensors for measuring air temperature, humidity and pressure, see Appendix C4. Based on averaged measurement data obtained from these sensors, i.e. A1 to A6, the following calculations could be conducted using the described methodology.

Calculation of the different air states was, mostly, done using *Psych* and *RnLib*. *Psych* is an open-source psychometric plug-in for Excel, which uses equations from ASHRAE 2005 Fundamentals Handbook, chapter 6; whereas *RnLib*

is an Excel plug-in developed by *SINTEF*, containing fluid property data for a number of refrigerants.

The measured air temperatures, i.e. dry bulb temperature, and the relative humidity (RH) of the AHU airstreams was examined at the different measuring points, i.e. A1, A2, A3 and A4, corresponding to the test chamber illustration in Appendix C4. The measured temperature and RH was then used, in Eq.(26), to determine the humidity ratio (x), i.e. the mass ratio between water vapor and dry air [$m_{H2O}/m_{dry\ air}$], presuming an atmospheric pressure of 101 325 Pa.

$$x_{A(n)} = \frac{p_{ws}(t_{A(n)}) \cdot RH}{p_{tot} - p_{ws}(t_{A(n)}) \cdot RH} \qquad \text{Eq.(26)}$$

Where p_{ws} (calculated in *Psych*) is the saturation pressure of water vapor and p_{tot} total pressure of the air. And the index A(n) represent the air measurement point (n), corresponding with Appendix C4.

Subsequently, the humid air specific enthalpy (I) could be determined using Eq.(27), as specified in the ASHRAE handbook.

$$I = 1.006 \cdot t_{A(n)} + x \cdot \left(2501 + 1.86 \cdot t_{A(n)}\right) \qquad \text{Eq.(27)}$$

The temperature, humidity ratio, relative humidity, dew point temperature, and specific enthalpy of the air at point A1 to A6, corresponding to the various test scenarios was calculated using *Psych*, and have been included Appendix D1, D2, and D3.

It was not clarified how *FTL* established the air volume rate used to calculate the air mass flow rate of the supply air fans ($\dot{m}_{a1}$). However, as the test rig did not include any sensors for measuring airflow or velocity, the air volume rate was most likely estimated based on the control signals, using the table included in Appendix B. Nevertheless, the *FTL* calculated supply air mass flow rates ($\dot{m}_{a1}$) was used in the calculations of this thesis.

The cooling capacity of HX1 ($\dot{Q}_{HX1}$) and the HVAC unit ($\dot{Q}_{HVAC}$) was calculated, using the difference in specific enthalpy (ΔI) and mass flow rate ($\dot{m}_{a1}$) of the supply air, as expressed in Eq.(28) and Eq.(29).

$$\dot{Q}_{HX1} = \dot{m}_{a1} \cdot \Delta I_{HX1} = \dot{m}_{a1} \cdot (I_{A3} - I_{A2}) \qquad \text{Eq.(28)}$$

$$\dot{Q}_{HVAC} = \dot{m}_{a1} \cdot \Delta I_{HVAC} = \dot{m}_{a1} \cdot (I_{A1} - I_{A4}) \qquad \text{Eq.(29)}$$

Where the indexes A1, A2, A3 and A4 corresponds with Appendix C4.

The reason for distinguishing between the cooling capacity of HX1 and the HVAC unit, was that $\dot{Q}_{HX1}$ was further used to calculate refrigerant mass flow ($\dot{m}_r$) through HX1, whereas $\dot{Q}_{HVAC}$ was used to specify the cooling capacity achieved by the whole HVAC unit, after sensible heat gain from casing transmission and equipment had been included. Consequently, an expression for the HVAC heat gains ($\dot{Q}_{gain}$) could be deduced, Eq.(30).

$$\dot{Q}_{gain} = \dot{Q}_{HX1} - \dot{Q}_{HVAC} \qquad \text{Eq.(30)}$$

Moreover, an expression describing the amount of water condensed on the HX1 ($\dot{X}_{cond}$) surface was established using $\dot{m}_{a1}$ and the inlet/outlet humidity ratio difference, Eq.(31).

$$\dot{X}_{cond} = \dot{m}_{a1} \cdot \Delta x_{HX1} = \dot{m}_{a1} (x_{A4} - x_{A3}) \qquad \text{Eq.(31)}$$

Furthermore, the amount of latent heat extracted from the air at HX1 ($\dot{Q}_{HX1,lat}$) could then be determined by multiplying the rate of condensed water with the specific latent heat of evaporation at atmospheric pressure (I_{sat} = 2254 kJ/kg (*RnLib*)), Eq.(32). Subsequently, the extracted sensible heat could be calculated with Eq.(33).

$$\dot{Q}_{HX1\_lat} = I_{sat} \cdot \dot{X}_{cond} \qquad \text{Eq.(32)}$$

$$\dot{Q}_{HX1\_sens} = \dot{Q}_{HX1} - \dot{Q}_{HX1\_lat} \qquad \text{Eq.(33)}$$

It is important to note that some of the calculated values were stated as kg/h.

The air volume rate over HX2 was not measured during the tests. Consequently, the two constant speed fans were assumed to provide 4000 m^3/h each, as specified earlier in *Table 7*. The corresponding air mass flow rate ($\dot{m}_{a2}$) over HX2 was calculated using the humid air density corresponding to the temperature downstream of HX2, as this was where the fans were located, again assuming atmospheric pressure. Finally, the heat rejected to the air at HX2 could be calculated using the expression in Eq.(34).

$$\dot{Q}_{HX2} = \dot{m}_{a2} \cdot C_{p,air} \cdot (t_{A6} - t_{A5}) \qquad \text{Eq.(34)}$$

Where the indexes of t_{A5} and t_{A6} corresponds with measuring point A5 and A6 in Appendix C4, and.

As explained in section 4.2.3.4, the voltage and frequency of the current supplied to the HX2 fan motors was increased to 480V and 60Hz, during some of the tests. Consequently, the air volume rate through HX2 during these tests could not be assumed to be 4000 m^3/h per fan.

4.2.2.3 Refrigerant basic circuit

As previously mentioned the test rig included numerous sensors for measuring refrigerant temperature and pressure in the basic circuit, illustrated in Appendix C2. Based on the data obtained from these sensors, the following calculations could be conducted using the methodology described below.

Calculation of the refrigerant properties at various measurement points was performed using the *Excel* plug-in *RnLib*. Additionally, the plot function in *CoolPack* was used to illustrate the various cycles in log(p)h-diagrams.

Moreover, due to issues related to some of the output values from *RnLib*, *CoolPack* served as a quality insurance. The issues experienced with *RnLib* stemmed from an incompatibility with the applied version of Excel.

Table 12 lists the various measuring points throughout the basic circuit, i.e. R7 to R19, and specifies the assumptions presumed in order to calculate the unknown refrigerant properties. All of the points listed in *Table 11* corresponds with the measuring points depicted in Appendix C2.

Table 11: Presumed assumptions used to calculating refrigerant states of basic circuit, where s and h abbreviates specific entropy and enthalpy respectively, and the points corresponds with the measuring points depicted in Appendix C2.

Assumptions basic circuit			
Point	Measured parameter	Assumption	Calculated properties
R7	Temperature, pressure	-	Spec. enthalpy (h) and entropy (s)
R8	Temperature	Similar pressure as R8	Spec. enthalpy (h) and entropy (s)
R9	Temperature	Similar pressure as R11	Spec. enthalpy (h) and entropy (s)
R10	Temperature	Similar pressure as R11	Spec. enthalpy (h) and entropy (s)
R11	Temperature, pressure	-	Spec. enthalpy (h) and entropy (s)
R12	Temperature	Similar pressure as R11	Spec. enthalpy (h) and entropy (s)
R13	Temperature	Similar pressure as R11	Spec. enthalpy (h) and entropy (s)
R14	Temperature	Isentropic fluid expansion from R13	Spec. enthalpy (h) and entropy (s), vapor fraction and saturation pressure
R15	Temperature	Similar pressure as R19	Superheat, spec. enthalpy (h) and entropy (s)
R16	Temperature	Similar pressure as R19	Superheat, spec. enthalpy (h) and entropy (s)
R17	Temperature	Similar pressure as R19	Superheat, spec. enthalpy (h) and entropy (s)
R18	Temperature	Similar pressure as R19	Superheat, spec. enthalpy (h) and entropy (s)
R19	Temperature, pressure	-	Superheat, spec. enthalpy (h) and entropy (s)

The saturation temperature (t_{sat}) in the points R15 to R19 was calculated using the pressure in point R19 as input variable, thus the amount of superheat (Δt_{sh}) could calculated by subtracting the saturation temperature (t_{sat}) from the refrigerant temperature, as shown in Eq.(35).

$$\Delta t_{sh,R(n)} = t_{R(n)} - t_{sat}\left(p_{R(n)}\right) \qquad \text{Eq.(35)}$$

Where the n in R(n) represents the number of the refrigerant measuring point.

With the refrigerant state at the measuring points in the circuit established, further calculations could be conducted in order to find, refrigerant mass flow rate, volumetric and isentropic efficiency of the compressor, and COP.

The refrigerant mass flow rate provided by the compressor could be estimated using a polynomial developed by *Bitzer;* however, the use of the polynomial was limited to calculating refrigerant flow through HX2 in the ejector circuit, and for both circuits during simultaneous operation. This due to the unknown accuracy of the polynomial.

The refrigerant mass flowrate in the basic circuit ($\dot{m}_{rb}$) during individual operation was calculated with expression Eq.(36), using $\dot{Q}_{HX1}$ previously calculated in Eq.(28).

$$\dot{m}_{rb} = \frac{-\dot{Q}_{HX1}}{h_{R15} - h_{R14}} \qquad \text{Eq.(36)}$$

Where the indices of specific enthalpies h_{R14} and h_{R15} corresponds with measuring point R14 and R15, i.e. refrigerant inlet and outlet of HX1, respectively.

Two COP values were calculated, where COP_{HX1}, Eq.(37), was based on $\dot{Q}_{HX1}$ thus excluding the sensible heat gains through the HVAC system ($\dot{Q}_{Gain}$), and COP_{HVAC}, Eq.(38), was based on $\dot{Q}_{HVAC}$ thus represented the COP of the HVAC unit. The electrical input power behind the two COPs was the measured active/true power supplied to the compressor ($\dot{P}_c$), thus excluding all the energy needed to drive the auxiliary HVAC equipment, such as supply air and HX2 fans.

$$COP_{HX1} = \frac{-\dot{Q}_{HX1}}{\dot{P}_c} \qquad \text{Eq.(37)}$$

$$COP_{HVAC} = \frac{-\dot{Q}_{HVAC}}{\dot{P}_c} \qquad \text{Eq.(38)}$$

The volumetric efficiency of the compressors (λ) was calculated with Eq.(7). The actual compressor displacement (V_i) was calculated with expression Eq.(39) using the specific gas volume (v_g) at compressor suction pressure and temperature in, i.e. R19, whereas the theoretical compressor displacement was specified by *Bitzer* (*Table 8*).

$$V_{i,b} = \dot{m}_{r,b} \cdot v_g(p_{R19}, t_{R19}) \qquad \text{Eq.(39)}$$

$$\lambda = \frac{V_i}{V_s} \qquad \text{Eq.(7)}$$

The isentropic efficiency was calculated using the active electrical input power to the compressor motor ($\dot{P}_c$). The specific enthalpy difference of isenthalpic compression (Δw_{is}), specific enthalpy at compressor discharge pressure, i.e. p_{R33}, and specific entropy at compressor inlet, i.e. s_{R33}, was calculated using *RnLib*.

$$\eta_{is,b} = \frac{\Delta w_{is}}{\dot{P}_c} \cdot \dot{m}_{rb} \qquad \text{Eq.(8)}$$

Consequently, the calculated isentropic efficiency included the compressor motor efficiency.

The heat transfer from the high-pressure liquid line to the low-pressure suction line in the SLHX of the basic circuit was calculated by Eq.(40) and Eq.(41), respectively.

$$\dot{Q}_{SLHX,HP,b} = (h_{R12} - h_{R11}) \cdot \dot{m}_{rb} \qquad \text{Eq.(40)}$$

$$\dot{Q}_{SLHX,LP,b} = (h_{R18} - h_{R17}) \cdot \dot{m}_{rb} \qquad \text{Eq.(41)}$$

4.2.2.4 Refrigerant ejector circuit

A similar methodology as for the basic circuit was carried out in order to establish the refrigerant properties of the ejector circuit at the various measuring points, i.e. point R20 to R33. However, due to some dissimilarities between the two circuits, e.g. two different mass flow rates and an intermediate pressure level, some additional assumptions and operations had to be made, as specified in *Table 12* and described further down in this section.

Table 12 lists the various measuring points throughout the ejector circuit, and specifies the necessary assumptions presumed in order to calculate the refrigerant properties. The points listed in *Table 12*, i.e. R20 to R33, corresponds with the measuring points illustrated in Appendix C3.

Table 12: Presumed assumptions for calculating refrigerant states in ejector circuit, where s and h abbreviates specific entropy and enthalpy respectively, and the points corresponds with the measuring points depicted in Appendix C3.

Presumed assumptions ejector circuit			
Point	Measured parameter	Assumption	Calculated properties
R20	Temperature, pressure	-	Spec. enthalpy (h) and entropy (s)
R21	Temperature	Similar pressure as R20	Spec. enthalpy (h) and entropy (s)
R22	Temperature	Similar pressure as R24	Spec. enthalpy (h) and entropy (s)
R23	Temperature	Similar pressure as R24	Spec. enthalpy (h) and entropy (s)
R24	Temperature, pressure	-	Spec. enthalpy (h) and entropy (s)
R25	Temperature	Similar pressure as R24	Spec. enthalpy (h) and entropy (s)
R26	Temperature	Similar pressure as R24	Spec. enthalpy (h) and entropy (s)
R27	Temperature	Isentropic fluid expansion from R30 and similar pressure as R28	Spec. enthalpy (h) and entropy (s), vapor fraction and saturation pressure
R28	Temperature, pressure	-	Superheat, spec. enthalpy (h) and entropy (s)
R29	Temperature	Ejector energy balance	Spec. enthalpy (h) and entropy (s), vapor fraction
R30	Temperature	Saturated liquid	Spec. enthalpy (h) and entropy (s)
R31	Temperature	Similar pressure as R33	Superheat, spec. enthalpy (h) and entropy (s)
R32	Temperature	Similar pressure as R33	Superheat, spec. enthalpy (h) and entropy (s)
R33	Temperature, pressure	-	Superheat, spec. enthalpy (h) and entropy (s)

Different methodologies were used to calculate the low-side and high-side mass flow rates of the ejector circuit, i.e. the mass flow rate through HX1 ($\dot{m}_{re,HX1}$) and HX2 ($\dot{m}_{re,HX2}$), respectively. The low-side mass flow rate ($\dot{m}_{re,HX1}$) was calculated similarly to that of the basic circuit, using the cooling capacity of HX1 via air ($\dot{Q}_{HX1}$) in Eq.(42).

$$\dot{m}_{re,HX1} = \frac{-\dot{Q}_{HX1}}{\Delta h_{e,HX1}} = \frac{-\dot{Q}_{HX1}}{(h_{R28} - h_{R27})} \qquad \text{Eq.(42)}$$

Whereas the high-side mass flow rate ($\dot{m}_{re,HX2}$) was estimated using the polynomial provided by *Bitzer*. The workings of this polynomial was not fully established, other than that the input variables were compressor discharge pressure and an intermediate temperature, additionally it presumed 5K of superheat at the compressor suction inlet.

Alternatively, $\dot{m}_{re,HX2}$ for individual operation could have been calculated using the heat rejection of HX2 via the air ($\dot{Q}_{HX2}$) which would have provided a similar accuracy as for the calculated $\dot{m}_{re,HX1}$. However, it was not known whether this would have yielded a more or less

correct estimate than the *Bitzer* polynomial, but comparisons of the two values showed that they were roughly in the same range during most of the tests.

In order to establish the specific enthalpy (h) and entropy (s) at the ejector discharge line, i.e. R29, an energy balance was established for the ejector, Eq.(43) and Eq.(44), thus threating it and the bypass through EV17 (Appendix C3) as a black box, as depicted in *Figure 4.2*. Heat loss through the ejector casing and the length of pipeline going to the various temperature sensors was neglected.

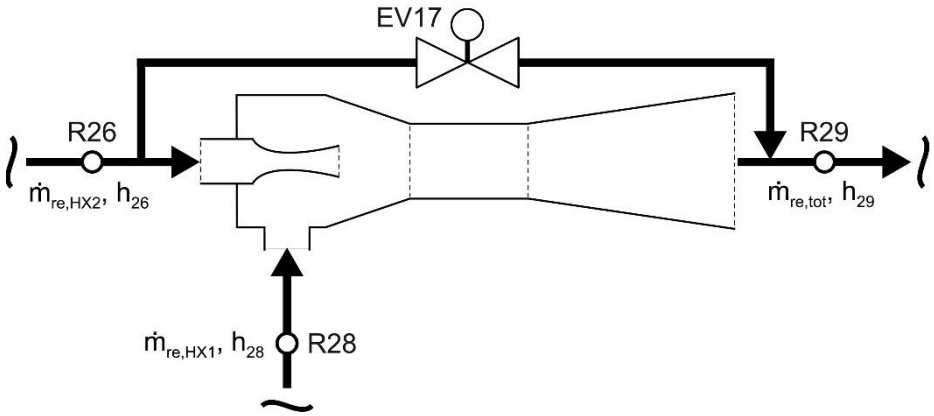

Figure 4.2: Ejector energy balance used to calculate the refrigerant state at the ejector outlet R29 in Eq.(44). Where h_{26}, h_{28} and h_{29} abbreviates specific enthalpy in point R26, R28 and R29, respectively, corresponding to Appendix C3.

$$\dot{m}_{re,tot} \cdot h_{R29} = \dot{m}_{re,HX2} \cdot h_{R26} + \dot{m}_{re,HX1} \cdot h_{R28} \qquad \text{Eq.(43)}$$

$$h_{R29} = \frac{\dot{m}_{re,HX2} \cdot h_{R26} + \dot{m}_{re,HX1} \cdot h_{R28}}{\dot{m}_{re,tot}} = \frac{\dot{m}_{re,HX2} \cdot h_{R26} + \dot{m}_{re,HX1} \cdot h_{R28}}{\dot{m}_{re,HX1} + \dot{m}_{re,HX2}} \qquad \text{Eq.(44)}$$

The vapor fraction corresponding to the temperature and specific enthalpy in R29 was calculated using *RnLib*.

The ejector suction pressure ratio (Π_s), mass entrainment ratio (Φ_m), and efficiency (η_{ej}) was calculated as described in section 2.2.5.2, using Eq.(19), Eq.(20), and Eq.(21), respectively.

$$\Pi_s = \frac{p_{diff,out}}{p_{sn,in}} = \frac{p_{33}}{p_{28}} \qquad \text{Eq.(19)}$$

$$\Phi_m = \frac{\dot{m}_{sn}}{\dot{m}_{mn}} = \frac{\dot{m}_{re,HX1}}{\dot{m}_{re,HX2}} \qquad \text{Eq.(20)}$$

$$\eta_{ej} = \frac{\dot{W}_{rec}}{\dot{W}_{rec,max}} = \Phi_m \cdot \frac{h_l - h_k}{h_c - h_m} = \frac{\dot{m}_{re,HX1}}{\dot{m}_{re,HX2}} \cdot \frac{h_l - h_{R28}}{h_{R26} - h_m} \qquad \text{Eq.(21)}$$

Where the indices R26, R28 and R33 corresponds with the measuring points in Appendix C3, and h_l and h_m have been shown in *Figure 2.29*.

As may be observed from *Figure 2.29* and deduced from Eq(x), h_m represents the specific enthalpy in the point corresponding to isentropic fluid expansion from R26 down to the intermediate pressure, i.e. compressor suction pressure (p_{33}). Hence, h_m could be calculated using the specific entropy in R26 and pressure in R33 as input values in *RnLib*.

Similarly, h_l represents the specific enthalpy in the point corresponding to isentropic compression from ejector suction pressure to compressor suction pressure, i.e. p_{R28} and p_{R33} respectively. Hence, h_l could be calculated using the specific entropy in R28 and pressure in R33 as input values in *RnLib*.

As a result of the EV17 bypass (Appedix C3), the η_{ej} was significantly reduced during operation with a high amount of bypass, as disclosed in section 4.2.4.5.

The heat transfer from the high-pressure liquid line to the low-pressure suction line in the SLHX of the ejector circuit was calculated using Eq.(45) and Eq.(46), respectively.

$$\dot{Q}_{SLHX,HP,e} = (h_{R25} - h_{R24}) \cdot \dot{m}_{re,HX2} \qquad \text{Eq.(45)}$$

$$\dot{Q}_{SLHX,LP,e} = (h_{R32} - h_{R31}) \cdot \dot{m}_{re,HX2} \qquad \text{Eq.(46)}$$

4.2.3 Individual circuit operation at various ambient temperatures

The pilot unit was tested at numerous conditions, with variations in supply air and HX2 air volume rate, at several different stages of part load, and for various ambient temperatures ranging from 15 to 40°C. A selected assortment of these tests, all of which maximum cooling load tests, were analyzed and have been presented in section 5.2.

A total of 14 individual operation tests were analyzed and the full results corresponding to these tests have been included in Appendix D1 and D2. The controlled ambient parameters during these tests were supply air volume rate, ambient air temperature and RH; hence, the state of the air at the inlet of both HX1 and HX2 was varied. *Table 13* lists the tests included in Appendix D1 and D2 and the corresponding controlled conditions behind them.

Table 13: Controlled conditions behind individual operation test scenarios where A1 and A5 corresponds with the measuring points in appendix C4.

Controlled parameters behind individual operation test scenarios							
Test number	**Circuit**	**Supply air volume [%]**	**HX2 air volume [%]**	**temperature**		**RH**	**Appendix**
				A5	A1		
1.1.5(1)	Basic	50%	100%	25°C	23°C	49%	D1.1
1.1.1(6)	Basic	50%	100%	28°C	23°C	48%	D1.2
1.1.1(5)	Basic	100%	100%	28°C	23°C	48%	D1.3
1.1.3(1)	Basic	50%	100%	35°C	28°C	56%	D1.4
1.1.3(3)	Basic	100%	100%	35°C	29°C	56%	D1.5
1.1.6(2)	Basic	50%	100%	40°C	31°C	59%	D1.6
1.1.6(1)	Basic	100%	100%	40°C	30°C	59%	D1.7
1.2.5(2)	Ejector	50%	100%	25°C	23°C	50%	D2.1
1.2.1(10)	Ejector	50%	100%	28°C	23°C	50%	D2.2
1.2.1(9)	Ejector	100%	100%	28°C	23°C	50%	D2.3
1.2.1(3)	Ejector (single EV19)	100%	100%	28°C	23°C	49%	D2.4
1.2.3(1)	Ejector	100%	100%	35°C	28°C	56%	D2.5
1.2.3(2)	Ejector (110 bar HP)	100%	100%	35°C	28°C	56%	D2.6
1.2.3(3)	Ejector (110 bar HP and 480V-3-60Hz HX2 fans)	100%	++100 %	35°C	28°C	56%	D2.7

In order to limit the extent of the results presented in section 5.2, the test scenarios with a 50% supply air volume rate reduction was omitted; hence, only test scenarios with a supply air volume rate of 100%, i.e. approximately 4000 m^3/h, have been presented in section 5.2.

Consequently, five individual-operation tests have been presented in section 5.2, where three of these are from operation of the basic circuit, i.e. 1.1.1(5), 1.1.3(3) and 1.1.6(1), and two from the ejector circuit, i.e. 1.2.1(9) and1.2.3(1).

The presentation of the results in section 5.2 include log(p)h-diagrams depicting the heat absorption at HX1, the compression process, and the heat rejection at HX2 corresponding to the various test scenarios, *Figure 5.2* and *5.3* for the basic and ejector circuit, respectively. The expansion, SLHX and ejector processes were excluded from the diagrams in order to reduce clutter. The log(p)h-diagrams also include refrigerant state data at the various measuring points, extracted from Appendix D1 and D2.

Additionally, key parameters corresponding to the five test scenarios have been compiled and listed in *Table 15*, thus further facilitating performance evaluation and comparison of the two circuits at the various temperatures.

4.2.4 Challenges and difficulties

As previously mentioned, several difficulties and challenges, especially with regard to the ejector circuit, were encountered over the course of the laboratory bench tests. Moreover, as will be explained in 4.2.4.4, the pilot unit did not meet the required cooling capacity at design load conditions.

4.2.4.1 Implementation of triple parallel expansion valves in the ejector circuit

The initial tests, conducted during the first visit to the *FTL* R&D laboratory, highlighted some substantial issues suspected to be a result of high flow resistance between the accumulator tank and HX1 in the ejector circuit. Consequently, resulting in excessive superheat at the HX1 refrigerant outlet, even during maximum feeding of HX1, i.e. EV19 depicted in Appendix C3 in fully open position.

The components and piping between the accumulator tank and HX1 were inspected, and it became evident that the expansion valves applied in the system was of a different type than those suggested by *Danfoss* in the design phase.

Due to difficulties concerning TÜV certification of *Danfoss* equipment, *FTL* had made the decision to switch to the manufacturer *Carel* for all expansion valves in the system. However, whereas *Danfoss* had suggested a selection of valves based on sizing calculations, all of the applied *Carel* expansion valves were of one identical sizes. Consequently, the expansion valve separating the intermedia pressure and ejector suction pressure, i.e. (21) in *Figure 3.12*, was suspected to be too small and the corresponding flow resistance too high.

The initial proposal was to, simply, switch to a larger model of the *Carel* valve as these came in several larger and smaller sizes. However, *FTL* estimated the delivery time of a new larger valve to be in the range of several months. Consequently, an alternative measure was suggested.

As *FTL* had several of the applied *Carel* valves in storage, a parallel installation of two additional similar size valves, as illustrated in Appendix C3, seemed like the most practical option. However, there was only one free output on the control unit, and the two additional valves had to be controlled in tandem. Nevertheless, it was decided that implementation of the three parallel EV19 expansion valves would be initiated starting the following week.

The tests corresponding to before and after implementation of triple parallel EV19 are 1.2.1(3) and 1.2.1(9), respectively The key results from these tests have been listed in *Table 14* in section 5.1. Additionally, a log(p)h-diagram depicting the two cycles have been included in *Figure 5.1*. The extended results from these tests, i.e. 1.2.1(3) and 1.2.1(9), can be found in Appendix D2.4 and D2.3, respectively.

As can be deduced from the results presented in chapter 5.1, a significant increase in refrigerant flow through HX1 was achieved by implementing two additional EV19s, thus substantially reducing the amount of superheat.

Further tests of the triple EV19 arrangement showed that an opening of the third valve had little to no effect on flow when two valves were fully open, thus suggesting further throttling upstream or downstream of EV19. However, the remaining superheat at R28 in test 1.2.1(9), was suspected to be caused by measurement deviations, as it took a lot of closing steps of EV19 to produce a further increase in superheat.

4.2.4.2 Accurate high-pressure control

As have been previously described in section 3.2.2.3, a bypass leading from the high-pressure liquid line, upstream of the ejector, to the discharge, downstream of the ejector, was included in the ejector circuit, depicted in *Figure 3.17*. A valve dictated the flow through the bypass and the purpose of this feature was to facilitate high-pressure control. The valve would be fully open during start up, and gradually be closed in order to achieve desired high-pressure. This valve is addressed as 20 in *Figure 3.17* and EV17 in Appendix C3.

However, as previously explained in section 4.2.4.1, *FTL* had diverged from the initial system design plans and implemented *Carel* expansion valves of identical size throughout the system, as opposed to the specifically sized *Danfoss* expansion valves suggested during design. Consequently, too little attention was paid to intended functionality of EV17, thus it was grossly oversized, and the corresponding regulation curve not suitable for fine adjustment of high-pressure.

Consequently, the test engineer found it challenging to achieve desired high-pressure during ambient temperatures above 24°C without tripping the high-pressure switch (set to approx. 102 bar) in the process. When the opening of EV17 neared a close, even the slightest reduction in flow area would produce a high-pressure peak of approximately 10-15 bar.

As can be seen in *Table 15*, the discharge pressure during test 1.2.1(9) was 94.3 bar, at that point, the EV17 was almost completely shut and a further reduction in flow area would set of the high-pressure switch. The only way to increase cooling capacity further during these conditions was to first reduce refrigerant mass flow through HX1 ($\dot{m}_{re,HX1}$) by throttling EV19, wait for the system pressure to drop, then fully close EV17, and slowly open EV19 until high-pressure reached the highest possible level. However, due to the tandem regulation of two of the three EV19s this procedure also proved challenging as high-pressure peaks would occur.

Moreover, during simultaneous operation of the two circuits high-pressure in both circuits increased due to interactions in HX2, consequently further intensifying the problem.

The scientific project advisor from *SINTEF* proposed a parallel bypass arrangement at EV17 as a measure to increase controllability. The additional bypass, or ideally several, would be regulated by a much smaller valve, or ideally several differently sized valves, thus enabling accurate fine-tuning of the high-pressure. However, as there were no free controller outputs available on the HVAC controller, an additional control device would have to be integrated to the system, and the solution was shelved by *FTL*.

4.2.4.3 Crankcase oil foaming

During some operating conditions, excessive oil foaming in the compressor crankcase was detected, as can be seen in the pictures taken from a sight glass located in the front of the compressor oil sump, at various levels of superheat, included in Appendix E.

The excessive oil foaming occurred when conditions in the compressor crankcase, at suction pressure, did not support R744 miscibility with the PAG oil. Thus, liquid R744 entrained in the oil started to evaporate out, consequently leading to foaming of oil.

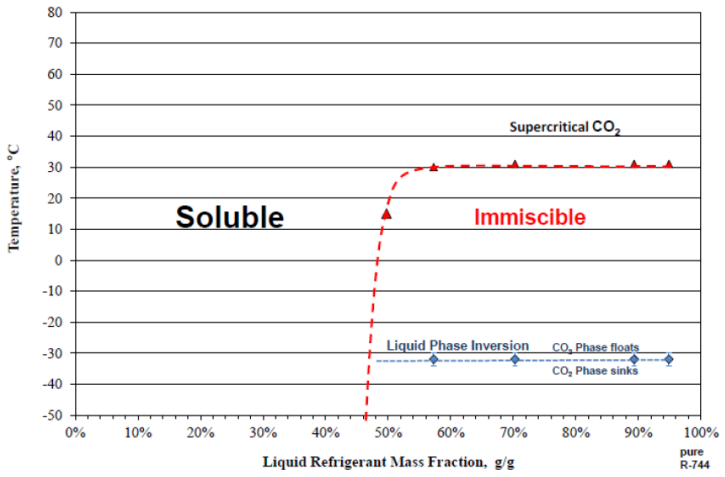

Figure 4.3: PAG oil and R744 immiscible area (Bitzer).

Figure 4.3 show the soluble and immiscible condition for R744 in the applied PAG oil.

Efforts were made in order to keep compressor suction conditions outside the immiscible area. However, the operation of the *CRII* capacity control, previously described in section 3.2.2.1, at part load led to large variations in compressor suction conditions, consequently making oil foaming inevitable during some stages of part load. In order to keep oil foaming at part load to a minimum, the modulation cycle interval of the *CRII* changed from 20 to 10 seconds.

4.2.4.4 Enhancement measures

The pilot unit design cooling load calculation, included in Appendix D4, was conducted by *FTL* in accordance with the European standard EN 13129. As previously described in section 2.1.2, the design load conditions for climatic zone III corresponds with a maximum passenger load, 28°C ambient air temperature, 45% ambient air relative humidity and an equivalent solar load of 600 W/m^3.

The *FTL* design cooling load calculation suggested an evaporator cooling demand of 24.1kW, where the internal, passenger, ventilation air, transmission and solar gains to the carriage constituted 23.0 kW. The sensible heat gain from auxiliary HVAC equipment was assumed 0.1 kW and an additional 1.0 kW was added as a redundancy measure. The pilot unit was sized based on *Modelica* CFD simulations presuming the evaporator cooling capacity specified in the *FTL* design load calculation.

According to the *FTL* design load calculations, each individual circuit would have to produce a cooling capacity of -12.05kW, during simultaneous operation, assuming a 50-50 capacity contribution. As can be observed in the results presented in section 5.2 (*Table 15)*, the basic and ejector circuit, test 1.1.1(5) and 1.2.1(9), achieved an evaporator cooling capacity, i.e. $\dot{Q}_{HX1}$, of -13.4 and -12.5kW, respectively, thus surpassing the individual circuit capacity requirement at the design conditions.

However, when $\dot{Q}_{HX1}$ and the HVAC cooling capacity ($\dot{Q}_{HVAC}$) was compared it became evident that the assumed 0.1 kW sensible heat gain from HVAC equipment was a gross underestimation, being approximately in the range of 2-3 kW during full supply air fan power.

Moreover, *FTL* also specified that the 1.0 kW, added for redundancy, was earmarked compartment heat gains. Thus, even though the *FTL* design load calculation had specified an evaporator cooling capacity requirement of -24.1kW, *FTL* later stated that this capacity applied

to $\dot{Q}_{HVAC}$, and not $\dot{Q}_{HX1}$. Consequently, the pilot unit had been "under-dimensioned" by approximately 2-3kW.

Furthermore, the CFD model used in the design phase had presumed a maximum high-pressure of 110 bar, whereas the maximum high-pressure limit during the bench tests was approximately 100 bar. Moreover, due to difficulties with regard to high-pressure control, described in section 4.2.4.2, not even a high-pressure of 100 bar could be achieved for the ejector circuit during some of the tested scenarios.

When the new requirement was applied, i.e. $\dot{Q}_{HVAC} \leq$ -24 kW, the individual operation tests of the basic and ejector circuit at design load conditions demonstrated shortcomings in cooling capacity, of 7.9 and 17.8%, respectively; as can be deduced from *Table 15*, test 1.1.1(5) and 1.2.1(9), respectively.

Furthermore, when both circuits of the pilot unit was operated simultaneously, the interaction between the two circuits resulted in further shortcomings in cooling capacity. As can be observed in from the results presented in section 5.3.2, *Table 17*, test 1.3.1(5).

Consequently, efforts were made in order to identify the components related to the largest drop in performance. However none of which feasible onboard the train, two enhancement measures were implemented and investigated. One of the enhancement measures was to increase the maximum operation high-pressure limit to 110bar by disconnecting the high-pressure switch, while the other was to increase the power supplied to the HX2 fans by increasing voltage and frequency to 480V-60Hz.

The improvements in cooling capacity generated by the two enhancement measures were tested for individual operation of the ejector circuit at 35°C ambient temperature, presented in section 5.3.1, and for simultaneous operation of both circuits at design load conditions, presented in 5.3.2.

As can may be observed in Appendix C3 and *Figure 3.12*, the ejector circuit did not include a high-pressure safety valve. Consequently, disconnecting the high-pressure switch did not come without risks, which was experienced first-hand by the test engineer who at one point had to activate the emergency power switch due to a large high-pressure spike, owing to a slight deviation in the control software input values.

4.2.4.5 Poor ejector efficiency

As a result of the EV17 bypass being in a partly open position during all of the analyzed tests, the achieved ejector efficiency (η_{ej}) in the presented results proved quite low, being in the range of 5 to 10%, whereas an efficiency of approximately 30% should be expected from a properly functioning ejector.

Hence, two hypothetical scenarios where the η_{ej} was 30%, was established. For both of these scenarios, most of the parameters from test 1.2.3(1) was used as a basis.

In scenario one, all of the additional work recovered by the ejector would go towards increasing the refrigerant mass flow rate through HX1 ($\dot{m}_{re,HX1}$), meanwhile, preserving the ejector pressure lift produced in test 1.2.3(1). Hence, the $\dot{m}_{re,HX1}$ could be calculated as expressed in Eq.(48), derived from Eq.(21).

$$\dot{m}_{re,HX1} = \eta_{ej} \cdot \dot{m}_{re,HX2} \cdot \frac{(h_{R26} - h_m)}{(h_l - h_{R28})} \qquad \text{Eq.(48)}$$

In scenario two, parts of the work recovered by the ejector was assumed to increase the refrigerant flowing through HX1 ($\dot{m}_{re,HX1}$) until 0K superheat was achieved at the outlet, i.e. point R28, whereas the remaining work would go towards compression, thus providing a higher compressor suction pressure, i.e. p_{33}. The required $\dot{m}_{re,HX1}$ was calculated using $\dot{Q}_{HX1}$ from test 1.2.3(1), presuming a specific enthalpy at the outlet of HX1, i.e. h_{R28}, equal to the specific enthalpy of saturated gas at p_{27} from test 1.2.3(1).

$$h_l = \frac{\eta_{ej} \cdot \dot{m}_{re,HX2} \cdot (h_{R26} - h_m)}{\dot{m}_{re,HX1}} + h_{R28} \qquad \text{Eq.(49)}$$

An expression to calculate the new h_l (Eq.(49)) was derived from Eq.(21), and the pressure corresponding to an isentropic process from h_{R28} to h_l was found in *CoolPack*, thus yielding the new compressor suction pressure p_{33}.

Further, assuming a linear characteristic for the active compressor power $\dot{P}_c$, the reduction in compressor power corresponding to the increased suction pressure could be estimated.

However, it must be stated that these calculations are highly theoretical and would not necessarily apply accurately to the real system. Moreover, the underlying assumptions are not entirely realistic, and additionally the increase in dynamic component losses related to the increased $\dot{m}_{re,HX1}$ in scenario one was ignored.

The results corresponding to the two scenarios, have been presented in section 5.4.

4.2.5 Improving on the *FTL* calculation model

As have been described in the preceding sub-sections, the student developed a calculation model in order to analyze the *FTL* measured data. Throughout this process, data from the thesis model was compared to that from the *FTL* model, thus some improvements measures for the *FTL* calculation model have been identified and presented in section 5.5.

5 Pilot unit laboratory bench test results

5.1 Implementation of triple parallel expansion valves in the ejector circuit

The below presented results represents maximum capacity operation of the ejector circuit before and after implementation of the triple parallel expansion valves (EV19 in Appendix C3), i.e. test 1.2.1(3) and 1.2.1(9).

The general methodology behind the results presented in this section have been described in section 4.2.2, whereas the specifics have been explained in section 4.2.4.

The ambient conditions during these tests corresponds with the design conditions specified in *Table 1*, i.e. an ambient air temperature and relative humidity of 28°C and 45%, respectively. Both HX2 fans were on (approx. 8000 m^3/h), and maximum supply air volume rate (approx. 4000 m^3/h) was supplied to HX1.

The extended results corresponding to the two tests 1.2.1 (3) and 1.2.1 (9) have been compiled in Appendix D2.4 and D2.3, respectively.

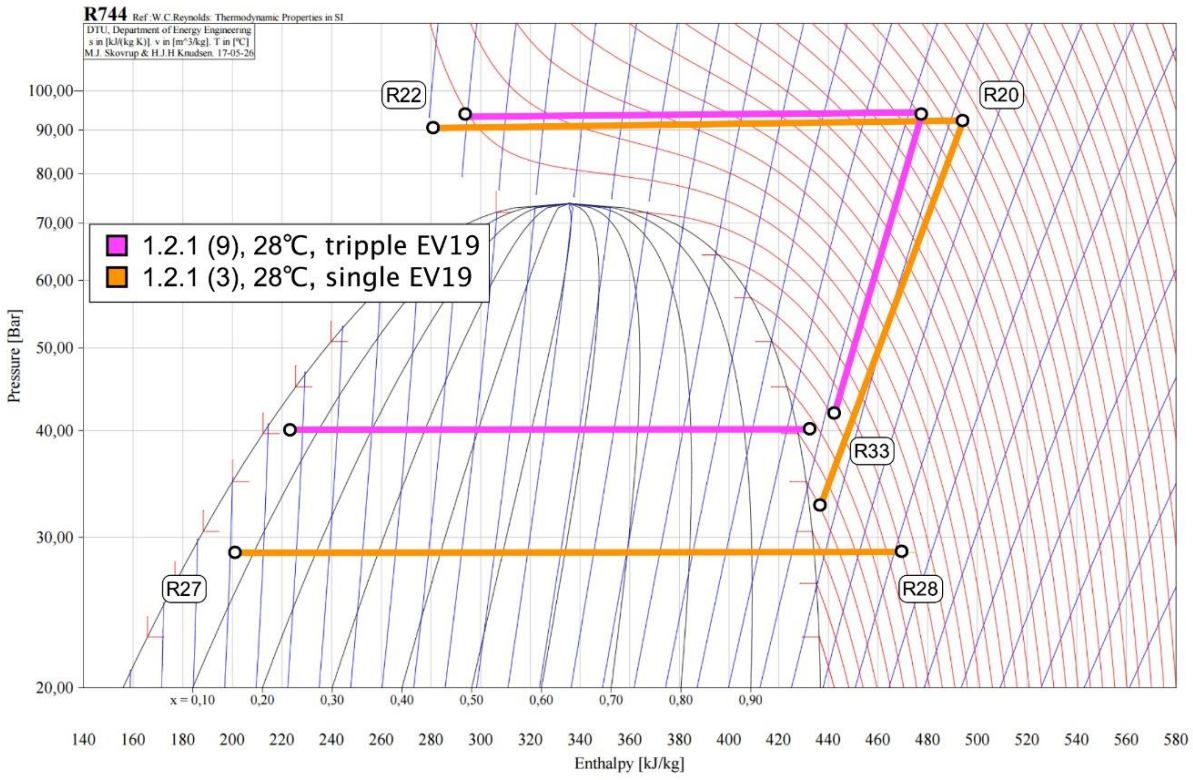

Figure 5.1: log(p)h-diagram cycle illustration of test 1.2.1 (3) and 1.2.1 (9), in green and black, respectively. Where the point R21, R22, R27, R28 and R33 corresponds with the measuring points depicted in Appendix C3.

As is clear when comparing the two test scenarios in *Figure 5.1*, the reduced flow resistance between the accumulator tank and HX1 inlet drastically increased evaporation pressure, and reduced superheat at R28; however, not completely.

Table 14: Comparison between test number 1.2.1(3) and 1.2.1(9) , i.e. before and after implementation of triple EV19 in the ejector circuit.

Key parameters from the results of test number 1.2.1(3) and 1.2.1(9)					
System layout			Single EV19	Tripple EV19	Designation
Circuit			Ejector	Ejector	
Test number			1.2.1(3)	1.2.1(9)	
Pressure	Compressor discharge	p_R20	92.2	94.3	[bar]
	Compressor suction	p_R33	32.3	41.6	[bar]
	Ejector suction	p_R28	28.8	40.1	[bar]
Temperature	Refrigerant gas cooler outlet	t_R22	30.6	34.4	[°C]
	Approach gas cooler outlet	Δt_ap,HX2	3.2	6.6	[K]
	Air inlet HX1	t_A2	23.8	23.5	[°C]
	Air outlet HX1	t_A3	17.2	14.2	[°C]
	Refrigerant HX1 inlet	t_R27	-3.5	7.7	[°C]
	Refrigerant superheat HX1	Δt_sh,HX1	30.1	3.0	[K]
Mass flow rate	Refrigerant HX1	m_re,HX1	125	211	[kg/h]
	Refrigerant HX2	m_re,HX2	216	312	[kg/h]
	Air HX1	m_a1	4816	4631	[kg/h]
Compressor	Isentropic efficiency	η_is	0.62	0.69	[-]
	Volumetric efficiency	λ	0.62	0.86	[-]
	Pressure ratio	π	2.9	2.3	[-]
	Active input power	P_c	4.267	4.382	[kW]
Ejector	Mass entrainment ratio	Φm	0.58	0.67	[-]
	Suction pressure ratio	Πs	1.12	1.04	[-]
	Efficiency	η_is	0.36	0.10	[-]
SLHX	Transferred from HP	Q̇_SLHX,HP	-1.2	-0.9	[kW]
	Recived at LP	Q̇_SLHX,LP	0.0	0.9	[kW]
Capacity		Q̇_HX1	-9.6	-12.5	[kW]
		Q̇_HVAC	-6.7	-9.9	[kW]
COP		COP_HVAC	1.6	2.3	[-]

As may be observed in *Table 14*, the $\dot{m}_{re,HX1}$ in test 1.2.1(9) is almost twice that in test 1.2.1(3), being 211 and 125 kg/h, respectively. Consequently, this yielded an increase in $|\dot{Q}_{HVAC}|$ of 47% and consequently an increase in COP_{HVAC} of 44%. Moreover, the refrigerant superheat at the outlet of HX1 was reduced by 27.1K, and evaporation and compressor suction pressure was increased by 11.3 and 9.3 bar, respectively.

Ideally, the refrigerant superheat at the R28 would be zero; however, as explained in section 4.2.4.1, the small superheat measured in test 1.2.1(9) could have been attributed measurement deviations, as all three EV19s were in fully open position.

The $\dot{Q}_{SLHX,HP}$ of zero in test number 1.2.1(3) can most likely be attributed to measurement deviations.

5.2 Individual circuit operation at various ambient temperatures

The below presented results represents maximum capacity operation of the individual circuits, at ambient temperatures of 28, 35 and 40°C. The extended results corresponding to these tests can be found in Appendix D1 and D2. The methodology behind the results have been described generally and specifically in section 4.2.2 and 4.2.3, respectively.

Figure 5.2 depicts parts of the basic circuit VCCs from test 1.1.1(5), 1.1.3(3) and 1.1.6(1) in a log(p)h-diagram; where point R9 is the refrigerant outlet of HX2, R14 and R15 are the inlet and outlet of HX1, respectively, and R19 and R7 are the compressor suction and discharge, respectively, as depicted in Appendix C2.

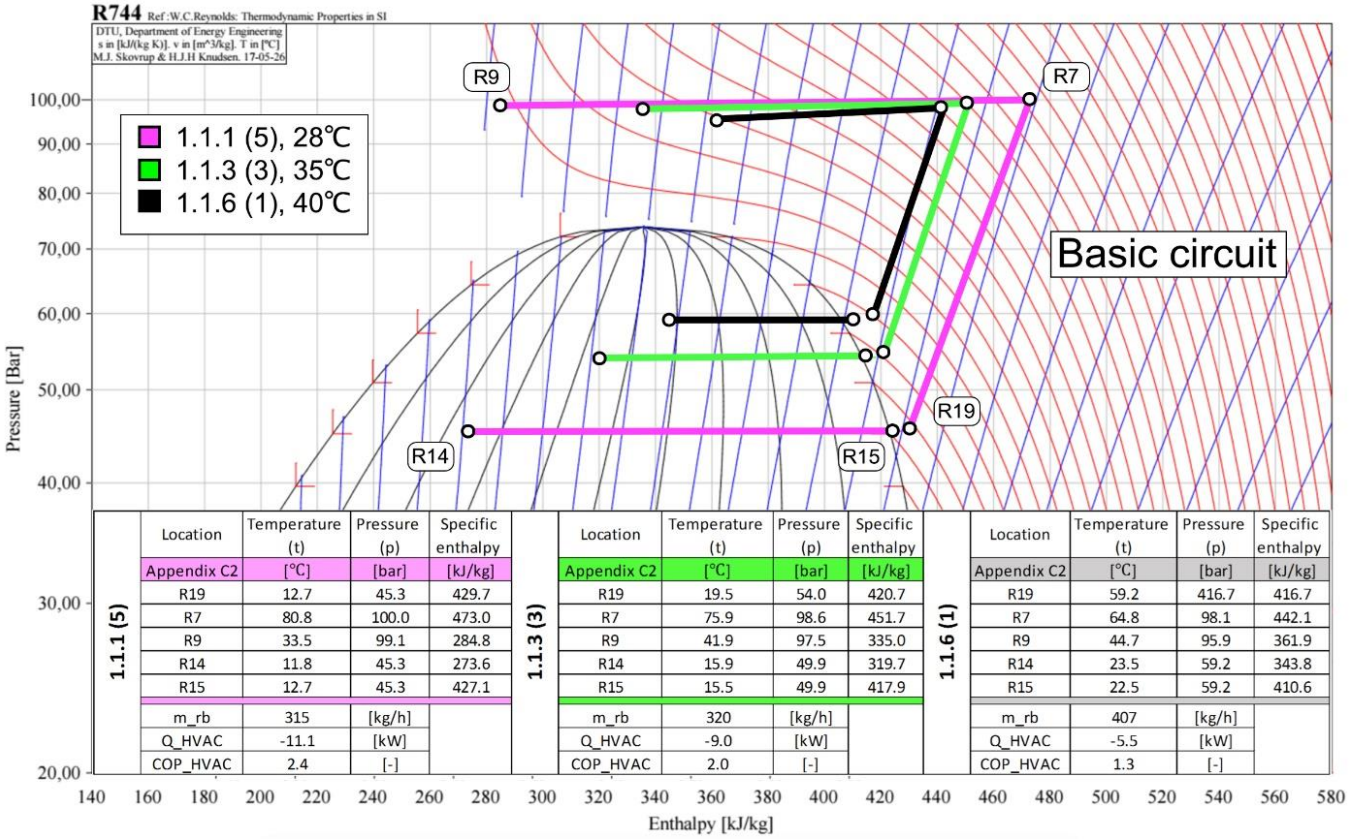

1.1.1 (5)	Location	Temperature (t)	Pressure (p)	Specific enthalpy
	Appendix C2	[°C]	[bar]	[kJ/kg]
	R19	12.7	45.3	429.7
	R7	80.8	100.0	473.0
	R9	33.5	99.1	284.8
	R14	11.8	45.3	273.6
	R15	12.7	45.3	427.1
	m_rb	315	[kg/h]	
	Q_HVAC	-11.1	[kW]	
	COP_HVAC	2.4	[-]	

1.1.3 (3)	Location	Temperature (t)	Pressure (p)	Specific enthalpy
	Appendix C2	[°C]	[bar]	[kJ/kg]
	R19	19.5	54.0	420.7
	R7	75.9	98.6	451.7
	R9	41.9	97.5	335.0
	R14	15.9	49.9	319.7
	R15	15.5	49.9	417.9
	m_rb	320	[kg/h]	
	Q_HVAC	-9.0	[kW]	
	COP_HVAC	2.0	[-]	

1.1.6 (1)	Location	Temperature (t)	Pressure (p)	Specific enthalpy
	Appendix C2	[°C]	[bar]	[kJ/kg]
	R19	59.2	416.7	416.7
	R7	64.8	98.1	442.1
	R9	44.7	95.9	361.9
	R14	23.5	59.2	343.8
	R15	22.5	59.2	410.6
	m_rb	407	[kg/h]	
	Q_HVAC	-5.5	[kW]	
	COP_HVAC	1.3	[-]	

Figure 5.2 Log(p)h-diagram of individual basic circuit operation at ambient temperatures of 28, 35 and 40°C. The full test results can be found in Appendix D1.3, D1.5 and D1.7, respectively.

As can be seen in *Figure 5.2*, the ambient temperature increase from 28 to 35°C and 35 to 40°C, resulted in an 8.4 and 2.8 K increase in refrigerant temperature at the outlet of HX2, i.e. R9, respectively.

Moreover, the reduced enthalpy difference between R14 and R15, results in an increase in $\dot{m}_{rb}$ and a reduction in HVAC cooling capacity and COP. Furthermore, due to the high-pressure limitation of 100 bar, a significant reduction in the specific enthalpy difference between R7 and R9 is seen for increasing ambient temperatures, due to the near critical point operation.

As can be seen from the shape of the isotherms at R9, a slight increase in high-pressure during test 1.1.3(3) and 1.1.6(1) would yield a relatively large difference in specific enthalpy, assuming a constant refrigerant temperature, whereas the high-pressure during test 1.1.1(5) being further away from the critical point, is closer to the optimum high-pressure.

Figure 5.3 depicts parts of the ejector circuit VCCs from test 1.2.1(9) and 1.2.3(1) in a log(p)h-diagram, where point R22 is the refrigerant outlet of HX2, R27 and R28 are the inlet and outlet of HX1, respectively, and R33 and R20 are the compressor suction and discharge line, respectively, as depicted in Appendix C3.

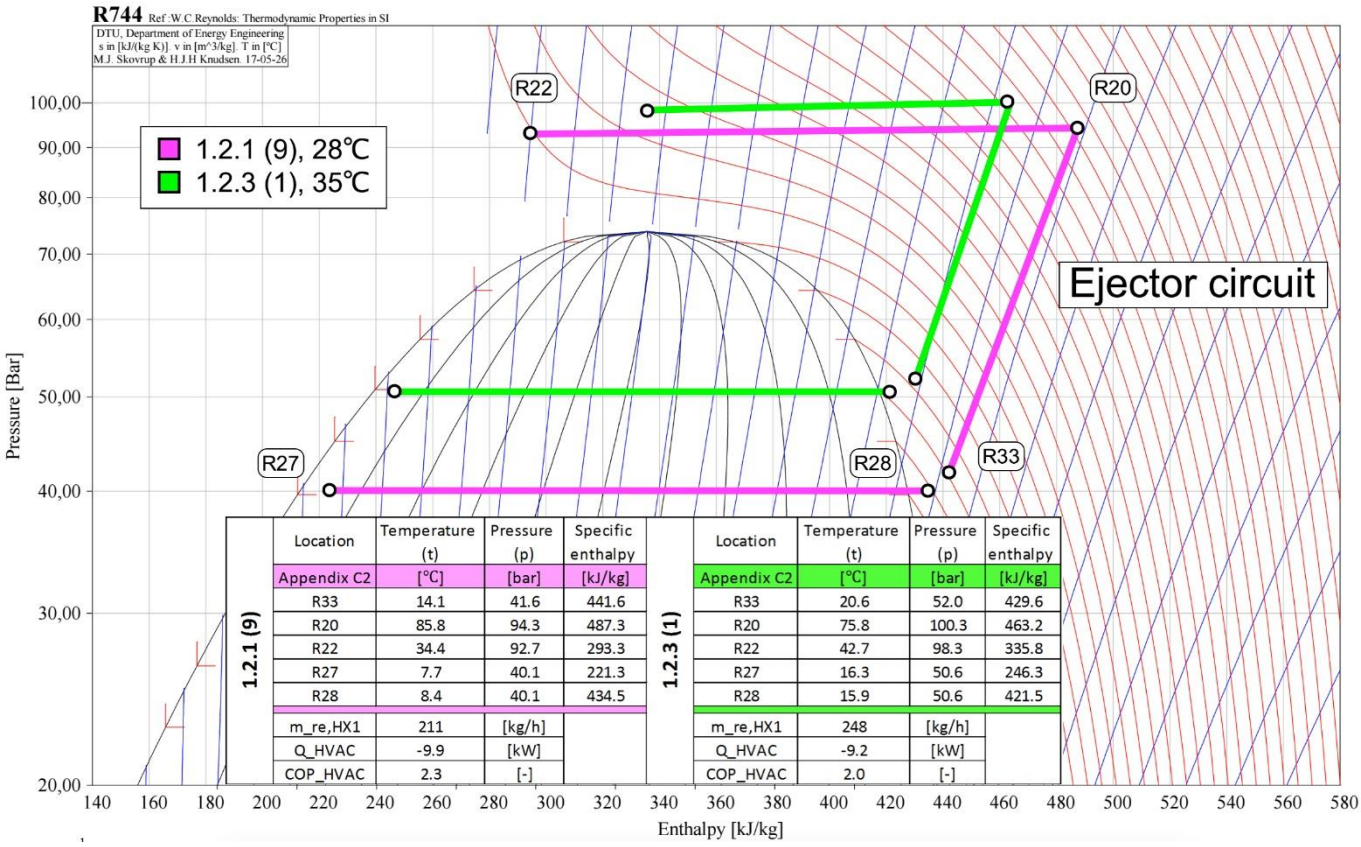

1.2.1 (9)

Location	Temperature (t)	Pressure (p)	Specific enthalpy
Appendix C2	[°C]	[bar]	[kJ/kg]
R33	14.1	41.6	441.6
R20	85.8	94.3	487.3
R22	34.4	92.7	293.3
R27	7.7	40.1	221.3
R28	8.4	40.1	434.5
m_re,HX1	211	[kg/h]	
Q_HVAC	-9.9	[kW]	
COP_HVAC	2.3	[-]	

1.2.3 (1)

Location	Temperature (t)	Pressure (p)	Specific enthalpy
Appendix C2	[°C]	[bar]	[kJ/kg]
R33	20.6	52.0	429.6
R20	75.8	100.3	463.2
R22	42.7	98.3	335.8
R27	16.3	50.6	246.3
R28	15.9	50.6	421.5
m_re,HX1	248	[kg/h]	
Q_HVAC	-9.2	[kW]	
COP_HVAC	2.0	[-]	

Figure 5.3 Log(p)h-diagram of individual ejector circuit operation at ambient temperatures of 28 and 35°C. The full test results can be found in Appendix D2.3 and D2.5, respectively.

As can be seen in *Figure 5.3*, the ambient temperature increase from 28 to 35°C results in a 8.3 K increase in refrigerant temperature at the outlet of HX2, i.e. R9. Moreover, the reduction in specific enthalpy difference between R27 and R28, results in a corresponding increase in $\dot{m}_{re,HX1}$

; however, as can be seen in *Table 15*, the increase in $\dot{m}_{re,HX2}$ is substantially higher due to the much larger decrease in specific enthalpy difference from R20 to R22.

Moreover, due to high-pressure control issues, described in section 4.2.4.2, the discharge pressure in test 1.2.1(9) is only 94.3 bar, consequently limiting achieved capacity.

When comparing *Figure 5.2* and *5.3*, it becomes evident that the specific enthalpy difference over HX1 in the ejector circuit was less sensitive to an increase in ambient temperature than the basic circuit.

As may be observed in *Figure 5.3* and *Table 15*, $\dot{m}_{re,HX1}$ was not enough to eliminate refrigerant superheat at the outlet, i.e. R28, in test 1.2.1(9) and 1.2.3(1).

Table 15: Key parameters from the basic and ejector individual operation test results during various ambient temperature operation.

Key parameters from the basic and ejector individual operation test results									
Ambient temperature			28°C		35°C		40°C		Designation
Circuit			Basic	Ejector	Basic	Ejector	Basic	Ejector	
Test number			1.1.1(5)	1.2.1(9)	1.1.3(3)	1.2.3(1)	1.1.6(1)	-	
Pressure	Compressor discharge	p_R7, p_R20	100.0	94.3	99.6	100.3	98.1	-	[bar]
	Compressor suction	p_R19, p_R33	45.3	41.6	54.0	52.0	59.2	-	[bar]
	Ejector suction	p_R28	-	40.1	-	50.6	-	-	[bar]
Temperature	Refrigerant HX2 outlet	t_R9, t_R22	33.5	34.4	42.6	42.7	44.7	-	[°C]
	Approach HX2 outlet	Δt_ap,HX2	5.8	6.6	7.7	7.9	5.7	-	[K]
	Air inlet HX1	t_A2	23.6	23.5	28.9	28.9	30.0	-	[°C]
	Air outlet HX1	t_A3	14.3	14.2	21.3	20.4	24.6	-	[°C]
	Refrigerant HX1 inlet	t_R14, t_R27	11.8	7.7	19.4	16.3	23.5	-	[°C]
	Refrigerant superheat HX1	Δt_sh,HX1	1.3	3.0	1.2	1.1	1.1	-	[K]
Mass flow rate	Refrigerant HX1	m_rb, m_re,HX1	315	211	381	248	407	-	[kg/h]
	Refrigerant HX2	m_rb, M_re,HX2	315	312	381	431	407	-	[kg/h]
	Air HX1	m_a1	4828	4631	4546	4543	4575	-	[kg/h]
Compressor	Isentropic efficiency	η_is	0.58	0.69	0.53	0.67	0.48	-	[-]
	Volumetric efficiency	λ	0.73	0.86	0.69	0.87	0.65	-	[-]
	Pressure ratio	π	2.2	2.3	1.8	1.9	1.7	-	[-]
	Active input power	P_c	4.618	4.382	4.392	4.479	4.099	-	[kW]
Ejector	Mass entrainment ratio	Φm	-	0.67	-	0.58	-	-	[-]
	Suction pressure ratio	Πs	-	1.04	-	1.03	-	-	[-]
	Efficiency	η_is	-	0.10	-	0.05	-	-	[-]
SLHX	Transferred from HP	Q̇_SLHX,HP	-0.9	-0.9	-1.4	-1.4	-1.7	-	[kW]
	Recived at LP	Q̇_SLHX,LP	0.4	0.9	0.7	1.1	1.2	-	[kW]
Capacity		Q̇_HX1	-13.4	-12.5	-10.4	-12.1	-7.5	-	[kW]
		Q̇_HVAC	-11.1	-9.9	-8.3	-9.2	-5.5	-	[kW]
COP		COP_HVAC	2.4	2.3	1.9	2.0	1.3	-	[-]

Table 15 lists the key results from the individual operation tests. The effective power supplied to the compressor of the ejector circuit is slightly lower than that of the basic, thus also yielding a higher η_{is} in the ejector circuit. Moreover, the ejector circuit also achieves a higher λ; however, it should be noted that λ in the ejector circuit was calculated using $\dot{m}_{re,HX2}$ which again was

calculated by the *Bitzer* polynomial, whereas λ of the basic circuit was calculated using $\dot{m}_{rb}$ (Eq.(36)).

During 28℃ ambient temperature operation, the HVAC unit cooling capacity, achieved by basic circuits exceeded that of the ejector circuit, in test number 1.1.1(5) and 1.2.1(9), respectively. However, much of this difference can be attributed to the lower high-pressure in the ejector circuit, moreover the mass flow rate of air over HX1 ($\dot{m}_{a1}$) was higher during the basic circuit test. Furthermore, the $\Delta t_{ap,HX2}$ in the ejector circuit was 0.8K higher than the in the basic circuit, most likely a result of the lower discharge pressure.

During 35℃ ambient temperature operation, the cooling capacity of the ejector circuit, i.e. test 1.2.3(1), exceeded that of the basic, i.e. test 1.1.3(3), owing to the lower sensitivity to high ambient temperature operation. As can be observed in *Figure 5.2* and *5.3*, both circuits have similar specific enthalpy at the inlet and outlet of HX2; however, the higher mass flow rate in the ejector circuit results in a greater heat rejection at HX2. As opposed to the 28℃ tests, the $\Delta t_{ap,HX2}$ in the two circuits is quite similar for the two circuits during 35℃ ambient temperature operation, all though quite high, keeping in mind that the heat exchanger is designed for simultaneous operation of two circuits.

The cooling capacity and performance of the basic circuit drops significantly during 40℃ ambient temperature operation, which surpass the limiting operating conditions, as specified in *Table 1*. Testing of the ejector circuit during these ambient conditions was not conducted due to issues with high-pressure control.

5.3 Enhancement measures

Due to insufficient cooling capacity at design load conditions, performance-enhancing measures were implemented and tested, as described in section 4.2.4.4.

Though implemented during laboratory bench tests, none of the evaluated measures were feasible onboard the trainset due to component certifications and limitations with regard to power supply.

5.3.1 Ejector circuit operation

The performance enhancing measures described in section 4.2.4.4 were implemented and tested during individual operation of the ejector circuit at an ambient temperature of 35℃.

The most relevant results from these tests have been presented in *Table 16*, whereas the extended results can be found in Appendix D2.5, D2.6 and D2.7. Moreover, a log(p)h-diagram

illustrating the heat absorption at HX1, heat rejection at HX2, and compression processes during the three tests have been included in *Figure 5.4*.

Test number 1.2.3(1) is the baseline scenario, whereas in test number 1.2.3(2) the maximum high-pressure limit have been raised to 110 bar, and test number 1.2.3(3) corresponds with simultaneous implementation of 110 bar high-pressure and 480V-60Hz HX2 fan power supply.

As may be observed in *Figure 5.4* the increased high-pressure in test number 1.2.3(2) and 1.2.3(3) yielded a lower evaporation pressure and a higher specific enthalpy difference over HX1. A flooded evaporator could not be achieved during any of the tests, as can be seen by the superheat at R28 (*Table 16*)

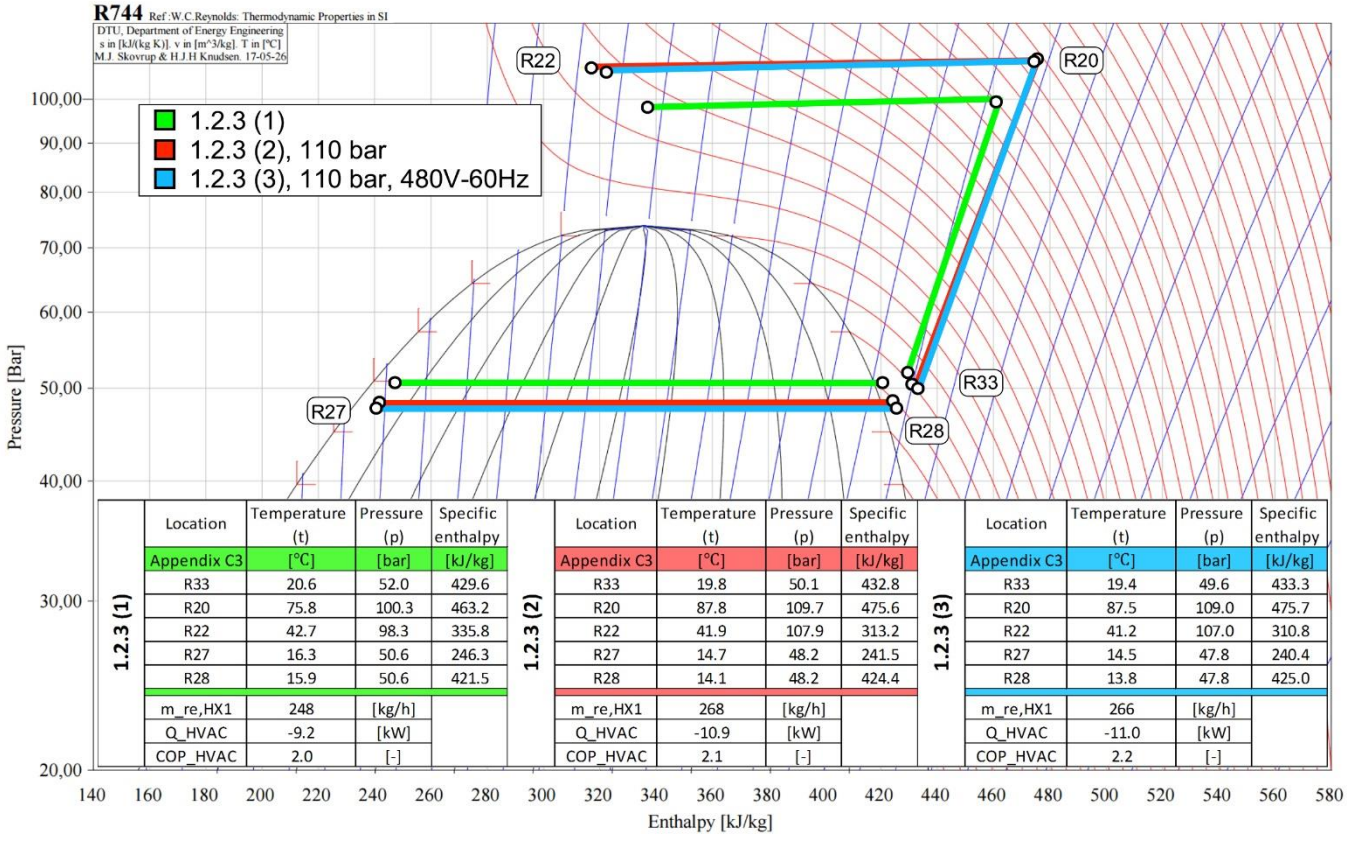

1.2.3 (1)	Location	Temperature (t)	Pressure (p)	Specific enthalpy
	Appendix C3	[°C]	[bar]	[kJ/kg]
	R33	20.6	52.0	429.6
	R20	75.8	100.3	463.2
	R22	42.7	98.3	335.8
	R27	16.3	50.6	246.3
	R28	15.9	50.6	421.5
	m_re,HX1	248	[kg/h]	
	Q_HVAC	-9.2	[kW]	
	COP_HVAC	2.0	[-]	

1.2.3 (2)	Location	Temperature (t)	Pressure (p)	Specific enthalpy
	Appendix C3	[°C]	[bar]	[kJ/kg]
	R33	19.8	50.1	432.8
	R20	87.8	109.7	475.6
	R22	41.9	107.9	313.2
	R27	14.7	48.2	241.5
	R28	14.1	48.2	424.4
	m_re,HX1	268	[kg/h]	
	Q_HVAC	-10.9	[kW]	
	COP_HVAC	2.1	[-]	

1.2.3 (3)	Location	Temperature (t)	Pressure (p)	Specific enthalpy
	Appendix C3	[°C]	[bar]	[kJ/kg]
	R33	19.4	49.6	433.3
	R20	87.5	109.0	475.7
	R22	41.2	107.0	310.8
	R27	14.5	47.8	240.4
	R28	13.8	47.8	425.0
	m_re,HX1	266	[kg/h]	
	Q_HVAC	-11.0	[kW]	
	COP_HVAC	2.2	[-]	

Figure 5.4: Log(p)h-diagram of individual ejector circuit enhanced operation at an ambient temperatures of 35°C. The extended test results can be found in Appendix D2.5, D2.6 and D2.7, respectively, and the measuring points R20, R22, R27, R28 and R33 corresponds with Appendix C3.

The increase in HX2 fan power in test 1.2.3(3) does not seem to have a significant effect, only reducing $\Delta t_{ap,HX2}$ by 0.8 K, when compared to 1.2.3(2). This is not surprising as the air volume rate over HX2 even during the baseline scenario is quite high when considering that only one circuit is being operated, thus further reductions in $\Delta t_{ap,HX2}$ will most likely require improvements to the heat exchanger design of HX2. As was explained in section 2.2.3.3, gas-

cooler design can have a substantial effect on transcritical system performance, as a large temperature glide is required in order to maximize heat transfer.

Table 16: Key results from individual ejector circuit performance enhancement tests. Where test number 1.2.3(2) corresponds with increased high-pressure limit to 110bar, and test number 1.2.3(3) corresponds with an 110bar high-pressure limit in addition to increased HX2 fan power**.*

Key parameters from ejector circuit enhancement measure test results						
Enhancement measure			-	110 bar HP*	110 bar HP 480V-60Hz**	Designation
Test number			1.2.3(1)	1.2.3(2)	1.2.3(3)	
Pressure	Compressor discharge	p_R20	100.3	109.7	109.0	[bar]
	Compressor suction	p_R33	52.0	50.1	49.6	[bar]
	Ejector suction	p_R28	50.6	48.2	47.8	[bar]
Temperature	Refrigerant HX2 outlet	t_R22	42.7	41.9	41.2	[°C]
	Approach HX2 outlet	Δt_ap,HX2	7.9	7.1	6.3	[K]
	Air inlet HX1	t_A2	28.9	28.7	28.9	[°C]
	Air outlet HX1	t_A3	20.4	19.9	20.1	[°C]
	Refrigerant HX1 inlet	t_R27	16.3	14.7	14.5	[°C]
	Refrigerant superheat HX1	Δt_sh,HX1	1.1	1.3	1.4	[K]
Mass flow rate	Refrigerant HX1	m_re,HX1	248	268	266	[kg/h]
	Refrigerant HX2	m_re,HX2	431	395	390	[kg/h]
	Air HX1	m_a1	4543	4615	4612	[kg/h]
Compressor	Isentropic efficiency	η_is	0.67	0.68	0.68	[-]
	Volumetric efficiency	λ	0.87	0.84	0.84	[-]
	Pressure ratio	π	1.9	2.2	2.2	[-]
	Active input power	P_c	4.479	5.070	5.011	[kW]
Ejector	Mass entrainment ratio	Φm	1.03	0.68	0.68	[-]
	Suction pressure ratio	Πs	1.03	1.04	1.04	[-]
	Efficiency	η_is	0.05	0.09	0.09	[-]
SLHX	Transferred from HP	Q̇_SLHX,HP	-1.4	-1.2	-1.2	[kW]
	Recived at LP	Q̇_SLHX,LP	1.1	1.0	1.0	[kW]
Capacity		Q̇_HX1	-12.1	-13.6	-13.6	[kW]
		Q̇_HVAC	-9.2	-10.9	-11.0	[kW]
COP		COP_HVAC	2.0	2.1	2.2	[-]

Table 16 lists the most relevant results from the three tests. As may be observed, increasing the high-pressure limit to 110bar yielded an increase in HVAC cooling capacity of -1.7 kW for a 0.6kW increase in $\dot{P}_{c,}$ while the additional HX2 fan power, in test number 1.2.3(3) provided an almost negligible increase in in cooling capacity compared to test 1.2.3(2).

5.3.2 Simultaneous operation

The performance-enhancing measures, described in section 4.2.4.4, were implemented and tested during simultaneous operation of both circuits at design load conditions, i.e. 28°C ambient temperature.

The most relevant results from these tests have been presented in *Table 17*, whereas the extended results can be found in Appendix D3.1, D3.2 and D3.3. Moreover, a log(p)h-diagram illustrating the heat absorption at HX1, heat rejection at HX2, and the compression processes of the three tests, have been included in *Figure 5.5* and *5.6*, for the basic and ejector circuit, respectively.

Test number 1.3.1(5) is the baseline scenario, whereas in test number 1.3.1(6) the voltage and current frequency supplied to the HX2 fan motors have been increased to 480V-60Hz, and in test number 1.2.3(3) the maximum high-pressure limit have been raised to 110bar for both circuits.

As can be observed in *Figure 5.5* both of the measures yielded an increase in the specific enthalpy difference through HX1 of the basic circuit. Even though air volume rate over HX2 was higher in test 1.3.1(6) than 1.3.1(10), the refrigerant temperature in at R9 is quite similar, owing to the higher superheat at the inlet of R19.

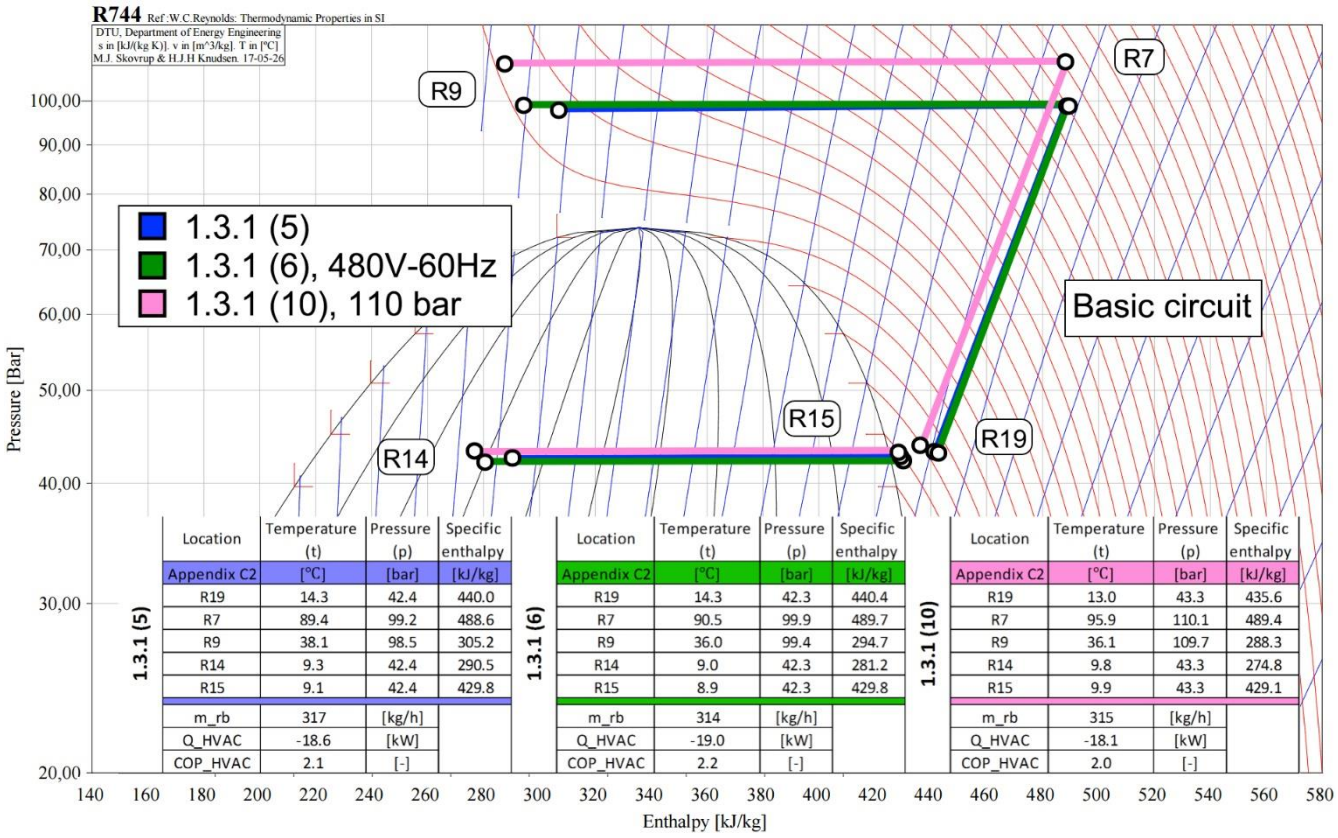

1.3.1 (5)	Location	Temperature (t)	Pressure (p)	Specific enthalpy
	Appendix C2	[°C]	[bar]	[kJ/kg]
	R19	14.3	42.4	440.0
	R7	89.4	99.2	488.6
	R9	38.1	98.5	305.2
	R14	9.3	42.4	290.5
	R15	9.1	42.4	429.8
	m_rb	317	[kg/h]	
	Q_HVAC	-18.6	[kW]	
	COP_HVAC	2.1	[-]	

1.3.1 (6)	Location	Temperature (t)	Pressure (p)	Specific enthalpy
	Appendix C2	[°C]	[bar]	[kJ/kg]
	R19	14.3	42.3	440.4
	R7	90.5	99.9	489.7
	R9	36.0	99.4	294.7
	R14	9.0	42.3	281.2
	R15	8.9	42.3	429.8
	m_rb	314	[kg/h]	
	Q_HVAC	-19.0	[kW]	
	COP_HVAC	2.2	[-]	

1.3.1 (10)	Location	Temperature (t)	Pressure (p)	Specific enthalpy
	Appendix C2	[°C]	[bar]	[kJ/kg]
	R19	13.0	43.3	435.6
	R7	95.9	110.1	489.4
	R9	36.1	109.7	288.3
	R14	9.8	43.3	274.8
	R15	9.9	43.3	429.1
	m_rb	315	[kg/h]	
	Q_HVAC	-18.1	[kW]	
	COP_HVAC	2.0	[-]	

Figure 5.5: Log(p)h-diagram of the basic circuit during simultaneous enhanced operation at design load conditions. The extended test results can be found in Appendix D3.1, D3.2 and D3.3, respectively, and the measuring points R20, R22, R27, R28 and R33 corresponds with Appendix C2.

As can be observed in *Figure 5.6*, the enhancement measures have little effect on the ejector circuit in the log(p)h-diagram. Due to issues related to high-pressure control, the discharge

pressure could not be increased to 110 bar in the ejector circuit during test number 1.3.1(10). Even though a slight reduction in HX2 refrigerant outlet temperature was achieved in test 1.3.1(6), the specific enthalpy difference through HX1 in the ejector circuit was almost unaffected by any of the measures.

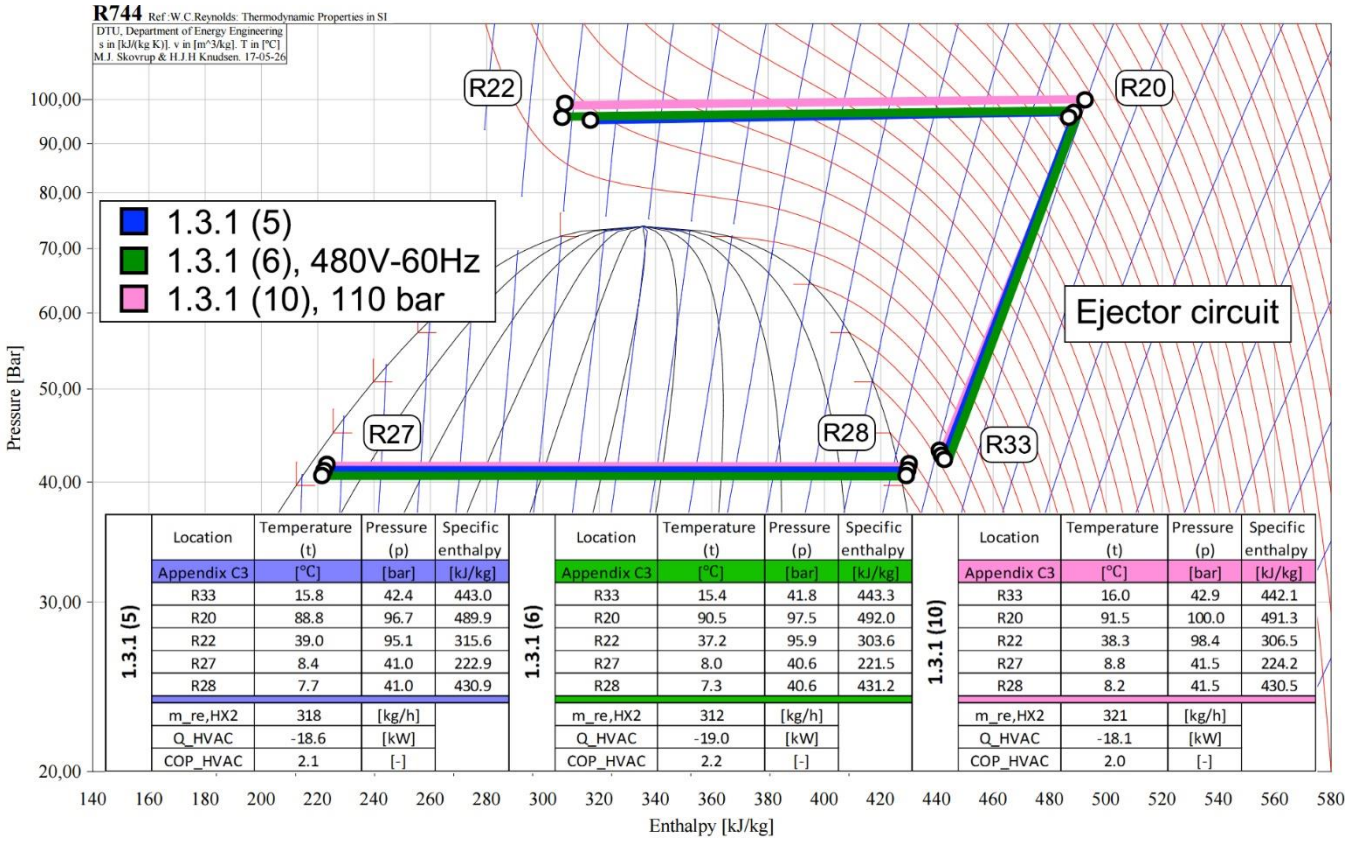

1.3.1 (5)	Location	Temperature (t)	Pressure (p)	Specific enthalpy
	Appendix C3	[°C]	[bar]	[kJ/kg]
	R33	15.8	42.4	443.0
	R20	88.8	96.7	489.9
	R22	39.0	95.1	315.6
	R27	8.4	41.0	222.9
	R28	7.7	41.0	430.9
	m_re,HX2	318	[kg/h]	
	Q_HVAC	-18.6	[kW]	
	COP_HVAC	2.1	[-]	

1.3.1 (6)	Location	Temperature (t)	Pressure (p)	Specific enthalpy
	Appendix C3	[°C]	[bar]	[kJ/kg]
	R33	15.4	41.8	443.3
	R20	90.5	97.5	492.0
	R22	37.2	95.9	303.6
	R27	8.0	40.6	221.5
	R28	7.3	40.6	431.2
	m_re,HX2	312	[kg/h]	
	Q_HVAC	-19.0	[kW]	
	COP_HVAC	2.2	[-]	

1.3.1 (10)	Location	Temperature (t)	Pressure (p)	Specific enthalpy
	Appendix C3	[°C]	[bar]	[kJ/kg]
	R33	16.0	42.9	442.1
	R20	91.5	100.0	491.3
	R22	38.3	98.4	306.5
	R27	8.8	41.5	224.2
	R28	8.2	41.5	430.5
	m_re,HX2	321	[kg/h]	
	Q_HVAC	-18.1	[kW]	
	COP_HVAC	2.0	[-]	

Figure 5.6:Log(p)h-diagram of the ejector circuit during simultaneous enhanced operation at design load conditions. The extended test results can be found in Appendix D3.1, D3.2 and D3.3, respectively, and the measuring points R20, R22, R27, R28 and R33 corresponds with Appendix C3.

As opposed to the individual operation of the ejector circuit in test 1.2.3(3) presented in section 5.3.1, the increase in air volume rate over HX2 during simultaneous operation, test 1.3.1(6), yielded a higher boost in performance as a larger part of the heat exchanger volume was occupied with high-temperature refrigerant. However, as was proposed in 5.3.1, a further reduction in $\Delta t_{ap,HX2}$ will most likely require improvements in the HX2 heat exchanger design.

Table 17 lists the most relevant results from the three tests. As may be observed, raising the high-pressure limit to 110 bar, in test number 1.3.1(10), reduced HVAC cooling capacity by 0.5 kW. The poor performance related to the measure was, most likely, attributed to internal interaction losses between the two circuits, as a high-pressure of 110 bar was not achieved in the ejector circuit consequently leading to increased transmission between the two circuits inside HX2.

*Table 17: Key results from simultaneous operation performance enhancement tests. Where test number 1.3.1(10) corresponds with an increase in high-pressure** limit to 110bar, and test number 1.3.1(6) corresponds with an increase in HX2 fan power**.*

Key parameters from simultaneous operation at design load conditions test results									
Enhancement measure			-		480V-60Hz*		110 bar HP**		Designation
Circuit			Basic	Ejector	Basic	Ejector	Basic	Ejector	
Test number			1.3.1(5)		1.3.1(6)		1.3.1(10)		
Pressure	Compressor discharge	p_R7, p_R20	99.2	96.7	99.9	97.5	110.1	100.0	[bar]
	Compressor suction	p_R19, p_R33	42.4	42.4	42.3	41.8	43.3	42.9	[bar]
	Ejector suction	p_R28	-	41.0	-	40.6	-	41.5	[bar]
Temperature	Refrigerant gas cooler outlet	t_R9, t_R22	38.1	39.0	36.0	37.2	36.1	38.3	[°C]
	Approach gas cooler outlet	Δt_ap,HX2	10.3	11.1	8.2	9.4	8.0	10.2	[K]
	Air inlet HX1	t_A2	23.6		23.5		23.8		[°C]
	Air outlet HX1	t_A3	10.8		10.4		11.3		[°C]
	Refrigerant HX1 inlet	t_R14, t_R27	9.3	8.4	9.0	8.0	9.8	8.8	[°C]
	Refrigerant superheat HX1	Δt_sh,HX1	1.4	1.5	1.4	1.4	1.4	2.1	[K]
Mass flow rate	Refrigerant HX1	m_rb, m_re,HX1	317	-	314	-	315	-	[kg/h]
	Refrigerant HX2	m_rb, M_re,HX2	317	312	314	312	315	321	[kg/h]
	Air HX1	m_a1	4754		4744		4798		[kg/h]
Compressor	Isentropic efficiency	η_is	0.71	0.72	0.71	0.73	0.69	0.75	[-]
	Volumetric efficiency	λ	0.85	0.87	0.84	0.86	0.80	0.86	[-]
	Pressure ratio	π	2.3	2.3	2.4	2.3	2.5	2.3	[-]
	Active input power	P_c	4.424	4.312	4.457	4.312	4.885	4.312	[kW]
Ejector	Mass entrainment ratio	Φm	-	-	-	-	-	-	[-]
	Suction pressure ratio	Πs	-	1.03	-	1.03	-	1.03	[-]
	Efficiency	η_is	-	-	-	-	-	-	[-]
SLHX	Transferred from HP	Q̇_SLHX,HP	-1.1	-1.1	-1.0	-1.0	-1.0	-1.0	[kW]
	Recived at LP	Q̇_SLHX,LP	1.1	1.0	1.0	0.9	0.7	0.9	[kW]
Capacity		Q̇_HX1	-20.5		-21.2		-20.3		[kW]
		Q̇_HVAC	-18.6		-19.0		-18.1		[kW]
COP		COP_HVAC	2.1		2.2		2.0		[-]

The increased air volume rate through HX2, in test 1.3.1(6), yielded a modest increase in cooling capacity, as a result of a slight reduction in $\Delta t_{ap,HX2}$, when compared to the baseline test 1.3.1(5).

None of the implemented measures yielded a sufficient improvement in capacity; however, if both measures had been simultaneously implemented and high-pressure in the ejector circuit could have been increased to 110 bar, increase in cooling capacity would most likely have been a bit higher. However, as may be observed in *Figure 5.5* and *5.6*, the isotherm shape at the HX2 outlet suggests a relatively limited increase in cooling capacity for an increase in high-pressure, at these ambient conditions.

5.4 Assuming optimal ejector efficiency

Due to the low ejector efficiency in the conducted tests, owing to the EV17 bypass, two hypothetical scenarios where a 30% ejector efficiency was assumed, as described in section 4.2.4.5, was established.

In scenario one, the increase in ejector efficiency yielded a $\dot{m}_{re,HX1}$ of 806 kg/h, corresponding to a 558 kg/h increase compared to the standard 1.2.3(1) test, provided the conditions described in section 4.2.4.5.

In scenario two, the suction pressure corresponding to the increased ejector efficiency was calculated to 58.8 bar, which is a 6.8 bar increase when compared to the 0.05% ejector efficiency in test 1.2.3(1). The increase in suction pressure would lead to a 0.6 kW reduction in $\dot{P}_c$, provided the assumption and conditions described in section 4.2.4.5.

Realistically, the increased ejector efficiency would result in something between these two scenarios.

However, as pointed out in section 4.2.4.5, these results are highly speculative.

5.5 Improvements to the FTL calculation model

As described in section 4.2, the student developed a calculation model in order to analyze the *FTL* measured data. Throughout this process, data from the thesis model have been compared to that from the *FTL* model, thus some improvement measures for the *FTL* calculation model have been identified and presented below.

It should be stated that none of the inconsistencies between the thesis and *FTL* model, disclosed below, had an effect on the reported cooling capacities.

The difference in specific enthalpy on the refrigerant side of HX1 in the ejector circuit, used to calculate the corresponding refrigerant mass flow rate ($\dot{m}_{re,HX1}$), was calculated differently in the thesis and *FTL* model, as can be seen from Eq.(50) and Eq.(51), respectively.

$$\Delta h_{e,HX1} = h_{R28} - h_{R27} \qquad \text{Eq.(50)}$$

$$\Delta h_{FTL} = h_{R28} - h_{R26} - (h_{R24} - h_{R25}) \qquad \text{Eq.(51)}$$

Where the indexes R24 to R28, corresponds with the illustration in Appendix C3.

The reasoning behind the calculated Δh_{FTL} is unclear; however, it is an incorrect representation of the specific enthalpy difference across HX1, as depicted in *Figure 5.7*, and will result in a higher calculated mass flow rate.

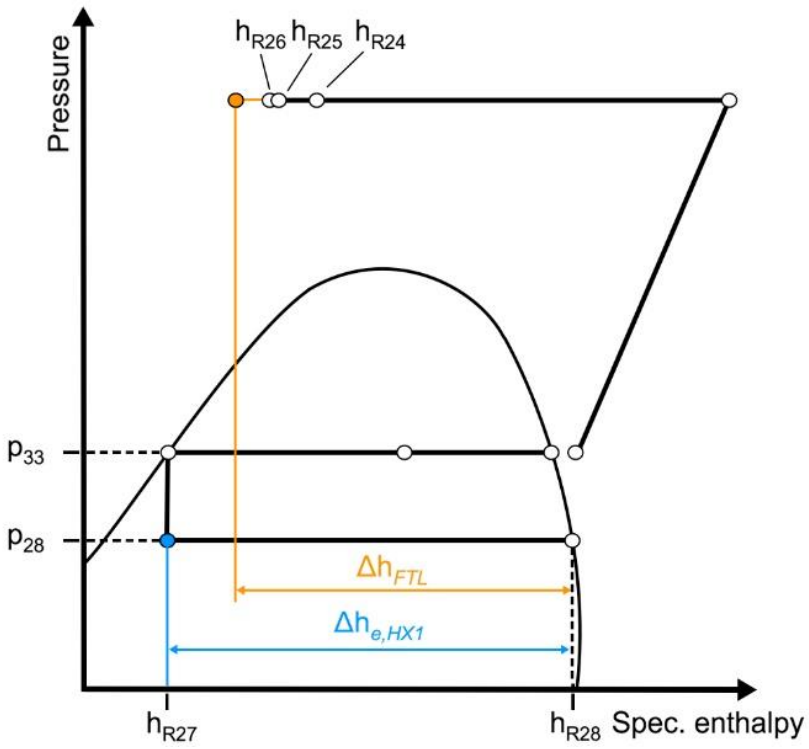

Figure 5.7: Methodology inconsistencies related to calculations of specific enthalpy difference across HX1 where Δh_{FTL} is used in the FTL calculation model, and $\Delta h_{e,HX1}$ is used in this thesis.

Moreover, when assessing the summary reports corresponding to the *FTL* measurement data, the reported HX2 temperature approach that did not correspond with those calculated for this thesis.

After some investigation, it appeared that *FTL* calculated temperature approach at HX2 ($\Delta t_{ap,FTL}$) by expression Eq.(52), while the HX2 temperature approach reported in this thesis ($\Delta t_{ap,HX2}$) have been calculated by expression Eq.(53).

$$\Delta t_{ap,FTL} = t_{R22} - t_{A6} \qquad \text{Eq.(52)}$$

$$\Delta t_{ap,HX2} = t_{R22} - t_{A5} \qquad \text{Eq.(53)}$$

Where the indexes A5 and A6 corresponds with the illustration in Appendix C4, and R22 with Appendix C3.

As may be observed when assessing Eq.(52), Eq.(53), and the corresponding illustrations in Appendix C3 and C4. The $\Delta t_{ap,FTL}$ yields a lower value as it is the difference between the air outlet and refrigerant outlet temperature, whereas $\Delta t_{ap,FTL}$ is the difference between air inlet and refrigerant outlet temperature, as previously depicted and explained in *Figure 2.19* and section 2.2.3.3, respectively. Thus, the $\Delta t_{ap,FTL}$ suggests more efficient heat transfer in HX2, than $\Delta t_{ap,HX2}$.

6 Discussion

Because of the simplified nature of the calculations conducted in this thesis, there are many uncertainties regarding the results presented in chapter 5, as pointed out several times throughout section 4.2.

It was not fully established to what extent the air temperature sensors realistically represented the dry bulb temperature; however, a short visual inspection indicated that efforts had been made in order to shield the sensors, at the inlet and outlet of HX1 and HX2, from radiative gains.

According to *FTL,* the temperature and humidity measurements upstream and downstream of the HVAC unit, i.e. A1 and A4 in Appendix C4, were based sensor values from a single point in the ducts. Hence, the calculated $\dot{Q}_{HVAC}$ was based on a uniform humid air enthalpy throughout the cross sectional area of the ducts, which might be one of the reasons for the larger than expected deviation from $\dot{Q}_{HX1}$, as disclosed in 4.2.4.4.

In order to facilitate simple calculations, the pressures in the refrigerant circuits was assumed uniform throughout most of the various pressure-sides, i.e. high-pressure, intermediate-pressure, and low-pressure. Consequently, the pressure drop corresponding to dynamic losses in components and piping was ignored, which have affected the reported results to some extent.

6.1 Performance of the ejector circuit

During the laboratory bench tests of the pilot unit, presented in chapter 5, performance of the ejector circuit was hampered by the high-pressure control difficulties, disclosed in 4.2.4.2. This may have been avoided if a more attentive approach had been applied to the selection of system valves.

The refrigerant mass flow rate through the ejector circuit side of HX1, was not sufficient to eliminate superheat at the outlet, thus one of the biggest advantages related to the two-phase ejector cycle, namely a flooded evaporator, could not be attained.

Moreover, as have been covered in section 4.2.4.5, the low ejector efficiency throughout testing, can largely be attributed the EV17 bypass being more or less open during all of the analyzed test scenarios.

Consequently, the full potential of the ejector circuit could not be realized in the test scenarios presented in this thesis.

An ejector with a larger motive nozzle, or ideally a parallel arrangement of several differently sized ejectors, could have eliminated the need for operation with flow through the EV17 bypass, thus yielding higher ejector efficiency, and consequently increased HX1 refrigerant mass flow rate, in addition to a higher compressor suction pressure.

6.2 Heat transfer at HX2

The results presented in 5.3.2, show a temperature approach at HX2 ($\Delta t_{ap,HX2}$) of 10.3 and 11.1 K for the basic and ejector circuit, respectively, during simultaneous operation at design conditions (test 1.2.3(1)).

The large $\Delta t_{ap,HX2}$ may be a result of excessive internal heat conduction between the horizontal tube passes in HX2. Moreover, as can be observed in *Figure 3.16* and *Table 10*, the design of the pilot unit HX2 is relatively compact compared to the standard unit HX2, having approximately half of the "depth", thus further limiting the temperature glide.

In order to maximize heat transfer efficiency at HX2 an alternative design, with vertically split sections on the first two or three horizontal tube passes, should be considered in order to minimize exergy losses related to heat conduction between "hot" and "cold" parts of HX2, thus facilitating a low $\Delta t_{ap,HX2}$. Alternatively, a HX2 design with eight horizontal tube passes, or ideally a combination of the two designs, should be considered for the same reasons.

6.3 Heat transfer at HX1

HX1 of, both, the standard and the pilot unit have the same amount of individual distribution feeds, i.e. 10 tubes per circuit, as depicted in *Figure 3.10* and *3.15*. As explained in section 2.3.2, the swept refrigerant volume in a R134a system is roughly 8 to 9 times that of a similar capacity R744 system. Thus, one would assume that the refrigerant velocity inside the HX1 tubing of the pilot unit would be lower than that in the standard; hence, possibly, leading to a less than optimal heat transfer coefficient.

When assessing the states of the two refrigerants at a comparable evaporator inlet temperature and vapor fraction, e.g. 10°C and 0.2, the values in *Table 18* can be found in *RnLib*.

Table 18: Comparisson of neccesary refrigerant volume rate R744 and R134a. where t_{sat} and p_{sat} is the saturation temperature and pressure, equal to the evaporator temperature and pressure, respectively. $Vv_{g,inlet}$ and $v_{g,sat}$ is the specific volume at the inlet and outlet of the hypothetical evaporator, respectively. Hh_{inlet}, h_{outlet} andΔh_{evao} is the inlet, outlet and difference in specific enthalpy of the evaporator, respectively. The values were calculated using RnLib, presuming a evaporator inlet vapor fraction of 0.2.

	t_{sat} [°C]	p_{sat} [bar]	$v_{g,inlet}$ [m^3/kg]	$v_{g,sat}$ [m^3/kg]	h_{inlet} [kJ/kg]	h_{outlet} [kJ/kg]	Δh_{evao} [kJ/kg]
R744	10	45.01 bar	0.0024	0.0073	265.08	423.30	158.22
R134a		4.15 bar	0.0105	0.0491	251.32	402.89	151.57
Ratio [R134a/R744]			4.38	6.72			0.96

If presuming saturated gas at the evaporator outlet, i.e. 0 K superheat, the refrigerant volume rate through the R134a evaporator will be approx. 5.3 times that in the R744, for a given capacity, assuming linearity for all the values. Thus, a relation can be derived as seen below Eq.(54).

$$\dot{V}_{R134a} = 5.3 \cdot \dot{V}_{R744} \qquad \text{Eq.(54)}$$

$$[A \cdot v]_{R134a} = 5.3 \cdot [A \cdot v]_{R744}$$

$$[d^2 \cdot v]_{R134a} = 5.3 \cdot [d^2 \cdot v]_{R744}$$

$$v_{R744} = \frac{[d^2 \cdot v]_{R134a}}{5.3 \cdot d_{R744}^2}$$

When applying the standard and pilot unit HX1 inner tube diameters of 9.53 and 4.53 mm, respectively, the following relation can be derived.

$$v_{R744} \approx 0.83 \cdot v_{R134a} \qquad \text{Eq.(55)}$$

Provided the above presumptions, Eq.(55) suggests that the refrigerant velocity (v) inside HX1 of the pilot unit is approximately 83% that of the standard unit during similar capacity operation. This may have a noticeable effect on the heat transfer coefficient on the inner tube walls, especially if the lower velocity corresponds with laminar flow.

Consequently, a lower heat transfer efficiency results in a lower evaporation temperature/pressure for a given cooling capacity, as explained in section 2.2.3.1.

Moreover, as the results presented in section 5.2 show, evaporation temperature in the ejector circuit is consistently lower than in the basic circuit, which may be partly attributed to the lower HX1 mass flow rate in the ejector circuit.

6.4 High-pressure

The presented results show that the high-pressure limit of 100 bar have an increased significance on performance during ambient temperatures above 28℃. This can be attributed to the refrigerant state at the outlet of HX2 being in close proximity to the critical point, thus a relatively small change in high-pressure, yields a relatively large change in specific enthalpy, owing to the "flat" shape of the isotherms, as depicted in *Figure 5.2*.

6.5 Inconsistencies with the *FTL* calculation model

The methodology applied by *FTL* to calculated refrigerant mass flow rate through HX1 was inconsistent with the methodology of this thesis, as have been shown in section 5.5.

Although not used to calculate any further parameters in the *FTL* results, the values would have given the test engineer the impression of a higher refrigerant mass flow rate through HX1, which in turn would make it more acceptable to assume that the superheat measured at R28 was a result of measurement deviations.

Moreover, as shown in section 5.5, the methodology applied by *FTL* to calculate temperature approach at HX2, suggests a higher HX2 heat transfer efficiency.

7 Conclusion

As explained in the introduction, the objective of this thesis had to be adjusted through the course of the thesis work. Consequently, the presented findings does not support any very substantial conclusions with regard to the initial scope, but lays a good foundation for the further work, proposed in chapter 8.

The description of the NSB *Stadler* FLIRT HVAC system and the related literature presented in this thesis, gives an important insight and basis knowledge, considered valuable for the future progress in the pilot R744 HVAC project.

Moreover, the reference unit DAQ system and record-file signal description, developed during the thesis work (Appendix A), facilitates the analysis of field measurement data to be gathered during the upcoming test campaign.

Through the analysis of data recorded from the reference unit, it could be established that the standard HVAC unit onboard the NSB *Stadler* FLIRT trainsets, have been unable to cover any of the ventilation air heating demand, due to an inadequate capacity control range. The find provide increased expectations for energy savings related to the implementation of the pilot unit, provided an effective control strategy can be developed and integrated.

Laboratory bench tests of the pilot unit showed a total HVAC unit cooling capacity of 18.6 kW, at the design load conditions, consequently falling 5.4 kW short of the 24 kW requirement, as can be seen in *Table 17* (test 1.3.1(5)).

Shortly summarized the shortcoming in capacity can largely be attributed to insufficient heat transfer efficiency at HX2, poor control of the ejector circuit high-pressure, and insufficient refrigerant mass flow rate through the ejector circuit side of HX1, as a result of the amount of refrigerant bypassed through EV17. A discussion of the presented results have been included in Chapter 6, in addition to some suggestions for improvements.

Future analysis of field data gathered in the upcoming test campaign, will determine if the pilot R744 HVAC unit is a viable replacement for the standard R134a HVAC units, onboard the NSB *Stadler* FLIRT trainsets.

8 Proposals for further work

As was explained in section 4.1, the vast majority of data recorded from the reference unit proved useless, due to a range of uncovered issues. However, some of the data may still serve a useful purpose. E.g. as may be deduced from Appendix A5, the record-file signal values from signal D_CRXPASSKL66 and D_CRXPASSKL33, can be used to establish a passenger load profile for the BM 75-41 commuter trainset, as these data proved reliable.

The data-logger outfitted on the reference unit have a sampling rate of 10 seconds, thus an immense amount of data will be made available during the test campaign. Hence, an effective method for processing and sorting the relevant data should be developed, e.g. using *Excel*, in order to facilitate analysis. The signal description included in Appendix A, will prove useful in this process.

When the pilot unit is part load operated, the conditions in the refrigerant circuit will fluctuate, due to the cycling intervals of the *CRIT* capacity modulation system, described in section 3.2.2.1. Consequently, this can result in unreliable measurement data onboard the trainset, owing to the 10-second sampling rate of the data-logger. Thus, the possibility for an increased sampling rate, or an averaging function, should be investigated and suggested for implementation to the logger software.

Analyze differences in operation patterns between the pilot and reference unit onboard the trainset, and evaluate the control strategy of the two units in cooling mode operation.

As explained in section 4.1, it was discovered that the standard unit is unable to cover any of the ventilation air heating demand. This find provide increased expectations for energy savings related to the implementation of the pilot unit, provided an effective control strategy can be developed and integrated.

Thus, an assessment of the ventilation air heating demand coverage provided by the pilot unit, should be conducted. However, as explained in Appendix A, the power supplied to the electrical heating coils is not registered by the CM4, thus it is not included in the record-file data. Consequently, alternative comparison parameters needs to be established, e.g. operating hours.

Further, the results from the coverage assessment can be used in order to establish if the control strategy for the pilot unit is sufficient during heat pump operation. Furthermore, based on these results, some suggestions for improvements to the control strategy can be presented for *FTL*.

The total heating demand coverage, provided by the HVAC unit, is relatively limited, due to the heat recovery system and the high ratio of recirculated compartment air, as described in chapter 3. Hence, alternative system solutions, enabling an increase in HVAC unit heating demand coverage, would significantly improve the energy saving potential related to the implementation of the pilot unit. Consequently, an investigation within this topic could prove beneficial for the further progress in the pilot R744 HVAC unit project.

Define criteria's for a passenger survey, to be conducted during the test campaign. Inspiration can be taken from the work of Xiaojiang Ye et al. [75], who in 2004 developed and conducted a survey for assessing the thermal comfort and indoor air quality onboard high-speed passenger railway vehicles in China.

References

1. George, C. and P.E. Briley, *100 Years of Refrigeration - A History of Refrigeration.* ASHRAE journal, 2004.
2. Lorentzen, G., *Revival of carbon dioxide as a refrigerant.* International Journal of Refrigeration, 1994. **17**(5): p. 292-301.
3. Protocol, M., *Montreal protocol on substances that deplete the ozone layer.* Washington, DC: US Government Printing Office, 1987. **26**.
4. EEA, *EEA Technical report No 22/2015, Fluorinated greenhouse gases 2014,* in *Summary of data reported by comapnies on the production, import and export of fluorinated greenhouse gases in the European Union*. 2015, European Environmental Agency: Publications office of the European Union, 2015.
5. European Parliament, *Regulation (EC) No 517/2014 of the European Parliament and of the council of 17 May 2006 on fluorinated greenhouse gases*, E. Union, Editor. 2006, Official Journal of the European Union: Strasbourg.
6. Parliament, E., *Regulation (EU) No 517/2014 of The European Parliament and of the council of 16 April 2014 on fluorinated greenhouse gases and repealing Regulation (EC) No 842/2006*, E. Union, Editor. 2014.
7. Stene, J., *"NARECO2" Master Module 7 CO2 Heat pumps.* Education and Culture Lifelong learning programme LEONARDO DA VINCI, 2009.
8. Hrnjak, P. *Thermodynamic possibilities and technological opportunities for improving the science of refrigeration in search for low global warming thermal systems*. in *Proc. Int. Symp. On Next-Generation Air Conditioning and Refrigeration Technology, Tokyo K*. 2010.
9. Hafner, A. and K. Banasiak. *R744 ejector technology future perspectives*. in *Journal of Physics: Conference Series*. 2016. IOP Publishing.
10. NSB, *NSB Persontogs miljøpolitikk*. 2016.
11. NSB, *NSB Togene kutter strømforbruken*. 2016.
12. Bentzrød, S., *Her fant NSB endelig tog som går - fra første dag*, in *Aftenposten*. 2015: aftenposten.no.
13. NSB-Group, *NSB Group Annual Report of 2016*. 2016.
14. IEA and UIC, *Railway handbook 2015 - Energy consumption and CO_2 emissions.* International Energy Agency, 2015.
15. UIC, *Technologies and potential developments for energy efficiency and CO_2 reduction in rail systems.* International Union of Railways, 2016.
16. Vetterli, N., et al. *Energy efficiency of railway vehicles*. in *Proceedings of International Conference CISBAT 2015 Future Buildings and Districts Sustainability from Nano to Urban Scale*. 2015. LESO-PB, EPFL.
17. ASHRAE, *Guideline 23P*, in *Guideline for the Design and Application of Heating, Ventilation and Air Conditioning Equipment for Rail Passenger Vehicles*. 2014.
18. Hafner, A., K. Banasiak, and L. Boeck, *R744 train HVAC unit.* 12th Gustav Lorentzen Conference on Natural Refrigerants GL2016: Proceedings, 2016.
19. Schwarz, W. and J.-M. Rhiemeier, *The analysis of the emissions of fluorinated greenhouse gases from refrigeration and air conditioning equipment used in the transport sector other than road transport and options for reducing these emissions Maritime, Rail, and Aircraft Sector.* Rail, and Aircraft Sector–Final report, European Commission, 2007.
20. IEA, U., *Railway Handbook 2016 "Energy Consumption and CO_2 emissions"*. International Energy Agency, 2016.

21. Ona, A., et al., *"NARECO2" Master Module 7 - Drivers for implementation of CO2 technology*. Education and Culture Lifelong learning programme LEONARDO DA VINCI, 2009.
22. Engelking, S. and H. Kruse, *Development of air cycle technology for transport refrigeration.* 1996.
23. Pearson, A., *Carbon dioxide—new uses for an old refrigerant.* international Journal of Refrigeration, 2005. **28**(8): p. 1140-1148.
24. Stockholm, J., *Large-Scale Cooling*, in *CRC Handbook of Thermoelectrics*. 1995, CRC Press.
25. Stockholm, J. *PROTOTYPE THERMOELECTRIC AIR CONDITIONING or A PASSENGER RAILWAY COACH*. in *Conference on Thermoelectric Energy Conversion. Arlington Texas*. 1982.
26. Ivanov, A., et al. *Thermoelectric air conditioner for railways-modifications, results, prospects*. in *Thermoelectrics, 2002. Proceedings ICT'02. Twenty-First International Conference on*. 2002. IEEE.
27. Yang, B., H. Ahuja, and T.N. Tran, *Review article: Thermoelectric technology assessment: Application to air conditioning and refrigeration.* HVAc&R Research, 2008. **14**(5): p. 635-653.
28. GmbH, V.K., *New CO2 air conditioning system—a milestone*, V.K. GmbH, Editor., 2016, Vossloh Kiepe GmbH.
29. Liebherr, *Liebherr - Transportation Systems carries out field data analysis of air cycle air conditioning system*. 2015.
30. DTU, *CoolPack, Simulation program for heat pumps and refrigeration plants (freeware)*. 2000, Technical University of Denmark.
31. Langley, B.C., *Heat pump technology: systems design, installation, and troubleshooting*. 1989: Prentice Hall.
32. Dincer, I. and M. Kanoglu, *Refrigeration Systems and Applications (2)*. 2010, Hoboken, GB: Wiley.
33. Hundy, G.F., A.R. Trott, and T.C. Welch, *Refrigeration, Air Conditioning and Heat Pumps (5th Edition)*. 2016, Elsevier.
34. Stene, J.r., *Varmepumper : grunnleggende varmepumpeteknikk*. Rev. utg. ed. SINTEF rapport (SINTEF. Kuldeteknikk : trykt utg.). Vol. STF84 A97302. 2001, Trondheim: SINTEF Energi, Klima- og kuldeteknikk.
35. Acca, P.E. Foundation, and Rses, *HVACR 401 : Heat Pumps*. 2011, Clifton Park, US: Cengage Learning.
36. Wujek, S.S. and P. Hrnjak, *Effects of Oil on aTranscritical Carbon Dioxide Air Conditioning Systems–some experiences.* 2006.
37. Nekså, P., H. Walnum, and A. Hafner, *CO2 - A refrigerant from the past with prospects of being one of the main refrigerants in the future.* SINTEF Energy Research,, 2010.
38. Pettersen, J., M.-H. Kim, and C.W. Bullard, *Fundamental process and system design issues in CO 2 vapor compression systems.* Progress in energy and combustion science, 2004. **30**(2): p. 119-174.
39. Hafner, A., *"NARECO2" Master Module 4 CO2/R744 Mobile air-conditioning (MAC).* Education and Culture Lifelong learning programme LEONARDO DA VINCI, 2009.
40. Becnel, C.J. and J.J. McLean, *Method for manufacturing a micro tube heat exchanger*. 2012, Google Patents.
41. Desireddy, V.R. and J.E. Field, *System and Method for Repairing Microchannel Heat Exchanger*. 2013, Google Patents.
42. Stene, J., *TEP4260 Varmepumper til bygningsklimatisering, Forelesningskompendie termodynamic*. 2016.

43. Austin, B.T. and K. Sumathy, *Transcritical carbon dioxide heat pump systems: A review.* Renewable and sustainable energy reviews, 2011. **15**(8): p. 4013-4029.
44. Nekså, P., *CO2 heat pump systems.* International Journal of Refrigeration, 2002. **25**(4): p. 421-427.
45. Beaver, A.C., et al., *An experimental investigation of transcritical carbon dioxide systems for residential air conditioning*. 1999, Air Conditioning and Refrigeration Center. College of Engineering. University of Illinois at Urbana-Champaign.
46. Bullard, C., J. Yin, and P. Hrnjak, *Compact counterflow gas cooler for R-744/Discussion.* ASHRAE Transactions, 2002. **108**: p. 482.
47. Domanski, P.A., D.A. Didion, and J.P. Doyle, *Evaluation of suction-line/liquid-line heat exchange in the refrigeration cycle.* International Journal of Refrigeration, 1994. **17**(7): p. 487-493.
48. Lorentzen, G. and J. Pettersen, *A new, efficient and environmentally benign system for car air-conditioning.* International Journal of Refrigeration, 1993. **16**(1): p. 4-12.
49. Robinson, D.M. and E.A. Groll, *Efficiencies of transcritical CO 2 cycles with and without an expansion turbine: Rendement de cycles transcritiques au CO2 avec et sans turbine d'expansion.* International Journal of Refrigeration, 1998. **21**(7): p. 577-589.
50. Torrella, E., et al., *Energetic evaluation of an internal heat exchanger in a CO 2 transcritical refrigeration plant using experimental data.* International Journal of refrigeration, 2011. **34**(1): p. 40-49.
51. Silberstein, E., *Heat Pumps*. 2003: Thomson/Delmar Learning.
52. Yoshino, H., *Electronic expansion valve*. 1986, Google Patents.
53. Fornasieri, E., et al., *"NARECO2" Master Module 1 Thermodynamic topics.* Education and Culture Lifelong learning programme LEONARDO DA VINCI, 2009.
54. Elbel, S. and N. Lawrence, *Review of recent developments in advanced ejector technology.* International journal of refrigeration, 2016. **62**: p. 1-18.
55. Sarkar, J., *Ejector enhanced vapor compression refrigeration and heat pump systems—A review.* Renewable and Sustainable Energy Reviews, 2012. **16**(9): p. 6647-6659.
56. Kornhauser, A.A., *The use of an ejector as a refrigerant expander.* 1990.
57. Banasiak, K., A. Hafner, and T. Andresen, *Experimental and numerical investigation of the influence of the two-phase ejector geometry on the performance of the R744 heat pump.* International Journal of Refrigeration, 2012. **35**(6): p. 1617-1625.
58. Lorentzen, G., *Throttling, the internal haemorrhage of the refrigeration process*. 1984: Place of publication not identified.
59. Brown, G.A., G.F. Harper, and C.A. Kemper, *Multiple-phase ejector refrigeration system*. 1966, Google Patents.
60. Elbel, S. and P. Hrnjak, *Experimental validation of a prototype ejector designed to reduce throttling losses encountered in transcritical R744 system operation.* International Journal of Refrigeration, 2008. **31**(3): p. 411-422.
61. Lawrence, N. and S. Elbel, *Analysis of two-phase ejector performance metrics and comparison of R134a and CO2 ejector performance.* Science and Technology for the Built Environment, 2015. **21**(5): p. 515-525.
62. Elbel, S., *Historical and present developments of ejector refrigeration systems with emphasis on transcritical carbon dioxide air-conditioning applications.* International Journal of Refrigeration, 2011. **34**(7): p. 1545-1561.
63. Liu, F., Y. Li, and E.A. Groll, *Performance enhancement of CO 2 air conditioner with a controllable ejector.* international journal of refrigeration, 2012. **35**(6): p. 1604-1616.
64. Hafner, A., S. Försterling, and K. Banasiak, *Multi-ejector concept for R-744 supermarket refrigeration.* International Journal of Refrigeration, 2014. **43**: p. 1-13.

65. Martinez-Frias, J. and S. Aceves, *Effects of evaporator frosting on the performance of an air-to-air heat pump.* TRANSACTIONS-AMERICAN SOCIETY OF MECHANICAL ENGINEERS JOURNAL OF ENERGY RESOURCES TECHNOLOGY, 1999. **121**: p. 60-65.
66. Pettersen, J., A. Hafner, and M. Brånås. *Some safety aspects of CO2 vapour compression systems*. in *Annex 27 workshop: Selected Issues on CO2 in Compression Systems, Final Report*. 2004.
67. Reid, R., *THE RAPID DEPRESSURIZATION OF HOT, HIGH PRESSURE LIQUIDS OR SUPERCRITICAL FLUIDS ME Kim-E Department of Chemical.* Chemical engineering at supercritical fluid conditions, 1983: p. 81.
68. Pettersen, J. and J. Hakenjos, *Boiling liquid expanding vapour explosions (BLEVE) in CO2 vessels: Initial experiments.* Science et technique du froid, 2001: p. 216-224.
69. Pettersen, J. *Experimental study on boiling liquid expansion in a CO2 vessel*. in *Annex 27 workshop: Selected Issues on CO2 in Compression Systems, Final Report*. 2004.
70. Bodinus, W.S., *The rise and fall of carbon dioxide systems: The first century of air conditioning.* ASHRAE journal, 1999. **41**(4): p. 37.
71. Lorentzen, G., J. Pettersen, and R.R. Bang, *Method and device for high side pressure regulation in transcritical vapor compression cycle*. 1993, Google Patents.
72. Liao, S. and T. Zhao, *Measurements of heat transfer coefficients from supercritical carbon dioxide flowing in horizontal mini/micro channels.* Transactions-American Society of Mechanical Engineers Journal of Heat Transfer, 2002. **124**(3): p. 413-420.
73. Stene, J., *TEP4260 Varmepumper til bygningsklimatisering, Arbeidsmedier*. 2016.
74. McCulloch, A. and A.A. Lindley, *From mine to refrigeration: a life cycle inventory analysis of the production of HFC-134a.* International Journal of Refrigeration, 2003. **26**(8): p. 865-872.
75. Ye, X., et al., *Thermal comfort and air quality in passenger rail cars.* International Journal of Ventilation, 2004. **3**(2): p. 183-192.

Appendix A: Data acquisitioning (DAQ) system reference R134a HVAC unit

The HVAC unit used as a reference to evaluate the performance of the pilot R744 HVAC unit during the measurement campaign is a standard R134a HVAC unit. However, the reference unit have been retrofitted with additional measuring equipment; i.e. a data acquisitioning (DAQ) system with additional temperature and pressure sensors, and current meters, which will be further described in this appendix.

A full description of all the signals assigned for logging, and their corresponding record-file, wiring-diagram and controller addresses have been prepared further down in Appendix A.

It should be mentioned that several issues with the DAQ system were detected during the thesis work, as have been disclosed in section 4.1. However, Appendix A describes the DAQ system as it was intended to function, and how it finally will function when the issues, disclosed in section 4.1, have been sorted.

The reference HVAC unit, does like the standard unit, hold a HVAC controller that governs control outputs for the HVAC system components based on data received from local sensors in the HVAC unit, and data transferred via the train system CAN-bus. Moreover, the HVAC controller also sends data to the train system CAN-bus. The HVAC controller (FPC24/2) is referred to as A1 in the wiring diagrams. A simplified block diagram representing the communication flow of the standard HVAC unit is depicted in *Figure 1*.

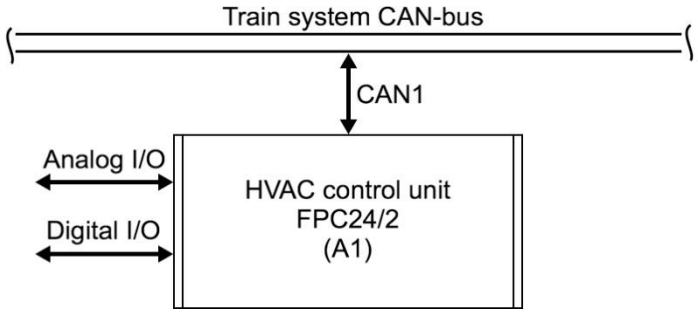

Figure 1: Data communication block diagram of standard R134a HVAC, where I/O abbreviates input/output.

To facilitate data logging of the reference unit, it have been retrofitted with two additional signal-processing devices, depicted in *Figure 1*, a data logger (CCM8) and a current measuring relay (CM4), addressed as A4 and A5 in the wiring diagrams, respectively.

The data assigned for logging is stored on a SD card inserted to the CCM8. The CCM8 also have integrated Ethernet connectivity, thus enabling the possibility of real-time online data

transfer, however, this feature is currently not in use. Consequently, the SD card have to be physically removed from the CCM8 and the content uploaded to an external computer at regular intervals in order to access the data. The sampling rate of the CCM8 is set to 10 seconds, i.e. every 10 second the momentary values from the equipment assigned for logging is stored.

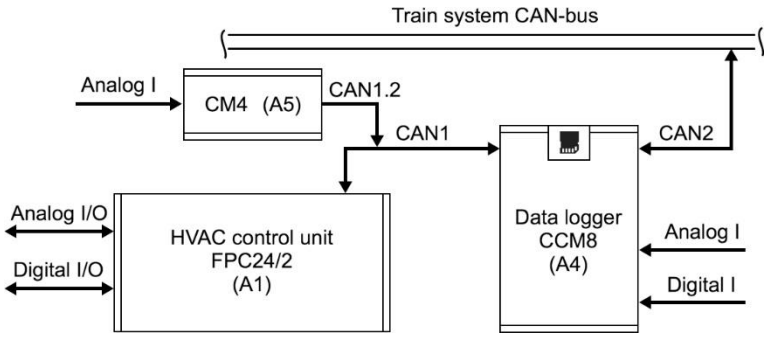

Figure 2: Data communication block diagram of reference R134a HVAC, where I and O abbreviates inputs and outputs, respectively.

Figure 2 is a block diagram representing the data communication on the reference unit. As may be observed, communication between the FPC24/2 (HVAC controller) and the train system CAN-bus flow via the retrofitted CCM8. Moreover, the figure show that the CCM8 also receives direct digital and analog input signals (Analog I and Digital I). These input signals are from the additional retrofitted sensors specially outfitted the reference unit, and measure pressure and temperature in the refrigerant circuit.

Furthermore, the CM4, depicted in *Figure 2*, measure the electrical current to the two compressors, the 110V DC system and the 400V AC system, which is subsequently transferred via the digital CAN1.2 and CAN1 data-bus to the CCM8 for logging. The majority of signals logged by the CCM8 is from the standard system layout connected to the FPC24/2.

Only sensors for measuring suction and discharge pressures are included in the refrigerant circuits of the standard HVAC unit, whereas the DAQ-system of the reference unit include several additional sensors for measuring pressure, temperature, and current, as depicted in *Figure 3*.

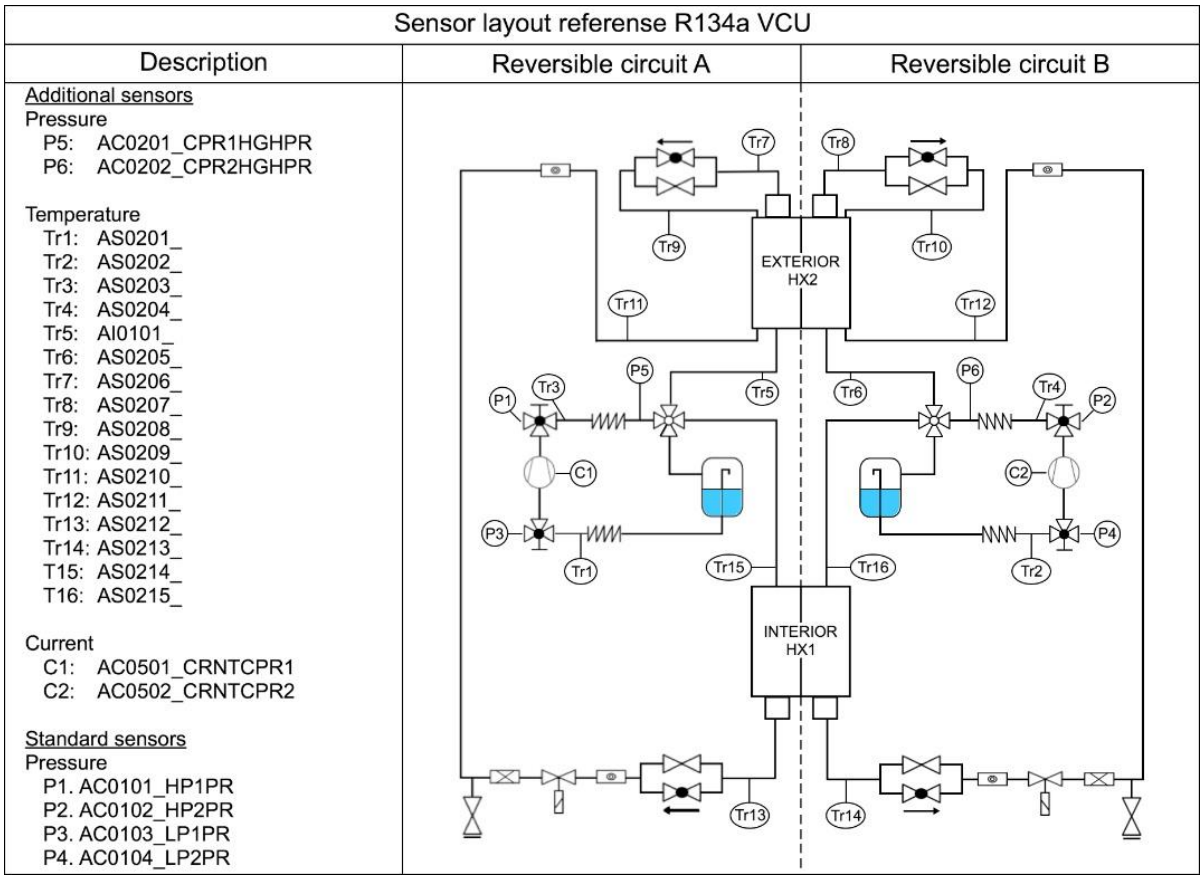

Figure 3: Sensor layout reference R134a VCU, showing the circuit location of the standard and additional sensors of the two refrigerant circuits.

The CCM8 also logs data from sensors located in the airstream of the AHU and HRS, these sensors are part of the standard unit layout, and are connected to the FPC24/2. The location of these sensors in the airstream can be found in *Figure 4*.

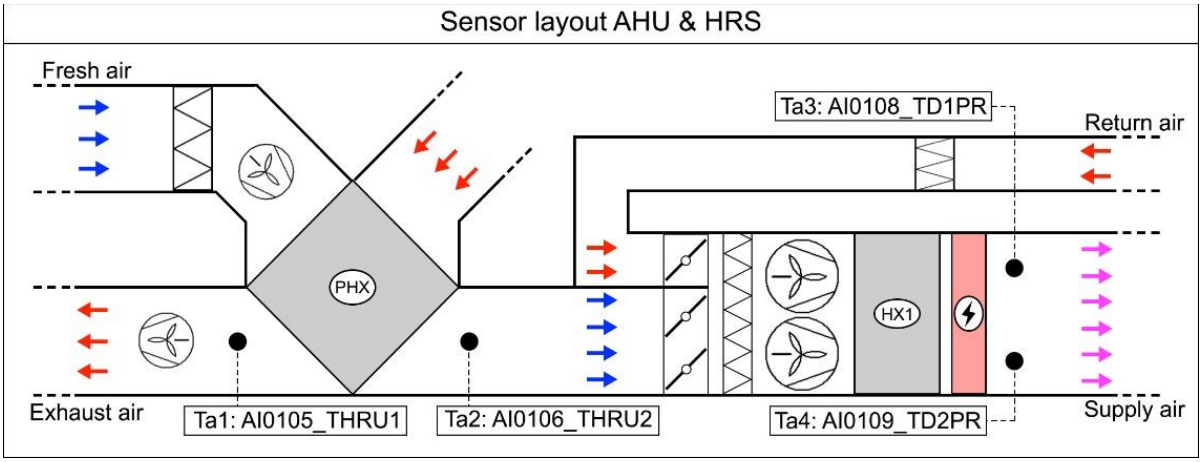

Figure 4: Sensor layout reference R134a HVAC fig.B, showing the location of the standard sensors in the AHU & HRS.

The sensors downstream of HX1, i.e. Ta3 and Ta4, measure the top and bottom outlet air temperature of HX1, respectively.

The record addresses corresponds with the naming system in the record DAT file from the SD card on CCM8, and is also used in the wiring diagrams. The figure addresses corresponds with the depictions in *Figure 3* and *4*. While the system address corresponds with the sensor/component marking on the physical system, also used in the wiring diagram. Consequently, the record address is the most essential for the purpose of analyzing the record file data.

The figure below depicts the header used in Appendix A, where the column headed by device states what device, i.e. CCM8, CM4, FPC24/2 or train system CAN-bus, the signal is sent via.

Address			Device	Connection			Value	Description	Location	Medium	VCU Circuit	VCU Flow
Record	Figure	Component		A/D	I/O	Connection						

Header Appendix A.

Moreover, the columns headed by connection specifies the signal type, i.e. digital or analog, input or output, and the corresponding connection on the controller. The connection signature can be very useful when navigating the wiring diagrams, as it is the most tangible reference.

Furthermore, as flow direction through many of the refrigerant circuit components is altered depending on operating mode, the mode of operation corresponding to the signal description is specified, if relevant, in the VCU flow column.

Refrigerant temperature sensors

Appendix A1 lists the additionally retrofitted refrigerant circuit temperature sensors equipped on the reference unit, depicted in *Figure 3*. All of these sensors are connected to a digital-bus (DigBus1/3), which is directly connected to the digital input X7:2/3 of the CCM8, apart from sensor AI0101, which is an analog temperature sensor, which for some reason is, connected to the FPC24/2. None of the signals listed in Appendix A1 have any other function than being logged by the CCM8, and are not communicated to other systems on the train.

Several issues related to these sensors were detected during the thesis work, as have been explained in section 4.1.

Refrigerant pressure sensors

Appendix A2 lists the standard and retrofitted refrigerant circuit pressure sensors, depicted in *Figure 3*. The standard sensors, i.e. AC010(1 to 4), sends analog 4-20 mA signals to the FPC24/2, which is subsequently sent the CCM8 via CAN1. Whereas the retrofitted sensors, i.e. AC0201 and AC0202, sends analog 4-20 mA signals directly to input X6:1/2/3/4 on the CCM8.

As may be observed from the description in Appendix A2, four of the sensors measure high-side/discharge pressure, the standard sensors are coupled to a nipple on the compressor cylinder head, whereas the retrofitted sensors are coupled to the discharge line downstream of the anti-vibration piping section, as depicted in *Figure 3*.

The 4-20 mA signal corresponds linearly to the pressures 0-10 bar and 0-40 bar for the standard low-pressure and high-pressure sensors, respectively. Whereas the retrofitted sensors have a range of 0-160 bar corresponding linearly to a 4-20 mA signal, which resulted in some issues, disclosed in section 4.1.

It should also be mentioned that the record addresses for the retrofitted sensors is differently referred to in the wiring diagram and the record file, as a result of a typing error in the record-file template on the SD card. Consequently, the retrofitted pressure sensors are addressed AC0201 and AC0202, and AC0401 and AC0402, in the record file and the wiring diagrams, respectively.

Electrical current meter

Appendix A3 lists signals from the retrofitted current meter CM4, some of which depicted in *Figure 3.* The electrical current supplied to compressor 1 and 2, all of the 400V-3-50Hz AC and 110V DC equipment is measured by CM4.

Moreover, the CM4 translate the flow of current into digital data signals and subsequently sends the data to the CCM8 via CAN1.2 and CAN1 (*Figure 2*). Furthermore, the electrical current data is also used to calculate electrical work.

The 110V DC system powers the support fresh and exhaust air fans, and some of the electrical controls and control objects of the HVAC unit. Whereas the 400V-3-50Hz AC system powers the rest of the HVAC unit equipment including the compressors, HX1 and HX2 fan motors, etc. However, the current supplied to the electrical heating coils of the AHU is supplied from the railway main lines and is not measured by the CM4, as explained further down.

Air temperature sensors

Appendix A4 lists the air temperature sensors assigned for logging by the CCM8, some of which depicted in *Figure 4*. These sensors are part of the standard layout and are located in the HVAC unit, the HRS, the passenger compartment, and the carriage exterior envelope.

As may be observed in Appendix A4, four measured compartment temperatures are used to establish an average compartment temperature A_PCTIAVRG, which is used as an estimate to

define the return air temperature to the AHU. All of the compartment temperature sensors are at ceiling height.

Control and reply signals ventilation system

Appendix A5 lists the logged control and reply signals for the ventilation system, i.e. fan motor operation, damper positions passenger compartment occupancy level, etc..

The signals that represents the damper opening of the fresh air bypass damper in the HRS, and the fresh/return air damper in the AHU are given as an electrical resistance 0.27-5.27 kOhm, where 0.27 and 5.27 kOhm corresponds with 0° and 90° damper angle, respectively. According to *FTL*, a linear characteristic can be assumed for the damper, and the air volume rates corresponding to the damper angles can be found in Appendix B, which is based on experiments conducted by *FTL*.

The fresh air bypass signal have the record address A_PRFPBPRES in the record file and AI0114_FpBpFre in the wiring diagram, whereas the fresh return air damper signal have the record address A_PRFPOARES in the record file and AI0115_FpFreRec in the wiring diagram.

The supply air fan speed, AQ0101_NFSF, is stated as a 0-100% signals, whereas the speed of the support fresh air fan, AQ0102_NFAF, is stated as a 0-10V signal where 0 and 10V represents 0 and 100%, respectively. The corresponding air volume rate can be established using Appendix B.

The exhaust air fan speed is represented by the signals, DQ0114_ and DQ0115_. The control signal values, i.e. 0-10V signal, corresponding to the record file values, i.e. 0, 1, can be found in the table below ,and the air volume rate corresponding to the control signal value can be read out of Appendix B.

Interperating exhaust air fan signals.

Exhaust air fan signals				
	Exhaust fan speed		DQ0114_EXFST1	DQ0115_EXFST2
Command	Switched off		0	0
	Low	3,7V	1	0
	Medium	5,2V	1	1
	High	7.2V	0	1

Control and reply signals vapor compression unit

Appendix A6 lists the logged control and reply signals from the main components in the VCU, most of which are sent via the FPC24/2 apart from “compressor start block”,

D_CRXNOSTRTCPR, which is sent from the train system CAN-bus. When this signal is active, i.e. a value of 1, compressor startup will be blocked. This can occur if the energy management system of the train detects low power from the main lines, and is not usual for normal operation.

Electrical heating coils

Appendix A7 lists the logged control signals to the two electric heating coils downstream of HX1 in the AHU. The total number of operating hours by the two coils is also logged.

The electrical heating coils of the HVAC unit is the only equipment supplied directly by the railway main power lines, however at a reduced voltage 400V-1-$16^{2/3}$Hz. This is largely attributed to the high power required by the two coils, approx. 11kW each, and the intermittent operation characteristic that would otherwise impose the need for a much larger 400V-3-50Hz generator on the train. Consequently, the current supplied to the electrical heating coils is not being measured by the CM4 current meter.

Control signals active system mode

Appendix A8 lists logged controller output signals dictating the HVAC systems active operating mode, not to be confused with the active operating mode of the VCU (HP or AC).

When pre-heating/cooling mode is active, only the supply fans are operated, thus precluding the intake of fresh air and discharge of exhaust air, whereas when automatic mode is active all fans are operated as stated in *Table 2* section 3.2.

Some issues related to these signals was detected, as was explained in section 4.1.

Power reduction

Appendix A9 lists logged input signals from the train system CAN-bus representing a reduction in power, these signals should always read 0 for normal operation.

Additionally, signal DI0123_ represent the 400V-3-50Hz power supply to the HVAC unit, should always be 1.

Appendix A1: Refrigerant temperature sensors

Appendix A1: Refrigerant temperature sensors												
Address			Device	Connection			Value	Description	Location	Medium	VCU	VCU
Record	Figure	Component		A/D	I/O	Connection					Circuit	Flow
AS0101_	Tr1	B20	CCM8	D	I	X7:2/3	Temperature [C]	Suction gas temperature 1	VCU	R134a	1	HP/AC
AS0102_	Tr2	B21	CCM8	D	I	X7:2/3	Temperature [C]	Suction gas temperature 2	VCU	R134a	2	HP/AC
AS0103_	Tr3	B22	CCM8	D	I	X7:2/3	Temperature [C]	Discharge temperature 1	VCU	R134a	1	HP/AC
AS0104_	Tr4	B23	CCM8	D	I	X7:2/3	Temperature [C]	Discharge temperature 2	VCU	R134a	2	HP/AC
AI0101_TCDROUT1	Tr5	B36	FPC24/2	A	I	P7:A3/B3	Temperature [C]	HX2 inlet 1	VCU	R134a	1	AC
AS0105_	Tr6	B25	CCM8	D	I	X7:2/3	Temperature [C]	HX2 Inlet 2	VCU	R134a	2	AC
AS0106_	Tr7	B26	CCM8	D	I	X7:2/3	Temperature [C]	HX2 Outlet 1	VCU	R134a	1	AC
AS0107_	Tr8	B27	CCM8	D	I	X7:2/3	Temperature [C]	HX2 Outlet 2	VCU	R134a	2	AC
AS0108_	Tr9	B28	CCM8	D	I	X7:2/3	Temperature [C]	HX2 Subcooling inlet 1	VCU	R134a	1	AC
AS0109_	Tr10	B29	CCM8	D	I	X7:2/3	Temperature [C]	HX2 Subcooling inlet 2	VCU	R134a	2	AC
AS0110_	Tr11	B30	CCM8	D	I	X7:2/3	Temperature [C]	HX2 Subcooling outlet 1	VCU	R134a	1	AC
AS0111_	Tr12	B31	CCM8	D	I	X7:2/3	Temperature [C]	HX2 Subcooling outlet 2	VCU	R134a	2	AC
AS0112_	Tr13	B32	CCM8	D	I	X7:2/3	Temperature [C]	HX1 Inlet 1	VCU	R134a	1	AC
AS0113_	Tr14	B33	CCM8	D	I	X7:2/3	Temperature [C]	HX1 Inlet 2	VCU	R134a	2	AC
AS0114_	Tr15	B34	CCM8	D	I	X7:2/3	Temperature [C]	HX1 Outlet 1	VCU	R134a	1	AC
AS0115_	Tr16	B35	CCM8	D	I	X7:2/3	Temperature [C]	HX1 Outlet 2	VCU	R134a	2	AC

Where: A, D, I, and O, abbreviates analog, digital, input and output, respectively.

Appendix A2: Refrigerant pressure sensors

Appendix A2: Refrigerant pressure sensors												
Address			Device	Connection			Value	Description	Location	Medium	VCU	VCU
Record	Figure	Component		A/D	I/O	Connection					Circuit	Flow
AC0101_HP1PR	P1	F2	FPC24/2	A	I	P6:A1/A2	Pressure [Bar]	High side pressure 1	VCU	R134a	1	AC/HP
AC0102_HP2PR	P2	F5	FPC24/2	A	I	P6:A3/A4	Pressure [Bar]	High side pressure 2	VCU	R134a	2	AC/HP
AC0103_LP1PR	P3	F1	FPC24/2	A	I	P6:A5/A6	Pressure [Bar]	Low side pressure 1	VCU	R134a	1	AC/HP
AC0104_LP2PR	P4	F4	FPC24/2	A	I	P6:A7/A8	Pressure [Bar]	Low side pressure 2	VCU	R134a	2	AC/HP
AC0201_CPR1HGHPR	P5	F11	CCM8	A	I	X6:3/4	Pressure [Bar]	Discharge pressure 1	VCU	R134a	1	AC/HP
AC0202_CPR2HGHPR	P6	F12	CCM8	A	I	X6:1/2	Pressure [Bar]	Discharge pressure 2	VCU	R134a	2	AC/HP

Where: A, D, I, and O, abbreviates analog, digital, input and output, respectively.

Appendix A3: CM4 Electrical current meter

Appendix A3: Electrical current meter											
Address			Device	Connection			Value		Description	Location	VCU
Record	Figure	Component		A/D	I/O	Connection					Curcuit
AC0501_CRNTCPR1	C1	A5	CM4	A	I	A5:1_1/2	Current	[A]	Average current compressor 1	VCU	1
AC0502_CRNTCPR2	C2	A5	CM4	A	I	A5:2_1/2	Current	[A]	Average current compressor 2	VCU	2
AC0503_CRNT400V	-	A5	CM4	A	I	A5:3_1/2	Current	[A]	El. Current 400V AC equipment	HVAC & HRS	-
AC0504_CRNT110V	-	A5	CM4	A	I	A5:4_1/2	Current	[A]	El. Current 110V DC equipment	HVAC & HRS	-
A_ELWORKCPR1CPLT	C1	A5	CM4	Calculated based on current input			Work	[kJ]	El. Work compressor 1	VCU	1
A_ELWORKCPR2CPLT	C2	A5	CM4				Work	[kJ]	El. Work compressor 2	VCU	2
A_ELWORK400VCPLT	-	A5	CM4				Work	[kJ]	El. Work 400V AC Equipment	HVAC & HRS	-
A_ELWORK110VCPLT	-	A5	CM4				Work	[kJ]	El. Work 110V DC Equipment	HVAC & HRS	-

Where: A, D, I, and O, abbreviates analog, digital, input and output, respectively.

Appendix A4: Air temperature sensors

Appendix A4: Air temperature sensors										
Address			Device	Connection			Value		Description	Location
Record	Figure	Component		A/D	I/O	Connection				
AI0103_THE1		B6	FPC24/2	A	I	P7:A5/B5	Temperature	[C]	HX2 Outlet top	VCU
AI0104_THE2		B7	FPC24/2	A	I	P7:A6/B6	Temperature	[C]	HX2 Outlet bottom	VCU
AI0105_THRU1	Ta1	X3	FPC24/2	A	I	P7:A7/B7	Temperature	[C]	Exhaust outlet HRS	HRS
AI0106_THRU2	Ta2	X3	FPC24/2	A	I	P7:A8/B8	Temperature	[C]	Fresh air outlet HRS	HRS
AI0107_Te		X3	FPC24/2	A	I	P7:A9/B9	Temperature	[C]	Ambient	Exterior
AI0108_TD1PR	Ta3	B2	FPC24/2	A	I	P7:A10/B10	Temperature	[C]	HX1 Outlet top	AHU
AI0109_TD2PR	Ta4	B3	FPC24/2	A	I	P11:A1/B1	Temperature	[C]	HX1 Outlet bottom	AHU
AI0110_TI1PR		X2	FPC24/2	A	I	P11:A2/B2	Temperature	[C]	Passenger compartment 1	Compartment
AI0111_TI2PR		X2	FPC24/2	A	I	P11:A3/B3	Temperature	[C]	Passenger compartment 2	Compartment
AI0112_TI3PR		X2	FPC24/2	A	I	P11:A4/B4	Temperature	[C]	Passenger compartment 3	Compartment
AI0113_TI4PR		X2	FPC24/2	A	I	P11:A5/B5	Temperature	[C]	Staff compartment 4	Compartment
A_PCTIAVRG		X2	FPC24/2	Calculated			Temperature	[C]	Compartment average	Compartment

Where: A, D, I, and O, abbreviates analog, digital, input and output, respectively.

Appendix A5: Control and reply signals ventilation system

Appendix A5: Control and reply signals ventilation system									
Address		Device	Connection			Value		Description	Location
Record	Component		A/D	I/O	Connection				
A_PRFPBPRES/ AI0114_FpBpFre	R7	FPC24/2	A	I	P11:A6/B6	(0.27 - 5.27)	[kOhm]	Fresh air bypass damper opening	HRS
A_PRFPOARES/ AI0115_FpFreRec	R6	FPC24/2	A	I	P11:A7/B7	(0.27 - 5.27)	[kOhm]	Fresh/Resirculation air damper opening	AHU
AQ0101_NFSF	M5	FPC24/2	A	O	P7:A1/B1	(0-100)	[%]	Supply air fan speed	AHU
AQ0102_NFAF	X3	FPC24/2	A	O	P7:A2/B2	(0-10)	[V]	Support fresh air fan speed	HRS
DI0101_SF1ON	M5	FPC24/2	D	I	P2:A2	[0, 1]	[Off, On]	Reply supply fan 1	AHU
DI0102_SF2ON	M6	FPC24/2	D	I	P2:B2	[0, 1]	[Off, On]	Reply supply fan 2	AHU
N	X2	FPC24/2	D	I	P2:B6	[0, 1]	[Off, On]	Emergancy ventilation on	AHU
DI0112_EXFON	X11	FPC24/2	D	I	P2:B7	[0, 1]	[Off, On]	Reply exhaust fan on	HRS
DI0113_AFON	X11	FPC24/2	D	I	P3:A2	[0, 1]	[Off, On]	Reply support fresh air fan on	HRS
D_CRXPASSKL66	CAN1	Train CAN	D	I	P1M:7/8	[0, 1]	[No, Yes]	66%	Compartment
D_CRXPASSKL33	CAN1	Train CAN	D	I	P1M:7/8	[0, 1]	[No, Yes]	Passenger occupancy < 33%	Compartment
D_CTXPRVENT	CAN1	Train CAN	D	I	-	[0, 1]	[No, Yes]	Only ventilation mode active	AHU
A_PCTIC	-	FPC24/2	D	O	-	Temperature	[C]	ventilation	HVAC
DQ0114_EXFST1	K14	FPC24/2	D	O	P5:A2	[0, 1]	[Off, On]	Exhaust air fan speed low	HRS
DQ0115_EXFST2	K15	FPC24/2	D	O	P5:A3	[0, 1]	[Off, On]	Exhaust air fan speed high	HRS

Where: A, D, I, and O, abbreviates analog, digital, input and output, respectively.

Appendix A6: Reply signals vapor compression unit

Appendix A6: Control and reply signals vapor compression unit									
Address		Device	Connection			Value		Description	VCU
Record	Component		A/D	I/O	Connection				Circut
DI0103_CPR1ON	MF1F1	FPC24/2	D	I	P2:A3	[0, 1]	[Off, On]	Reply compressor 1 on	1
DI0104_CPR2ON	MF2F1	FPC24/2	D	I	P2:B3	[0, 1]	[Off, On]	Reply compressor 2 on	2
DI0116_CF1ON	M3F1	FPC24/2	D	I	P3:B3	[0, 1]	[Off, On]	Reply HX2 fan 1 On	-
DI0117_CF2ON	M4F1	FPC24/2	D	I	P3:A4	[0, 1]	[Off, On]	Reply HX2 fan 2 On	-
DI0118_CPR1THNOK	M1F1	FPC24/2	D	I	P3:B4	[0, 1]	[Off, On]	Overload protection switch compressor 1	1
DI0119_CP21THNOK	M2F1	FPC24/2	D	I	P3:A5	[0, 1]	[Off, On]	Overload protection switch Compressor 2	2
DQ0105_SV1ON	Y1	FPC24/2	D	I	P4:A4	[0, 1]	[Shut, Open]	Solenoid valve liquid line 1	1
DQ0106_SV2ON	Y3	FPC24/2	D	I	P4:B4	[0, 1]	[Shut, Open]	Solenoid valve liquid line 2	2
DQ0107_BP1ON	M1Y1	FPC24/2	D	I	P4:A5	[0, 1]	[Off, On]	Cylinder unloading compressor 1	1
DQ0108_BP2ON	M2Y2	FPC24/2	D	I	P4:B5	[0, 1]	[Off, On]	Cylinder unloading compressor 2	2
DQ0123_C1HEAT	Y2	FPC24/2	D	I	P5:A8	[0, 1]	[Off, On]	Heat pump mode active 1	1
DQ0124_C2HEAT	Y4	FPC24/2	D	I	P5:B8	[0, 1]	[Off, On]	Heat pump mode active 2	2
D_CRXNOSTRTCPR	X2	Train CAN	D	I	PM1:7/8	[0, 1]	[No, Yes]	Compressor start blocked by train system	1 & 2

Where: A, D, I, and O, abbreviates analog, digital, input and output, respectively.

Appendix A7: Electrical heating coils

Appendix A7: Electrical heating coils									
Address		Device	Connection			Value		Description	Location
Record	Component		A/D	I/O	Connection				
DQ0110_HAT1ON	K11	FPC24/2	D	O	P4:B7	[0, 1]	[Off, On]	Electric heat coil 1 On	AHU
DQ0111_HAT2ON	K12	FPC24/2	D	O	P4:A8	[0, 1]	[Off, On]	Electric heat coil 2 On	AHU
A_OPHHTR1	-	FPC24/2	-	-	-	-	[Hours]	Operating hours heater 1	AHU
A_OPHHTR2	-	FPC24/2	-	-	-	-	[Hours]	Operating hours heater 2	AHU

Where: A, D, I, and O, abbreviates analog, digital, input and output, respectively.

Appendix A8: Control signals active system mode

Appendix A8: Control signals system mode								
Address		Device	Connection			Value		Description
Record	Component		A/D	I/O	Connection			
D_CTXPRAUTO	-	Train CAN	D	O	P1M:7/8	[0, 1]	[No, Yes]	Automatic mode active
D_CTXPRHEAT	-	Train CAN	D	O	P1M:7/8	[0, 1]	[No, Yes]	Pre-heating mode active
D_CTXPRCOOL	-	Train CAN	D	O	P1M:7/8	[0, 1]	[No, Yes]	Pre-cooling mode active
D_CTXPRVENT	-	Train CAN	D	O	P1M:7/8	[0, 1]	[No, Yes]	Ventilation mode active
D_CTXPROFF	-	Train CAN	D	O	P1M:7/8	[0, 1]	[No, Yes]	System Off
D_CRXVGR5KMH	-	Train CAN	D	I	P1M:7/8	[0, 1]	[No, Yes]	Train speed>5km/h

Where: A, D, I, and O, abbreviates analog, digital, input and output, respectively.

Appendix A9: Power reduction

Appendix A9: Power reduction									
Address		Device	Connection			Value		Description	System
Record	Component		A/D	I/O	Connection				
D_CRXEMRG11KW	-	Train CAN	D	I	P1M:7/8	[0,1]	[No, Yes]	Power reduction 11 kW	400V-1-16.7Hz
D_CRXEMRG28KW	-	Train CAN	D	I	P1M:7/8	[0,1]	[No, Yes]	Power reduction 28 kW	400V-1-16.7Hz
D_CRXEMRG5KVA	-	Train CAN	D	I	P1M:7/8	[0,1]	[No, Yes]	Power reduction 5 kVA	400V-3-50 Hz
D_CRXEMRG10KVA	-	Train CAN	D	I	P1M:7/8	[0,1]	[No, Yes]	Power reduction 10 kVA	400V-3-50 Hz
DI0123_AC400OK	-	FPC24/2	D	I	P3:A7	[0, 1]	[No, Yes]	AC power supply OK	400V-3-50 Hz

Where: A, D, I, and O, abbreviates analog, digital, input and output, respectively.

Appendix B: Damper settings NSB FLIRT middle car BMb.

Table 2-1: Damper setting FLIRT NSB middle car BMb												
Step	Operating mode	PWM signal Supply air fans [%]		PWM signal Exhaust air fans [%]	Voltage Support fan motor [V]	ΔP_inside,outside [Pa]		Outside air [m3/h]		Supply air [m3/h]		Flap position [deg]
		Set point	Is	Is	Is	Set point	Is	Set point	Is	Set point	Is	Is
A-1.1	Heating Occupation > 66% -40C < ta < -5C	33	30	low	4.5	10	10	690	728	2000		60
A-1.2	Heating 66%>Occupation > 33% -40C < ta < -5C	33	30	low	3.2	10	7	460	496	2000		40
A-1.3	Heating Occupation < 33% -40C < ta < -5C	33	30	off	3	10	7	230	302	2000		15
B-1.1	Heating Occupation > 66% -40C < ta < -5C	33	30	low	3.5	10	9	690	708	2000		40
B-1.2	Heating 66%>Occupation > 33% -40C < ta < -5C	33	30	low	3	10	6	460	448	2000		15
B-1.3	Heating Occupation < 33% -40C < ta < -5C	33	30	off	3	10	8	230	320	2000		10
A-2.1	Heating Occupation > 66% -5C < ta < 13C	33	30	med	6	10	7	1035	1050	2000		60
A-2.2	Heating 66%>Occupation > 33% -5C < ta < 13C	33	30	low	4,5	10	9	690	740	2000		60
A-2.3	Heating Occupation < 33% -5C < ta < 13C	33	30	off	3	10	8	345	364	2000		20
B-2.1	Heating Occupation > 66% -5C < ta < 13C	33	30	med	5	10	7	1035	1050	2000		40
B-2.2	Heating 66%>Occupation > 33% -5C < ta < 13C	33	30	low	3.5	10	9	690	708	2000		40
B-2.3	Heating Occupation < 33% -5C < ta < 13C	33	30	off	3	10	9	345	348	2000		10
A-3.1	Transition Occupation > 66% -5C < ta < 13C	53	46	med	8.5	10	25	1380	1430	3200		30
A-3.2	Transition 66%>Occupation > 33% -5C < ta < 13C	53	46	med	5.5	10	12	920	948	3200		30
A-3.3	Transition Occupation < 33% -5C < ta < 13C	53	46	off	3.5	10	15	460	460	3200		15
B-3.1	Transition Occupation > 66% -5C < ta < 13C	53	46	med	7	10	29	1380	1449	3200		30
B-3.2	Transition 66%>Occupation > 33% -5C < ta < 13C	53	46	med	4.5	10	6	920	1010	3200		30
B-3.3	Transition Occupation < 33% -5C < ta < 13C	53	46	low	off	10	10	460	488	3200		20
A-4.1	Cooling Occupation > 66% 13C < ta < 26C	53	46	med	6.5	10	9	1035	1130	3200		30
A-4.2	Cooling 66%>Occupation > 33% 13C < ta < 26C	53	46	low	4	10	8	690	716	3200		30

Appendix C: Pilot R744 HVAC lab setup

Appendix C1: Photographs of test chamber and HVAC unit

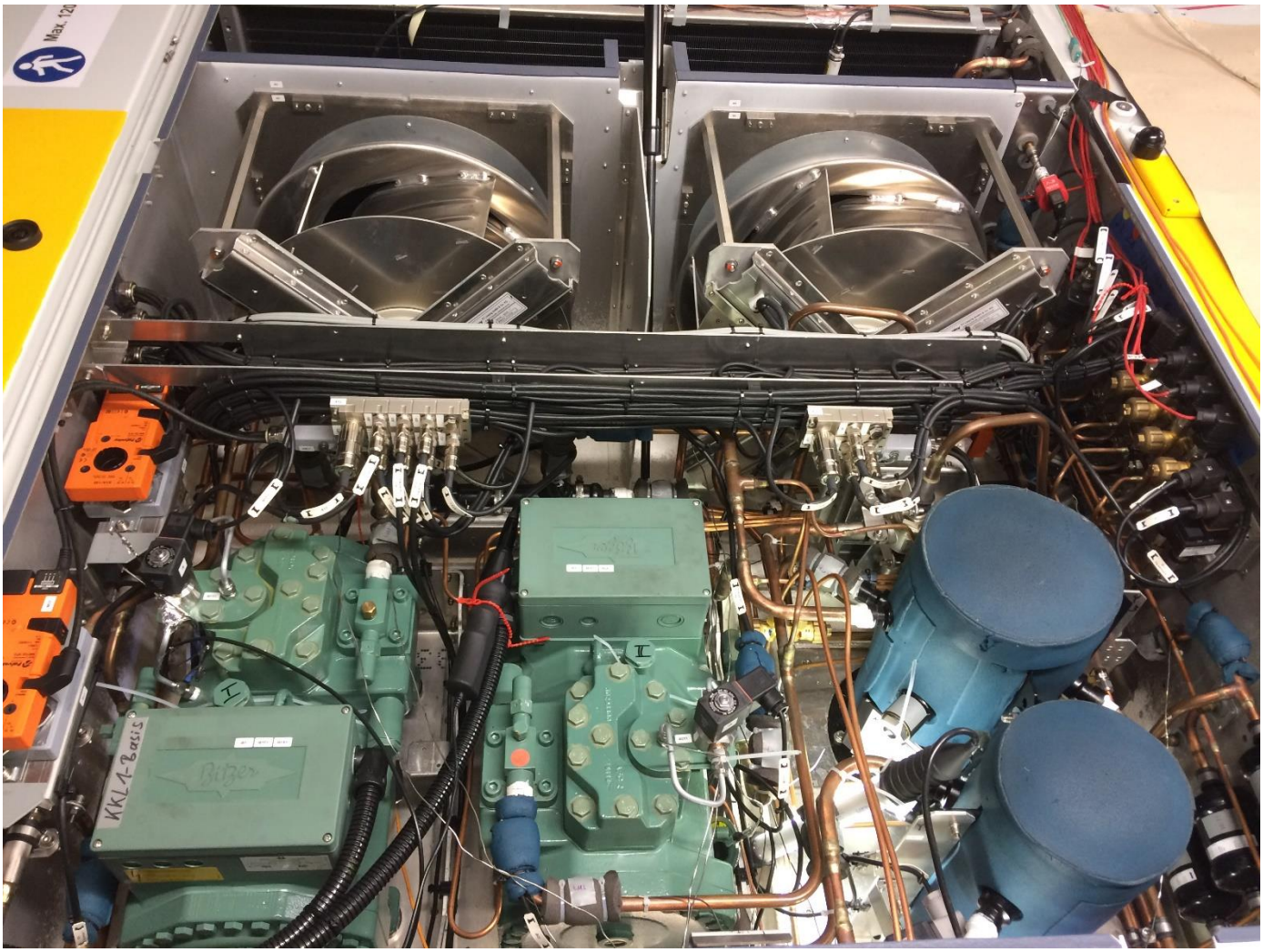

VCU assembly pilot R744 HVAC

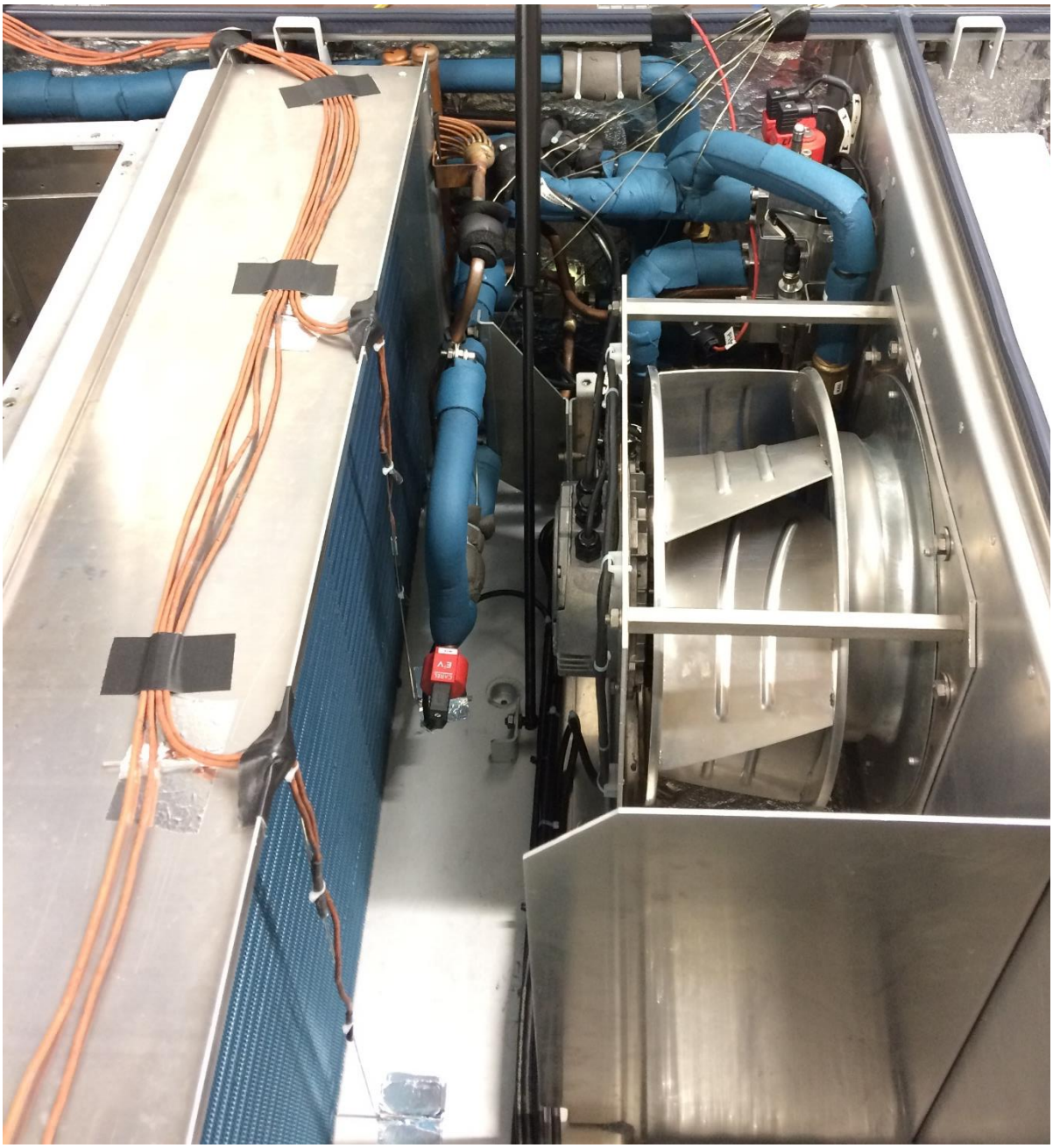

AHU assembly pilot R744 HVAC

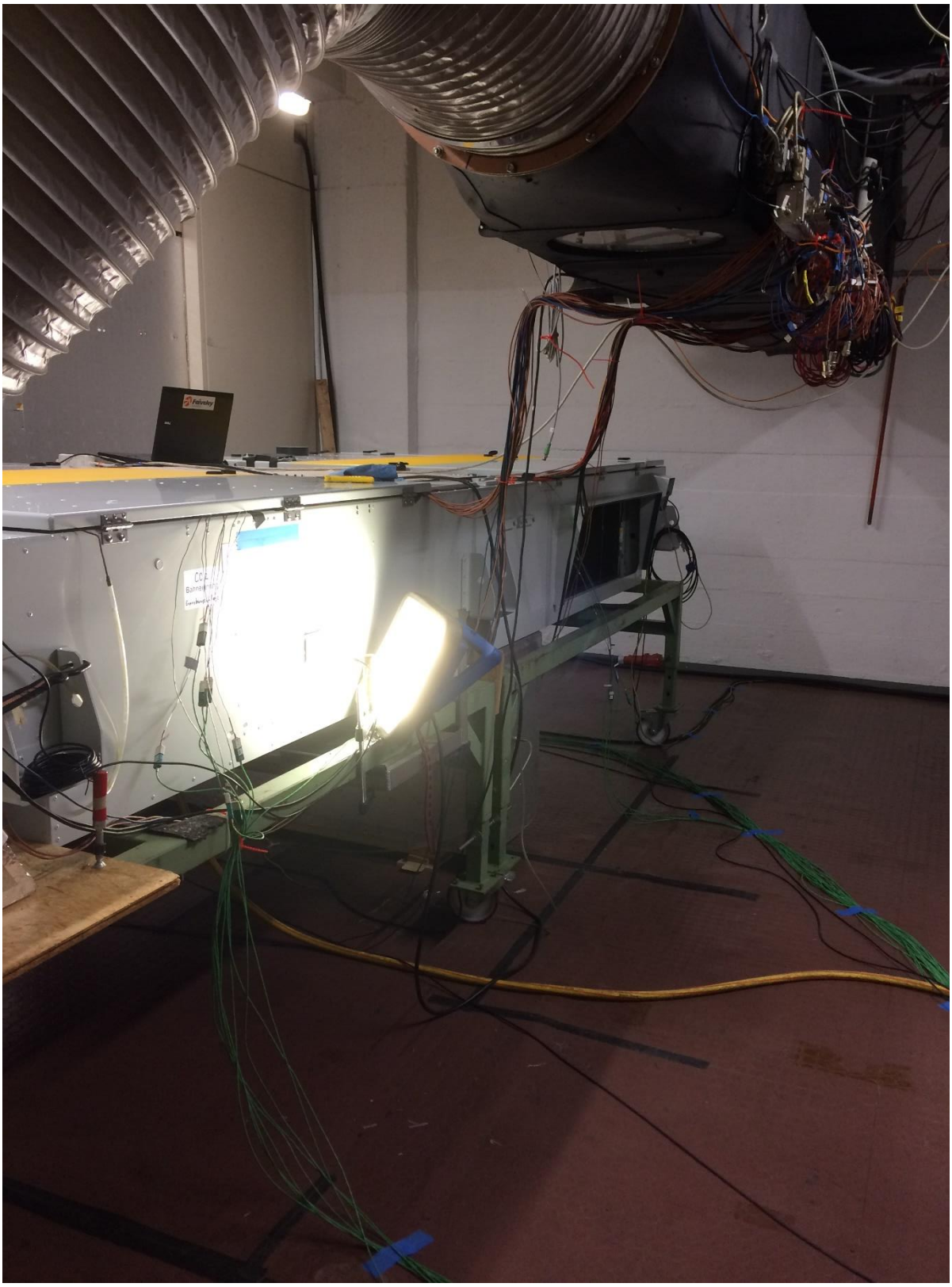

Pilot R744 HVAC unit casing inside the FTL test chamber

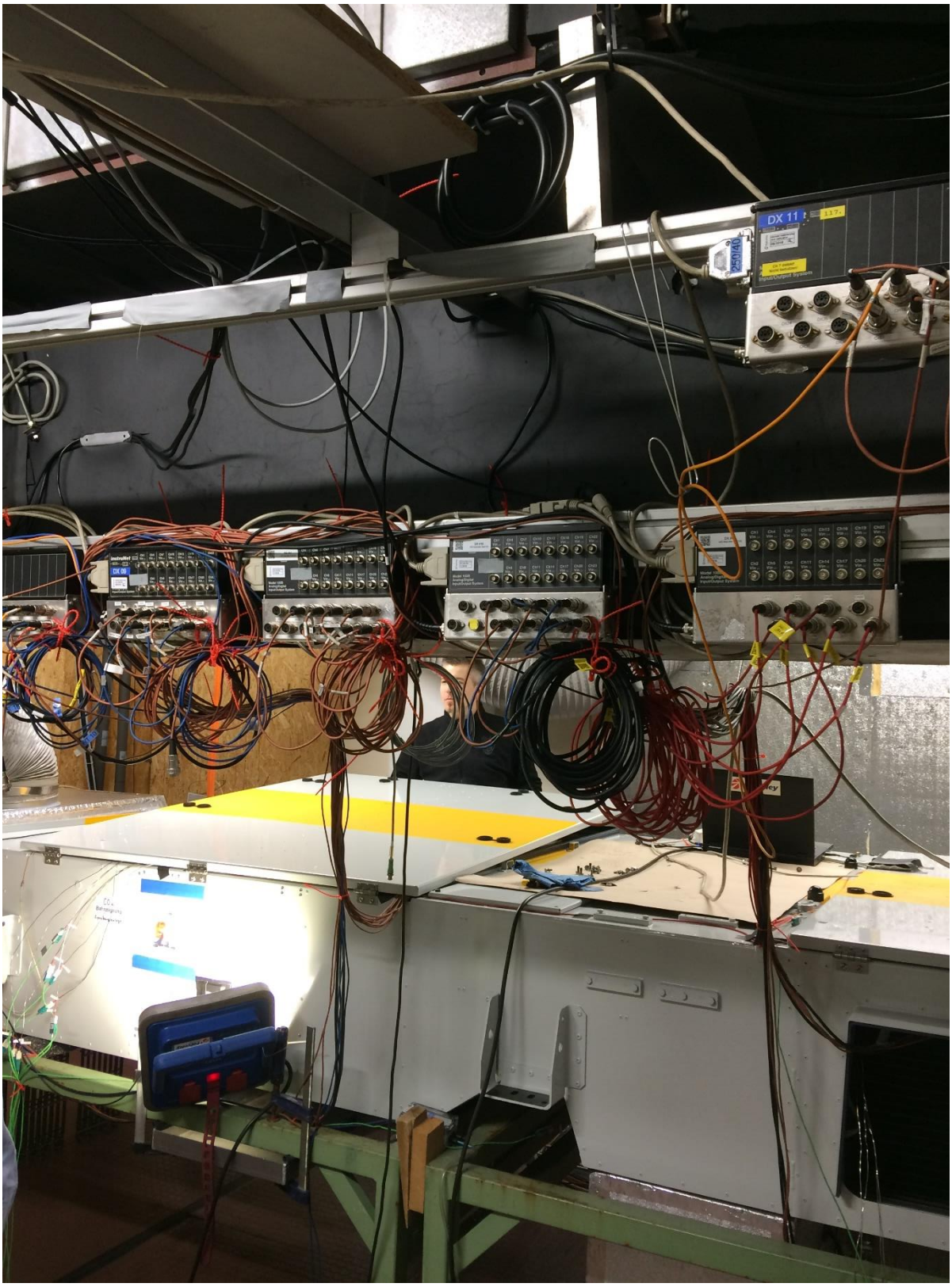

FTL test chamber

Appendix C2: Basic circuit sensor layout R744 HVAC lab tests

Measuring point	Basic circuit sensor layout during laboratory cooling load tests
Refrigerant temperature and pressure: R7: t_dl1, p_dl1 R8: t_02h_ext1 R9: t_cu_ext1 R10: t_EV_ext1 R11: t_HPiHtEx11, p_cu1 R12: t_HPiHtEx12 R13: t_EV_int1 R14: t_cu_int1 R15: t_02h_int1 R16: t_Lr_in1 R17: t_LPiHtEx11 R18: t_LPiHtEx12 R19: t_0h1, p_0h2 Air temperature: A2: t_EvAir1 A3: t_EvAir2 A5: t_CAir1 A6: t_CAir2	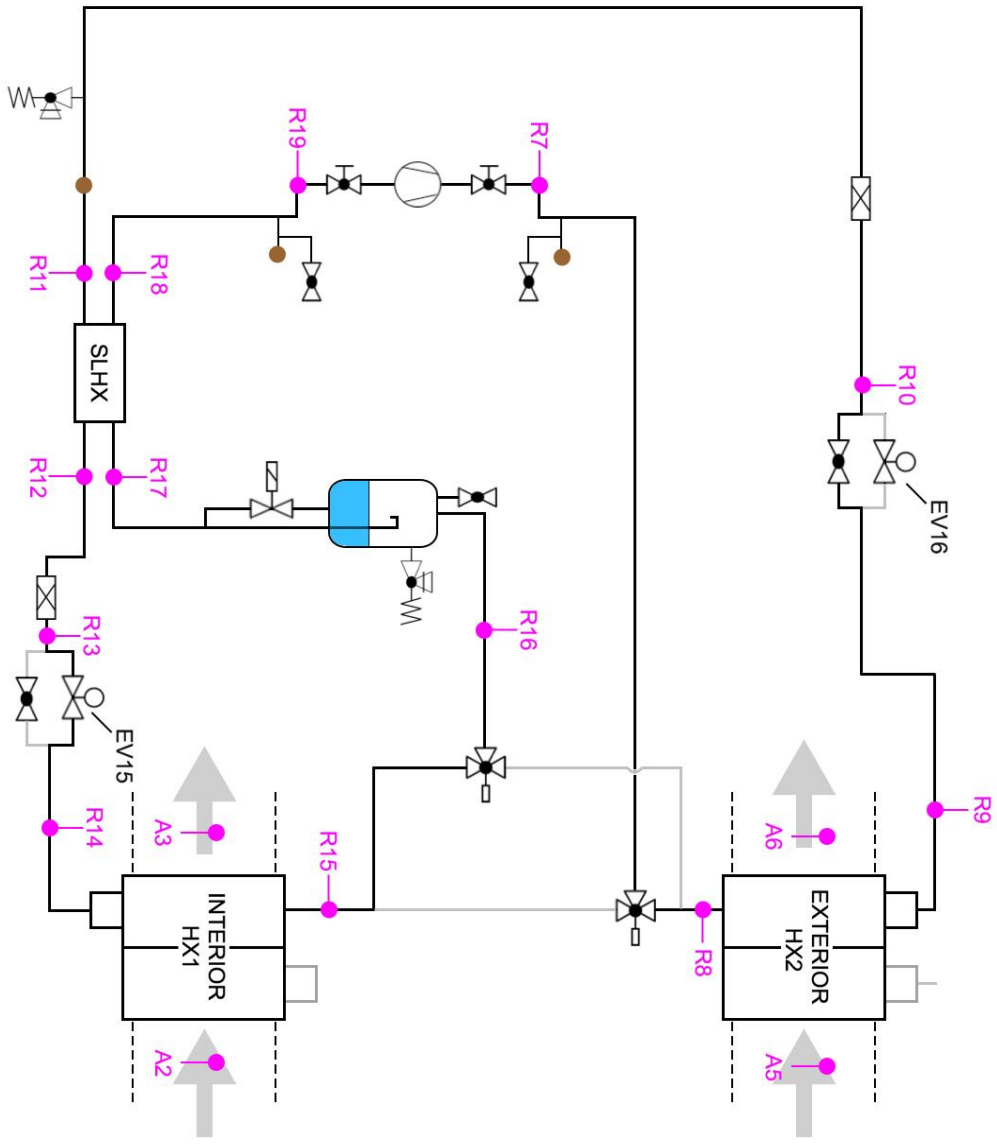

Appendix C3: Ejector circuit sensor layout R744 HVAC lab tests

Measuring point	Ejector circuit sensor layout during laboratory cooling load tests
Refrigerant temperature and pressure: R20: t_dl2, p_dl2 R21: t_02h_ext2 R22: t_cu_ext2 R23: t_EV_ext2 R24: t_HPiHtEx21, p_cu2 R25: t_HPiHtEx22 R26: t_EV_ejec R27: t_cu_int2 R28: t_02h_int2, p_ejec R29: t_Lr_in2 R30: t_EV_int2 R31: t_LPiHtEx21 R32: t_LPiHtEx22 R33: t_0h2, p_0h2 Air temperature: A2: t_EvAir1 A3: t_EvAir2 A5: t_CAir1 A6: t_CAir2	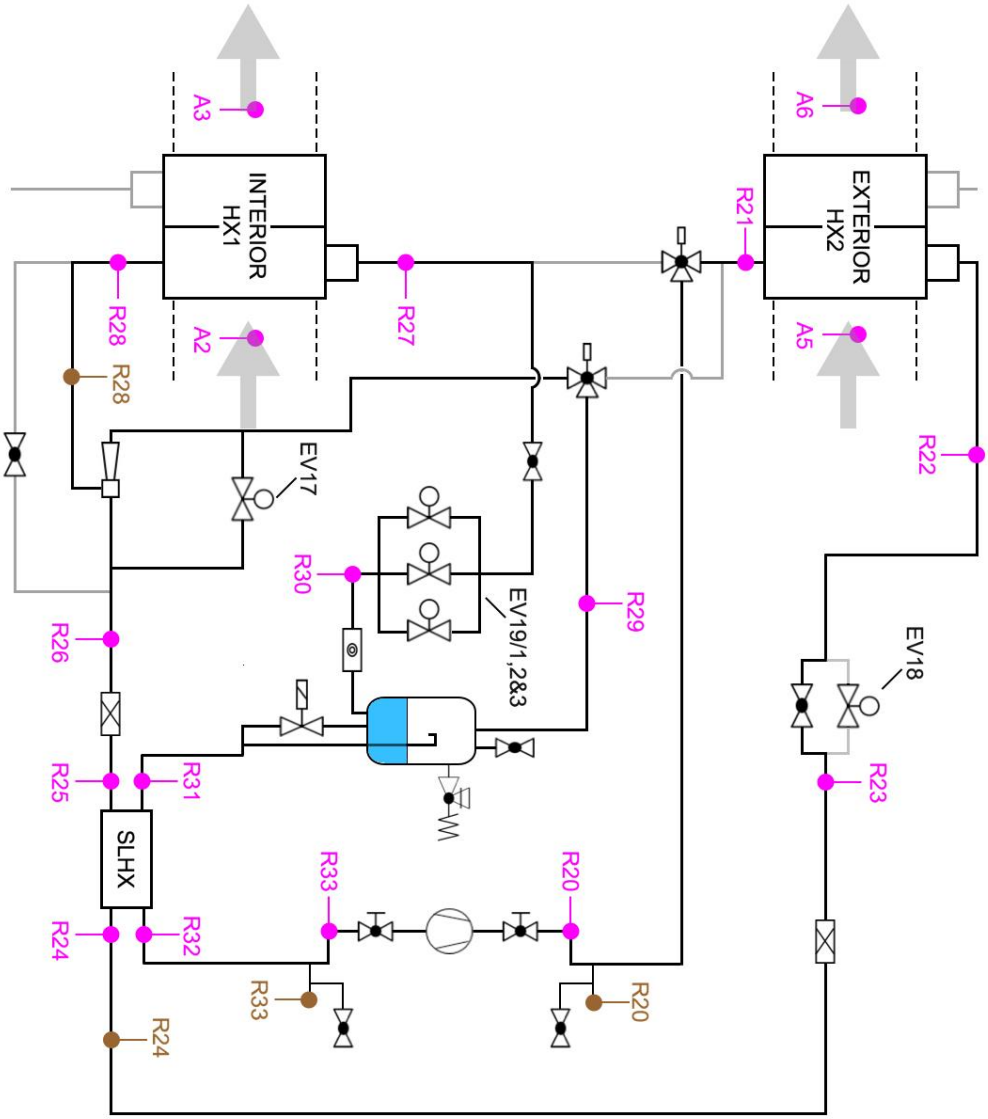

Appendix C4: Air stream sensor layout R744 HVAC lab tests

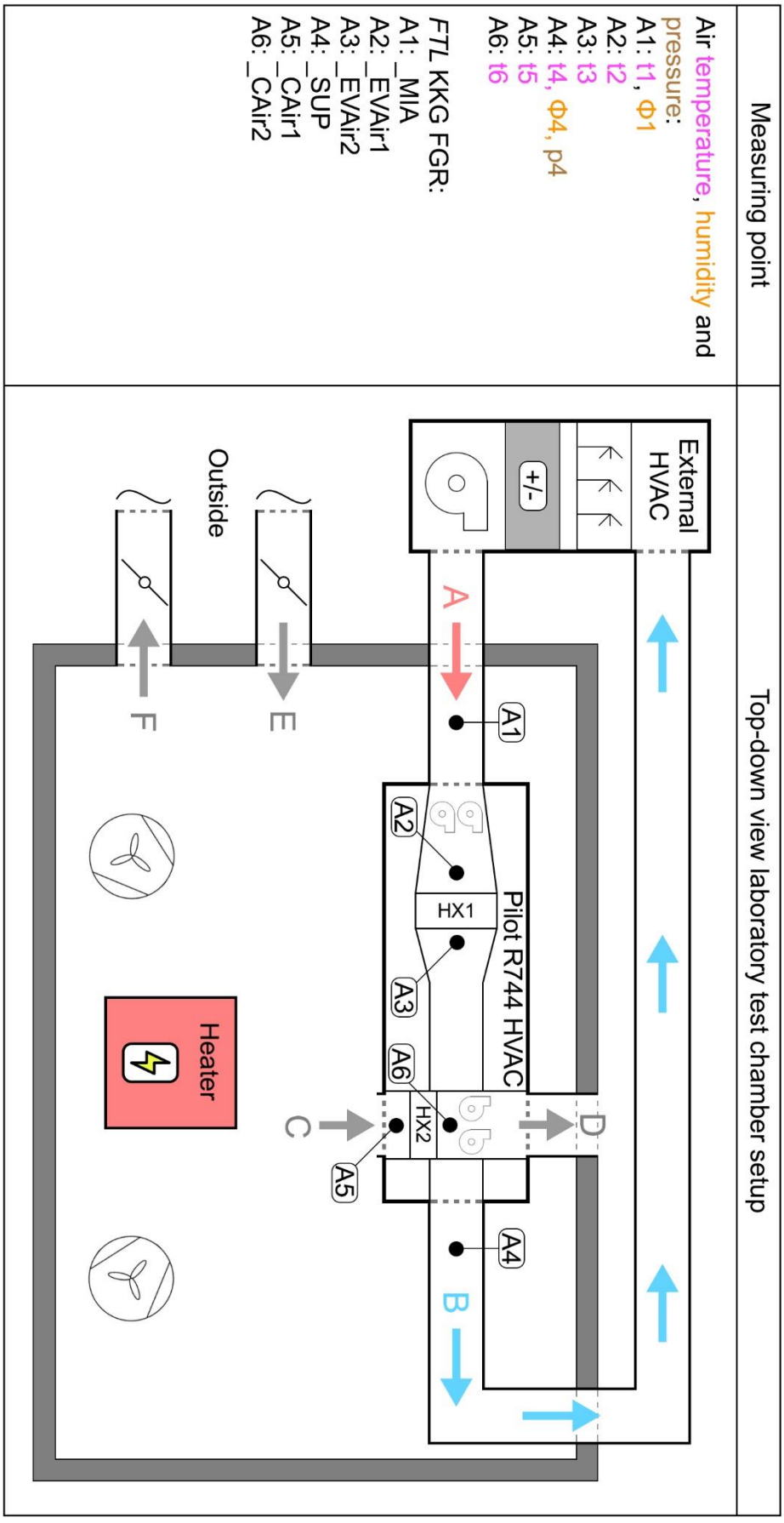

Appendix D: Pilot R744 HVAC lab tests complete results

Appendix D1: Individual operation of basic circuit

The following sub-sections, i.e. Appendix D1.1 to D1.7, include the complete measured and calculated test results from the individual operation tests of the basic circuit.

Appendix D1.1: 1.1.5 (1), 25℃ and 2000 m³/h supply air

1.1.5 (1)

Air

Location		Temperature (t)		Humidity (x)		Specific Enthalpy (I)	Density
		Dry bulb	Saturation	Ratio (x)	Relative (RH)		
Appendix C4	*FTL* KKG FGR	[°C]	[°C]	[kg_H20/Kg_dry]	[-]	[kJ/kg]	[kg/m3]
A1	_MIA	23.3	12.0	0.0087	0.49	45.60	1.18
A2	_EVAir1	22.3	12.0	0.0087	0.52	44.65	1.19
A3	_EVAir2	8.6	8.7	0.0070	1.01	26.14	1.25
A4	_SUP	10.1	8.7	0.0070	0.91	27.71	1.24
A5	_CAir1	23.5	11.0	0.0081	0.45	44.33	1.18
A6	_CAir2	30.3	11.0	0.0081	0.30	51.29	1.16

Air mass flow rate HX2 (m_a2) (8000 [m3/h]) approx.		9259	[kg/h]
Heat rejected at HX2 (Q_HX2)		17.90	[kW]
Air mass flow rate HX1 (m_a1)		2439	[kg/h]
Rate of condesed water (X_cond)		4.26	[kg/h]
Cooling capacity via air HX1	Sensible (Q_HX1_sens)	-9.87	[kW]
	Latent (Q_HX1_lat)	-2.67	[kW]
	Total (Q_HX1)	-12.54	[kW]
Cooling capacity via air HVAC unit (Q_HVAC)		-12.13	[kW]
Internal heat gains HVAC unit (Q_gain)		0.41	[kW]

1.1.5 (1)

Refrigerant basic circuit

Location		Temperature (t)	Pressure (p)	Specific		Vapor Fraction	Saturation Temperature	Superheat
				Enthalpy (h)	Entropy (s)			
Appendix C2	*FTL* KKG FGR	[°C]	[bar]	[kJ/kg]	[kJ/kgK]	[-]	[°C]	[K]
R7	_dl1	80.8	100.0	472.98	1.846	-	-	-
R8	_02h_ext1	76.6	100.0	465.05	1.824	-	-	-
R9	_cu_ext1	33.5	99.1	284.80	1.269	-	-	-
R10	_EV_ext1	34.1	-	-	-	-	-	-
R11	_HPiHtEx11	33.4	99.1	284.53	1.268	-	-	-
R12	_HPiHtEx12	30.6	99.1	274.60	1.235	-	-	-
R13	_EV_int1	30.2	99.1	273.56	1.232	-	-	-
R14	_cu_int1	11.8	45.3	273.56	1.257	0.225	-	-
R15	_02h_int1	11.5	45.3	427.11	1.801	-	10.2	1.3
R16	_LR_in1	10.8	45.3	425.41	1.795	-	10.2	0.6
R17	_LPiHtEx11	10.5	45.3	424.56	1.792	-	10.2	0.2
R18	_LpiHTtEx12	12.2	45.3	428.76	1.807	-	10.2	2.0
R19	_0h1	12.7	45.3	429.74	1.811	-	10.2	2.4

Refrigerant mass flow rate (m_rb)			294	[kg/h]
Compressor	Compression power (W)		3.530	[kW]
	Real el. input power (P_c) [kW]		4.665	[kW]
	Apparent el. input power (E_Sn)		6.245	[kW]
	Pressure ratio (π)		2.2	[-]
	Volumetric efficiency (λ)		0.68	[-]
	Isentropic efficiency (η_is)		0.54	[-]
COP		HX1 (COP_HX1)	2.7	[-]
		HVAC unit (COP_HVAC)	2.6	[-]

Appendix D1.2: 1.1.1 (6), 28℃ and 2000 m³/h supply air

1.1.1 (6)

Air

Location		Temperature (t)		Humidity (x)		Specific Enthalpy (I)	Density
		Dry bulb	Saturation	Ratio (x)	Relative (RH)		
Appendix C4	*FTL* KKG FGR	[°C]	[°C]	[kg_H20/Kg_dry]	[-]	[kJ/kg]	[kg/m3]
A1	_MIA	23.0	11.5	0.0084	0.48	44.55	1.19
A2	_EVAir1	22.3	11.5	0.0084	0.50	43.86	1.19
A3	_EVAir2	9.6	9.2	0.0072	0.97	27.81	1.24
A4	_SUP	11.3	9.2	0.0072	0.87	29.56	1.24
A5	_CAir1	27.9	14.9	0.0106	0.45	55.07	1.17
A6	_CAir2	34.2	14.9	0.0106	0.31	61.57	1.14

Air mass flow rate HX2 (m_a2) (approx. 8000 [m3/h])		9128	[kg/h]
Heat rejected at HX2 (Q_HX2)		16.46	[kW]
Air mass flow rate HX1 (m_a1) (approx. 2000 m3/h)		2433	[kg/h]
Rate of condesed water (X_cond)		2.95	[kg/h]
Cooling capacity via air HX1	Sensible (Q_HX1_sens)	-9.00	[kW]
	Latent (Q_HX1_lat)	-1.84	[kW]
	Total (Q_HX1)	-10.84	[kW]
Cooling capacity via air HVAC unit (Q_HVAC)		-10.13	[kW]
Internal heat gains HVAC unit (Q_gain)		0.71	[kW]

1.1.1 (6)

Refrigerant basic circuit

Location		Temperature (t)	Pressure (p)	Specific		Vapor Fraction	Saturation	Superheat	State
				Enthalpy (h)	Entropy (s)				
Appendix C2	*FTL* KKG FGR	[°C]	[bar]	[kJ/kg]	[kJ/kgK]	[-]	[°C]	[K]	
R7	_dl1	83.2	92.2	485.14	1.891	-	-	-	Gas
R8	_02h_ext1	77.7	92.2	476.01	1.865	-	-	-	Gas
R9	_cu_ext1	33.7	91.7	291.15	1.293	-	-	-	Gas
R10	_EV_ext1	33.8	-	-	-	-	-	-	-
R11	_HPiHtEx11	33.6	91.7	290.79	1.292	-	-	-	Gas
R12	_HPiHtEx12	31.0	91.7	279.94	1.256	-	-	-	Gas
R13	_EV_int1	30.8	91.7	278.99	1.253	-	-	-	Gas
R14	_cu_int1	8.1	41.2	278.99	1.280	0.285	-	-	Two-phase
R15	_02h_int1	8.0	41.2	430.83	1.826	-	6.5	1.5	Gas
R16	_LR_in1	7.1	41.2	429.05	1.820	-	6.5	0.7	Gas
R17	_LPiHtEx11	6.7	41.2	428.17	1.816	-	6.5	0.2	Gas
R18	_LpiHTtEx12	11.8	41.2	438.28	1.852	-	6.5	5.3	Gas
R19	_0h1	11.9	41.2	438.40	1.853	-	6.5	5.4	Gas

Refrigerant mass flow rate (m_rb)		257	[kg/h]
Compressor	Compression power (W)	3.337	[kW]
	Real el. input power (P_c) [kW]	4.281	[kW]
	Apparent el. input power (E_Sn)	5.939	[kW]
	Pressure ratio (π)	2.2	[-]
	Volumetric efficiency (λ)	0.70	[-]
	Isentropic efficiency (η_is)	0.56	[-]
COP	HX1 (COP_HX1)	2.5	[-]
	HVAC unit (COP_HVAC)	2.4	[-]

Appendix D1.3: 1.1.1 (5), 28℃ and 4000 m³/h supply air

1.1.1 (5)

Air

Location		Temperature (t)		Humidity (x)		Specific Enthalpy (I)	Density
		Dry bulb	Saturation	Ratio (x)	Relative (RH)		
Appendix C4	*FTL* KKG FGR	[°C]	[°C]	[kg_H20/Kg_dry]	[-]	[kJ/kg]	[kg/m3]
A1	_MIA	23.2	11.6	0.0085	0.48	44.84	1.19
A2	_EVAir1	23.6	11.6	0.0085	0.47	45.27	1.18
A3	_EVAir2	14.3	11.2	0.0083	0.82	35.26	1.22
A4	_SUP	15.5	11.2	0.0083	0.75	36.56	1.22
A5	_CAir1	27.7	14.7	0.0104	0.45	54.45	1.17
A6	_CAir2	34.9	14.7	0.0104	0.30	61.86	1.14

Air mass flow rate HX2 (m_a2) (approx. 8000 [m3/h])		9110	[kg/h]
Heat rejected at HX2 (Q_HX2)		18.73	[kW]
Air mass flow rate HX1 (m_a1) (approx. 4000 [m3/h])		4828	[kg/h]
Rate of condesed water (X_cond)		0.95	[kg/h]
Cooling capacity via air HX1	Sensible (Q_HX1_sens)	-12.84	[kW]
	Latent (Q_HX1_lat)	-0.59	[kW]
	Total (Q_HX1)	-13.43	[kW]
Cooling capacity via air HVAC unit (Q_HVAC)		-11.10	[kW]
Internal heat gains HVAC unit (Q_gain)		2.33	[kW]

1.1.1 (5)

Basic circuit

Location		Temperature (t)	Pressure (p)	Specific		Vapor Fraction	Saturation	Superheat
				Enthalpy (h)	Entropy (s)			
Appendix C2	*FTL* KKG FGR	[°C]	[bar]	[kJ/kg]	[kJ/kgK]	[-]	[°C]	[K]
R7	_dl1	80.8	100.0	472.98	1.846	-	-	-
R8	_02h_ext1	76.6	100.0	465.05	1.824	-	-	-
R9	_cu_ext1	33.5	99.1	284.80	1.269	-	-	-
R10	_EV_ext1	34.1	-	-	-	-	-	-
R11	_HPiHtEx11	33.4	99.1	284.53	1.268	-	-	-
R12	_HPiHtEx12	30.6	99.1	274.60	1.235	-	-	-
R13	_EV_int1	30.2	99.1	273.56	1.232	-	-	-
R14	_cu_int1	11.8	45.3	273.56	1.257	0.225	-	-
R15	_02h_int1	11.5	45.3	427.11	1.801	-	10.2	1.3
R16	_LR_in1	10.8	45.3	425.41	1.795	-	10.2	0.6
R17	_LPiHtEx11	10.5	45.3	424.56	1.792	-	10.2	0.2
R18	_LpiHTtEx12	12.2	45.3	428.76	1.807	-	10.2	2.0
R19	_0h1	12.7	45.3	429.74	1.811	-	10.2	2.4

Refrigerant mass flow rate (m_rb)			315	[kg/h]
Compressor	Compression power (W)		3.782	[kW]
	Real el. input power (P_c) [kW]		4.618	[kW]
	Apparent el. input power (E_Sn)		6.227	[kW]
	Pressure ratio (π)		2.2	[-]
	Volumetric efficiency (λ)		0.73	[-]
	Isentropic efficiency (η_is)		0.58	[-]
COP		HX1 (COP_HX1)	2.9	[-]
		HVAC unit (COP_HVAC)	2.4	[-]

Appendix D1.4: 1.1.3 (1), 35℃ and 2000 m³/h supply air

1.1.3 (1)

Air

Location		Temperature (t)		Humidity (x)		Specific Enthalpy (I)	Density
		Dry bulb	Saturation	Ratio (x)	Relative (RH)		
Appendix C4	*FTL* KKG FGR	[°C]	[°C]	[kg_H20/Kg_dry]	[-]	[kJ/kg]	[kg/m3]
A1	_MIA	28.4	18.9	0.0136	0.56	63.41	1.16
A2	_EVAir1	27.8	18.9	0.0136	0.58	62.83	1.16
A3	_EVAir2	17.3	17.1	0.0122	0.99	48.17	1.21
A4	_SUP	18.7	17.1	0.0122	0.90	49.62	1.20
A5	_CAir1	35.0	21.3	0.0160	0.45	76.18	1.13
A6	_CAir2	41.4	21.3	0.0160	0.32	82.81	1.11

Air mass flow rate HX2 (m_a2) (approx. 8000 [m3/h])		8892	[kg/h]
Heat rejected at HX2 (Q_HX2)		16.40	[kW]
Air mass flow rate HX1 (m_a1) (approx. 2000 [m3/h])		2339	[kg/h]
Rate of condesed water (X_cond)		3.48	[kg/h]
Cooling capacity via air HX1	Sensible (Q_HX1_sens)	-7.34	[kW]
	Latent (Q_HX1_lat)	-2.18	[kW]
	Total (Q_HX1)	-9.53	[kW]
Cooling capacity via air HVAC unit (Q_HVAC)		-8.96	[kW]
Internal heat gains HVAC unit (Q_gain)		0.57	[kW]

1.1.3 (1)

Basic circuit

Location		Temperature (t)	Pressure (p)	Specific		Vapor Fraction	Saturation Temperatur	Superheat
				Enthalpy (h)	Entropy (s)			
Appendix C2	*FTL* KKG FGR	[°C]	[bar]	[kJ/kg]	[kJ/kgK]	[-]	[°C]	[K]
R7	_dl1	75.9	98.6	465.34	1.826	-	-	-
R8	_02h_ext1	73.2	98.6	459.95	1.811	-	-	-
R9	_cu_ext1	41.9	97.5	330.87	1.417	-	-	-
R10	_EV_ext1	41.2	-	-	-	-	-	-
R11	_HPiHtEx11	41.8	97.5	330.33	1.415	-	-	-
R12	_HPiHtEx12	39.8	97.5	316.19	1.371	-	-	-
R13	_EV_int1	39.7	97.5	315.66	1.369	-	-	-
R14	_cu_int1	15.9	49.9	315.66	1.400	0.421	-	-
R15	_02h_int1	15.5	49.9	422.68	1.775	-	14.2	1.3
R16	_LR_in1	14.7	49.9	420.44	1.767	-	14.2	0.5
R17	_LPiHtEx11	14.5	49.9	419.62	1.764	-	14.2	0.2
R18	_LpiHTtEx12	17.8	49.9	428.51	1.795	-	14.2	3.5
R19	_0h1	17.4	49.9	427.63	1.792	-	14.2	3.2

Refrigerant mass flow rate (m_rb)			320	[kg/h]
Compressor	Compression power (W)		3.356	[kW]
	Real el. input power (P_c) [kW]		4.428	[kW]
	Apparent el. input power (E_Sn)		6.025	[kW]
	Pressure ratio (π)		2.0	[-]
	Volumetric efficiency (λ)		0.66	[-]
	Isentropic efficiency (η_is)		0.52	[-]
COP		HX1 (COP_HX1)	2.2	[-]
		HVAC unit (COP_HVAC)	2.0	[-]

Appendix D1.5: 1.1.3 (3), 35℃ and 4000 m³/h supply air

1.1.3 (3)

Air

Location		Temperature (t)		Humidity (x)		Specific Enthalpy (I)	Density
		Dry bulb	Saturation	Ratio (x)	Relative (RH)		
Appendix C4	*FTL* KKG FGR	[°C]	[°C]	[kg_H20/Kg_dry]	[-]	[kJ/kg]	[kg/m3]
A1	_MIA	28.4	18.7	0.0135	0.56	63.00	1.16
A2	_EVAir1	28.9	18.7	0.0135	0.54	63.60	1.16
A3	_EVAir2	21.3	18.5	0.0134	0.84	55.38	1.19
A4	_SUP	22.4	18.5	0.0134	0.79	56.46	1.18
A5	_CAir1	34.9	21.2	0.0158	0.45	75.73	1.14
A6	_CAir2	41.5	21.2	0.0158	0.32	82.54	1.11

Air mass flow rate HX2 (m_a2) (approx. 8000 [m3/h])		8891	[kg/h]
Heat rejected at HX2 (Q_HX2)		16.83	[kW]
Air mass flow rate HX1 (m_a1) (approx. 4000 [m3/h])		4546	[kg/h]
Rate of condesed water (X_cond)		0.66	[kg/h]
Cooling capacity via air HX1	Sensible (Q_HX1_sens)	-9.97	[kW]
	Latent (Q_HX1_lat)	-0.41	[kW]
	Total (Q_HX1)	-10.38	[kW]
Cooling capacity via air HVAC unit (Q_HVAC)		-8.26	[kW]
Internal heat gains HVAC unit (Q_gain)		2.13	[kW]

1.1.3 (3)

Basic circuit

Location		Temperature (t)	Pressure (p)	Specific		Vapor Fraction	Saturation Temperature	Superheat
				Enthalpy (h)	Entropy (s)			
Appendix C2	*FTL* KKG FGR	[°C]	[bar]	[kJ/kg]	[kJ/kgK]	[-]	[°C]	[K]
R7	_dl1	69.9	99.6	451.69	1.786	-	-	-
R8	_02h_ext1	67.9	99.6	447.36	1.773	-	-	-
R9	_cu_ext1	42.6	98.1	334.96	1.430	-	-	-
R10	_EV_ext1	42.0	-	-	-	-	-	-
R11	_HPiHtEx11	42.5	98.1	334.03	1.427	-	-	-
R12	_HPiHtEx12	40.6	98.1	320.56	1.384	-	-	-
R13	_EV_int1	40.5	98.1	319.73	1.382	-	-	-
R14	_cu_int1	19.4	54.0	319.73	1.409	0.423	-	-
R15	_02h_int1	18.7	54.0	417.93	1.750	-	17.5	1.2
R16	_LR_in1	18.1	54.0	415.88	1.743	-	17.5	0.6
R17	_LPiHtEx11	18.0	54.0	415.80	1.742	-	17.5	0.5
R18	_LpiHTtEx12	20.0	54.0	422.08	1.764	-	17.5	2.5
R19	_0h1	19.5	54.0	420.66	1.759	-	17.5	2.0

Refrigerant mass flow rate (m_rb)		381	[kg/h]
Compressor	Compression power (W)	3.280	[kW]
	Real el. input power (P_c) [kW]	4.392	[kW]
	Apparent el. input power (E_Sn)	5.950	[kW]
	Pressure ratio (π)	1.8	[-]
	Volumetric efficiency (λ)	0.69	[-]
	Isentropic efficiency (η_is)	0.53	[-]
COP	HX1 (COP_HX1)	2.4	[-]
	HVAC unit (COP_HVAC)	1.9	[-]

Appendix D1.6: 1.1.6 (2), 40℃ and 2000 m³/h supply air

1.1.6 (2)

Air

Location		Temperature (t)		Humidity (x)		Specific Enthalpy (I)	Density
		Dry bulb	Saturation	Ratio (x)	Relative (RH)		
Appendix C4	*FTL* KKG FGR	[°C]	[°C]	[kg_H20/Kg_dry]	[-]	[kJ/kg]	[kg/m3]
A1	_MIA	31.3	22.2	0.0169	0.59	74.75	1.15
A2	_EVAir1	31.1	22.2	0.0169	0.59	74.56	1.15
A3	_EVAir2	22.8	21.7	0.0163	0.93	64.39	1.18
A4	_SUP	23.9	21.7	0.0163	0.87	65.55	1.18
A5	_CAir1	39.7	25.5	0.0207	0.45	93.22	1.11
A6	_CAir2	44.3	25.5	0.0207	0.35	98.01	1.10

Air mass flow rate HX2 (m_a2) (approx. 8000 [m3/h])		8788	[kg/h]
Heat rejected at HX2 (Q_HX2)		11.68	[kW]
Air mass flow rate HX1 (m_a1) (approx. 2000 [m3/h])		2240	[kg/h]
Rate of condesed water (X_cond)		1.31	[kg/h]
Cooling capacity via air HX1	Sensible (Q_HX1_sens)	-5.51	[kW]
	Latent (Q_HX1_lat)	-0.82	[kW]
	Total (Q_HX1)	-6.32	[kW]
Cooling capacity via air HVAC unit (Q_HVAC)		-5.72	[kW]
Internal heat gains HVAC unit (Q_gain)		0.60	[kW]

1.1.6 (2)

Basic circuit

Location		Temperature (t)	Pressure (p)	Specific		Vapor Fraction	Saturation Temperatur	Superheat
				Enthalpy (h)	Entropy (s)			
Appendix C2	*FTL* KKG FGR	[°C]	[bar]	[kJ/kg]	[kJ/kgK]	[-]	[°C]	[K]
R7	_dl1	64.2	96.3	443.68	1.766	-	-	-
R8	_02h_ext1	62.9	96.3	440.45	1.757	-	-	-
R9	_cu_ext1	44.5	94.1	368.97	1.540	-	-	-
R10	_EV_ext1	44.2	-	-	-	-	-	-
R11	_HPiHtEx11	44.3	94.1	367.57	1.535	-	-	-
R12	_HPiHtEx12	42.6	94.1	351.22	1.484	-	-	-
R13	_EV_int1	42.6	94.1	350.95	1.483	-	-	-
R14	_cu_int1	22.2	57.4	350.95	1.511	0.624	-	-
R15	_02h_int1	21.2	57.4	413.64	1.729	-	20.1	1.2
R16	_LR_in1	20.7	57.4	411.48	1.721	-	20.1	0.6
R17	_LPiHtEx11	20.7	57.4	411.39	1.721	-	20.1	0.6
R18	_LpiHTtEx12	22.9	57.4	419.39	1.748	-	20.1	2.8
R19	_0h1	22.4	57.4	417.69	1.742	-	20.1	2.3

Refrigerant mass flow rate (m_rb)			363	[kg/h]
Compressor	Compression power (W)		2.622	[kW]
	Real el. input power (P_c) [kW]		4.036	[kW]
	Apparent el. input power (E_Sn)		5.654	[kW]
	Pressure ratio (π)		1.7	[-]
	Volumetric efficiency (λ)		0.61	[-]
	Isentropic efficiency (η_is)		0.45	[-]
COP		HX1 (COP_HX1)	1.6	[-]
		HVAC unit (COP_HVAC)	1.4	[-]

Appendix D1.7: 1.1.6 (1), 40℃ and 4000 m³/h supply air

1.1.6 (1)

Air

Location		Temperature (t)		Humidity (x)		Specific Enthalpy (I)	Density
		Dry bulb	Saturation	Ratio (x)	Relative (RH)		
Appendix C4	*FTL* KKG FGR	[°C]	[°C]	[kg_H20/Kg_dry]	[-]	[kJ/kg]	[kg/m3]
A1	_MIA	29.2	19.6	0.0143	0.56	65.90	1.16
A2	_EVAir1	30.0	19.6	0.0143	0.54	66.72	1.15
A3	_EVAir2	24.6	19.4	0.0142	0.73	60.79	1.18
A4	_SUP	25.4	19.4	0.0142	0.70	61.58	1.17
A5	_CAir1	39.0	24.9	0.0199	0.45	90.49	1.12
A6	_CAir2	44.0	24.9	0.0199	0.34	95.77	1.10

Air mass flow rate HX2 (m_a2) (approx. 8000 [m3/h])		8798	[kg/h]
Heat rejected at HX2 (Q_HX2)		12.91	[kW]
Air mass flow rate HX1 (m_a1) (approx. 4000 [m3/h])		4575	[kg/h]
Rate of condesed water (X_cond)		0.65	[kg/h]
Cooling capacity via air HX1	Sensible (Q_HX1_sens)	-7.13	[kW]
	Latent (Q_HX1_lat)	-0.40	[kW]
	Total (Q_HX1)	-7.54	[kW]
Cooling capacity via air HVAC unit (Q_HVAC)		-5.50	[kW]
Internal heat gains HVAC unit (Q_gain)		2.04	[kW]

1.1.6(1)

Basic circuit

Location		Temperature (t)	Pressure (p)	Specific		Vapor Fraction	Saturation Temperature	Superheat
				Enthalpy (h)	Entropy (s)			
Appendix C2	*FTL* KKG FGR	[°C]	[bar]	[kJ/kg]	[kJ/kgK]	[-]	[°C]	[K]
R7	_dl1	64.8	98.1	442.07	1.759	-	-	-
R8	_02h_ext1	63.5	98.1	438.87	1.750	-	-	-
R9	_cu_ext1	44.7	95.9	361.95	1.516	-	-	-
R10	_EV_ext1	44.2	-	-	-	-	-	-
R11	_HPiHtEx11	44.5	95.9	360.44	1.512	-	-	-
R12	_HPiHtEx12	42.9	95.9	345.37	1.464	-	-	-
R13	_EV_int1	42.7	95.9	343.84	1.459	-	-	-
R14	_cu_int1	23.5	59.2	343.84	1.485	0.573	-	-
R15	_02h_int1	22.5	59.2	410.57	1.715	-	21.4	1.1
R16	_LR_in1	22.0	59.2	408.36	1.708	-	21.4	0.6
R17	_LPiHtEx11	21.9	59.2	408.18	1.707	-	21.4	0.5
R18	_LpiHTtEx12	24.6	59.2	418.64	1.742	-	21.4	3.2
R19	_0h1	24.0	59.2	416.65	1.736	-	21.4	2.6

Refrigerant mass flow rate (m_rb)			407	[kg/h]
Compressor	Compression power (W)		2.870	[kW]
	Real el. input power (P_c) [kW]		4.099	[kW]
	Apparent el. input power (E_Sn)		5.653	[kW]
	Pressure ratio (π)		1.7	[-]
	Volumetric efficiency (λ)		0.65	[-]
	Isentropic efficiency (η_is)		0.48	[-]
COP		HX1 (COP_HX1)	1.8	[-]
		HVAC unit (COP_HVAC)	1.3	[-]

Appendix D2: Individual operation of ejector circuit

The following sub-sections, i.e. Appendix D2.1 to D2.7, include the complete measured and calculated test results from the individual operation tests of the ejector circuit.

Appendix D2.1: 1.2.5 (2), 25℃ and 2000 m³/h supply air

1.2.5 (2)

Air

Location		Temperature (t)		Humidity (x)		Specific Enthalpy (I)	Density
		Dry bulb	Saturation	Ratio (x)	Relative (RH)		
Appendix C4	*FTL* KKG FGR	[℃]	[℃]	[kg_H20/Kg_dry]	[-]	[kJ/kg]	[kg/m3]
A1	_MIA	23.1	12.2	0.0088	0.50	45.72	1.19
A2	_EVAir1	21.8	12.2	0.0088	0.54	44.45	1.19
A3	_EVAir2	7.8	8.6	0.0069	1.05	25.22	1.25
A4	_SUP	9.9	8.6	0.0069	0.91	27.34	1.24
A5	_CAir1	23.9	11.3	0.0083	0.45	45.30	1.18
A6	_CAir2	30.6	11.3	0.0083	0.31	52.07	1.16

Air mass flow rate HX2 (m_a2) (approx. 8000 [m3/h])		9251	[kg/h]
Heat rejected at HX2 (Q_HX2)		17.40	[kW]
Air mass flow rate HX1 (m_a1) (approx. 2000 [m3/h])		2411	[kg/h]
Rate of condesed water (X_cond)		4.69	[kg/h]
Cooling capacity via air HX1	Sensible (Q_HX1_sens)	-9.945	[kW]
	Latent (Q_HX1_lat)	-2.935	[kW]
	Total (Q_HX1)	-12.880	[kW]
Cooling capacity via air HVAC unit (Q_HVAC)		-12.303	[kW]
Internal heat gains HVAC unit (Q_gain)		0.577	[kW]

1.2.5 (2)

Refrigerant ejector circuit

Location		Temperature (t)	Pressure (p)	Specific Enthalpy (h)	Specific Entropy (s)	Vapor Fraction	Saturation Temperature	Superheat
Appendix C2	*FTL* KKG FGR	[℃]	[bar]	[kJ/kg]	[kJ/kgK]	[-]	[℃]	[K]
R20	_dl2	96.0	100.2	498.17	1.915	-	-	-
R21	_02h_ext2	90.0	100.2	488.48	1.888	-	-	-
R22	_cu_ext2	27.5	98.9	264.94	1.203	-	-	-
R23	_EV_ext2	27.8	98.9	265.94	1.207	-	-	-
R24	_HPiHtEx21	27.7	98.9	265.60	1.206	-	-	-
R25	_HPiHtEx22	24.9	98.9	257.02	1.177	-	-	-
R26	_EV_ejec	25.0	98.9	257.06	1.177	-	-	-
R27	_cu_int2	3.4	36.1	211.39	1.041	0.013	1.4	2.1
R28	_02h_int2	2.6	36.1	433.77	1.853	-	1.4	1.3
R29	_Lr_in2	4.6	37.2	336.04	1.490	0.573	2.5	2.2
R30	_EV_int2	4.6	37.2	211.39	1.853	-	2.5	-
R31	_LPiHtEx21	5.3	37.2	435.94	1.857	-	2.5	2.8
R32	_LPiHtEx22	10.4	37.2	444.58	1.888	-	2.5	7.9
R33	_02h2	10.7	37.2	445.13	1.890	-	2.5	8.2

Refrigerant mass flow rate HX1 (m_re,HX1)		209	[kg/h]
Refrigerant mass flow rate HX2 (m_re,HX2) (*Bitzer*)		258	[kg/h]
Heat transfered to the compressor suction line (Q̇_SLHX,LP)		0.619	[kW]
Heat transfered from the high pressure liquid line (Q̇_SLHX,HP)		-0.615	[kW]
Compressor	Compression power (W)	3.801	[kW]
	Real el. input power (P_c)	4.718	[kW]
	Apparent el. input power (E_Sn)	6.284	[kW]
	Pressure ratio (π)	2.7	[-]
	Volumetric efficiency (λ)	0.82	[-]
	Isentropic efficiency (η_is)	0.67	[-]
Ejector	Suction pressure ratio (Πs)	1.03	[-]
	Mass entrainment ratio (Φm)	0.81	[-]
	Efficiency (η_ej)	0.10	[-]
COP	COP_HX1	2.7	[-]
	COP_HVAC	2.6	[-]

Appendix D2.2: 1.2.1 (10), 28℃ and 2000 m³/h supply air

1.2.1 (10)

Air

Location		Temperature (t)		Humidity (x)		Specific Enthalpy (I)	Density
		Dry bulb	Saturation	Ratio (x)	Relative (RH)		
Appendix C4	*FTL* KKG FGR	[°C]	[°C]	[kg_H20/Kg_dry]	[-]	[kJ/kg]	[kg/m3]
A1	_MIA	23.3	12.4	0.0090	0.50	46.25	1.18
A2	_EVAir1	22.6	12.4	0.0090	0.53	45.45	1.19
A3	_EVAir2	9.1	9.9	0.0076	1.05	28.16	1.24
A4	_SUP	11.4	9.9	0.0076	0.90	30.56	1.23
A5	_CAir1	28.1	15.1	0.0107	0.45	55.53	1.16
A6	_CAir2	34.6	15.1	0.0107	0.31	62.22	1.14

Air mass flow rate HX2 (m_a2) (approx. 8000 [m3/h])		9117	[kg/h]
Heat rejected at HX2 (Q_HX2)		16.94	[kW]
Air mass flow rate HX1 (m_a1) (approx. 2000 [m3/h])		2383	[kg/h]
Rate of condesed water (X_cond)		3.34	[kg/h]
Cooling capacity via air HX1	Sensible (Q_HX1_sens)	-9.358	[kW]
	Latent (Q_HX1_lat)	-2.089	[kW]
	Total (Q_HX1)	-11.447	[kW]
Cooling capacity via air HVAC unit (Q_HVAC)		-10.388	[kW]
Internal heat gains HVAC unit (Q_gain)		1.059	[kW]

1.2.1 (10)

Refrigerant ejector circuit

Location		Temperature (t)	Pressure (p)	Specific		Vapor Fraction	Saturation Temperatur	Superheat
				Enthalpy (h)	Entropy (s)			
Appendix C2	*FTL* KKG FGR	[°C]	[bar]	[kJ/kg]	[kJ/kgK]	[-]	[°C]	[K]
R20	_dl2	87.5	92.1	492.21	1.911	-	-	-
R21	_02h_ext2	83.0	92.1	484.96	1.890	-	-	-
R22	_cu_ext2	34.5	90.4	296.23	1.310	-	-	-
R23	_EV_ext2	34.7	90.4	297.11	1.313	-	-	-
R24	_HPiHtEx21	34.6	90.4	296.63	1.311	-	-	-
R25	_HPiHtEx22	32.2	90.4	285.68	1.275	-	-	-
R26	_EV_ejec	32.0	90.4	284.63	1.272	-	-	-
R27	_cu_int2	6.0	38.6	216.20	1.057	0.005	3.9	2.2
R28	_02h_int2	5.5	38.6	432.91	1.842	-	3.9	1.6
R29	_Lr_in2	6.6	39.7	342.99	1.511	0.600	5.0	1.6
R30	_EV_int2	6.5	39.7	216.20	1.834	-	5.0	-
R31	_LPiHtEx21	7.2	39.7	433.22	1.839	-	5.0	2.2
R32	_LPiHtEx22	13.1	39.7	443.85	1.877	-	5.0	8.1
R33	_02h2	13.4	39.7	444.38	1.879	-	5.0	8.4

Refrigerant mass flow rate HX1 (m_re,HX1)		190	[kg/h]
Refrigerant mass flow rate HX2 (m_re,HX2) (*Bitzer*)		293	[kg/h]
Heat transfered to the compressor suction line (Q̇_SLHX,LP)		0.865	[kW]
Heat transfered from the high pressure liquid line (Q̇_SLHX,HP)		-0.891	[kW]
Compressor	Compression power (W)	3.893	[kW]
	Real el. input power (P_c)	4.296	[kW]
	Apparent el. input power (E_Sn)	6.068	[kW]
	Pressure ratio (π)	2.3	[-]
	Volumetric efficiency (λ)	0.86	[-]
	Isentropic efficiency (η_is)	0.69	[-]
Ejector	Suction pressure ratio (Πs)	1.03	[-]
	Mass entrainment ratio (Φm)	0.65	[-]
	Efficiency (η_ej)	0.08	[-]
COP	COP_HX1	2.7	[-]
	COP_HVAC	2.4	[-]

Appendix D2.3: 1.2.1 (9), 28℃ and 4000 m³/h supply air

1.2.1 (9)

Air

Location		Temperature (t)		Humidity (x)		Specific Enthalpy (I)	Density
		Dry bulb	Saturation	Ratio (x)	Relative (RH)		
Appendix C4	*FTL* KKG FGR	[℃]	[℃]	[kg_H20/Kg_dry]	[-]	[kJ/kg]	[kg/m3]
A1	_MIA	23.0	11.8	0.0086	0.49	45.07	1.19
A2	_EVAir1	23.5	11.8	0.0086	0.48	45.52	1.18
A3	_EVAir2	14.2	11.7	0.0085	0.85	35.82	1.22
A4	_SUP	15.7	11.7	0.0085	0.77	37.38	1.22
A5	_CAir1	27.8	14.8	0.0105	0.45	54.66	1.17
A6	_CAir2	34.8	14.8	0.0105	0.30	61.91	1.14

Air mass flow rate HX2 (m_a2) (approx. 8000 [m3/h])			9112	[kg/h]
Heat rejected at HX2 (Q_HX2)			18.36	[kW]
Air mass flow rate HX1 (m_a1) (approx. 4000 [m3/h])			4631	[kg/h]
Rate of condesed water (X_cond)			0.32	[kg/h]
Cooling capacity via air HX1	Sensible (Q_HX1_sens)		-12.274	[kW]
	Latent (Q_HX1_lat)		-0.197	[kW]
	Total (Q_HX1)		-12.471	[kW]
Cooling capacity via air HVAC unit (Q_HVAC)			-9.885	[kW]
Internal heat gains HVAC unit (Q_gain)			2.586	[kW]

1.2.1 (9)

Refrigerant ejector circuit

Location		Temperature (t)	Pressure (p)	Specific		Vapor Fraction	Saturation Temperatur	Superheat
				Enthalpy (h)	Entropy (s)			
Appendix C2	*FTL* KKG FGR	[℃]	[bar]	[kJ/kg]	[kJ/kgK]	[-]	[℃]	[K]
R20	_dl2	85.8	94.3	487.35	1.894	-	-	-
R21	_02h_ext2	81.8	94.3	480.69	1.875	-	-	-
R22	_cu_ext2	34.4	92.7	293.32	1.299	-	-	-
R23	_EV_ext2	34.6	92.7	294.26	1.302	-	-	-
R24	_HPiHtEx21	34.5	92.7	293.94	1.301	-	-	-
R25	_HPiHtEx22	32.1	92.7	283.64	1.268	-	-	-
R26	_EV_ejec	31.7	92.7	282.14	1.263	-	-	-
R27	_cu_int2	7.7	40.1	221.25	1.075	0.009	5.4	2.3
R28	_02h_int2	8.4	40.1	434.51	1.842	-	5.4	3.0
R29	_Lr_in2	8.4	41.6	343.53	1.509	0.598	6.8	1.6
R30	_EV_int2	8.4	41.6	221.25	1.825	-	6.8	-
R31	_LPiHtEx21	8.6	41.6	431.19	1.826	-	6.8	1.8
R32	_LPiHtEx22	13.8	41.6	441.10	1.861	-	6.8	7.0
R33	_02h2	14.1	41.6	441.65	1.863	-	6.8	7.3

Refrigerant mass flow rate HX1 (m_re,HX1)			211	[kg/h]
Refrigerant mass flow rate HX2 (m_re,HX2) (*Bitzer*)			312	[kg/h]
Heat transfered to the compressor suction line (Q̇_SLHX,LP)			0.859	[kW]
Heat transfered from the high pressure liquid line (Q̇_SLHX,HP)			-0.893	[kW]
Compressor	Compression power (W)		3.961	[kW]
	Real el. input power (P_c)		4.382	[kW]
	Apparent el. input power (E_Sn)		5.920	[kW]
	Pressure ratio (π)		2.3	[-]
	Volumetric efficiency (λ)		0.86	[-]
	Isentropic efficiency (η_is)		0.69	[-]
Ejector		Suction pressure ratio (Πs)	1.04	[-]
		Mass entrainment ratio (Φm)	0.67	[-]
		Efficiency (η_ej)	0.10	[-]
COP		COP_HX1	2.8	[-]
		COP_HVAC	2.3	[-]

Appendix D2.4: 1.2.1 (3), 28℃ and 4000 m³/h supply air (Single EV19)

1.2.1 (3)

Air

Location		Temperature (t)		Humidity (x)		Specific Enthalpy (I)	Density
		Dry bulb	Saturation	Ratio (x)	Relative (RH)		
Appendix C4	*FTL* KKG FGR	[℃]	[℃]	[kg_H20/Kg_dry]	[-]	[kJ/kg]	[kg/m3]
A1	_MIA	23.0	11.8	0.0086	0.49	44.98	1.19
A2	_EVAir1	23.8	11.8	0.0086	0.47	45.81	1.18
A3	_EVAir2	17.2	11.5	0.0084	0.69	38.64	1.21
A4	_SUP	18.5	11.5	0.0084	0.63	39.98	1.20
A5	_CAir1	27.4	14.4	0.0102	0.45	53.68	1.17
A6	_CAir2	32.7	14.4	0.0102	0.33	59.11	1.15

Air mass flow rate HX2 (m_a2) (approx. 8000 [m3/h])		9177	[kg/h]
Heat rejected at HX2 (Q_HX2)		13.84	[kW]
Air mass flow rate HX1 (m_a1) (approx. 4000 [m3/h])		4816	[kg/h]
Rate of condesed water (X_cond)		0.80	[kg/h]
Cooling capacity via air HX1	Sensible (Q_HX1_sens)	-9.083	[kW]
	Latent (Q_HX1_lat)	-0.503	[kW]
	Total (Q_HX1)	-9.586	[kW]
Cooling capacity via air HVAC unit (Q_HVAC)		-6.687	[kW]
Internal heat gains HVAC unit (Q_gain)		2.898	[kW]

1.2.1 (3)

Refrigerant ejector circuit

Location		Temperature (t)	Pressure (p)	Specific Enthalpy (h)	Specific Entropy (s)	Vapor Fraction	Saturation Temperature	Superheat
Appendix C2	*FTL* KKG FGR	[℃]	[bar]	[kJ/kg]	[kJ/kgK]	[-]	[℃]	[K]
R20	_dl2	89.2	92.2	494.60	1.917	-	-	-
R21	_02h_ext2	83.2	92.2	485.25	1.891	-	-	-
R22	_cu_ext2	30.6	90.9	278.90	1.253	-	-	-
R23	_EV_ext2	30.9	90.9	280.01	1.257	-	-	-
R24	_HPiHtEx21	30.7	90.9	279.23	1.254	-	-	-
R25	_HPiHtEx22	24.8	90.9	258.72	1.186	-	-	-
R26	_EV_ejec	24.9	90.9	259.12	1.187	-	-	-
R27	_cu_int2	-3.5	28.8	198.52	0.995	0.028	-7.0	3.5
R28	_02h_int2	23.1	28.8	474.65	2.030	-	-7.0	30.1
R29	_Lr_in2	-0.8	32.3	338.12	1.508	0.597	-2.8	2.1
R30	_EV_int2	-0.6	32.3	198.52	1.881	-	-2.8	-
R31	_LPiHtEx21	-0.7	32.3	437.28	1.880	-	-2.8	2.1
R32	_LPiHtEx22	-0.9	32.3	437.03	1.879	-	-2.8	2.0
R33	_02h2	-1.0	32.3	436.84	1.879	-	-2.8	1.9

Refrigerant mass flow rate HX1 (ṁ_re,HX1)			125	[kg/h]
Refrigerant mass flow rate HX2 (ṁ_re,HX2) (*Bitzer*)			216	[kg/h]
Heat transfered to the compressor suction line (Q̇_SLHX,LP)			-0.015	[kW]
Heat transfered from the high pressure liquid line (Q̇_SLHX,HP)			-1.231	[kW]
Compressor	Compression power (W)		3.465	[kW]
	Real el. input power (P_c)		4.267	[kW]
	Apparent el. input power (E_Sn)		5.906	[kW]
	Pressure ratio (π)		2.9	[-]
	Volumetric efficiency (λ)		0.75	[-]
	Isentropic efficiency (η_is)		0.62	[-]
Ejector		Suction pressure ratio (Πs)	1.12	[-]
		Mass entrainment ratio (Φm)	0.58	[-]
		Efficiency (η_ej)	0.36	[-]
COP		COP_HX1	2.2	[-]
		COP_HVAC	1.6	[-]

Appendix D2.5: 1.2.3 (1), 35℃ and 4000 m³/h supply air

1.2.3 (1)

Air

Location		Temperature (t)		Humidity (x)		Specific Enthalpy (I)	Density
		Dry bulb	Saturation	Ratio (x)	Relative (RH)		
Appendix C4	*FTL* KKG FGR	[°C]	[°C]	[kg_H20/Kg_dry]	[-]	[kJ/kg]	[kg/m3]
A1	_MIA	28.4	18.8	0.0136	0.56	63.35	1.16
A2	_EVAir1	28.9	18.8	0.0136	0.54	63.84	1.16
A3	_EVAir2	20.4	18.4	0.0133	0.88	54.28	1.19
A4	_SUP	22.1	18.4	0.0133	0.79	56.07	1.19
A5	_CAir1	34.9	21.2	0.0158	0.45	75.70	1.14
A6	_CAir2	44.3	21.2	0.0158	0.27	85.41	1.10

Air mass flow rate HX2 (m_a2) (approx. 8000 [m3/h])		8813	[kg/h]
Heat rejected at HX2 (Q_HX2)		23.78	[kW]
Air mass flow rate HX1 (m_a1) (approx. 2000 [m3/h])		4543	[kg/h]
Rate of condesed water (X_cond)		1.44	[kg/h]
Cooling capacity via air HX1	Sensible (Q_HX1_sens)	-11.172	[kW]
	Latent (Q_HX1_lat)	-0.901	[kW]
	Total (Q_HX1)	-12.073	[kW]
Cooling capacity via air HVAC unit (Q_HVAC)		-9.178	[kW]
Internal heat gains HVAC unit (Q_gain)		2.895	[kW]

1.2.3 (1)

Refrigerant ejector circuit

Location		Temperature (t)	Pressure (p)	Specific		Vapor Fraction	Saturation Temperature	Superheat
				Enthalpy (h)	Entropy (s)			
Appendix C2	*FTL* KKG FGR	[°C]	[bar]	[kJ/kg]	[kJ/kgK]	[-]	[°C]	[K]
R20	_dl2	75.8	100.3	463.21	1.818	-	-	-
R21	_02h_ext2	73.8	100.3	459.25	1.807	-	-	-
R22	_cu_ext2	42.7	98.3	335.81	1.432	-	-	-
R23	_EV_ext2	42.9	98.3	337.31	1.437	-	-	-
R24	_HPiHtEx21	42.8	98.3	336.56	1.435	-	-	-
R25	_HPiHtEx22	41.3	98.3	324.86	1.398	-	-	-
R26	_EV_ejec	40.8	98.3	321.18	1.386	-	-	-
R27	_cu_int2	16.3	50.6	246.32	1.159	0.014	14.8	1.5
R28	_02h_int2	15.9	50.6	421.48	1.769	-	14.8	1.1
R29	_Lr_in2	17.2	52.0	357.82	1.543	0.664	15.9	1.3
R30	_EV_int2	17.1	52.0	246.32	1.762	-	15.9	-
R31	_LPiHtEx21	17.2	52.0	420.50	1.763	-	15.9	1.3
R32	_LPiHtEx22	20.5	52.0	429.30	1.793	-	15.9	4.5
R33	_02h2	20.6	52.0	429.57	1.794	-	15.9	4.7

Refrigerant mass flow rate HX1 (m_re,HX1)			248	[kg/h]
Refrigerant mass flow rate HX2 (m_re,HX2) (*Bitzer*)			431	[kg/h]
Heat transfered to the compressor suction line (Q̇_SLHX,LP)			1.054	[kW]
Heat transfered from the high pressure liquid line (Q̇_SLHX,HP)			-1.400	[kW]
Compressor	Compression power (W)		4.028	[kW]
	Real el. input power (P_c)		4.479	[kW]
	Apparent el. input power (E_Sn)		6.016	[kW]
	Pressure ratio (π)		1.9	[-]
	Volumetric efficiency (λ)		0.87	[-]
	Isentropic efficiency (η_is)		0.67	[-]
Ejector		Suction pressure ratio (Πs)	1.03	[-]
		Mass entrainment ratio (Φm)	0.58	[-]
		Efficiency (η_ej)	0.05	[-]
COP		COP_HX1	2.7	[-]
		COP_HVAC	2.0	[-]

Appendix D2.6: 1.2.3 (2), 35℃ and 4000 m³/h supply air (110 Bar HP)

1.2.3 (2)

Air

Location		Temperature (t)		Humidity (x)		Specific Enthalpy	Density
		Dry bulb	Saturation	Ratio (x)	Relative (RH)		
Appendix C4	*FTL* KKG FGR	[°C]	[°C]	[kg_H20/Kg_dry]	[-]	[kJ/kg]	[kg/m3]
A1	_MIA	28.3	18.8	0.0136	0.56	63.14	1.16
A2	_EVAir1	28.7	18.8	0.0136	0.55	63.55	1.16
A3	_EVAir2	19.9	18.1	0.0130	0.89	52.92	1.20
A4	_SUP	21.5	18.1	0.0130	0.81	54.66	1.19
A5	_CAir1	34.9	21.2	0.0158	0.45	75.68	1.14
A6	_CAir2	42.2	21.2	0.0158	0.30	83.28	1.11

Air mass flow rate HX2 (m_a2) (approx. 8000 [m3/h])			8870	[kg/h]
Heat rejected at HX2 (Q_HX2)			18.73	[kW]
Air mass flow rate HX1 (m_a1) (approx. 4000 [m3/h])			4615	[kg/h]
Rate of condesed water (X_cond)			2.71	[kg/h]
Cooling capacity via air HX1	Sensible (Q_HX1_sens)		-11.929	[kW]
	Latent (Q_HX1_lat)		-1.700	[kW]
	Total (Q_HX1)		-13.629	[kW]
Cooling capacity via air HVAC unit (Q_HVAC)			-10.868	[kW]
Internal heat gains HVAC unit (Q_gain)			2.761	[kW]

1.2.3 (2)

Refrigerant ejector circuit

Location		Temperature (t)	Pressure (p)	Specific Enthalpy (h)	Specific Entropy (s)	Vapor Fraction	Saturation Temperature	Superheat
Appendix C2	*FTL* KKG FGR	[°C]	[bar]	[kJ/kg]	[kJ/kgK]	[-]	[°C]	[K]
R20	_dl2	87.8	109.7	475.58	1.841	-	-	-
R21	_02h_ext2	84.9	109.7	470.22	1.826	-	-	-
R22	_cu_ext2	41.9	107.9	313.25	1.356	-	-	-
R23	_EV_ext2	42.2	107.9	314.32	1.359	-	-	-
R24	_HPiHtEx21	42.1	107.9	313.90	1.358	-	-	-
R25	_HPiHtEx22	39.7	107.9	303.17	1.324	-	-	-
R26	_EV_ejec	39.2	107.9	301.30	1.318	-	-	-
R27	_cu_int2	14.7	48.2	241.52	1.143	0.015	12.8	1.9
R28	_02h_int2	14.1	48.2	424.41	1.785	-	12.8	1.3
R29	_Lr_in2	15.7	50.1	351.09	1.523	0.625	14.4	1.3
R30	_EV_int2	15.6	50.1	241.52	1.773	-	14.4	-
R31	_LPiHtEx21	15.8	50.1	423.11	1.776	-	14.4	1.5
R32	_LPiHtEx22	19.5	50.1	432.32	1.808	-	14.4	5.2
R33	_02h2	19.8	50.1	432.79	1.809	-	14.4	5.4

Refrigerant mass flow rate HX1 (m_re,HX1)			268	[kg/h]
Refrigerant mass flow rate HX2 (m_re,HX2) (*Bitzer*)			395	[kg/h]
Heat transfered to the compressor suction line (Q̇_SLHX,LP)			1.010	[kW]
Heat transfered from the high pressure liquid line (Q̇_SLHX,HP)			-1.177	[kW]
Compressor	Compression power (W)		4.695	[kW]
	Real el. input power (P_c)		5.070	[kW]
	Apparent el. input power (E_Sn)		6.534	[kW]
	Pressure ratio (π)		2.2	[-]
	Volumetric efficiency (λ)		0.84	[-]
	Isentropic efficiency (η_is)		0.68	[-]
Ejector		Suction pressure ratio (Πs)	1.04	[-]
		Mass entrainment ratio (Φm)	0.68	[-]
		Efficiency (η_ej)	0.09	[-]
COP		COP_HX1	2.7	[-]
		COP_HVAC	2.1	[-]

Appendix D2.7: 1.2.3 (3), 35℃ and 4000 m³/h supply air (110 bar HP and 480V-60Hz HX2 fans)

1.2.3 (3)

Air

Location		Temperature (t)		Humidity (x)		Specific Enthalpy (I)	Density
		Dry bulb	Saturation	Ratio (x)	Relative (RH)		
Appendix C4	*FTL* KKG FGR	[°C]	[°C]	[kg_H20/Kg_dry]	[-]	[kJ/kg]	[kg/m3]
A1	_MIA	28.5	18.8	0.0136	0.56	63.35	1.16
A2	_EVAir1	28.9	18.8	0.0136	0.54	63.80	1.16
A3	_EVAir2	20.1	18.1	0.0130	0.88	53.15	1.19
A4	_SUP	21.7	18.1	0.0130	0.80	54.79	1.19
A5	_CAir1	34.9	21.2	0.0159	0.45	75.80	1.14
A6	_CAir2	41.4	21.2	0.0159	0.32	82.49	1.11

Air mass flow rate HX2 (m_a2) 480V-3-50Hz		8894	[kg/h]
Heat rejected at HX2 (Q_HX2)		16.53	[kW]
Air mass flow rate HX1 (m_a1) (approx. 4000 [m3/h])		4612	[kg/h]
Rate of condesed water (X_cond)		2.76	[kg/h]
Cooling capacity via air HX1	Sensible (Q_HX1_sens)	-11.905	[kW]
	Latent (Q_HX1_lat)	-1.730	[kW]
	Total (Q_HX1)	-13.636	[kW]
Cooling capacity via air HVAC unit (Q_HVAC)		-10.964	[kW]
Internal heat gains HVAC unit (Q_gain)		2.672	[kW]

1.2.3 (3)

Refrigerant ejector circuit

Location		Temperature (t)	Pressure (p)	Specific Enthalpy (h)	Specific Entropy (s)	Vapor Fraction	Saturation Temperature	Superheat
Appendix C2	*FTL* KKG FGR	[°C]	[bar]	[kJ/kg]	[kJ/kgK]	[-]	[°C]	[K]
R20	_dl2	87.5	109.0	475.70	1.842	-	-	-
R21	_02h_ext2	84.3	109.0	469.83	1.826	-	-	-
R22	_cu_ext2	41.2	107.0	310.75	1.348	-	-	-
R23	_EV_ext2	41.4	107.0	311.74	1.352	-	-	-
R24	_HPiHtEx21	41.3	107.0	311.23	1.350	-	-	-
R25	_HPiHtEx22	38.9	107.0	300.60	1.316	-	-	-
R26	_EV_ejec	38.5	107.0	298.99	1.311	-	-	-
R27	_cu_int2	14.5	47.8	240.42	1.140	0.013	12.5	2.0
R28	_02h_int2	13.8	47.8	425.01	1.788	-	12.5	1.4
R29	_Lr_in2	15.3	49.6	350.08	1.520	0.620	14.0	1.3
R30	_EV_int2	15.2	49.6	240.42	1.776	-	14.0	-
R31	_LPiHtEx21	15.5	49.6	423.63	1.779	-	14.0	1.5
R32	_LPiHtEx22	19.2	49.6	432.72	1.810	-	14.0	5.2
R33	_02h2	19.4	49.6	433.25	1.812	-	14.0	5.5

Refrigerant mass flow rate HX1 (m_re,HX1)			266	[kg/h]
Refrigerant mass flow rate HX2 (m_re,HX2) (*Bitzer*)			390	[kg/h]
Heat transfered to the compressor suction line (Q̇_SLHX,LP)			0.986	[kW]
Heat transfered from the high pressure liquid line (Q̇_SLHX,HP)			-1.152	[kW]
Compressor	Compression power (W)		4.599	[kW]
	Real el. input power (P_c)		5.011	[kW]
	Apparent el. input power (E_Sn)		6.521	[kW]
	Pressure ratio (π)		2.2	[-]
	Volumetric efficiency (λ)		0.84	[-]
	Isentropic efficiency (η_is)		0.68	[-]
Ejector		Suction pressure ratio (Πs)	1.04	[-]
		Mass entrainment ratio (Φm)	0.68	[-]
		Efficiency (η_ej)	0.09	[-]
COP		COP_HX1	2.7	[-]
		COP_HVAC	2.2	[-]

Appendix D3: Simultaneous operation of both circuits

The following sub-sections, i.e. Appendix D3.1 to D3.3, include all the measured and calculated data used to produce the results presented in chapter 5.4.

Appendix D3.1: 1.3.1 (10), 28℃ and 4000 m³/h supply air

1.3.1 (5)

Air

Location		Temperature (t)		Humidity (x)		Specific Enthalpy (I)	Density
		Dry bulb	Saturation	Ratio (x)	Relative (RH)		
Appendix C4	*FTL* KKG FGR	[°C]	[°C]	[kg_H20/Kg_dry]	[-]	[kJ/kg]	[kg/m3]
A1	_MIA	23.7	12.1	0.0088	0.48	46.14	1.18
A2	_EVAir1	23.6	12.1	0.0088	0.48	46.06	1.18
A3	_EVAir2	10.8	10.3	0.0078	0.97	30.54	1.24
A4	_SUP	12.3	10.3	0.0078	0.87	32.07	1.23
A5	_CAir1	27.8	14.8	0.0105	0.45	54.83	1.17
A6	_CAir2	40.0	14.8	0.0105	0.23	67.31	1.12

Air mass flow rate HX2 (m_a2) (approx. 8000 [m3/h])		8961	[kg/h]
Heat rejected at HX2 (Q_HX2)		31.06	[kW]
Air mass flow rate HX1 (m_a1) (approx. 4000 [m3/h])		4754	[kg/h]
Rate of condesed water (X_cond)		4.68	[kg/h]
Cooling capacity via air HX1	Sensible (Q_HX1_sens)	-17.568	[kW]
	Latent (Q_HX1_lat)	-2.931	[kW]
	Total (Q_HX1)	-20.499	[kW]
Cooling capacity via air HVAC unit (Q_HVAC)		-18.578	[kW]
Internal heat gains HVAC unit (Q_gain)		1.921	[kW]

1.3.1 (5) (Basic)

Basic circuit

Location		Temperature (t)	Pressure (p)	Specific		Vapor Fraction	Saturation Temperature	Superheat
				Enthalpy (h)	Entropy (s)			
Appendix C2	*FTL* KKG FGR	[°C]	[bar]	[kJ/kg]	[kJ/kgK]	[-]	[°C]	[K]
R7	_dl1	89.4	99.2	488.58	1.890	-	-	-
R8	_02h_ext1	84.0	99.2	479.39	1.865	-	-	-
R9	_cu_ext1	38.1	98.5	305.24	1.335	-	-	-
R10	_EV_ext1	38.5	-	-	-	-	-	-
R11	_HPiHtEx11	38.0	98.5	304.85	1.334	-	-	-
R12	_HPiHtEx12	35.3	98.5	292.44	1.294	-	-	-
R13	_EV_int1	34.9	98.5	290.51	1.288	-	-	-
R14	_cu_int1	9.3	42.4	290.51	1.320	0.332	-	-
R15	_02h_int1	9.1	42.4	429.80	1.819	-	7.6	1.4
R16	_LR_in1	8.4	42.4	428.30	1.813	-	7.6	0.8
R17	_LPiHtEx11	8.3	42.4	428.18	1.813	-	7.6	0.7
R18	_LpiHTtEx12	14.4	42.4	440.31	1.856	-	7.6	6.8
R19	_0h1	14.3	42.4	440.00	1.855	-	7.6	6.6

Refrigerant mass flow rate (m_rb) (*Bitzer*)			317	[kg/h]
Compressor	Compression power (W)		4.277	[kW]
	Real el. input power (P_c) (*Bitzer)*		4.424	[kW]
	Apparent el. input power (E_Sn)		6.025	[kW]
	Pressure ratio (π)		2.3	[-]
	Volumetric efficiency (λ)		0.85	[-]
	Isentropic efficiency (η_is)		0.71	[-]
COP		HX1 (COP_HX1)	-	[-]
		HVAC unit (COP_HVAC)	-	[-]

1.3.1 (5) (Ejector)

Refrigerant ejector circuit

Location		Temperature (t)	Pressure (p)	Specific Enthalpy (h)	Specific Entropy (s)	Vapor Fraction	Saturation Temperature	Superheat
Appendix C2	*FTL* KKG FGR	[°C]	[bar]	[kJ/kg]	[kJ/kgK]	[-]	[°C]	[K]
R20	_dl2	88.8	96.7	489.92	1.897	-	-	-
R21	_02h_ext2	84.8	96.7	483.35	1.879	-	-	-
R22	_cu_ext2	39.0	95.1	315.64	1.370	-	-	-
R23	_EV_ext2	39.3	95.1	317.64	1.376	-	-	-
R24	_HPiHtEx21	39.1	95.1	316.89	1.374	-	-	-
R25	_HPiHtEx22	37.2	95.1	304.97	1.336	-	-	-
R26	_EV_ejec	36.6	95.1	301.84	1.326	-	-	-
R27	_cu_int2	8.4	41.0	222.89	1.080	0.009	6.3	2.1
R28	_02h_int2	7.7	41.0	430.88	1.827	-	6.3	1.5
R29	_Lr_in2	9.1	42.4	-	-	-	-	-
R30	_EV_int2	9.0	42.4	222.89	1.819	-	7.6	-
R31	_LPiHtEx21	9.6	42.4	431.11	1.824	-	7.6	2.0
R32	_LPiHtEx22	15.5	42.4	442.33	1.863	-	7.6	7.9
R33	_02h2	15.8	42.4	442.99	1.865	-	7.6	8.3

Refrigerant mass flow rate HX1 (m_re,HX1)		-	[kg/h]
Refrigerant mass flow rate HX2 (m_re,HX2) (*Bitzer*)		318	[kg/h]
Heat transfered to the compressor suction line ($\dot{Q}$_SLHX,LP)		-	[kW]
Heat transfered from the high pressure liquid line ($\dot{Q}$_SLHX,HP)		-	[kW]
Compressor	Compression power (W)	4.146	[kW]
	Real el. input power (P_c) (*Bitzer)*	4.312	[kW]
	Apparent el. input power (E_Sn)	-	[kW]
	Pressure ratio (π)	2.3	[-]
	Volumetric efficiency (λ)	0.87	[-]
	Isentropic efficiency (η_is)	0.72	[-]
Ejector	Suction pressure ratio (Πs)	1.03	[-]
	Mass entrainment ratio (Φm)	-	[-]
	Efficiency (η_ej)	-	[-]
COP	COP_HX1	-	[-]
	COP_HVAC	-	[-]

Appendix D3.2: 1.3.1 (6), 28℃ and 4000 m³/h supply air (480V-3-60Hz HX2 fans)

1.3.1 (6)

Air

Location		Temperature (t)		Humidity (x)		Specific Enthalpy (I)	Density
		Dry bulb	Saturation	Ratio (x)	Relative (RH)		
Appendix C4	*FTL* KKG FGR	[°C]	[°C]	[kg_H20/Kg_dry]	[-]	[kJ/kg]	[kg/m3]
A1	_MIA	23.4	12.1	0.0088	0.49	45.87	1.18
A2	_EVAir1	23.5	12.1	0.0088	0.49	45.90	1.18
A3	_EVAir2	10.4	10.2	0.0077	0.99	29.84	1.24
A4	_SUP	11.9	10.2	0.0077	0.89	31.44	1.23
A5	_CAir1	27.8	14.8	0.0105	0.45	54.74	1.17
A6	_CAir2	38.6	14.8	0.0105	0.25	65.81	1.13

Air mass flow rate HX2 (m_a2) 480V-3-60Hz		-	[kg/h]
Heat rejected at HX2 (Q_HX2)		-	[kW]
Air mass flow rate HX1 (m_a1) (approx. 4000 [m3/h])		4744	[kg/h]
Rate of condesed water (X_cond)		5.01	[kg/h]
Cooling capacity via air HX1	Sensible (Q_HX1_sens)	-18.021	[kW]
	Latent (Q_HX1_lat)	-3.138	[kW]
	Total (Q_HX1)	-21.158	[kW]
Cooling capacity via air HVAC unit (Q_HVAC)		-19.014	[kW]
Internal heat gains HVAC unit (Q_gain)		2.145	[kW]

1.3.1 (6) (Basic)

Basic circuit

Location		Temperature (t)	Pressure (p)	Specific		Vapor Fraction	Saturation Temperatu	Superheat
				Enthalpy (h)	Entropy (s)			
Appendix C2	*FTL* KKG FGR	[°C]	[bar]	[kJ/kg]	[kJ/kgK]	[-]	[°C]	[K]
R7	_dl1	90.5	99.9	489.68	1.892	-	-	-
R8	_02h_ext1	84.1	99.9	478.97	1.863	-	-	-
R9	_cu_ext1	36.0	99.4	294.71	1.301	-	-	-
R10	_EV_ext1	36.7	-	-	-	-	-	-
R11	_HPiHtEx11	36.0	99.4	294.37	1.300	-	-	-
R12	_HPiHtEx12	33.1	99.4	283.07	1.263	-	-	-
R13	_EV_int1	32.6	99.4	281.24	1.257	-	-	-
R14	_cu_int1	9.0	42.3	281.24	1.287	0.289	-	-
R15	_02h_int1	8.9	42.3	429.82	1.819	-	7.5	1.4
R16	_LR_in1	8.2	42.3	428.35	1.814	-	7.5	0.7
R17	_LPiHtEx11	8.4	42.3	428.84	1.816	-	7.5	0.9
R18	_LpiHTtEx12	14.5	42.3	440.73	1.858	-	7.5	7.0
R19	_0h1	14.3	42.3	440.42	1.857	-	7.5	6.8

Refrigerant mass flow rate (m_rb) (*Bitzer*)			314	[kg/h]
Compressor	Compression power (W)		4.296	[kW]
	Real el. input power (P_c) (*Bitzer)*		4.457	[kW]
	Apparent el. input power (E_Sn)		-	[kW]
	Pressure ratio (π)		2.4	[-]
	Volumetric efficiency (λ)		0.84	[-]
	Isentropic efficiency (η_is)		0.71	[-]
COP		HX1 (COP_HX1)	-	[-]
		HVAC unit (COP_HVAC)	-	[-]

1.3.1 (6) (Ejector)

Refrigerant ejector circuit

Location		Temperature (t)	Pressure (p)	Specific Enthalpy (h)	Specific Entropy (s)	Vapor Fraction	Saturation Temperatur	Superheat
Appendix C2	*FTL* KKG FGR	[°C]	[bar]	[kJ/kg]	[kJ/kgK]	[-]	[°C]	[K]
R20	_dl2	90.5	97.5	491.95	1.902	-	-	-
R21	_02h_ext2	85.9	97.5	484.34	1.881	-	-	-
R22	_cu_ext2	37.2	95.9	303.64	1.331	-	-	-
R23	_EV_ext2	37.5	95.9	305.43	1.337	-	-	-
R24	_HPiHtEx21	37.4	95.9	304.88	1.335	-	-	-
R25	_HPiHtEx22	35.1	95.9	293.59	1.299	-	-	-
R26	_EV_ejec	34.6	95.9	291.45	1.292	-	-	-
R27	_cu_int2	8.0	40.6	221.52	1.076	0.007	5.9	2.1
R28	_02h_int2	7.3	40.6	431.16	1.829	-	5.9	1.4
R29	_Lr_in2	8.6	41.8	-	-	-	-	-
R30	_EV_int2	8.5	41.8	221.52	1.822	-	7.1	-
R31	_LPiHtEx21	9.3	41.8	431.97	1.828	-	7.1	2.3
R32	_LPiHtEx22	15.0	41.8	442.65	1.866	-	7.1	7.9
R33	_02h2	15.4	41.8	443.29	1.868	-	7.1	8.3

Refrigerant mass flow rate HX1 (m_re,HX1)			-	[kg/h]
Refrigerant mass flow rate HX2 (m_re,HX2) (*Bitzer*)			312	[kg/h]
Heat transfered to the compressor suction line (Q̇_SLHX,LP)			-	[kW]
Heat transfered from the high pressure liquid line (Q̇_SLHX,HP)			-	[kW]
Compressor	Compression power (W)		4.218	[kW]
	Real el. input power (P_c) (*Bitzer)*		4.312	[kW]
	Apparent el. input power (E_Sn)		-	[kW]
	Pressure ratio (π)		2.3	[-]
	Volumetric efficiency (λ)		0.86	[-]
	Isentropic efficiency (η_is)		0.73	[-]
Ejector		Suction pressure ratio (Πs)	1.03	[-]
		Mass entrainment ratio (Φm)	-	[-]
		Efficiency (η_ej)	-	[-]
COP		COP_HX1	-	[-]
		COP_HVAC	-	[-]

Appendix D3.3: 1.3.1 (5), 28℃ and 4000 m³/h supply air (110 bar high pressure)

1.3.1 (10)

Air

Location		Temperature (t)		Humidity (x)		Specific Enthalpy (I)	Density
		Dry bulb	Saturation	Ratio (x)	Relative (RH)		
Appendix C4	*FTL* KKG FGR	[°C]	[°C]	[kg_H20/Kg_dry]	[-]	[kJ/kg]	[kg/m3]
A1	_MIA	23.7	12.8	0.0092	0.50	47.20	1.18
A2	_EVAir1	23.8	12.8	0.0092	0.50	47.31	1.18
A3	_EVAir2	11.3	11.1	0.0082	0.99	32.05	1.23
A4	_SUP	12.8	11.1	0.0082	0.89	33.65	1.23
A5	_CAir1	28.1	15.1	0.0107	0.45	55.58	1.16
A6	_CAir2	40.4	15.1	0.0107	0.23	68.22	1.12

Air mass flow rate HX2 (m_a2) (approx. 8000 [m3/h])		8948	[kg/h]
Heat rejected at HX2 (Q_HX2)		31.42	[kW]
Air mass flow rate HX1 (m_a1) (approx. 4000 [m3/h])		4798	[kg/h]
Rate of condesed water (X_cond)		4.69	[kg/h]
Cooling capacity via air HX1	Sensible (Q_HX1_sens)	-17.402	[kW]
	Latent (Q_HX1_lat)	-2.935	[kW]
	Total (Q_HX1)	-20.337	[kW]
Cooling capacity via air HVAC unit (Q_HVAC)		-18.056	[kW]
Internal heat gains HVAC unit (Q_gain)		2.281	[kW]

1.3.1 (10) (Basic)

Basic circuit

Location		Temperature (t)	Pressure (p)	Specific		Vapor Fraction	Saturation Temperature	Superheat
				Enthalpy (h)	Entropy (s)			
Appendix C2	*FTL* KKG FGR	[°C]	[bar]	[kJ/kg]	[kJ/kgK]	[-]	[°C]	[K]
R7	_dl1	95.9	110.1	489.38	1.878	-	-	-
R8	_02h_ext1	89.5	110.1	478.35	1.848	-	-	-
R9	_cu_ext1	36.1	109.7	288.26	1.275	-	-	-
R10	_EV_ext1	37.4	-	-	-	-	-	-
R11	_HPiHtEx11	36.0	109.7	288.19	1.275	-	-	-
R12	_HPiHtEx12	32.4	109.7	276.45	1.237	-	-	-
R13	_EV_int1	31.9	109.7	274.82	1.231	-	-	-
R14	_cu_int1	9.8	43.3	274.82	1.264	0.250	-	-
R15	_02h_int1	9.9	43.3	429.06	1.814	-	8.5	1.4
R16	_LR_in1	9.2	43.3	427.53	1.808	-	8.5	0.8
R17	_LPiHtEx11	9.2	43.3	427.54	1.808	-	8.5	0.8
R18	_LpiHTtEx12	13.1	43.3	435.77	1.837	-	8.5	4.7
R19	_0h1	13.0	43.3	435.60	1.837	-	8.5	4.6

Refrigerant mass flow rate (m_rb) (*Bitzer*)			315	[kg/h]
Compressor	Compression power (W)		4.705	[kW]
	Real el. input power (P_c) (*Bitzer)*		4.885	[kW]
	Apparent el. input power (E_Sn)		-	[kW]
	Pressure ratio (π)		2.5	[-]
	Volumetric efficiency (λ)		0.80	[-]
	Isentropic efficiency (η_is)		0.69	[-]
COP		HX1 (COP_HX1)	-	[-]
		HVAC unit (COP_HVAC)	-	[-]

1.3.1 (10) (Ejector)

Refrigerant ejector circuit

Location		Temperature (t)	Pressure (p)	Specific Enthalpy (h)	Specific Entropy (s)	Vapor Fraction	Saturation Temperature	Superheat
Appendix C2	*FTL* KKG FGR	[°C]	[bar]	[kJ/kg]	[kJ/kgK]	[-]	[°C]	[K]
R20	_dl2	91.5	100.0	491.26	1.896	-	-	-
R21	_02h_ext2	87.4	100.0	484.37	1.878	-	-	-
R22	_cu_ext2	38.3	98.4	306.45	1.339	-	-	-
R23	_EV_ext2	38.6	98.4	308.11	1.344	-	-	-
R24	_HPiHtEx21	38.5	98.4	307.60	1.343	-	-	-
R25	_HPiHtEx22	36.2	98.4	296.16	1.306	-	-	-
R26	_EV_ejec	35.7	98.4	293.94	1.299	-	-	-
R27	_cu_int2	8.8	41.5	224.19	1.085	0.009	6.8	2.1
R28	_02h_int2	8.2	41.5	430.52	1.824	-	6.8	1.5
R29	_Lr_in2	9.7	42.9	-	-	-	-	-
R30	_EV_int2	9.5	42.9	224.19	1.816	-	8.1	-
R31	_LPiHtEx21	10.3	42.9	430.96	1.821	-	8.1	2.2
R32	_LPiHtEx22	15.7	42.9	441.46	1.858	-	8.1	7.6
R33	_02h2	16.0	42.9	442.07	1.860	-	8.1	7.9

Refrigerant mass flow rate HX1 (m_re,HX1)			-	[kg/h]
Refrigerant mass flow rate HX2 (m_re,HX2) (*Bitzer*)			321	[kg/h]
Heat transfered to the compressor suction line (Q̇_SLHX,LP)			-	[kW]
Heat transfered from the high pressure liquid line (Q̇_SLHX,HP)			-	[kW]
Compressor	Compression power (W)		4.387	[kW]
	Real el. input power (P_c) (*Bitzer)*		4.312	[kW]
	Apparent el. input power (E_Sn)		-	[kW]
	Pressure ratio (π)		2.3	[-]
	Volumetric efficiency (λ)		0.86	[-]
	Isentropic efficiency (η_is)		0.75	[-]
Ejector		Suction pressure ratio (Πs)	1.03	[-]
		Mass entrainment ratio (Φm)	-	[-]
		Efficiency (η_ej)	-	[-]
COP		COP_HX1	-	[-]
		COP_HVAC	-	[-]

Appendix D4: FTL *Design cooling load calculation for R744 HVAC*

The datasheet presented below is the design cooling load calculations the R744 HVAC unit conducted by *FTL* in accordance with EN 13129, thus corresponding to full passenger load and 28°C ambient air temperature and 45% ambient relative air humidity.

DATENBLATT LASTRECHNUNG KÜHLEN WAGGON ================ VERS. 4.20 === 19.03.2015
FGR_Kühlen

LASTEN KÜHLEN ==========
Einsatzort / Bemerkung Flirt NSB

Umgebungstemperatur	28	°C	Passagierzahl	69	
Luftfeuchtigkeit	45	%	Frischluftmenge	1035	m³/h
Höhe	100	m	dT Frischluft	0	K
Sonnenstrahlung	600	W/m²	diffuse Strahlung	110	W/m²
Einfallswinkel	30	°			
Geschwindigkeit	12	km/h			
innere Wärmelast sens.	1	kW	Druckverl. Kanalsystem	100	Pa
innere Wärmelast lat.	0.0	kW	CO2 je Passagier	17	l/h

WAGGONBEDINGUNGEN ==========

Länge	20,9	m	(k-Werte bei akt. Geschwindigkeit)		
Höhe	2,45	m	Dach	1,2	W/m²/K
Breite	3,2	m	Seitenwand	1,2	W/m²/K
Fensterhöhe	1,0	m	Stirnseite 1		W/m²/K
Fensterbreite	1,5	m	Stirnseite 2		W/m²/K
Fensterzahl Sonne	10		Boden	1,2	W/m²/K
Fensterzahl Schatten	10		Fenster	1,7	W/m²/K
Absorptionsfakt. Dach	0,8				
Absorptionsfakt. Seite	0,7				
Transmissionsfaktor	0,4				

VERDAMPFER ========== VERFLÜSSIGER ==========

Anzahl	1	
Luftmenge	2000	m³/h

ERGEBNISSE ==========

STRAHLUNG ==========		SONNENWAND ====	SCHATTENWAND ==	DACH ==========
Intensität	W/m²/K	630	110	410

LASTEN ==========		SENSIBEL ======	LATENT ==========
Frischluft	kW	1.973	4.874
Passagiere	kW	5.824	2.332
Wärmedurchgang Wände	kW	1.484	
Wärmedurchgang Fenster	kW	0.306	
Strahlung Wände+Fenster	kW	6.243	
Lüfterleistung	kW	0.111	
Sonstige	kW	1.000	0.000

WÄRMEÜBERTRAGER ==========		VERDAMPFER ==========	
Leistung	kW	24.1	
Lufteintrittstemperatur	°C	25.1	0.000
rel. Eintrittsfeuchte	%	39	
Luftaustrittstemperatur	°C	-1.0	
rel. Austrittsfeuchte	%	100	

==========

benötigte Kälteleistung	kW	24.1
Feuchte im Raum	%	30
Temperatur im Raum	°C	22.0

==========

Appendix E: Pilot R744 HVAC oil foaming

Refrigerant foaming at various amounts of superheat during laboratory testing of the R744 HVAC, as explained in section 4.2.4.3.

1. *Superheat compressor suction 5K*

2 . *Superheat compressor suction 8K*

3. *Superheat compressor suction 10K*

4. *Superheat compressor suction 13K*

5. *Superheat compressor suction 17K*

Appendix F: HSE documentation

Risk assessment

Field trip for master thesis

Sundland Drammen, Norway, January 2017

Project title	R744 HVAC for NSB Flirt trains
Project leader	Armin Hafner
Unit	EPT
HSE coordinator	Morten Grønli
Line manager	Olav Bolland
Risk assessment conducted by	Armin Hafner, Eirik Trygstad

Table of contents

1 Introduction

The purpose of this field trip is to observe the installation and start-up of a modified R134a HVAC unit on one of NSBs Stadler FLIRT trainsets, at NSBs workshop in Drammen. A team from Stadler will conduct the installation, and a service technician from a subcontractor will perform the commissioning of the HVAC unit.

2 Organization

Role	**NTNU**
Tour manager	Krzysztof Banasiak
Line manager	Olav bolland
HSE manager	Armin Hafner
HSE coordinator	Morten Grønli

3 Risk of trip

Main activities	**Documentation**	**Date**
Trip to Drammen	Program, risk assessment	10.01.2017
Program in Drammen (Facility tour)	Program, risk assessment	10.01.2017
Trip to Lysaker	Program, risk assessment	10.01.2017
Trip to Drammen	Program, risk assessment	12.01.2017
Program in Drammen (Observation of HVAC)	Program, risk assessment	12.01.2017
Trip to Lysaker	Program risk assessment	12.01.2017

4 In advance and risk reduction measures

Program with tour guide and high visibility vest. Sign-in and –out at gatekeeper.

Phonebook of all participants placed at the department office and with tour

5 Program

Time	Activity	Participants
Tuesday, 10.01.2017, Day 2 in week 2		
Morning	Meeting At Sundland workshop in Drammen. Meeting with tour-guide and sign-in at gatekeeper. High visibility vest required. Tour of the facility	Eirik Trygstad
Midday	Tour of the facility by representative from NSB	Eirik Trygstad
Thursday, 12.01.2017, Day 4 in week 2		
Morning	Meeting At Sundland workshop in Drammen. Meeting with tour-guide and sign-in at gatekeeper. High visibility vest required. Tour of the facility	All

Midday	Observation of HVAC unit commissioning	All

6 Risk matrix

CONSEQUENCE						
	Extremely serious	E1	E2	E3	E4	E5
	Serious	D1	D2	D3	D4	D5
	Moderate	C1	C2	C3	C4	C5
	Minor	B1	B2	B3	B4	B5
	Not significant	A1	A2	A3	A4	A5
		Very low	Low	Medium	High	Very high
		LIKELIHOOD				

Principle for acceptance criteria. Explenation of the colours used in the risk matrix

Colour		Description
Red		Unacceptable risk. Measures must be taken to reduce the risk.
Yellow		Assessment range. Measures must be considered.
Green		Acceptable risk Measures can be considered based on other considerations.

Risk assessment

Field trip for master thesis

Leipzig, Germany, January 2017

Project title	R744 HVAC for NSB Flirt trains
Project leader	Armin Hafner
Unit	EPT
HSE coordinator	Morten Grønli
Line manager	Olav Bolland
Risk assessment conducted by	Armin Hafner, Eirik Trygstad

Table of contents

1 Introduction

The purpose of this field trip is to observe laboratory tests of a prototype R744 HVAC unit at the Faivaly test laboratory in Leipzig.

2 Organization

Role	**NTNU**
Tour manager	Krzysztof Banasiak
Line manager	Olav bolland
HSE manager	Armin Hafner
HSE coordinator	Morten Grønli

3 Risk of trip

Main activities	**Documentation**	**Date**
Trip to Leipzig	Program, risk assessment	06.02.17
Program Faivaley (Laboratory tests)	Program, risk assessment	07.02.17
Program Faivaley (Laboratory tests)	Program, risk assessment	08.02.17
Program Faivaley (Laboratory tests)	Program, risk assessment	09.02.17
Trip to Trondheim	Program, risk assessment	10.02.17

4 In advance and risk reduction measures

Preparations Review of safety memo for the prototype R744 HVAC unit.

Program In accordance with Faivaleys HSE regulations.

Phonebook of all participants placed at the department office and with tour

5 Program

Time	Activity	Participants
Monday, 06.02.2017, Day 1 in week 6		
Morning	Meeting at Værnes airport in Outside Trondheim. Travel by plane to OSL Gardermoen airport.	All
Midday	Travel by plane to Berlin airport and then by train to Leipzig	All
Tuesday, 07.02.2017, Day 2 in week 6		
Morning	Travel by train to Faivaleys test facility and observe laboratory tests	All
Midday	Observe laboratory tests	All
Evening	Travel by train to the hotel	All
Wednesday, 08.02.2017, Day 3 in week 6		

Morning	Travel by train to Faivaleys test facility and observe laboratory tests	All
Midday	Observe laboratory tests	All
Evening	Travel by train to the hotel	All
Thursday, 09.02.2017, day 4 in week 6		
Morning	Travel by train to Faivaleys test facility and observe laboratory tests	All
Midday	Observe laboratory tests	All
Evening	Travel by train to the hotel	All
Friday, 10.02.2017, day 5 om week 7		
Morning	Travel by train to Berlin airport. Travel by plane to OSL Gardermoen airport	Eirik Trygstad
Midday	Travel by plane to TRD Værnes airport	Eirik Trygstad

6 Risk matrix

CONSEQUENCE	Extremely serious	E1	E2	E3	E4	E5
	Serious	D1	D2	D3	D4	D5
	Moderate	C1	C2	C3	C4	C5
	Minor	B1	B2	B3	B4	B5
	Not significant	A1	A2	A3	A4	A5
		Very low	Low	Medium	High	Very high
		LIKELIHOOD				

Principle for acceptance criteria. Explenation of the colours used in the risk matrix

Colour	Description
Red	Unacceptable risk. Measures must be taken to reduce the risk.
Yellow	Assessment range. Measures must be considered.
Green	Acceptable risk Measures can be considered based on other considerations.